# Exploring the determinants of brown adipose tissue function in early life using infrared thermography

Lindsay J Robinson

BMedSc (Hons), MB ChB (Hons)

Division of Child Health, Obstetrics and Gynaecology

School of Medicine

Supervised by Professor Helen Budge and Professor Michael Symonds

**Thesis submitted to the University of Nottingham for the degree of Doctor of Philosophy**

**November 2019**

## Abstract

There are significant gaps in our understanding of the developmental physiology of brown adipose tissue (BAT) between the neonatal period and adulthood. Studies of BAT in childhood are limited to the retrospective analysis of radiolabelled positron emission tomography (PET) imaging untaken for paediatric oncological diagnosis, treatment or monitoring. This thesis aimed to utilise supraclavicular skin temperature ($T_{SCR}$), derived from infrared thermography (IRT), as a non-invasive, surrogate marker of BAT thermogenic function in children and, to use this methodology to identify determinants of BAT function in early life.

Study I was undertaken in primary school-age children (6 – 11 years) within a free-living school environment, it explored the impact of age, sex, ambient room temperature and body mass index (BMI) on $T_{SCR}$, and also sought to quantify the thermogenic response ($\Delta T_{SCR}$) to a localised mild cold stimulus (single-hand immersion in cool tap water c.20˚C). BMI and ambient room temperature were identified as significant determinants of $T_{SCR}$ and $\Delta T_{SCR}$. The magnitude of the thermogenic response to cold exposure was less than expected (c. 0.1˚C) and a second study was undertaken to confirm the findings of Study II. Study II also explored the impact of dietary intake, activity and eating behaviour on $T_{SCR.}$ In line with Study I, an inverse relationship was identified between BMI and $T_{SCR,}$ but no other persistent relationships were observed. In addition, $T_{SCR}$ and $\Delta T_{SCR}$ were higher in boys than girls in this slightly older study group (aged 8.5 – 11 years). Similar findings were also identified retrospectively in the Study I cohort of children when limited to children aged 8.5 years and above. The whole group thermogenic response to cooling in Study II was still unexpectedly small, and Studies III – V were undertaken to explore why this may have been.

Study III identified that $T_{SCR}$ and $\Delta T_{SCR}$ were higher in participants exposed to mild anticipatory psychological stress (confirmed by raised cortisol) than when relaxed. The study protocol also unintentionally resulted in passive cooling, indicated by a gradual

reduction in overall mean skin temperature ($T_{MSK}$). Conversely, $T_{SCR}$ did not fall. During the relaxation phase, a significant increase in $T_{SCR}$ was observed in parallel to a reduction in $T_{MSK}$, indicating that BAT may have been activated in response to passive cooling in addition to anticipatory psychological stress.

Study IV evaluated the effect of ambient room temperature under controlled laboratory conditions. A differential effect of ambient temperature on supraclavicular heat production was observed. When acclimated to a warm room both $T_{SCR}$ and energy expenditure (EE) increased, when acclimated to a cool room, despite an ongoing decline in $T_{MSK}$ neither $T_{SCR}$ nor EE changed significantly after exposure to an additional localised cold stimulus. Suggesingt that BAT may respond to very small changes in room temperature, and may have been near maximally activated at 18˚C in light clothing.

Study V examined whether a more severe and prolonged localised cold stimulus would enhance the supraclavicular thermogenic response. Using a water-perfused blanket, the forearm was selectively cooled at 14˚C for 45 minutes and the time course and magnitude of changes in $T_{SCR}$ were investigated. In this group of participants, the maximal $T_{SCR}$ response of c.0.4˚C was observed after thirty minutes. Participants also underwent MRI, from which subcutaneous adipose tissue (SCAT) depth was measured on the dorsal aspect of the upper thorax. The inverse relationship between BMI and $T_{SCR}$ in Studies II and II were also observed in this group of young adults and persisted even after adjustment for the insulative effect of regional SCAT.

In conclusion, small changes in $T_{SCR}$ are detectable using infrared thermography in children and young adults. Sex, BMI, ambient temperature and psychological state all impact upon $T_{SCR}$ indicative of an effect on BAT thermogenesis.

## Acknowledgements

I sincerely thank Professor Helen Budge and Professor Michael Symonds for giving me the opportunity to undertake the research described in this thesis.

I am exceptionally grateful for the technical expertise provided by Victoria Wilson, Mark Pope, Sara Brown and Elizabeth Simpson and am naturally indebted to the volunteers for taking part in these studies, without whom, these studies would not have been possible.

On a personal note I would like to thank all those who have had cake and tea with me in the coffee room over the years. Most of all thank you to Neil for his patience and Annabel and Madeleine for providing much needed perspective on what it means to be successful and happy.

# Table of Contents

Abstract ..... i
Acknowledgements ..... iii
Table of Contents ..... iv
Declaration ..... viii
Abbreviations and Acronyms ..... ix
List of Figures ..... xi
List of Tables ..... xiv

**Chapter 1 Introduction** ..... 1
1.1 Principal aims ..... 2
1.2 Childhood obesity ..... 4
1.3 The adipose tissue organ structure and function ..... 8
1.4 Mitochondrial oxidation ..... 10
1.5 Uncoupling protein 1 and the principles of thermogenesis ..... 11
1.6 Non-shivering thermogenesis and energy balance ..... 14
1.7 Clinical implications of dysfunctional BAT ..... 16
1.8 Human supraclavicular BAT in early life ..... 17
1.9 Classification of human brown adipose tissue ..... 22
1.10 Sympathetic control of BAT ..... 24
1.11 In vivo assessment of human BAT morphology and function ..... 26
1.11.1 Radiolabelled uptake of BAT substrates ..... 27
1.11.2 Adipose tissue lipid content ..... 34
1.11.3 Oxygenation and tissue perfusion ..... 36
1.11.4 Supraclavicular skin temperature as a surrogate marker of BAT activity ..... 37
1.11.5 Cooling protocols for activation of human BAT ..... 51
1.12 Human BAT in early life ..... 52
1.12.1 Relationship between BAT and age in early life ..... 56
1.12.2 Relationship between BAT and sex in early life ..... 61
1.12.3 Relationship between BAT and height, weight and body composition ..... 63
1.12.4 Effect of ambient temperature and pre-PET scan warming measures ..... 68
1.12.5 Effect of season and outdoor temperature ..... 69
1.12.6 Impact of sedation, anxiolytics, opiates and anaesthesia ..... 70
1.12.7 BAT function during childhood ill-health ..... 71
1.13 Aims and hypotheses ..... 74

**Chapter 2 General materials and methods** ..... 77
2.1 Overview of studies ..... 78
2.2 Ethical approval ..... 78
2.3 Participants ..... 79
2.4 Cooling protocols ..... 80
2.4.1 Acclimatisation and clothing ..... 80
2.42 Ambient room temperature ..... 82
2.4.3 Hand cooling ..... 83
2.4.4 Prolonged hand cooling ..... 84
2.4.5 Forearm cooling with the Blanketrol® II ..... 84
2.5 Mild mental stress protocol ..... 85
2.5.1 Mental arithmetic test ..... 85
2.5.2 Corresponding control period ..... 86
2.5.3 Measurement of salivary cortisol ..... 86
2.6 Infrared thermography ..... 89
2.6.1 Acquisition of thermal images ..... 93
2.6.2 Thermal image analysis ..... 99
2.6.2.1 Manual supraclavicular ROI placement using FLIR software ..... 101
2.6.2.2 Calculating a summary measure of supraclavicular skin temperature ..... 109
2.6.2.3 Semi-automated ROI placement using a custom MATLAB script ..... 110
2.7 Non-BAT skin temperature measurement ..... 111
2.7.1 Skin temperature measurement using iButton devices ..... 111
2.7.2 Skin temperature measurement using thermography ..... 114
2.7.3 Tympanic membrane temperature ..... 114
2.8 Anthropometrics ..... 114
2.8.1 Height and body weight ..... 114
2.8.2 Body mass index ..... 115
2.8.3 Bioelectrical impedance ..... 116
2.8.4 Subcutaneous adipose tissue thickness ..... 117
2.9 Metabolic and cardiovascular ..... 118
2.9.1 Indirect calorimetry ..... 118
2.9.2 Dietary intake, activity and eating behaviour ..... 119
2.9.3 Blood pressure and heart rate ..... 121
2.10 Safety precautions ..... 121
2.11 Statistical analysis and data presentation ..... 122

**Chapter 3 Exploring the determinants of supraclavicular skin temperature in young children** ..... 125
3.1 Preface ..... 126
3.2 Study I ..... 128
3.2.1 Abstract ..... 128
3.2.2 Introduction ..... 129
3.2.3 Methods ..... 130
3.2.4 Results ..... 134
3.2.5 Discussion ..... 140
3.3 Study II ..... 144
3.3.1 Abstract ..... 144
3.3.2 Introduction ..... 145
3.3.3 Methods ..... 147
3.3.4 Statistics ..... 153
3.3.5 Results ..... 154
3.3.6 Discussion ..... 163
3.4 Studies I and II conclusions ..... 167

**Chapter 4 The effect of mild psychological stress on supraclavicular skin temperature in young females**. ..... 178
4.1 Preface ..... 179
4.2 Study III ..... 181
4.2.1 Abstract ..... 181
4.2.2 Introduction ..... 182
4.2.3 Methods ..... 184
4.2.4 Statistical analysis ..... 187
4.2.5 Results ..... 188
4.2.5.1 Salivary cortisol response ..... 189
4.2.5.2 Anticipation is associated with increased supraclavicular skin temperature ..... 190
4.2.5.3 Supraclavicular skin temperature increases following MA and R and is associated with baseline $T_{SCR}$ and salivary cortisol concentration ..... 190
4.2.6 Discussion ..... 194
4.3 Study III conclusions in 2019 ..... 198

**Chapter 5 The physiological response to mild cold exposure and the effect of ambient temperature** ..... 202
5.0 Preface ..... 203
5.1 Study IV ..... 207
5.1.1 Abstract ..... 207

5.1.2 Introduction ..... 208
5.1.3 Methods ..... 210
5.1.3.1 Participants ..... 210
5.1.3.2 Cooling protocol ..... 211
5.1.3.3 Energy expenditure ..... 211
5.1.3.4 Infrared thermography ..... 212
5.1.3.5 Mean skin temperature ..... 213
5.1.3.6 Statistical analysis ..... 213
5.2.4 Results ..... 214
5.2.5 Discussion ..... 217
5.2 Study V ..... 221
5.2.1 Abstract ..... 221
5.2.2 Introduction ..... 222
5.2.3 Methods ..... 224
5.2.3.1 Study protocol and participants ..... 225
5.2.3.2 Anthropometric measurements ..... 227
5.2.3.3 Statistical analysis ..... 229
5.2.3.4 Sample size and power ..... 230
5.2.4 Results ..... 231
5.2.4.1 Time course and magnitude of the $T_{SCR}$ response to forearm cooling ..... 232
5.2.4.2 Relationship between $T_{SCR}$ and body composition ..... 236
5.2.5 Discussion ..... 238
5.3 Study IV and V conclusions ..... 243

**Chapter 6 Conclusions** ..... 251
6.1 General aims ..... 252
6.2 Summary of study findings ..... 253
6.3 Limitations ..... 254
6.4 Future perspectives ..... 260
6.5 Final remarks ..... 261

**Appendices**
Appendices to Study I to V ..... 263
Publications in journal format ..... 286
Other authors' declarations ..... 313
Permissions for reproduction of material ..... 314

**References** ..... 316

## Declaration

The work presented in this thesis, for submission of Doctor of Philosophy was undertaken within the Department of Child Health, Obstetrics and Gynaecology, University of Nottingham between June 2013 and August 2019. I hereby declared that this thesis and the attached publications represent my own work. I am responsible for all aspects of the experimental work with the exception of the participant recruitment, anthropometry and acquisition of thermograms in Study II, which were undertaken by Taoli Zhang (School of Psychology, University of Nottingham). No part of this thesis has been submitted in any previous application for a higher degree.

**Lindsay Robinson**

**November 2019**

.

# Abbreviations and Acronyms

| | |
|---|---|
| ACTH | adrenocorticotrophic hormone |
| ANCOVA | Analysis of covariance analysis |
| ANOVA | Analysis of variance analysis |
| ATP | Adenosine triphosphate |
| BAR | Beta adrenoreceptors |
| BAT | Brown adipose tissue |
| BIA | Bioelectrical impedance analysis |
| BMI | Body mass index |
| BRITE | Brown in white |
| BSA | Body surface area |
| BW | Body weight |
| CI | Confidence interval |
| $CO_2$ | Carbon dioxide |
| COG | Child Health Obstetrics and Gynaecology |
| CT | Computed tomography |
| DIT | Dietary induced thermogenesis |
| EE | Energy expenditure |
| ELISA | Enzyme linked immunosorbent assay |
| EMG | Electromyography |
| ETC | Electron transport chain |
| $FADH_2$ | Reduced flavin adenine dinucleotide |
| FDG | Fluorodeoxyglucose |
| FF | Fat fraction |
| FLIR | Forward looking infrared |
| FOV | Field of view |
| FPA | Focal plane array |
| FSH | Follicle-stimulating hormone |
| HPA | Hypothalamic-pituitary-axis |
| ICC | Intraclass correlation coefficient |
| IOTF | International obesity task force |
| IR | Infrared |
| IRT | Infrared thermography |

| | |
|---|---|
| LBW | Lean body weight |
| MA | Mental arithmetic |
| MCSDS | Marlowe crowne social desirability scale |
| MRI | Magnetic resonance imaging |
| NA | Noradrenaline |
| NADH | Reduced nicotinamide adenine diphosphate |
| NST | Non shivering thermogenesis |
| $O_2$ | Oxygen |
| $O_2$ | Oxygen |
| PET | Positron-emission tomography |
| PET-CT | Positron-emission tomography computed-tomography |
| RCPCH | Royal College of Paediatrics and Child Health |
| ROI | Region of interest |
| SCAT | Subcutaneous adipose tissue |
| SD | Standard deviation |
| SEM | Standard error of the mean |
| SUV | Standard uptake values |
| SUVmax | Maximum standard uptake value |
| SUVmean | Mean standard uptake value |
| SUVpeak | Peak standard uptake value |
| TMB | tetramethylbenzidine |
| $T_{MSK}$ | Mean skin temperature |
| $T_{SCR}$ | Supraclavicular skin temperature |
| UCP1 | Uncoupling protein one |
| $VO_2$ | Oxygen consumption |
| WHO | World Health Organisation |
| $\Delta T_{SCR}$ | Change in supraclavicular skin temperature |
| $^{11}$C-HED | $^{11}$C-meta-hydroxyephedrine |
| $^{18}$F-THA | $^{14}$(*R,S*)-[$^{18}$F]fluoro-6-thia-heptadecanoic acid |

# List of Figures

Figure 1.1. The microscopic appearance of brown and white adipose tissue ..... 9

Figure 1.2. Diagrammatic representation of mitochondrial oxidative phosphorylation ..... 10

Figure 1.3 Diagrammatic representation of the proton leak generated by uncoupling protein (UCP)1 on the inner mitochondrial membrane ..... 12

Figure 1.4 Four frequently discussed models of UCP1 operation ..... 13

Figure 1.5 Bertholet's proposed model of UCP1 operation based on electrophysiological patch-clamp data ..... 13

Figure 1.6. The components of energy balance in humans ..... 15

Figure 1.7A – C. Anatomy of Bonnot's interscapular gland at dissection ..... 20

Figure 1.8 Structure of the radiolabelled glucose analogue 18F-Flurodeoxyglucose (FDG) ..... 27

Figure 1.9. A) High 18F-Flurodeoxyglucose uptake in the neck and upper thorax of a representative subject on positron emission tomography ..... 29

Figure 1.10 A-G Examples of thermal images presented in publicationsusing infrared thermographic assessment of supraclavicular skintemperature for assesment of brown adipose tissue activity ..... 42

Figure 1.11 Correlation between BAT activity and age ..... 59

Figure 2.1 The left posterior triangle of the neck ..... 95

Figure 2.2 Thermogram visualised in a high-resolution rainbow palette in FLIR ThermaCAM pro 2.1 and the output of the temperature data displayed in Excel ..... 102

Figure 2.3 Example of the left supraclavicular region of interest isolated manually using FLIR software ..... 104

Figure 2.4 Bland-Altman plot using A) the size B) sum temperature and C) average temperature of the polygonal supraclavicular region of interest (ROI) isolated using manual placement with FLIR ThermaCAM Pro 2.1. ..... 105

Figure 2.5 Figure 2.5 Procedure for thermal image analysis of supraclavicular brown adipose tissue in MATLAB ..... 110

Figure 3.1 Anterior thermal images of the neck and upper thorax in A, B a 7 year of normal BMI ($25^{th}$percentile) and C, D a 7 year old of high BMI ($98^{th}$ percentile). ..... 137

Figure 3.2 Relationship between $T_{SCR}$ measured by infrared thermography in response to immersion of a hand into cool tap water at 20.1˚C and BMI percentile in healthy volunteer children aged 6 – 11 years ..... 138

Figure 3.3 Change in supraclavicular skin temperature following 5 minutes single hand immersion in cool water ..... 155

Figure 4.1 Summary of the study protocol, demonstrating the timing of thermal imaging and salivary cortisol assessment relative to mental arithmetic (MA) testing or exposure to the audiovisual relaxation film (R), which were conducted at the same time on different days ..... 186

Figure 4.2 Salivary cortisol concentrations (in micrograms per decilitre) at baseline (B) and after mental arithmetic testing (MA) or exposure to audiovisual relaxation film, in lean, Caucasian female subjects (n = 5) ..... 189

Figure 4.3 Supraclavicular temperature ($T_{SCR}$) A) and temperature region and mean skin temperature ($T_{Diff} = T_{SCR} – T_{MSK}$;B) 20 and 10 min prior to mental arithmetic testing (filled bars) and the audiovisual relaxation film (open bars) in lean, Caucasian white female subjects (n = 5) ..... 191

Figure 4.4 Mean changes in supraclavicular and reference point skin temperature .. 192

Figure 4.5 Relationship between minimal baseline supraclavicular temperature ($T_{SCR}$) and maximal change in supraclavicular temperature ($\Delta T_{SCRmax}$) throughout the duration of the study periods (Pearson's correlation coefficient r = −0.72, P = 0.017) in lean, Caucasian female subjects (n = 5) ..... 193

Figure 4.6 Relationship between supraclavicular temperature ($T_{SCR}$) and salivary cortisol during the baseline period prior to mental arithmetic testing ..... 194

Figure 5.1 Summary of the study protocol, demonstrating the timing of hand cooling and the assessment of energy expenditure (EE), supraclavicular skin temperature ($T_{SCR}$) and mean skin temperature ($T_{MSK}$) during baseline and cold stimulation ..... 210

Figure 5.2 Effect of single-hand immersion in cool water on supraclavicular temperature at 18˚C and 23˚C ambient room temperature ..... 214

Figure 5.3 Change in resting energy expenditure after 30 minutes hand cooling at 18˚C and 23˚C ..... 215

Figure 5.4 Skin temperature of the anterior thigh and supraclavicular region prior to and following 30 minutes' hand cooling at 23˚C ..... 216

Figure 5.5 Time course of changes in mean skin temperature after 30 minutes hand cooling at an ambient room temperature of 18˚C and 23˚C ..... 217

Figure 5.6 MRI of the upper thorax demonstrating measurements of subcutaneous adipose tissue thickness ..... 229

Figure 5.7 Supraclavicular BAT response to forearm cooling in adults ..... 232

Figure 5.8 Mean overall skin temperature response to forearm cooling in adults ..... 234

Figure 5.9 Relationship between supraclavicular skin temperature and body mass index (BMI), body surface area (BSA) and subcutaneous adipose tissue thickness (SCAT) .. 235

Figure 5.10 Diagrammatic representation of supraclavicular temperature for individuals with A) active BAT with low basal activity, B) active BAT with high basal activity and C) dysfunctional BAT with low basal activity and low response to stimulation ..... 237

Figure 6.1 Anterior and lateral thermograms of a male subject taken using a FLIR T540 thermal camera (resolution 464 x 348 pixels) ..... 258

**Appendix**

Figure A3.1A Diagrammatic representation of the 25$^{th}$ upper percentile of temperature values in the thermal ROI..... 264

Figure A3.1B Representative thermograms of the 55 children who underwent thermography in Study I ..... 265

Figures A3.2A – F Scatter plot and line of best fit ± 95% confidence intervals for A) age, B) ambient room temperature, C) height, D) weight and E) BMI percentile against left $T_{SCR}$ and, F) left baseline $T_{SCR}$ against response to hand cooling ($\Delta T_{SCR}$) ..... 266

Figures A3.3A – E. Scatter plot and line of best fit ± 95% confidence intervals for A) age, B) ambient room temperature, C) height, D) weight and E) BMI percentile against left-sided change in $T_{SCR}$ ($\Delta T_{SCR}$) ..... 267

Figures A3.4A – F Scatter plot and line of best fit ± 95% confidence intervals for A) age, B) ambient room temperature, C) height, D) weight and E) BMI percentile against right $T_{SCR}$ and, F) right baseline $T_{SCR}$ against response to hand cooling ($\Delta T_{SCR}$) ..... 268

Figures A3.5A – E Scatter plot and line of best fit ± 95% confidence intervals for A) age, B) ambient room temperature, C) height, D) weight and E) BMI percentile against left-sided change in $T_{SCR}$ ($\Delta T_{SCR}$) ..... 269

Figure A3.6 Left and right sided baseline supraclavicular temperature (A and B) and response to hand cooling in males and females (C and D)..... 70

Figure A3.7 Adjusted means for the left and right supraclavicular skin response to 5 minutes hand cooling (adjusted for BMI percentile) in the girls and boys from Study I aged 102 months and over ..... 271

Figure A3.8 Agreement between baseline TSCR87.5$^{F}$ and TSCR$^{M}$ in Study I ..... 273

Figure A5.1 A – B Supraclavicular skin temperature measured at 1 minute interval using infrared thermography prior to and during hand cooling at an ambient room temperature of A) 23˚C and B) 18˚C ..... 281

Figure A5.2A – H Mean average skin temperature during the last 5 minutes of baseline (B) and hand cooling (C), measured using iButtons sited on the left side of the A) forehead, C) pectoral muscle, D) anterior mid-thigh E) mid forearm F) dorsum of the hand, G) mid-tibial plateau, H) dorsum of the foot and skin temperature from the right sided supraclavicular region measured using infrared thermography..... 282

Figure A5.3 A) Blood pressure and B) heart rate during baseline and active forearm cooling..... 284

Figure A5.4 Right sided tympanic membrane temperature during baseline and active forearm cooling with the Blanketrol II X device ..... 285

**List of Tables**

Table 1.1 Summary of human studies using supraclavicular skin temperature as a surrogate marker of supraclavicular BAT activity published since 2011 ..... 43

Table 1.2 Positron-emission-tomography and computed-tomography assessment of BAT in children. Author, year of publication, location and dates of scans, and underlying diagnoses of research subjects ..... 54

Table 2.1 Technical summary of the FLIR cameras used in the Department of Child Health, Obstetrics and Gynaecology, the University of Nottingham for the assessment of supraclavicular skin temperature as a proxy measure of brown adipose tissue activity between 2011 and 2019 ..... 98

Table 2.2 Calibration formulae used for the set of iButtons used in Studies I – V ..... 112

Table 3.1 Demographic and anthropometric variables in healthy children aged 6 – 11 years (n = 55)..... 135

Table 3.2 $T_{SCR}$ at baseline and in response to a cool stimulus (placing a hand in cool water at 20.1˚C for 5 minutes) in healthy children aged 6 – 11 years (n = 55) ..... 135

Table 3.3 Multiple regression analyses for left and right $T_{SCR}$ as dependent variables and age, BMI percentile, ethnicity, sex and ambient temperature as independent variables (n = 55) ..... 136

Table 3.4 Multiple regression analyses for left and right $\Delta T_{SCR}$ as dependent variables age, BMI percentile, ethnicity, sex and ambient temperature as independent variables (n = 55) ..... 139

Table 3.5 Demographic and anthropometric variables in healthy girls and boys aged 8 – 11 years (n = 36)..... 149

Table 3.6 Unadjusted means (SEM) for left and right supraclavicular skin temperatures ($T_{SCR}$) and means (SEM) adjusted for BMI percentile in healthy girls and boys before and after 5 minutes of cold exposure (n = 36)..... 157

Table 3.7 Relationship between supraclavicular skin temperature ($T_{SCR}$) measured by infrared thermography and food consumption score in healthy volunteer boys and girls aged 8 – 11 years before and after 5 minutes cold exposure (n = 36)..... 159

Table 3.8 Means (SEM) for left and right supraclavicular skin temperature ($T_{SCR}$), unadjusted and adjusted for BMI percentile, in sedentary and active healthy children at baseline, and following 5 minutes cold-exposure (n = 36).....160

Table 3.9 Means (SEM) for the left and right supraclavicular skin temperature, unadjusted and adjusted for BMI percentile, in children classified as picky or non-picky eaters at baseline and following 5 minutes cold-exposure (n = 36).....162

Table 4.1 Summary of the anthropometric measures of the study participants and room temperature on each study day.....188

Table 5.1 Participant demographics, anthropometry and room conditions.....231

**Appendix**

Table A3.1 Correlation (Pearson's r) between supraclavicular skin temperature ($T_{SCR}$) values calculated in Study I using different methods of isolation of the supraclavicular region .....272

Table A3.2 Multiple regression analyses for left and right $T_{SCR95}$ as dependent variables and age, BMI percentile, ethnicity, sex and ambient temperature as independent variables for Study I (n = 55) .....274

Table A3.3 Multiple regression analyses for left and right $\Delta T_{SCR95}$ as dependent variables age, BMI percentile, ethnicity, sex and ambient temperature as independent variables for Study I (n = 55).....275

Table 3.1 Foods included for calculation of food consumption sum scores, reliability assessment of parental responses (Cronbach's alpha), and mean food consumption sum score in each food group .....277

Table 3.2 Relationship between Marlow-Crowne Social Desirability Score (MC-SDS) and responses to parental questionnaires regarding dietary intake, fussy eating behaviour, food consumption score and duration of TV watching .....278

Table 3.3A and B Relationship between supraclavicular skin temperature ($T_{SCR}$) measured by infrared thermography and BMI percentile in healthy volunteer boys (A) and girls (B) aged 8 – 11 years (n = 36).....279

# CHAPTER ONE

## Introduction

### 1.1 Principal Aims

The principal aims of this thesis were to i) investigate the feasibility of using infrared thermography (IRT) for the assessment of supraclavicular brown adipose tissue (BAT) activity in childhood and, using this methodology, to ii) identify the key determinants of BAT thermogenic function during early life.

---

Brown adipose tissue is the main site of non-shivering thermogenesis (NST) in the new-born and is essential for the adaptation to the extrauterine environment after birth (Dawkins and Scopes, 1965). New-born infants do not initially have the capacity to shiver and postnatal thermoregulation is, therefore, dependent on the heat produced from BAT (Schubring, 1986). As the thermoregulatory system matures, and muscle mass increases, shivering takes over as the primary mechanism maintaining core temperature (Dawkins and Scopes, 1965, Hull, 1976).

For many years, conventional teaching was that BAT mass peaks at birth, decreases over the first few weeks of life and becomes largely absent by adulthood. Even during the course of my medical studies (2000 – 2006), I was taught that there was no role for BAT in adulthood. In 2009, the New England Journal of Medicine published three independent research papers, each of which, reported the presence of cold-responsive, metabolically active, adipose tissue in the neck and upper thorax of adult humans consistent with functional BAT (Virtanen et al., 2009, Cypess et al., 2009, van Marken Lichtenbelt et al., 2009). Using a radiolabelled glucose analogue, high

metabolic activity was identified in regions with the radiodensity of fat on computed tomography (CT). Subsequent biopsy of these regions demonstrated the presence of uncoupling protein (UCP)1 (Zingaretti et al., 2009, Virtanen et al., 2009, Cypess et al., 2009), a protein typically found in depots of BAT in neonates, rodents and hibernating mammals (Cannon and Nedergaard, 2004).

Current research is primarily focussed on how the thermogenic properties of adult BAT can be exploited to improve energy balance and cardiometabolic health in the context of obesity (Harms and Seale, 2013, Porter et al., 2015, Yoneshiro et al., 2013, Broeders et al., 2015a). It is well established that the origins of obesity and the metabolic syndrome lie in early life (Barker, 2007), and that there are few effective strategies for successful long term weight loss in adulthood (Varkevisser et al., 2019, Montesi et al., 2016). Prevention in childhood may be the key to the adult obesity epidemic (Pandita et al., 2016) and optimising BAT development during early life may be an alternative means of maintaining metabolic health in adulthood. However, few studies have examined the normal, developmental physiology of BAT during infancy, childhood or adolescence, knowledge that is a prerequisite to understanding how this tissue maybe manipulated for metabolic gain.

BAT research in children has been restricted by the lack of suitable methods for functional assessment. Quantification of glucose uptake using positron-emission tomography and computed tomography (PET-CT) is commonly used in adults as a marker of metabolic activity in BAT (Chen et al., 2016), but this not considered to be appropriate for dedicated BAT imaging in children due to the associated radiation dose

(estimated at 8mSv, the equivalent of 160 chest radiographs in a 35Kg child (Symonds et al., 2012a)). Identifying an alternative non-radiative, non-invasive method that can be used in children of all ages is critical to elucidating the developmental physiology of BAT in early life.

### 1.2 Childhood obesity

The State of Child Health Report published by the Royal College of Paediatrics and Child Health (RCPCH) in 2017 (Viner, 2017) identifies childhood weight status as an important predictor of health outcomes in later life. Data from the National Childhood Measurement Programme England highlights little improvement in the proportions of children considered overweight or obese over the last decade. Figures from 2015/2016 state that, at the start of primary school, 23% of children are considered to be an unhealthy weight, with almost 1 in 5 classified as overweight or obese. Alarmingly, at the time of transition to secondary school, this proportion rises further to 1 in 3 (Viner, 2017).

Using projections of current obesity trends in England, the RCPCH State of Child Health Report 2018 short report predicts that, by 2030, around 23% of 10 – 11 year old boys will be clinically obese, with figures for obesity rising to almost a third in the most deprived areas of England (Viner et al., 2018).

The obesity epidemic is not limited to developed countries like the UK, the numbers of overweight and obese children are also rising worldwide. The World Health Organisation (WHO) identifies childhood obesity as one of the most serious global

public health challenges of the 21st century (WHO, 2018) with over 38 million children under the age of 5 years in 2017 classified as overweight or obese (UNICEF, 2018). Over the last four decades, the total number of obese school-age children and adolescents has risen from 11 million to an estimated 124 million (Collaboration, 2017). Three hundred and thirty two million children aged 5 – 19 years were defined as either overweight or obese in 2016, with the prevalence increasing in all regions worldwide, particularly in the South-East Asian and Western Pacific WHO regions where prevalence had increased by over 40% (WHO, 2018).

The associations between obesity and ill-health in adulthood are well established (Must et al., 1999, Bray, 2004, Pi‐Sunyer, 2002, Larsson et al., 1981). Obesity is linked with many disorders including cardiovascular disease (Manson et al., 1995), malignancy (Schapira et al., 1994), gall bladder and liver disease (Stampfer et al., 1992, Ratziu et al., 2000) and the metabolic syndrome (Chan et al., 1994). Furthermore, there is also strong evidence to support a link between increased body mass index (BMI) in childhood and Type 2 diabetes (Morrison et al., 2010, Barker et al., 2002, Eriksson et al., 2003, Nguyen et al., 2008, Tirosh et al., 2011), hypertension (Field et al., 2005, Israeli et al., 2007, Li et al., 2007) and cardiovascular disease (Silventoinen et al., 2009, Barker et al., 2002, Falkstedt et al., 2006, Gunnell et al., 1998, Tirosh et al., 2011) in later life.

Although few studies have sought to identify whether the associations between cardiometabolic disease in adulthood and childhood BMI are independent of adult adiposity, it is clear that excess adiposity tracks from early life into adulthood. For

example, children who are obese are over five times more likely to be obese as adults than non-obese children (Simmonds et al., 2016). BMI percentile in childhood is a good predictor for adolescent obesity and has high specificity for predicting overweight and obesity in adult life (Field et al., 2005, Guo et al., 1994). Nonetheless, there is some evidence to suggest that childhood obesity alone is an independent risk factor for coronary heart disease (Tirosh et al., 2011) and atherosclerosis (Must et al., 1992).

While obesity is simply defined by the WHO as abnormal or excessive fat accumulation that presents a risk to health (WHO, 2019), diagnosing obesity in childhood is more complex, and at present there is no consensus definition of childhood obesity. Measuring body fat percentage is ideal but not easy to do in practice, particularly in children. BMI percentile is considered by the RCPCH as a simple and reliable indicator of healthy weight and recommends measurement and monitoring of children in whom excess adiposity is suspected using serial BMI percentile measurements on their BMI sex-specific growth charts (RCPCH, 2013). The fixed BMI thresholds used in adults to define overweight and obesity (e.g. >25 and >30 $kg/m^2$ respectively) are inappropriate in children as body composition naturally changes throughout childhood and adolescence and differs between girls and boys. Therefore, in children, BMI thresholds are age and sex dependent, and often defined in terms of percentile on a growth reference chart (Dinsdale et al., 2011). A range of BMI reference charts are available, each based on different population data. Furthermore, the BMI thresholds used to define overweight and obese can differ from chart to chart and can also vary for the same reference data for clinical diagnosis and population monitoring (RCPCH, 2013).

In England, the British 1990 growth reference (UK90) is recommended for population monitoring and clinical assessment in children over the age of 4 years, and the WHO data is used for younger children. A clinical diagnosis of overweight and obesity is made using cut off of >91$^{st}$ and 98$^{th}$ percentiles respectively, whereas for population monitoring the cut-offs are less lenient at the >85$^{th}$ and 95$^{th}$ percentiles. The UK90 data and these cut-offs are rarely used outside the UK. Internationally, the Centre for Disease Control and Prevention, International Obesity Task Force (IOTF) or WHO charts may be used, these are derived from different reference populations and utilised with different threshold cut-offs for overweight and obesity, although the IOTF thresholds are considered to be the most widely used (Cole and Lobstein, 2012). All epidemiological and research studies that focus on obesity before the age of 19 years should be understood in the context of how excess adiposity may be defined differently in different parts of the world. The origins and details of the commonly used reference data and growth charts are beyond the scope of this thesis but are comprehensively summarised elsewhere (Dinsdale et al., 2011).

The pathogenesis of obesity is poorly understood, and the mechanisms by which the excess fat deposition characteristic of obesity occur in childhood is yet to be elucidated. Considering the first law of thermodynamics, that the total energy of an isolated system is constant, and that energy cannot be created or destroyed, obesity may be explained in simple terms as the result of a chronic state of positive energy imbalance; where energy intake exceeds expenditure and caloric excess is stored as white adipose tissue or fat. However, the regulation of intake and expenditure,

particularly during early life is complex, mediated by both environmental and genetic factors, the detail of which is beyond the scope of this thesis.

At present, there are fundamental gaps in our knowledge regarding the components of energy expenditure in early life. It is now well established that functional BAT persists beyond the neonatal period into adulthood, although the degree to which it contributes to energy expenditure in the physiological state is unknown, estimates from adults studies range from 5 – 20% (Muzik et al., 2013, Carpentier et al., 2018). How this tissue contributes to bio-energetic metabolism in children, or whether it plays a role in the development of energy imbalance associated with obesity, has yet to be defined.

### 1.3 The adipose organ structure and function

The adipose organ consists of both white and brown adipose tissue. However, the adipocytes within each depot type differ significantly in their morphology and function. While white adipose tissue (WAT) stores energy, and releases hormones, cytokines and adipokines (Adamczak and Wiecek, 2013, Ronti et al., 2006), the main function of BAT is to produce heat, facilitating adaptive thermogenesis. There is also increasing evidence that supports an endocrine role for BAT, although the full complement of substances released from this tissue are not yet known (Villarroya et al., 2013, Villarroya and Giralt, 2015).

White adipocytes are large (25 – 200µm) spherical cells, with few mitochondria and one large lipid droplet, reflecting their role in energy storage. In contrast, brown

adipocytes are small (15 – 60µm) polygonal cells, typically arranged in highly vascularised clusters divided into gland-like lobules. Classical brown adipocytes contain multiple lipid droplets, many mitochondria and a centrally located spherical nucleus. Their dense vascularity and abundant mitochondria impart their characteristic brown colouring both micro and macroscopically (see Figure 1.1).

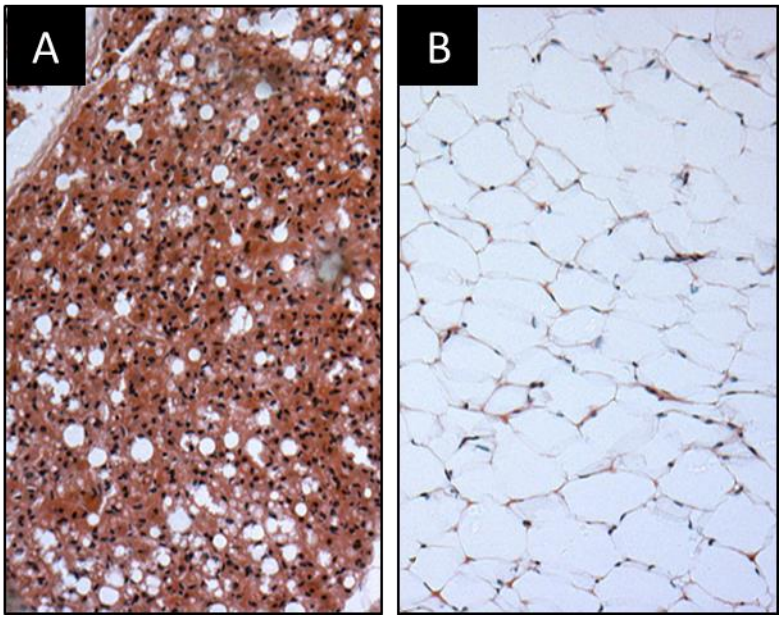



**Figure 1.1. The microscopic appearance (haematoxylin and eosin staining) of A) brown and B) white adipose tissue.** Brown adipose tissue is distinguished from white adipose tissue by the presence of multiple lipid droplets, dense granular cytoplasm containing mitochondria. Samples are from perirenal fat of the A) new-born sheep and B) 30 day old sheep.

BAT mitochondria are double membrane organelles that contain a well-developed system of cristae formed by the inner mitochondrial membrane. These cristae create two distinct compartments, the intermembrane space, and the matrix. In addition to the enzymes of the electron transport chain that are embedded in the inner

mitochondrial membrane, in brown adipocytes this is also the location of UCP1, the protein that mediates heat production during BAT thermogenesis.

### 1.4 Mitochondrial oxidation and UCP1 activation

Mitochondria are considered cellular power houses, producing up to 95% of a cell's energy, they also play a significant role in calcium homeostasis, apoptosis and hormones production (Duchen and Szabadkai, 2010). The structure and activity of mitochondria can vary from cell to cell and, may depend on energy needs.

Cellular energy is produced by mitochondrial oxidative phosphorylation, in brief, a process whereby adenosine triphosphate (ATP) is formed as a result of the transfer of electrons from reduced nicotinamide adenine diphosphate (NADH) or reduced flavin adenine dinucleotide ($FADH_2$) to oxygen ($O_2$) by a series of electron carriers within the electron transport chain. This movement of electrons generates a proton gradient across the inner mitochondrial membrane, and the flow of electrons down this gradient drives ATPase to produce ATP (Figure 1.2).

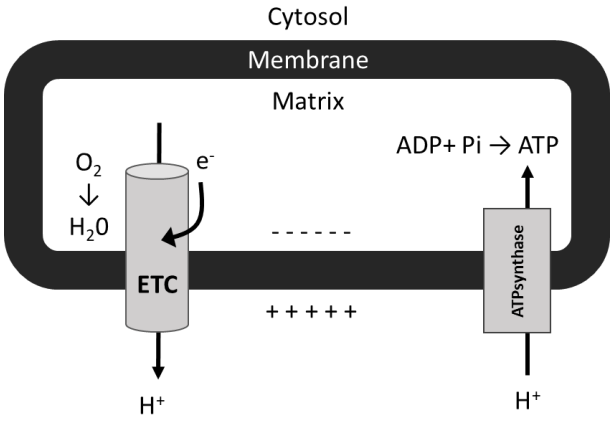



**Figure 1.2. Diagrammatic representation of mitochondrial oxidative phosphorylation.** Electrons are donated to the electron transport chain (ETC) from

nicotinamide adenine diphosphate and reduced Flavin adenine dinucleotide, generating a proton gradient across the mitochondrial membrane which drives ATP synthase to produce cellular energy in the form of ATP. ATP – adenosine triphosphate, Pi – phosphate.

NADH and $FADH_2$ are predominantly produced within the mitochondrial matrix and are primarily derived from the oxidation of acetyl coenzyme A in the tricarboxylic acid cycle. These products may be produced during the degradation of glucose (by glycolysis), β oxidation of fatty acids or from the breakdown of protein/amino acids, depending on glucose levels. When ATP is abundant electrons can no longer enter the electron transport chain, and mitochondrial fuel oxidation ceases.

### 1.5 Uncoupling protein 1 and the principles of thermogenesis

UCP1 is a 32 – 33kDa protein that is located on the inner mitochondrial membrane of thermogenic adipocytes (Ricquier et al., 1979, Lin and Klingenberg, 1980) and functions as a long-chain fatty acid and proton symporter (Bertholet and Kirichok, 2017). Activation of UCP1 allows the passage of protons into the matrix, bypassing ATP synthase and uncoupling cellular respiration from ATP synthesis. Therefore, in cells with UCP1 where fuel oxidation is not limited by high concentrations of ATP, all steps of the tricarboxylic acid cycle and electron transport chain are accelerated in a metabolically futile cycle, and the excess chemical energy is dissipated as heat (Figure 1.3).

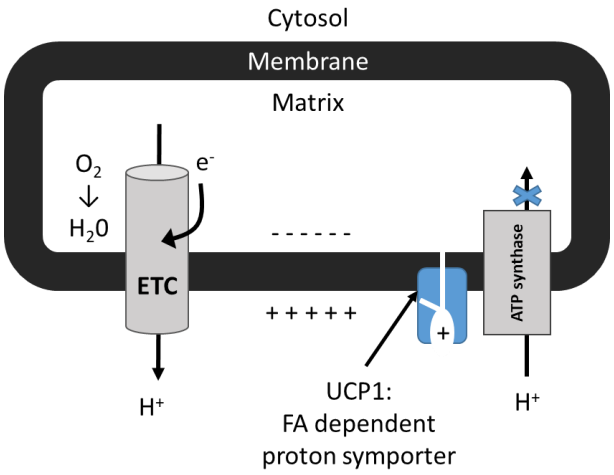



**Figure 1.3 Diagrammatic representation of the proton leak generated by uncoupling protein (UCP)1 on the inner mitochondrial membrane.** Fatty acids activate UCP1 which functions as a proton symporter, dissipating the electrochemical gradient generated by the electron transport chain (ETC), at the expense of ATP generation by ATP synthase. Excess chemical energy is dissipated as heat.

There are two main regulators of UCP1, long-chain fatty acids and purine nucleotides (e.g. ATP, guanosine diphosphate [GDP]) which activate and inhibit UCP1 respectively (Nicholls and Rial, 1999, Nicholls and Locke, 1984). The $H^+$ channel opens in response to neural stimulation of BAT, releasing noradrenaline (NA) at the sympathetic nerve terminals. NA activates lipoprotein lipase and fatty acid levels rise, activating UCP1 and providing substrate to fuel thermogenesis. The exact molecular mechanisms by which UCP1 facilitates proton transport across the inner mitochondrial membrane continue to be debated and some of the commonly dicussed models are summarised in Figure 1.4.

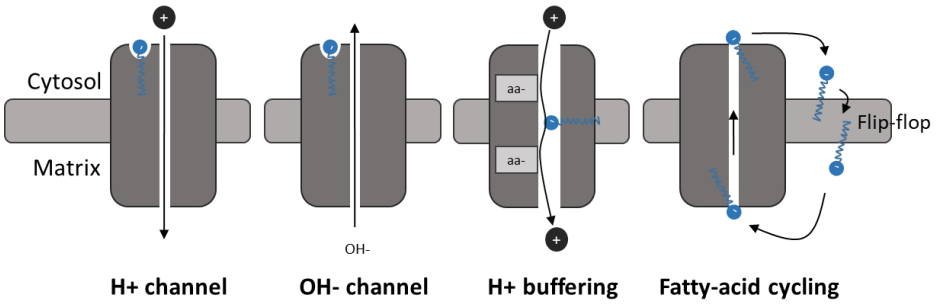



**Figure 1.4 Four frequently discussed models of UCP1 operation, adapted and redrawn from (Bertholet and Kirichok, 2017)**. $H^+$ channel activated by allosteric binding of fatty-acids (blue symbol), OH- channel activated by allosteric binding of fatty acids, "$H^+$ buffering" model, and "Fatty-acid cycling" model.

The recent application of the patch-clamp technique has allowed the high-resolution study of UCP1 within the native inner mitochondrial membrane in response to various ligands (Fedorenko et al., 2012). In light of these studies, a refined model has been proposed that suggests that UCP1 functions as a long chain fatty-acid anion/H+ symporter (Figure 1.5).

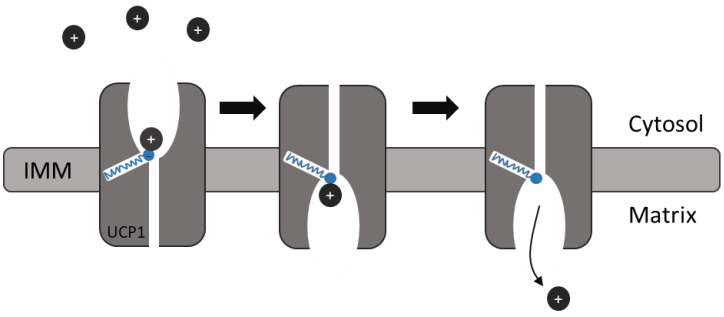



**Figure 1.5 Bertholet's proposed model of UCP1 operation based on electrophysiological patch-clamp data**. Adapted and redrawn from (Bertholet and Kirichok, 2017).

This model proposes that while bound to UCP1 at the cytosolic face of the inner mitochondrial membrane, long-chain fatty acid anions also binds an $H^+$ ion. Upon a conformational change in UCP1 the H+ ion is then translocated from the cytosol into

the matrix (Bertholet and Kirichok, 2017). Strong hydrophobic interactions between the carbon tail of the long-chain fatty acid and UCP1 leave it tightly bound to UCP1 for further cycles of $H^+$ transport. In contrast, when the UCP1 substrate binding site binds short-chain fatty acids these are merely translocated from one side of the membrane to the other, without simultaneous transport of H+ ions (Bertholet and Kirichok, 2018). This model, alongside electrophysiological data highlights that long-chain fatty acids are integral to UCP1 activation and BAT thermogenesis.

### 1.6 Non-shivering thermogenesis and energy balance

Energy expenditure in adult humans can be divided into three main components: adaptive thermogenesis, obligatory energy expenditure and the energy expenditure of physical activity (Garrow, 1987, Tam and Ravussin, 2012). Adaptive thermogenesis may be considered shivering, non-shivering and dietary-induced (DIT); obligatory thermogenesis is the energy required for all cellular and organ functions (also referred to as basal metabolism), and physical activity may be further subdivided as exercise and non-exercise activity thermogenesis (Figure 1.6). An additional, but important, component of energy expenditure in childhood is the energy expended during growth and tissue development (Wiskin et al., 2011, Tam and Ravussin, 2012).

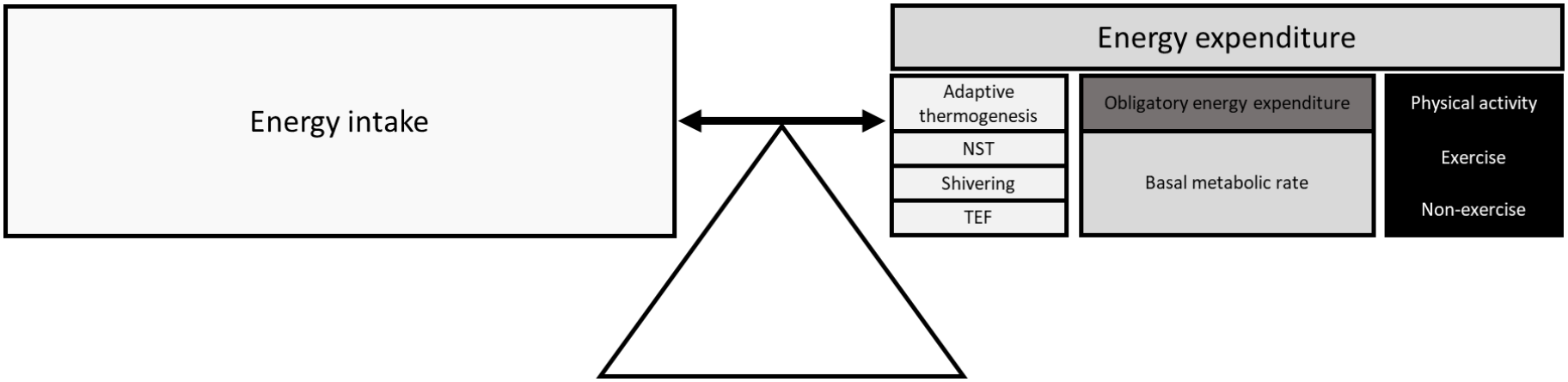



**Figure 1.6. The components of energy balance in humans.** A state of energy balance may be considered when intake is equal to expenditure. In adults energy expenditure may be considered as three components: the expenditure of physical activity, the obligatory expenditure associated with basal cellular function (basal metabolic rate) and adaptive thermogenesis. Adaptive thermogenesis is the energy expended during the regulated production of heat in response to environmental changes in temperature and diet (thermic effect of food (TEF)). The adaptive response to changes in temperature may be regulated by shivering or non-shivering mechanisms (i.e. non-shivering thermogenesis (NST)). Heat produced by brown adipose tissue in response to cold is one mechanism of non-shivering thermogenesis. In children, the energy expended during growth must also be taken into account (although not shown in the diagram above).

BAT is a major site of adaptive thermogenesis in rodents and small mammal hibernators (Smith, 1964, Smith and Hock, 1963), where activation of UCP1 results in heat production in response to environmental temperature change or diet (Cannon and Nedergaard, 2004). In addition, activation of human BAT by cold (Orava et al., 2011, Yoneshiro et al., 2011a, Ouellet et al., 2012), β3-agonists (Loh et al., 2019, Cypess et al., 2015, Baskin et al., 2018) and some dietary stimuli (test meal and individual components (Saito et al., 2016, Yoneshiro et al., 2012, Blondin et al., 2017b) has been associated with an increase in overall energy expenditure.

### 1.7 Clinical implications of dysfunctional BAT

In the late 1970s, it was observed that some genetically obese rodents (e.g. the ob/ob and db/db mouse and the fa/fa rat) demonstrated impaired NST alongside atrophied interscapular BAT (Trayhurn et al., 1977, Himms-Hagen and Desautels, 1978). This relationship between dysfunctional BAT and obesity was further confirmed by Lowell et al. and Feldman et al. who established that mice genetically engineered without UCP1 were not only devoid of BAT but also became obese at thermoneutrality (Lowell et al., 1993, Feldmann et al., 2009). More recent rodent studies also demonstrate that activated BAT has the capacity to clear plasma triglycerides (Bartelt et al., 2011, Schlein et al., 2016) and glucose, although latterly glucose uptake was shown to be independent of UCP1 (Olsen et al., 2014, Olsen et al., 2017).

A similar relationship has been observed in humans, whereby obese individuals have been repeatedly shown to have reduced uptake of the radiolabelled glucose analogue fluorodeoxyglucose (FDG) in BAT on PET-CT (Vijgen et al., 2011, Wang et al., 2015) and

supraclavicular adipose tissue with magnetic resonance properties more consistent with WAT than BAT (Deng et al., 2018, Deng et al., 2015). The recent findings of Entringer and co-workers, that BAT composition at birth is inversely related to body fat accumulation in the first 6 months of life, shows that BAT may also be related to adiposity in early life, prior to the onset of pathological obesity (Entringer et al., 2017).

How BAT may contribute to human energy balance, the metabolic regulation of weight and body composition is uncertain. Even the bio-energetics of obesity are far from fully understood. It is frequently stated that obesity can result from mild prolonged positive energy imbalance, whereby excess calories are stored as fat, providing a plausible explanation whereby BAT dysfunction may lead to obesity. It has also been counter-argued that due to the compensatory increase in expenditure that occurs with increased energy storage, this hypothesis is incorrect (Tam and Ravussin, 2012). With this in mind, an alternative hypotheses must also be considered.

### 1.8 Human supraclavicular BAT in early life

Brown adipose tissue has been extensively studied in perinatal and neonatal periods (Merklin, 1974, Dawkins and Hull, 1965, Hatai, 1902, Bonnot, 1908, Aherne and Hull, 1966, Hull, 1976, Gupta et al., 2011, Hu et al., 2014, Lean et al., 1986, Ponrartana et al., 2016, Rasmussen et al., 2013). Canon and Nedergaard report that six major depots of BAT have been identified in the human infant (Cannon and Nedergaard, 2017), including, perirenal, interscapular, cervical and periaortic and minor depots have also been observed elsewhere, typically around, or in close proximity to large blood vessels (Merklin, 1974).

The most well-studied depot of human BAT in early life is often referred to as interscapular BAT, and it has been suggested that it is analogous to the interscapular depot observed in rodents (Lidell et al., 2013). However, some of the earliest anatomical descriptions of human BAT contradict this. Hatai described BAT in human embryos as a gland located under the sternocleidomastoid and trapezius muscles, which runs laterally and in parallel with the neck (Hatai, 1902). In addition, following the study of 20 adults and 12 fetuses Bonnot also eloquently described the anatomy of what can now be presumed to be BAT as follows (Bonnot, 1908):

"the gland is a paired organ, very irregular in shape, but definite in outline, situated on the shoulder and the side of the neck, between the superior border of the scapular and clavicle, with a large process extending upward to the mastoid process of the temporal bone. The gland may be divided for convenience, into five parts, the body, and the mastoid clavicular, glenoid and scapular processes……

…. The thickest part, or body of the gland is about 1.5 inches posterior to the junction of the outer and middle third of the clavicle, in the region uncovered by the trapezius and sternocleidomastoid muscle. The deep fascia forms the external covering, and the prevertebral fascia the internal. Along the border of the gland is found the chain of deep lymphatic glands, the lower division of the cervical plexus passes through this part of the gland. The omohyoid muscle, after passing over and beyond the internal jugular vein for 2cm, enters and passes diagonally through the body of the gland…..

….. the largest process, the mastoid extends up to and under the insertion of the sternocleidomastoid muscle, along and under the insertion of the posterior belly of the digastric muscle, filling a space between the splenius muscle and sheath of the large blood vessels, and extending some distance both over and under this sheath towards the trachea. This process is partially covered by the sternocleidomastoid muscle, the remainder by the deep fascia. From the dorsal side of the process a secondary process projects into the posterior triangle of the neck. This secondary process is continuous with a ridge extending downward and forward along the posterior border of the sternocleido muscle……

….the clavicular process is very irregular in shape, forming a right angle with the clavicle at a point where the internal jugular vein passes under the clavicle.

…….the glenoid process fills the acute angle formed between the clavicle and the scapula, and extends some distance under the acromion process. This process is entirely covered by the trapezius muscle….

….. the scapula process joins the gland at a point near the superior-posterior angle of the scapula and extends horizontally towards the centre of the interscapular region, where it forms a somewhat T-shaped mass over and between the rhomboidii muscles….. " (Bonnot 1908).

In addition to these detailed descriptions, his anatomical drawings are some of the most comprehensive available to date. These clearly demonstrate that the anatomy of neonatal BAT is not exclusively interscapular as is often stated but is found extensively throughout the neck and upper thorax in a pattern similar to that observed in adults more recently using FDG-PET-CT (Figure 1.7). Bonnot himself referred to the inaccuracy of the term "interscapular" in the footnotes of his paper, but, confusingly, this terminology was still used in the manuscript title and was adopted in many subsequent publications.




**A** **B** **C**

**Figure 1.7A – C. Anatomy of Bonnot's interscapular gland at dissection in relation to regional musculature, lymphatics and vasculature in an A) 4 months old fetus, B) newborn infant and C) adult. Reproduced from Bonnot (1908), no longer under copyright.**
*a* – large compound lymph and haemolymph; *ax* – axillary glands; *ap* – axillary process; *b* – ;*cp* – clavicle process; *gp* – glenoid process; *mp* – mastoid process; *sm* – submaxillary gland) and C) adult (*a* – large compound lymph and haemolymph gland; *b* – parotid gland; *c* – submaxillary gland; *cp* – cervical process*; gp* – glenoid process; *g* – interscapular gland; *J* – internal jugular vein; *mp* – mastoid process; *n* – gland nodes; *sp* – scapular process) (Bonnot, 1908).

One of the most extensive studies of human neonatal BAT was undertaken by Aherne in the mid '60s, in over 400 infants (from 29 weeks gestation up to 4 weeks postnatal age) also he reported small masses of multilocular, granular tissue consistent with BAT around the vasculature and muscles of the neck, with the largest following the course of the internal jugular vein (Aherne and Hull, 1966). A similar pattern was also observed during a series of exploratory dissections by Merklin. Merklin described neonatal BAT as a "high collared vest" with the largest depots found within the posterior cervical triangle, coursing along large vessels such as the internal jugular vein further supportive evidence for the existence of neonatal supraclavicular BAT (Merklin, 1974).

Although before 2009 it was frequently taught that neonatal BAT does not persist into childhood (terminology notwithstanding), review of the literature published between Hatai's original description of BAT in the supraclavicular region of infants and adults in 1902, and the seminal papers of 2009, identifies some key publications that suggest that this was not accurate. As UCP1 was not discovered until the late 1970's (Heaton et al., 1978, Ricquier and Kader, 1976) many of these historic studies rely on the characteristic microscopic and macroscopic appearance of the tissue for identification. In 1909 Shattock confirmed the anatomical location, macroscopic findings and histology of Bonnot's interscapular gland, reporting highly vascular, multilocular fatty deposits within the posterior triangle of the neck, located between the sternocleidomastoid and trapezius in children and adults with congenital hypothyroidism (Shattock, 1909).

Heaton also reported the wide distribution of multilocular adipose tissue in the neck and upper thorax consistent with BAT. She also confirmed the presence of BAT around the vessels and musculature of the neck and clavicles in all the young children she examined (aged 0 – 10 years). Furthermore, she also reported that this adipose tissue depot persists into mid-adulthood, and was visible in many specimens until the fourth decade of life (Heaton, 1972).

Indirect evidence of BAT persisting beyond the immediate neonatal period is also seen from the numerous case studies describing supraclavicular BAT necrosis in infants with congenital cyanotic heart disease. In these infants, extensive calcification has been frequently visualised within the neck and axillae on chest radiograph in the anatomical location of BAT described above (Raboi and Smith, 1999, Higgins et al., 1993, Golden et al., 2018).

**1.9 Classification of human BAT**

Whether the UCP1 containing adipocytes obtained from human supraclavicular adipose tissue depots are classical brown adipocytes analogous to rodent interscapular BAT continues to be debated (Lidell et al., 2013, Cannon and Nedergaard, 2012, Nedergaard and Cannon, 2013, Jespersen et al., 2013). Evidence is emerging that the separation of adipose tissue into brown and white is too simplistic, and that a third population of adipocytes exist in humans and other mammals. These adipocytes are often termed brown in white (BRITE), beige or inducible brown adipocytes. Evidence suggests that these so-called beige adipocytes have distinct molecular signatures when compared to classical rodent interscapular BAT (Wu et al.,

2012, Guller et al., 2015) and may be derived from different cellular precursors (Seale et al., 2008, Timmons et al., 2007) via separate developmental pathways (Xue et al., 2007, Sanchez-Gurmaches and Guertin, 2014). With the right stimuli, beige adipocytes are inducible and are able to take on a thermogenic phenotype analogous to that of the brown adipocyte, upregulating UCP1 and energy expenditure (Bartelt and Heeren, 2014, Wu et al., 2012, Petrovic et al., 2010). Whether induced beige adipocytes arise de novo from distinct progenitor cells or convert from mature white adipocytes is unclear as evidence for both exists (Kiefer, 2016, Barbatelli et al., 2010, Wang et al., 2013, Rosenwald et al., 2013, Lee et al., 2012, Walden et al., 2012) and may, in fact, be both species and depot specific.

Some research groups claim that adult human supraclavicular BAT is composed of exclusively beige adipocytes (Wu et al., 2012, Sharp et al., 2012, Lee et al., 2014c) whereas others present evidence that this depot is a heterogeneous mix of white, beige and classical brown (Cypess et al., 2013). Lidell et al. examined the adipose tissue obtained from four human infants post mortem and concluded that samples from the interscapular region appeared classically brown, whereas those from the supraclavicular region appeared beige (Lidell et al., 2013). Composition may, therefore, vary by depot, location, or stage of development. Understanding the true composition of the human adipose organ and how this changes throughout the life cycle is essential to the future development of BAT research, particularly with respect to the relevance of rodent interscapular BAT to human BAT physiology.

Nonetheless, for clarity in this thesis, and in keeping with the terminology used in current literature, metabolically active, UCP1 containing adipose tissue found in the neck and upper thorax of humans will be referred to throughout as BAT.

### 1.10 Sympathetic control of BAT

Animal studies show that BAT is extensively innervated by the sympathetic nervous system with little opposing parasympathetic innervation (Himms-Hagen et al., 1990, Bartness et al., 2010), postganglionic neurones release NA, which acts on β-adrenoreceptors (βAR) on the brown adipocyte cell surface initiating an intracellular cascade that results in the activation of UCP1. The precise role of the sympathetic nervous system and UCP1 activation in human BAT is less clear. However, both sympathetic innervation (Zingaretti et al., 2009) and expression of βAR's (Virtanen et al., 2009, Deng et al., 1996, Cypess et al., 2013, Baskin et al., 2018) have also been demonstrated in adult and neonatal human BAT, and indirect evidence from human in vivo studies also indicates that BAT is under sympathetic control.

Even prior to the FDG-PET-CT studies published in 2009, bilateral symmetrical uptake of a radiolabelled NA analogue $^{123}$I-meta-iodobenzylguanidine was observed in the upper thorax in a pattern consistent with that of FDG uptake in BAT on PET (Okuyama et al., 2003, Okuyama et al., 2002, Admiraal et al., 2013). Furthermore, Fukuchi et al. reported a paediatric case where this pattern of $^{123}$I-meta-iodobenzylguanidine uptake became asymmetrical following surgical unilateral sympathetic denervation (Fukuchi et al., 2004), a pattern which was also observed on FDG-PET-CT in two adult patients with Horner's syndrome (Lebron et al., 2010).

FDG uptake in BAT is significantly reduced following administration of the β-antagonist propranolol (Soderlund et al., 2007, Jacobsson et al., 2005), and βAR blockade can even reduce FDG uptake in the hypermetabolic BAT of patients with phaeochromocytoma (Cheng et al., 2012). These patients typically show high levels of BAT activity due to excess circulating catecholamines (Kuji et al., 2008) and also appear to demonstrate significant FDG uptake indicative of browning within atypical adipose tissue depots (Cheng et al., 2012). Interestingly, when these tumours are surgically excised FDG uptake in BAT is reduced or no longer observed (Yamaga et al., 2008, Kuji et al., 2008).

Exogenous stimulation of the β-adrenergic part of the sympathetic nervous system using sympathomimetics in humans has been met with varying success. The non-selective β-adrenoreceptor agonist isoprenaline fails to elicit an increase in FDG uptake on PET-CT (Vosselman et al., 2012), yet has been shown to produce an increase in BAT temperature during acute infusion (Scotney et al., 2017) and rise in energy expenditure (Vosselman et al., 2012).

Stimulation of BAT has also been attempted with the mixed sympathomimetic amine ephedrine, as it enhances the activity of NA at the post-synaptic membrane, it is expected to increase BAT activity. Research to date yields variable results, including no effect at all (Cypess et al., 2012, Astrup et al., 1984), increased BAT activity in lean subjects only (Carey et al., 2013); and reduced BAT activity following chronic administration (Carey et al., 2015).

Isoprenaline and ephedrine are non-selective β agonists, recent use of mirabegron, a selective $\beta_3$-adrenoreceptor agonist results in FDG uptake in BAT on PET-CT (Cypess et al., 2015), and an increase in resting metabolic rate (Cypess et al., 2015, Loh et al., 2019) indicative of BAT activation.

Using tissue uptake of the NA analogue $^{11}$C-meta-hydroxyephedrine as an indirect measure of the density of sympathetic innervation Muzik et al. (2019) more recently reported sympathetic activity within human supraclavicular BAT which correlated with BAT mass even under thermoneutral conditions. Further evidence that like rodent BAT, human BAT is widely innervated by the sympathetic nervous system.

**1.11 In vivo assessment of human BAT morphology and function**

Several methods have been used to try and quantify BAT activity and describe BAT distribution and morphology. At present, radiolabelled glucose uptake visualised with PET-CT is considered the "gold standard", a term that is slightly misleading but frequently repeated throughout the BAT literature. While it may be regarded as the best of currently available methods; this should not be interpreted to mean that it is a good one. The limitations of PET-CT for quantification of BAT activity are commonly overlooked or minimised, and studies using this methodology for the assessment of BAT function should be interpreted with this in mind.

### 1.11.1 Radiolabelled uptake of BAT substrates on PET-CT as surrogate markers of tissue activity

Radiolabelled PET is commonly used in conjunction with CT to identify anatomical regions with high metabolic activity and is predominantly used in clinical medicine for the investigation and follow up of malignant disease. FDG is used in over 90% of clinically indicated scans and, as a glucose analogue (where Fluorine-18 substitutes the hydroxyl group at the second position of glucose, as shown in Figure 1.8) it is avidly taken up by hypermetabolic cells. It is this property that is central to its ability to detect cancer, and brown and beige adipose tissue during PET imaging.

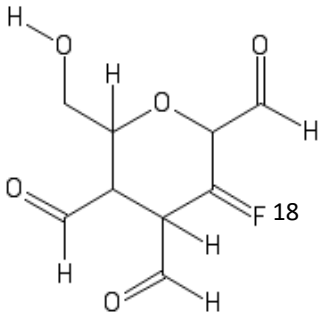



**Figure 1.8 Structure of the radiolabelled glucose analogue 18F-Fluorodeoxyglucose.**

Unlike glucose, FDG cannot be metabolised beyond the first step of glycolysis and becomes trapped within cells as FDG-6-phosphate. In some tissues, in some species dephosphorylation of FDG-6-phosphate may be significant, but, in humans, this is thought to be negligible (Kuwabara and Gjedde, 1991). The positrons emitted from FDG trapped within cells are detected by the PET scanner, and the anatomical location of regions with high signal intensity is determined by fusion with simultaneously acquired CT. Since the introduction of routine PET imaging in clinical medicine, symmetrical regions of FDG uptake in the neck and upper thorax have been observed

(Engel et al., 1996, Barrington and Maisey, 1996). These were initially deemed to be an artefact of muscular in origin and were subsequently dismissed.

With the increasing use of concomitant CT imaging, it became clear that these areas consistently had the radiodensity of adipose tissue, raising the question that they may, be metabolically active BAT (Hany et al., 2002, Cohade et al., 2003, Yeung et al., 2003). Subsequent dedicated PET-CT imaging revealed a similar pattern of uptake in healthy research volunteers, which was even more apparent after stimulating BAT with cold exposure (van Marken Lichtenbelt et al., 2009). Samples of tissue from supraclavicular and cervical regions with high FDG uptake have since been repeatedly identified as multilocular adipocytes containing UCP1 (Virtanen et al., 2009, Lidell et al., 2013, Cypess et al., 2013, Jespersen et al., 2013, van Marken Lichtenbelt et al., 2009, Broeders et al., 2015b), confirming these regions as BAT (Figure 1.9).

SUVs obtained during BAT imaging are frequently calculated using different methods; including the intensity value of the highest voxel within the volume of interest ($SUV_{max}$), as an average of the voxels within the volumes of interest ($SUV_{mean}$) or as an average of a region with a fixed size that contains the hottest voxel ($SUV_{peak}$). These SUVs are then presented as semi-quantitative measures of tissue activity or may be used to estimate BAT volume using threshold or region growing techniques.

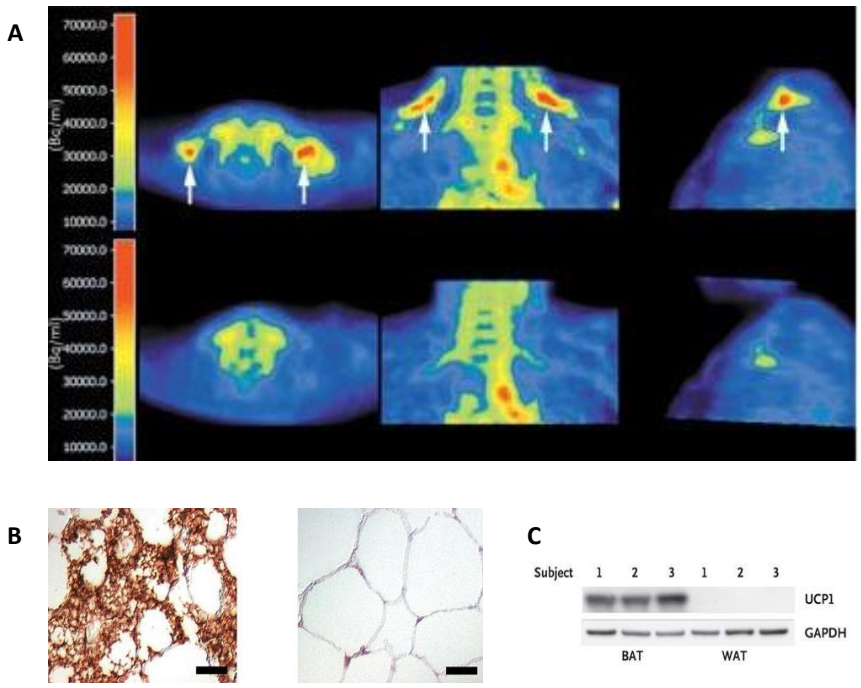



**Figure 1.9. A) High 18F-Flurodeoxyglucose uptake in the neck and upper thorax of a representative subject on positron emission tomography (PET)** indicated by white arrows; top row – cold stimulated PET; bottom row – PET under warm conditions; images are in the axial, coronal and lateral plane respectively, **B) comparative histology of supraclavicular brown adipose tissue sample, and subcutaneous white adipose tissue (WAT) sample and C) confirmation of UCP1 protein in supraclavicular adipose tissue using Western Blot analysis**. Reproduced with permission from Virtanen et al., 2009.

The reproducibility for each of these methods varies, and, current recommendations advise a combination of $SUV_{max}$ and $SUV_{peak}$ as a standard approach for tumour imaging (Wahl et al., 2009, Joo Hyun et al., 2016). The standards for the assessment of BAT with PET-CT were not outlined until 2016 in the BARCIST 1.0 guidelines (Chen et al., 2016) and it must be noted that these guidelines serve merely as recommendations from experts within the field. The evidence base for best practice with regard to PET-CT in BAT imaging is lacking. The BARCIST 1.0 guidelines/recommendations suggest that ideally SUVs should be reported as $SUV_{max}$ and $SUV_{peak}$ for six regions including, the left and right supraclavicular region, neck and

mediastinum and, should be normalised to lean body weight (LBW) (or body weight). Even if these guidelines are followed, there may be significant variation between research groups, limiting comparability between studies.

Parameters of FDG uptake should be considered as a surrogate markers for BAT thermogenesis with uncertain reliability. Whilst FDG uptake in healthy men is directly proportional to the change in energy expenditure during non-shivering thermogenesis (van der Lans et al., 2013, Cypess et al., 2015, Ouellet et al., 2012) there is increasing evidence which suggests that FDG uptake does not accurately represent BAT thermogenic activity and that glucose is not the primary substrate for BAT oxidation (Blondin et al., 2015a, Blondin et al., 2017a, Carpentier et al., 2018).

For example, cold stimulated FDG-PET imaging in the UCP1 knockout mouse (animals with defective capacity for BAT mediated non-shivering thermogenesis) still results in FDG uptake in interscapular BAT that is indistinguishable from that observed in wild type mice (Jeanguillaume et al., 2013). Similarly, $\beta_3$ adrenergic stimulation in these UCP1 knockout mice also produces a pattern of FDG uptake suggestive of active BAT (Hankir et al., 2017, Olsen et al., 2017), despite these animals having no functional UCP1 and demonstrating a blunted metabolic response (reduced oxygen consumption) as compared to animals with intact BAT. Furthermore, rodent in vitro studies also confirm that although glucose is required for thermogenesis, glucose uptake occurs independently of UCP1 mediated thermogenesis (Olsen et al., 2017, Hankir et al., 2017, Winther et al., 2018). Whether a similar dissociation exists during

human brown adipocyte thermogenesis is unknown and should be a priority for future studies.

Rather than peripheral circulating glucose, evidence suggests that BAT mainly combusts fats (Schilperoort et al., 2016) and primarily uses endogenous intracellular fatty acids as fuel (Blondin et al., 2017a) (but, may also take up fatty acids from the circulation if the endogenous supply is deplete). How glucose uptake from the circulation (which is fundamentally all that FDG-PET-CT measures) relates to fatty acid metabolism, thermogenesis or UCP1 activity in human BAT is not known. Evidence that glucose uptake can be used as a direct measure of thermogenesis is weak and FDG uptake may merely reflect a metabolic process that is secondary to thermogenesis (i.e. enhanced glycolysis in response to demand for ATP during UCP1 mediated thermogenesis). Likewise, a more recent study indicates that FDG uptake in human BAT does not correlate with cold-induced thermogenesis (expressed as a proportional change in resting metabolic rate) or with estimations of cold-induced carbohydrate or fat oxidation (Sanchez-Delgado et al., 2018).

Although the repeatability and reproducibility of SUV parameters in tumour assessment have been shown to be good (Rockall et al., 2014, Minn et al., 1995), whether this is also demonstrated in BAT is not clear. Extensive assessment of reproducibility for the assessment of BAT using FDG-PET-CT imaging has not yet been undertaken. Crandall et al. attempted to quantify the repeatability of cold stimulated static FDG-PET, whilst the qualitative assessment of FDG uptake in BAT was consistent (i.e. “BAT positive” and “BAT negative”), the test-retest repeatability of the

quantitative measures $SUV_{max}$ and BAT mass volume was low (Crandall et al., 2019). However, it must be noted that the method of cooling used in this study was crude (2h exposed to room temperature of 18 – 20˚C, with intermittent placement of feet on a block of ice) and resulted in shivering in almost 50% of volunteers, meaning that this study did not examine BAT derived NST in isolation.

It has been suggested that FDG-PET may underestimate (Carpentier et al., 2018, Lee et al., 2010) or overestimate (Leitner et al., 2017) the volumes of active BAT present in humans, and may be particularly unreliable in individuals with aberrant glucose metabolism or insulin sensitivity, particularly when comparing to individuals with normal physiology. This is particularly important in BAT research where the focus is on individuals with obesity or diabetes.

While SUVs are not recommended for absolute quantitation, estimation of the metabolic rate of glucose during dynamic PET-CT has been described as a means of more accurately quantifying glucose uptake, and thus BAT activity, and, may also be used to quantify the response to stimulation. Dynamic PET-CT is, however, less frequently used as it is technically more complex, requires longer scan times, sampling of arterial, or arterialised blood and necessitates more sophisticated image analysis. The use of dynamic FDG-PET for the assessment of BAT is in its infancy, up to 2019 only a handful of studies reported human BAT activity using dynamic FDG-PET-CT (Salem et al., 2016, Law et al., 2018, Hanssen et al., 2015b, Blondin et al., 2015a, Virtanen et al., 2009, Blondin et al., 2014, Hanssen et al., 2015a, Koskensalo et al.,

2017, Orava et al., 2011) and, at present, there is no data regarding the reproducibility of dynamic FDG-PET-CT for the quantitative assessment of BAT.

Aside from the aforementioned limitations of FDG-PET, the use of FDG-PET-CT for research purposes is also limited by its radiation dose. The estimated absorbed radiation dose during PET-CT in humans varies by tissue and age. Absorption is higher in infants and children in all tissues as compared to adults. For example, a newborn infant of 3.4 kg may absorb up to 4.3 rem/mCi within the bladder wall, as compared to 0.32 rem/mCi in a 70 kg adult, and the total absorption in a 9.8 kg 1 year-old almost six times more than that of an adult (FDA, 2005). This degree of radiation exposure is not insignificant and, whilst justified for clinical indications, prohibits its use for scanning healthy children or large groups of individuals for research purposes.

In addition to FDG, a number of other tracers are available for clinical and research PET imaging, and depending on the radiolabelled biologically active compound used a whole host of metabolic pathways can be evaluated. Quantification of mitochondrial fatty acid uptake in BAT has been explored using $^{14}$(*R,S*)-[$^{18}$F]fluoro-6-thia-heptadecanoic acid ($^{18}$F-THA)-PET (UDin et al., 2016, Ouellet et al., 2012, Blondin et al., 2015a), BAT oxidative metabolism using $^{11}$C acetate-PET (Ouellet et al., 2012) and sympathetic innervation of BAT using (*S,S*)-[$^{11}$C]O-methylreboxetine ($^{11}$C-MRB-PET) (Hwang et al., 2015) and 11C-meta-hydroxyephedrin ($^{11}$C-HED) (Muzik et al., 2017). Whilst these may be more reflective of tissue thermogenesis than glucose, these methods remain in their infancy and require further development.

### 1.11.2 Adipose tissue lipid content to discriminate between BAT and WAT

Magnetic resonance imaging (MRI) is increasingly being used in adults (Holstila et al., 2017, Gifford et al., 2016) and children (Deng et al., 2015, Franz et al., 2015, Hu et al., 2012, Hu et al., 2013, Andersson et al., 2019) to delineate BAT morphology, and may also have the capacity to measure metabolic activity using relative fat content (i.e. proton density fat fraction [FF]) without significant exposure to radiation. Some authors even report detectable changes in T2* relaxation times (Gashi et al., 2019, Oreskovich et al., 2019) and fat fraction (Lundstrom et al., 2015, Koskensalo et al., 2017, Oreskovich et al., 2019) in response to cold exposure protocols that have previously been shown to induce BAT activation. These findings are not ubiquitous and other groups report no significant changes in either of these measures after cooling (Holstila et al., 2017).

Using chemical-shift water-fat imaging, the lipid content of tissues can be estimated using a multi-echo Dixon method of water fat separation to calculate FF. Considered simply, the more lipid a tissue contains, the higher the FF on chemical-shift water-fat MRI. Fat fraction of supraclavicular human BAT has been repeatedly shown to be lower than a comparative WAT region in both adults (Holstila et al., 2013, Deng et al., 2018, Gashi et al., 2019, Gifford et al., 2016) and children (Franz et al., 2015, Deng et al., 2015, Hu et al., 2014). Basal non-stimulated FF in supraclavicular BAT depots correlates with FDG uptake on FDG-PET-CT (Holstila et al., 2017), and changes in lipid content with cooling were negatively correlated with both BAT volume and total BAT activity as estimated from FDG-PET-CT (Deng et al., 2018).

T2* relaxation times are another measure derived during chemical-shift water-fat MRI that is frequently being reported alongside FF and used to discriminate between BAT and WAT in humans. T2* is defined as the decay of the MR signal in the transverse plane of an in homogenous magnetic field (Ong et al., 2018), and as brown adipocytes contain a high density of mitochondria, cellular iron content is higher in BAT than WAT, which result in faster relaxation times (lower T2* values). T2* values differ between BAT and WAT in adults and children, and have been shown by at least one group to inversely correlate with glucose uptake on dynamic FDG-PET-CT in a small adult cohort (Holstila et al., 2017).

Whilst most of these studies using both MRI and FDG-PET-CT have been undertaken only in adults these findings suggest that chemical-shift water-fat imaging holds potential as an alternative to PET, particularly for the study of BAT in children.

### 1.11.3 Oxygenation and perfusion as an indicator of BAT activation

T2* relaxation times may also reflect the ratio of deoxyhaemoglobin and oxyhaemoglobin within a tissue, and shorter T2 relaxation times may indicate tissue oxygenation of BAT during activation. Studies have identified shortening of T2* relaxation times in BAT as compared to WAT which, may reflect the differences in vascularity and perfusion rather than BAT activity per se. Similarly, tissue perfusion has been measured with functional MRI using blood-oxygen-level-dependent (BOLD) contrast MRI as an indicator of BAT activity in mice (Khanna and Branca, 2012) although to date this has not been used successfully in humans.

Total haemoglobin concentrations within superficial adipose tissue depots can be assessed by near-infrared time-resolved spectroscopy (NIRS) as another index of blood volume/vasculature. Nirengi et al. showed that baseline measures of total-Hb within the supraclavicular region were correlated with $SUV_{mean}$ from FDG-PET-CT and were significantly higher in individuals with FDG-detected BAT as compared to those without (Nirengi et al., 2015) and also that this measure could detect changes in blood flow after stimulation with capsinoids (Nirengi et al., 2016).

### 1.11.4 Supraclavicular skin temperature as a surrogate marker of BAT activity

In 2013, at the time of registration for this PhD, supraclavicular skin temperature ($T_{SCR}$) was not a well-established surrogate marker of BAT activity. In 2011, Lee et al. described localised areas of maximal skin temperature overlying the supraclavicular fossae during whole-body cooling, consistent with the anatomical location of FDG-detected BAT in a 32 year old volunteer (Lee et al., 2011). Whole-body cooling is associated with a reduction in skin temperature due to the systemic cutaneous vasoconstriction that occurs to reduce heat loss. Whilst this response was observed on the skin overlying the chest in this participant, the decline in supraclavicular skin temperature was significantly attenuated. It was concluded that these findings were suggestive of a local thermogenic response originating from the underlying supraclavicular BAT.

Subsequently, several studies, including those presented in this thesis, have been published that utilise $T_{SCR}$ as a surrogate measure of BAT activity (summarised in Table 1.1). Although some of the more recent studies have validated measures of

supraclavicular temperature against FDG uptake on PET-CT, their findings are by no means consistent.

Most of these studies have assessed the $T_{SCR}$ response to cold stimulation. Some authors report a comparatively attenuated drop in $T_{SCR}$ as indicated by Lee et al (2011) (van der Lans et al., 2016, Yoneshiro et al., 2016, Ramage et al., 2016, Thuzar et al., 2018, Thuzar et al., 2019, Coolbaugh et al., 2018, Lee et al., 2011), others report maintenance of $T_{SCR}$ despite a reduction in skin temperature at other sites (Jang et al., 2014, Yoneshiro et al., 2011a, Chondronikola et al., 2016, Levy et al., 2018, Gashi et al., 2019), and some report an increase in $T_{SCR}$ (Symonds et al., 2012a, Boon et al., 2014, El Hadi et al., 2016, Ang et al., 2017, Haq et al., 2017, Malpique et al., 2018, Lee et al., 2016). The likely reason for this apparent inconsistency lies in the different methodology utilised to achieve cooling. These vary from study to study and comprise a range of approaches from single limb cooling to whole-body cooling using air, ice, water or specialised clothing (see section 1.11.5). Overall, it seems that whole-body cooling is accompanied by a fall in $T_{SCR}$ (but less so than non-BAT regions), but when the supraclavicular region is itself not directly exposed to cold, $T_{SCR}$ is maintained or increases (Table 1.1).

The absolute change in $T_{SCR}$ following cold exposure has been shown to correlate with BAT volume (Chondronikola et al., 2016), $SUV_{mean}$ (Lee et al., 2016, van der Lans et al., 2016) and energy expenditure (van der Lans et al., 2016) and, when expressed as a value relative to a non-BAT control region, correlates to BAT volume (Jang et al., 2014) and MRgluc (Law et al., 2018). Although more recently, Martinez-Tellez explored cold-

induced changes in supraclavicular skin temperature in a large mixed sex group of adults, and identified that although $T_{SCR}$ was positively associated with BAT activity (in the warm and during cold exposure) the change from baseline ($\Delta T_{SCR}$) was not. Furthermore, when considered by sex these associations were only present in women (Martinez-Tellez et al., 2019a). This is in contrast to the other studies mentioned above that exclusively studied men.

Positive associations between cold stimulated absolute $T_{SCR}$, and both $SUV_{max}$ and BAT volume have also been reported elsewhere (Boon et al., 2014, Thuzar et al., 2019), whereas baseline $T_{SCR}$ prior to cold exposure has not been identified as correlating with any measure of FDG uptake on PET-CT previously. Gatidis et al. explored single time point thermography of the supraclavicular region at room temperature and concluded that once adjustments were made for age, sex and BMI that there were no differences in $T_{SCR}$ between those with significant FDG uptake ("BAT +ve") and those without ("BAT –ve") (Gatidis et al., 2016). Moreover, Sarasniemi et al. failed to find any relationship between FF on MRI and basal $T_{SCR}$ although the study methodology reported in this short report with respect to IRT was suboptimal in my opinion (Sarasniemi et al., 2018).

These inconsistencies are not surprising given the variety of techniques used in these studies, both for cooling and for the assessment of $T_{SCR}$ (discussed in detail in section 1.11.5) in addition to variability in the PET-CT criteria used to quantify BAT. This is somewhat highlighted by another publication from Martinez-Tellez (2019a) where $T_{SCR}$ was measured using both iButtons and IRT. In contrast to the aforementioned

Martinez-Tellez study, no relationship between $T_{SCR}$ (measured using iButton or IRT) and BAT activity on FDG-PET-CT was observed in this smaller group of individuals (n = 12) but $T_{SCR}$ was negatively correlated with BAT volume, but only when $T_{SCR}$ was derived from IRT not iButtons (Martinez-Tellez et al., 2019b).

To date, two methods have emerged as the most frequently used to measure $T_{SCR}$, infrared thermography and assessment of skin temperature using wireless temperature sensors applied directly to the skin (e.g. iButtons, SubCue). With the exception of the two studies presented in this thesis (Robinson et al., 2014, Robinson et al., 2016) and three others (Martinez-Tellez et al., 2019a, van der Lans et al., 2016, Martinez-Tellez et al., 2018), none of the studies identified during my literature search for Table 1.1 specify the model or resolution of wireless data logger they had used.

At present, the Thermacron family of iButtons produced by Maxim is comprised of more than five versions of their standard Thermochron iButton models (DS1921/DS1922) with the capacity to detect temperatures within the range of human physiological skin temperature. These all function at different resolutions, ranging from 0.0625 to 0.5˚C. The observed $T_{SCR}$ changes in response to cold-stimulation reported to date are reasonably small (mostly < 0.5˚C), and how precisely these are detected will be dependent on the resolution of the equipment used. As this information is rarely specified in any of these publications, it is not clear how robust the conclusions made from this data are.

In addition, the supraclavicular region in adults is a large area compared to the size of these data loggers, and the temperature profile of the skin within this region is not homogenous (Figure 1.10). The anatomical detail of where these were placed and what measures that were taken to ensure that they were placed consistently and had reached stability in recording is also lacking in these publications.

Measuring skin temperature with infrared thermography may appear simple, but is in practicality complex due to the influence of external factors such as environmental temperature, humidity and airflow. It is also somewhat dependent not only on the specification of the camera but also on the software available for analysis. A range of methods have been used (and are summarised in Table 1.1) to calculate a summary value for supraclavicular temperature, with differing regions of interest (ROIs) (see Figure 1.10); including fixed size, proportioned relative to the participant, derived using threshold segmentation, or identified using a modified seed region growing algorithm and calculated using different mathematical approaches (mean, percentiles, maximum etc.). The images included in some of the publications summarised in Table 1.1 also elude to possible issues with data quality in some of these studies, which may also have contributed to the discrepancies observed between studies. For example, in Figure 1.10G there has been noticeable movement of the participant as they have moved to place their hand in the water for cooling, not only changing the contour of the shoulders but also moving towards the thermal imaging camera, movement certain to affect these authors measure of BAT given that this was calculated based on an absolute supraclavicular thermal area.

“Personalised cooling protocols” are commonly used to stimulate BAT for research purposes, and these aim to elicit maximal NST. In contrast to fixed protocols where all participants are exposed to the same cold stimulus (e.g. water perfused cooling vest set to deliver water at 8˚C) these personalised protocols cool participants to the threshold at which they begin to shiver, and then gradually increase the temperature of the cooling medium until shivering stops (or to an arbitrary value above this). The assumption is then made that this is maximal NST; however at present time, the evidence for this is lacking.

A large proportion of these studies also relied on self-reporting and/or visual assessment of shivering rather than using electromyography (EMG). It is well recognised in clinical medicine that patients may shiver without this being clinically apparent to an observer and that visual assessment alone is not an optimal method of detection (discussed in detail 1.10.5).

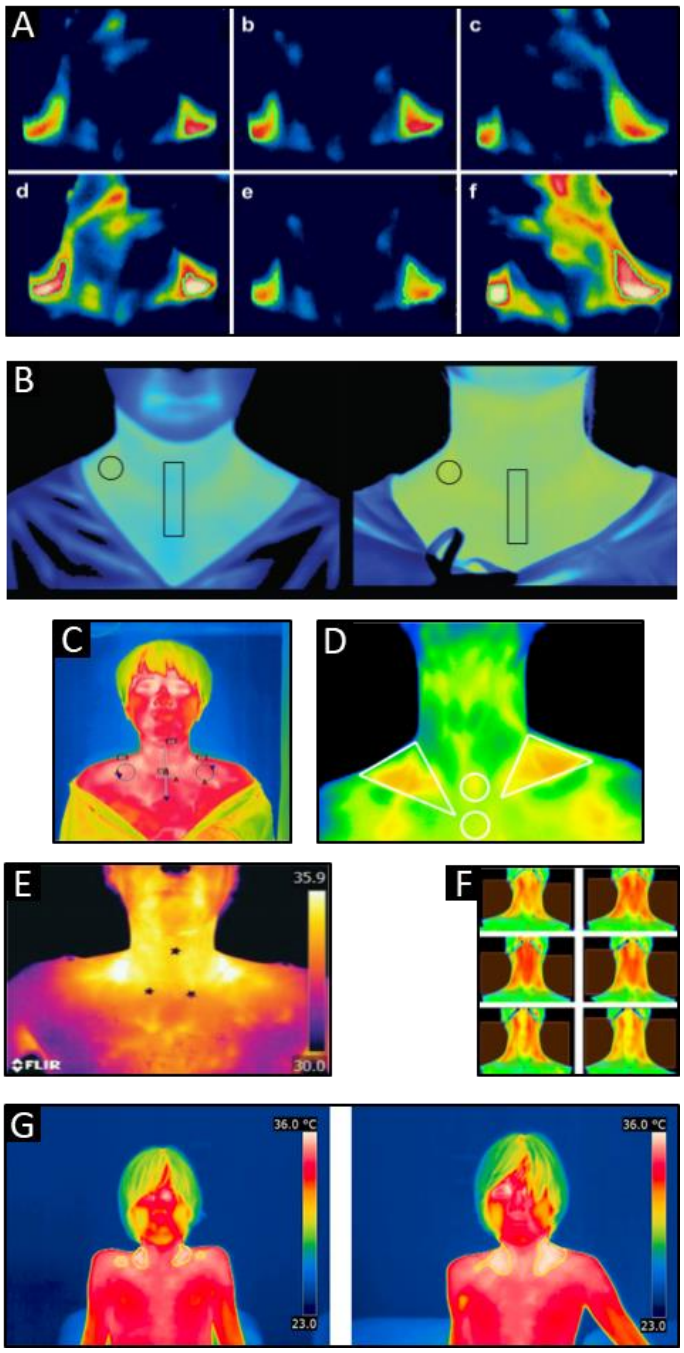



**Figure 1.10 A-G Examples of thermal images presented in publications using infrared thermographic assessment of supraclavicular skin temperature for assesment of brown adipose tissue activity.** Images reproduced with permission or are under Creative Commons licences (See Appendix for details) and demonstrate the variation between research groups in field of view, colour palette, size and shape of regions of interest and positioning of the participant for the assessment of supraclavicular BAT. A) (Ang et al., 2017) B) (Kim et al., 2014) C) (Zhou et al., 2018) D) (Gatidis et al., 2016) E) (Salem et al., 2016) F) (Haq et al., 2017) G) (Malpique et al., 2018).

**Table 1.1 Summary of human studies using supraclavicular skin temperature as a surrogate marker of supraclavicular BAT activity published since 2011, identified by a MEDLINE search (May 2019) using search terms BAT, brown adipose tissue and supraclavicular temperature.** Bold type indicates publications that aimed to, or have validated $T_{SCR}$ as a measure of BAT activity.

| Author | Subjects | Intervention | BAT activity assessment | Shivering | Method of $T_{SCR}$ assessment | 'Validation of $T_{SCR}$' or observed change in $T_{SCR}$ with cold exposure |
|---|---|---|---|---|---|---|
| (Lee et al., 2011) | Adult (M)<br>n = 1<br>32y | - Cold (WB; air; 17˚C; 30mins)<br>- Standard meal | Absolute $T_{SCR}$<br>Relative $T_{SCR}$ | NS | IRT; oval ROI in SCR | $T_{SCR}$ ↓<br>$T_{mediastinum}$ ↓↓<br>Relative $T_{SCR}$ ↑ |
| (Yoneshiro et al., 2011a) | Adults(M)<br>n = 13<br>20 – 28y | - Cold (WB; air; 19˚C; plus feet on/off ice; 2h) | $T_{SCR}$<br>sFDG-PET-CT ($SUV_{max}$)<br>EE (IC – hood) | NS | Disc-type data logger;<br>Thermochron G with SCR | FDG +ve $T_{SCR}$ ↔<br>FDG -ve $T_{SCR}$ ↓<br>EE ↑correlates with $SUV_{max}$ |
| (Symonds et al., 2012a) | Adults/children (M/F)<br>n = 26<br>3 – 58y | - Cold (hand; water; 20˚C; 5min) | Absolute $T_{SCR}$<br>Area SCR | NS | IRT (FLIR b60; QuickReport; $T_{SCR}$ – 95$^{th}$ perpercentile of rectangular ROI) | $T_{SCR}$ ↑ |
| (Yoneshiro et al., 2012) | Adults (M)<br>n = 18<br>20 – 32y | - Cold (WB; air; 19˚C; 2h)<br>Capsinoids | $T_{SCR}$<br>sFDG-PET-CT ($SUV_{max}$)<br>EE (IC – hood) | NS | Disc-type data logger<br>Thermochron G within SCR | - |
| **(Jang et al., 2014)** | **Adults (M/F)<br>n = 17<br>36 ± 8.6y<br>(mean ± SD)** | **Cold (WB; air; 19˚C; 2h)** | **Absolute $T_{SCR}$<br>Relative $T_{SCR}$<br>sFDG-PET-CT ($SUV_{max}$, BAT volume)** | **NS** | **IRT (FLIR 425; RIR; maximal temp in midclavicular circular ROI, non-BAT ROI – lateral upper chest)** | **Absolute $T_{SCR}$ ↔<br>Relative $T_{SCR}$ ↑<br>BAT volume correlates with Δrelative $T_{SCR}$** |
| (Robinson et al., 2014) | Children (M/F)<br>n = 55<br>6 – 11y | Cold (hand; water; 20.1˚C; 5min) | Absolute $T_{SCR}$ | SR<br>VA | IRT (FLIR 425; ThermaCAM Researcher Pro; $T_{SCR}$ –87.5$^{th}$ perpercentile of SCR ROI, sternal non-BAT ROI) | $T_{SCR}$ ↑in ~ 50%<br>$T_{sternum}$ ↔ |

| | | | | | | |
|---|---|---|---|---|---|---|
| **(Boon et al., 2014)** | **Adult (M)<br>n = 24<br>18 – 28y** | **Cold (WB; water perfused mattress; personalised protocol; 2h)** | **Absolute $T_{SCR}$<br>sFDG-PET-CT ($SUV_{max}$, $SUV_{mean}$/BAT volume)<br>EE (IC – hood)** | **VA<br>SR** | **iButton$^{NS}$** | **$T_{SCR}$ ↑ and EE ↑<br>Correlation between cold exposed $T_{SCR}$ and:<br>- BAT vol ($R^2$ = 0.28)<br>- SUV max ($R^2$ = 0.32)<br>No correlation with $\Delta T_{SCR}$** |
| (Kim et al., 2014) | Adolescent (F)<br>n = 1 Hypothyroidism | Thyroid hormone replacement | Absolute $T_{SCR}$<br>Relative $T_{SCR}$<br>Water-fat MRI | - | IRT (FLK-Ti32; $T_{SCR}$- circular ROI; non-BAT rectangular ROI at suprasternal notch | Following TH replacement:<br>Absolute $T_{SCR}$ ↑<br>Relative $T_{SCR}$ ↓<br>FF ↑ |
| (Lee et al., 2014a) | Adults<br>n = 10<br>27 ± 5y | Cold (water circulating blanket; 27→12˚C)<br>Exercise | Relative $T_{SCR}$<br>sFDG-PET-CT<br>EE (IC – hood) | EMG X2 | iButtons$^{NS}$ on the i) supraclavicular fossae and ii) pectoralis major (non-BAT region) | ↑ relative $T_{SCR}$ with increased cooling<br>↑ EE |
| **(van der Lans et al., 2016)** | **Adults (M)<br>n = 36<br>23.4 ± 3.6y** | **Cold (WB; air; individualised protocol; 90min)** | **sFDG-PET-CT ($SUV_{mean/Max}$)** | **EMG$^{NS}$** | **iButton (precision 0.05˚C) on the SCR<br>multiple non-BAT sites** | **↓ $T_{SCR}$<br>↓↓ $T_{MSK}$<br>In BAT+ correlation between:<br>- $SUV_{mean}$ and $\Delta T_{SCR}$ $R^2$ = 0.23<br>- NST (ΔEE) and $\Delta T_{SCR}$ $R^2$ = 0.18<br>No correlation with SUVmax** |
| (Yoneshiro et al., 2016) | Adults (M)<br>n = 45<br>20 – 31y | Cold (air; 19˚C; 2h) and (feet on ice intermittently) | Absolute $T_{SCR}$<br>FDG-PET-CT (FDG high/low)<br>EE (IC- hood) | EMG - pectoral | Disc-type data logger Thermacron G in SCR<br>Parasternal non-BAT region | $T_{SCR}$ ↓ with cold exposure - less than non-BAT areas<br>Cold exposed $T_{SCR}$ ↑ in winter (noted at other sites also) |

| | | | | | | |
|---|---|---|---|---|---|---|
| **(Chondronikola et al., 2016)** | **Adults (M)<br>n = 18<br>46.9 ± 18.1y** | **- Cold (personalised; circulating liquid vest and blanket; 6h)** | **Absolute $T_{SCR}$<br>sFDG-PET-CT<br>($SUV_{mean}$, FDG +ve, FDG –ve)** | **VA<br>SR** | **iButton$^{NS}$ over left supraclavicular adipose tissue depot (n = 16)<br>trunk** | **$T_{SCR}$ ↔ in FDG +ve<br>$T_{SCR}$ ↓↓ in FDG -ve<br>$\Delta T_{SCR}$ correlated with $log_{10}$BAT volume r = 0.58<br>BAT volume + associated with $\Delta T_{SCR}$ after adjustment for age, adiposity** |
| (Salem et al., 2016) | Adults (M)<br>n = 11<br>20.8 – 39.8y | - Cold (torso; water-perfused vest; 8˚C 55min)<br>- Glucagon | Absolute $T_{SCR}$<br>dFDG-PET-CT<br>(MRgluc)<br>EE (IC – hood) | SR<br>VA | FLIR T440bx, FLIR tools +, ThermaCAM Researcher Pro, $T_{SCR}$ – mean of hottest 10% of anatomical SCR<br>Non-BAT ROI – triangle over deltoid. | $T_{SCR}$ ↑ in FDFG +ve<br>$T_{SCR}$ ↔ in FDG –ve<br>↑EE<br>↑MRgluc |
| (Gatidis et al., 2016) | Adults (M/F)<br>n = 102<br>58 ± 17y | None | Absolute $T_{SCR}$<br>Relative $T_{SCR}$<br>sFDG-PET-CT<br>(clinically indicated) | | IRT; Varioscan 3021 ST (accuracy±2K,resolution 0.03K)<br>Mean/max temp of triangular SCR ROI.<br>Jugular temp | FDG +ve ↑ mean $T_{CSR}$ and max $T_{SCR}$ compared to FDG -ve<br>No effect of FDG status after adjustment for age, sex and BMI |
| (El Hadi et al., 2016) | Adults (M)<br>n = 30<br>lean/obese<br>24 ± 2.2/29 ±6y | - Cold (hands; water; 5˚C; 20min) | Absolute $T_{SCR}$<br>EE (IC – face mask) | VA | FLIR T450sc; triangular ROI in the supraclavicular fossa; mean temp of ROI; “FLIR R&D software”<br>Sternal as non-BAT control ROI | $T_{SCR}$ ↑ (lean only)<br>↑ EE (lean only)<br>↑RQ (lean only)<br>No correlation between $\Delta T_{SCR}$ and ΔEE (data not shown) |
| (Robinson et al., 2016) | Adults (F)<br>n = 5<br>21 – 29y | Mild mental stress | Absolute $T_{SCR}$<br>Relative $T_{SCR}$ | | FLIR B425; FLIR RIR; $T_{SCR}$ – 97.5$^{th}$ perpercentile of SCR | - |

| | | | | | | |
|---|---|---|---|---|---|---|
| (Lee et al., 2016) | Adults<br>n = 18<br>29 ± 4y | Cold (WB; circulating water blanket; personalised cooling 14-18˚C; 2h) | Absolute $T_{SCR}$<br>sFDG-PET-CT<br>($SUV_{mean}$) | EMG | iButton (model: not stated ∴ unknown resolution) | $T_{SCR}$ ↑<br>$T_{MSK}$ ↓<br>$T_{core}$ ↔<br>$\Delta T_{SCR}$ correlated with $SUV_{mean}$ |
| Ramage et al 2016 | Adults | Glucocorticoid (prednisolone)<br>Cold (Whole-body; air; 2h; 16-17C) | Absolute $T_{SCR}$<br>sFDG-PET-CT (not paired to IRT), EE | | FLIR T650sc; Oval ROI in SCR; mean and max temp, RIR<br>Non-BAT ROI – chest | $T_{SCR}$ ↓, $T_{chest}$ ↓↓<br>EE ↑ |
| (Ang et al., 2017) | Adults (M)<br>n = 24<br>23 ± 0.4 (mean ± SEM) | Cold (hand/feet; water; 18˚C; 5min)<br>Capsinoid supplementation<br>Test meal | $T_{SCR}$ ($\Delta T_{SCR}$, area, heat output defined high BAT and low BAT groups)<br>EE (IC) | NS | FLIR T440; Heat output calculated using $T_{SCR}$ and AreaSCR from a Modified SRG algorithm; RIR; | $T_{SCR}$ ↑ with cold<br>Correlation between C-SCV heat output and BMR |
| (Scotney et al., 2017) | Adults (M)<br>n = 8<br>18 – 34y | Isocaloric meal<br>Isoprenaline<br>Hydrocortisone | Absolute $T_{SCR}$ | | FLIR E60; FLIR Tools; 95$^{th}$ percentile of SCR ROI; | - |
| (Peterson et al., 2017) | Adults (M)<br>n = 14<br>24 ± 3y | Cold (cold; feet: ice water; 2min)<br>Overfeeding | Relative $T_{SCR}$ | NS | FLIR SC5500M (software; MATLAB)<br>Torso as non-BAT region | Relative $\Delta T_{SCR}$ c. -0.04˚C |
| (Haq et al., 2017) | Adults (M)<br>n = 62<br>18 – 39y | Cold (torso; circulating water blanket; 12˚C; 1h) | Absolute $T_{SCR}$<br>EE | EMG | FLIR T650sc; Amide software; top 10% of rectangular ROI. | $T_{SCR}$ ↑ (c. 0.13 – 0.34˚C) |
| (Hartwig et al., 2017) | Adults (F)<br>Lean/overweight<br>n = 10 | Oral glucose followed by cold (hand; water; 5-9˚C; 5mins | Absolute $T_{SCR}$<br>NIRS | NS | Fluke Ti9 Thermal imager<br>10x10mm ROI in SCR | - |

| | | | | | | |
|---|---|---|---|---|---|---|
| (Sarasniemi et al., 2018) | Adults (M/F)<br>48 ± 5y<br>n = 24 | none | Absolute $T_{SCR}$<br>MRS | - | FLIR A325 IR camera<br>Mean of rectangular ROI in 5 positions lateral neck and SCR<br>Dubious methodology | Association between MRS and IR temperature only in non-obese<br>Inverse correlation in obese |
| (Martinez-Tellez et al., 2018) | Adults<br>n = 11<br>23.3 ± 0.5 (mean ± SE) | Cold (air + water perfused jacket; personalised; 90min) | Absolute $T_{SCR}$<br>Relative $T_{SCR}$<br>$T_{SCR}$ gradient | VA/SR<br>EMG | iButtons DS1922 L (0.0625˚C) | $T_{SCR}$ ↔ |
| (Malpique et al., 2018) | Children<br>n = 86<br>8.5 ± 0.1y<br>AGA/SGA | Cold (hand; water; 17-18˚C; 5min) | Absolute $T_{SCR}$<br>$Area_{SCR}$ | NS | FLIR b60; QuickReport; max temp in ROI, area >35.2˚C | $T_{SCR}$ ↑ (c.0.4˚C)<br>$Area_{SCR}$ ↑ |
| **(Law et al., 2018)** | **Adults (M)<br>n = 8<br>18 – 35y<br>FDG +ve** | **Cold (torso; water-perfused vest; 8˚C 55min)** | **Absolute $T_{SCR}$<br>Relative $T_{SCR}$<br>dFDG-PET-CT** | **VA<br>SR** | **FLIR T440bx, FLIR tools+, ThermaCAM Researcher Pro, $T_{SCR}$ – mean of hottest 10% of anatomical SCR<br>MATLAB** | **MRgluc correlated with relative $\Delta T_{SCR}$ at 10 mins of cooling.<br>Trend to correlation with absolute $T_{SCR}$ at baseline and cold exposed.** |
| (Zhou et al., 2018) | Adults (F)<br>n = 164<br>GDM | None | Absolute $T_{SCR}$ | NA | FLIR B425, circular ROI, upper thorax (overlying the clavicle) | - |
| (Levy et al., 2018) | Adults (M/F)<br>28.8 ± 8/27.4 ± 8.7y<br>n = 74 | Cold (WB; water perfused suit; personalised; 30min | Absolute $T_{SCR}$<br>EE ($IC^{NS}$)<br>RQ | VA | FLIR E60; $T_{SCR}$ – max temp of SCR ROI, FLIR tools<br>Non-BAT ROI at sternum | $T_{SCR}$ ↔<br>$T_{sternum}$ ↓<br>Correlation between $\Delta T_{SCR}$ and %ΔEE |

| | | | | | | |
|---|---|---|---|---|---|---|
| (Thuzar et al., 2018) | Adults (M/F)<br>28 ± 2y<br>n = 13 | Glucocorticoids<br>Cold (whole-body; air; 19˚C; 3h) | Absolute $T_{SCR}$<br>sFDG-PET-CT ($SUV_{max}$, BAT volume)<br>EE ($IC^{NS}$) | | IRT (FLIR B425; $T_{SCR}$ – Mean of midclavicular circular ROI; RIR)<br>Non-BAT ROI – mid sternum | $T_{SCR}$ ↓<br>EE ↑ |
| (Sanchez-Delgado et al., 2018) | Adults (M/F)<br>n = 57<br>23 ± 2.4y | Cold (air; 19.5-20˚C; plus perfused vest at 3.8˚C above shivering threshold; 2h) | EE – IC<br>Absolute $T_{SCR}$<br>sFDG-PET-CT (BAT vol, SUVmean/peak) | VA<br>SR | iButton DS 1922L (resolution 0.0625˚C) minimal detail on placement | No relationship between $\Delta T_{SCR}$ and CIT or cold exposed $T_{SCR}$ and CIT |
| (Coolbaugh et al., 2018) | Adults (M/F)<br>26.2 ± 1.4y<br>n = 12 | Cold (water perfused blanket; personalised cooling) | Absolute $T_{SCR}$ | EMG<br>SR | Temperature thermistor probe Model MLT422/A above the clavicle | $T_{SCR}$ ↓ |
| (Senn et al., 2018) | Adults (M/F)<br>n = 56 | Cold (torso; circulating water; personalised; 90-120 min) | $T_{SCR}$<br>EE – IC hood | VA<br>SR | $iButton^{NS}$ | - |
| (Thuzar et al., 2019) | Adults (M/F)<br>28 ± 1y<br>n = 10 | Mineralocorticoids<br>Cold (WB; air; 19˚C; 3h)<br>Meal | Absolute $T_{SCR}$<br>sFDG-PET-CT ($SUV_{max}$, BAT volume)<br>EE (IC – hood) | | IRT (FLIR B425; $T_{SCR}$ – mean of midclavicular circular ROI; RIR) | $T_{SCR}$ ↓<br>Correlation between $SUV_{max}$ and cold exposed $T_{SCR}$ (r = 0.62) |
| (Gashi et al., 2019) | Adults (M/F)<br>18 – 47y<br>n = 20 | Cold (trunk and arm; personalised; 120 mins) | Absolute $T_{SCR}$<br>FDG-PET-CT<br>Dynamic Water-fat MRI | VA<br>SR | $iButton^{NS}$ | $T_{SCR}$ ↔ (skin temp at 7 non-BAT locations all ↓↓)<br>EE ↑<br>Correlation between $\Delta T_{SCR}$ and ΔEE (r = 0.56) |

| | | | | | | |
|---|---|---|---|---|---|---|
| (Robinson et al., 2019) | Children (M/F)<br>n = 36<br>8 – 11y | Cold (hand; water; 20˚C; 5min) | Absolute $T_{SCR}$ | | IRT (FLIR 425; ThermaCAM Researcher Pro; $T_{SCR}$ – 95$^{th}$ perpercentile of anatomical SCR | $T_{SCR}$ ↑ (boys) |
| (Shorakae et al., 2019) | Adults (F)<br>30 ± 6.2y<br>PCOS<br>n = 55 | PCOS versus control | Absolute $T_{SCR}$ | | SubCue wireless dataloggers (resolution$^{NS}$) | - |
| (Loh et al., 2019) | Adults<br>18 – 35y<br>n = 17 | 4 doses of mirabegron (50-200mg) | Absolute $T_{SCR}$<br>EE | | iButton (model and resolution$^{NS}$) | $T_{SCR}$ ↑ (50,100,150mg doses)<br>EE ↑ (100, 150, 200mg doses) |
| **(Martinez-Tellez et al., 2019b)** | **Adults (M/F)<br>n = 12<br>18 – 25y** | **Personalised cooling Cold (water-perfused vest, 3.8˚C above shivering threshold, 2h)** | **sFDG-PECT-CT** | **SR<br>VA** | **iButton resolution 0.0625˚C – placed contralateral side to IRT FLIR E60 – 4 images; 2 selected for analysis pre/post<br>ROI – max/mean/min** | **$T_{SCR}$(mean) – not associated with BAT activity<br>$T_{SCR\ (mean)}$ neg associated with BAT volume<br>$T_{SCR(max)}$ positively associated with BAT activity at baseline** |
| **(Martinez-Tellez et al., 2019a)** | **Adults (M/F)<br>21.9 ± 2.1 years<br>n = 88** | **Personalised cooling Cold (water-perfused vest, 3.8˚C above shivering threshold, 2h)** | **sFDG-PET-CT (SUVmean/peak)** | **SR<br>VA** | **iButton resolution 0.0625˚C on right SCR** | **$T_{SCR}$ ↔<br>No association between $T_{SCR}$ and BAT volume<br>$T_{SCR}$ positively associated with BAT activity<br>No association between $\Delta T_{SCR}$ and BAT activity<br>Women only** |

Abbreviations: SCR – supraclavicular region; $T_{SCR}$ – supraclavicular skin temperature; NST – non-shivering thermogenesis; IRT – infrared thermography; EE – energy expenditure; F – female; M – male; NS – not specified; EMG – electromyography; SR – self reported; VA – visually assessed; ROI – region of interest; IC – indirect calorimetry; AGA – appropriate for gestational age; SGA – small for gestational age; GDM – gestational diabetes; PCOS – polycystic ovarian syndrome; FDG – flurodeoxyglucose; s FDG-PET-CT – static fusion FDG positron-emission tomography and computed tomography; WB – whole-body

How well $T_{SCR}$ or changes in $T_{SCR}$ may approximate to true BAT activity remains to be seen, and may become more evident when the measurement of BAT activity moves beyond that of glucose uptake.

Indirect evidence also supports $T_{SCR}$ as a marker of BAT activity. Two notable studies have evaluated the $T_{SCR}$ response to β adrenergic stimulation, Scotney et al. demonstrated an increase in $T_{SCR}$ after the administration of the non-selective β agonist isoprenaline (Scotney et al., 2017), and Loh et al. reported increases in $T_{SCR}$ after the administration of the $\beta_3$ selective agonist mirabegron in conjunction with an increase in energy expenditure (Loh et al., 2019).

There continue to be many criticisms of $T_{SCR}$ as a surrogate measure of supraclavicular BAT activity (Gatidis et al., 2016, Sarasniemi et al., 2018). The temperature at the skin surface reflects just that, supraclavicular BAT is the most superficial depot but often extends deep into the upper thorax. Any heat produced by BAT in these depots is conducted into the local tissues, and given its proximity to the vasculature, some of this heat will inevitably be carried away by the blood. How much makes it to the skin surface requires further study, and how this may be modified by overlying subcutaneous adipose tissue is unknown.

To date, just one study has attempted to measure the temperature within BAT and compare this to the temperature of the overlying skin measured with IRT. The author of this study concluded that there was no relationship between $T_{SCR}$ and BAT temperature, or between $T_{SCR}$ and FF on MRI, suggesting that basal $T_{SCR}$ is not related

to BAT activity. The temperature of BAT was assessed indirectly using MRS thermometry using the temperature of a single voxel, and $T_{SCR}$ was assessed using IRT (Sarasniemi et al., 2018). However, in this study, participant preparation, control, standardisation or documentation of ambient temperature were minimal calling into question the validity of $T_{SCR}$ measurements.

### 1.11.5 Cooling protocols for activation of human BAT

Cooling protocols are frequently used in all modes of BAT assessment. These vary from regional cooling of limbs to whole-body cooling with air or water. Some research groups utilise fixed cooling methods whereas others use individualised cooling protocols intended to elicit maximal BAT stimulation (Table 1.1). There is no standardisation as to which method is best, and no guidance at all for their use in children. Most protocols are designed around the timings of PET scanning, whereby the radiotracer must be administered around 40 minutes prior to acquisition of the scan, subsequent cooling times often reflect this, and usually comprise an hour of cooling prior to, and after injection of FDG.

Cooling for the comprehensive assessment of BAT should aim to elicit pure NST, and, when using $T_{SCR}$ as a proxy measure of BAT activity, should limit significant systemic cardiovascular change (e.g. cold pressor response) which may induce local changes in blood flow unrelated to BAT activation. Despite the relative severity of some of the cool stimuli used (e.g. 2 hours of exposure to room temperature at 18˚C plus cooling of the feet on ice) monitoring of shivering is often limited to participant self-reporting alongside visual checks from a study investigator (summarised in Table 1.1). The

research groups that have used EMG to identify shivering have done so using one or two superficial muscle groups monitored using surface rather than intramuscular electrodes (Coolbaugh et al., 2018, Haq et al., 2017, Lee et al., 2014b, Martinez-Tellez et al., 2018). The contribution of skeletal muscle to cold-induced thermogenesis is thought to be greater in the centrally located deep muscles rather than the superficial muscles observed in these studies and activity in these deep muscles has been observed during some BAT cooling protocols without noticeable shivering (UDin et al., 2016, Acosta et al., 2018).

As surface EMG does not detect deep muscular activity, this alone cannot ensure that cold-induced thermogenesis observed in these studies is exclusively derived from BAT. Consequently, studies using these personalised maximal non-shivering thermogenesis cooling protocols without comprehensive EMG assessment may not be evaluating BAT thermogenesis in isolation as intended (Martinez-Tellez et al., 2018, van der Lans et al., 2016). In addition, significant muscular activity may confound concomitant measures of energy expenditure and plasma metabolites, and may also affect SUVs in BAT (as these are measures of signal intensity in BAT, normalised for administered dose, skeletal muscle contraction may compete for glucose uptake, lowering the overall "dose" available for BAT uptake).

### 1.12 Human BAT in early life

At the time of writing, a comprehensive review of the literature revealed only a small number of research studies focussing exclusively on BAT in children (using FDG-PET-CT, of which all were retrospective review of clinically indicated scans) (Table 1.2) and a

handful of review articles (Hong et al., 2011, Gilsanz et al., 2013, Drubach et al., 2011, Ponrartana et al., 2013). A large proportion of these original research articles describing the use of FDG-PET-CT in children were derived from scans undertaken at the Children's Hospital of Los Angeles over similar time periods (Table 1.2). At first glance, the findings of these studies support each other. However detailed examination reveals considerable overlap with regard to the children involved in these studies. This is explicitly stated in at least one paper, but not referred to in others. The results of these individual studies and how they sit amongst the rest of the BAT literature must be interpreted in the context of this overlap given that they may not represent individual study populations as one might initially assume.

**Table 1.2 Positron-emission-tomography and computed-tomography assessment of supraclavicular BAT in children. Author, year of publication, location and dates of scans, and underlying diagnoses of research subjects.** Studies including the same children indicated by *.

| Author (year) | Method | Study dates | Location | Paediatric subject diagnoses (number of children) |
|---|---|---|---|---|
| (Gelfand et al., 2005) | PET | Dec '02 - Apr '04 | Cincinnati Children's Hospital | Solid tumours (n = 69) |
| (Zukotynski et al., 2009) | PET | Dec '06 – Mar '07<br>Dec '07 – Mar '08 | Children's Hospital Boston | Patients referred for whole-body FDG-PET scan (n = 85) |
| (Zukotynski et al., 2010) | PET | Dec '06 – Dec '07<br>Jan '08 – Dec '08 | Children's Hospital Boston | Patients referred for whole-body FDG-PET scan (n = 103) |
| (Gupta et al., 2011) | CT | Apr '08 – Oct '09 | Hospital for Sick Children, Toronto | Congenital thoracic malformations or CHD (n = 188) |
| (Hu et al., 2011) | PET-CT | Oct '08 – Feb '10 | Children's Hospital of Los Angeles | Lymphoma (n = 75), neuroblastoma (n = 12), ewing's sarcoma (n = 4)<br>Melanoma (n = 3)<br>Thyroid, RMS, NP, liver, cardiac angiosarcoma, adenosarcoma (n = 1) |
| (Gilsanz et al., 2011) | PET-CT | Unspecified dates*.<br>But overlap identified with Gilsanz 2012 | Children's Hospital of Los Angeles | Lymphoma (n = 56), neuroblastoma (n = 3), ewing's sarcoma (n = 2)<br>ALL (n = 2)<br>Thyroid, RMS, NP, liver, cardiac angiosarcoma, adenosarcoma, melanoma (n = 1) |

| | | | | |
|---|---|---|---|---|
| (Gilsanz et al., 2012a) | PET-CT | Jan '09 – Jan '11* | Children's Hospital of Los Angeles | Hodgkin lymphoma (n = 21)<br>Non-Hodgkin lymphoma (n = 10) |
| (Gilsanz et al., 2012b) | PET-CT | Unspecified dates. But overlap with Hu et al and Gilsanz 2011* | Children's Hospital of Los Angeles | Lymphoma (n = 57)<br>Neuroblastoma (n = 4)<br>ALL (n = 3)<br>Castleman's syndrome, Ewing's sarcoma, MB, melanoma, RMS, post-transplant LPD, thyroid cancer (n = 1), cancer ruled out (n = 2) |
| (Chalfant et al., 2012) | PET-CT | Oct '08 – sept '11 | Children's Hospital of Los Angeles | Lymphoma (n = 28)<br>ALL, melanoma, MB, RMS (n = 1) |
| (Ponrartana et al., 2012) | PET-CT | Oct '08 – Jan '12* | Children's Hospital of Los Angeles | Lymphoma (n = 35)<br>ALL (n = 2)<br>Ewing sarcoma, melanoma, neuroblastoma (n = 1). |
| (Brendle et al., 2018) | PET-CT | Aug '04 – July '09 | Germany | Clinically indicated – unspecified (n = 31) |
| (Drubach et al., 2011) | PET-CT | Nov '04 – Nov '07 | Children's Hospital Boston | Hodgkin lymphoma, Non-Hodgkin lymphoma, mesenchymal tumours, CNS tumours, other (n = 172) |

Abbreviations: PET – Positron-emission-tomography; CT – computed-tomography; FDG – flurodeoxyglucose; CHD – congenital heart disease; RMS – rhabdomyosarcoma; NP – nasopharyngeal carcinoma; ALL – acute lymphoblastic leukaemia; MB – medulloblastoma; LPD – lymphoproliferative disease; CNS – central nervous system.

### 1.12.1 Relationship between BAT and age in early life

The most frequently reported and consistent finding from the assessment of supraclavicular BAT irrespective of the method used, is that of a negative relationship between BAT and age (Cypess et al., 2009, Brendle et al., 2018, Pfannenberg et al., 2010, Yoneshiro et al., 2011b, Yeung et al., 2003, Steinberg et al., 2017, Ouellet et al., 2011, Lean et al., 1986, Kim et al., 2008, Truong et al., 2004). Even before the discovery of UCP1 in the late 197o's, autopsy-based studies identified adipose tissue in the neck and upper thorax of adults and children with histology consistent with what is currently described as thermogenic brown/beige adipose tissue (Heaton, 1972, Lean et al., 1986, Bonnot, 1908). Some these studies also demonstrate a transition from well vascularised, mitochondrion rich multilocular adipose tissue, to unilocular white adipose tissue occurring with advancing age (Heaton, 1972). This is in line with more recent data from both FDG-PET-CT and chemical-shift water-fat MRI studies whereby supraclavicular BAT prevalence and activity decline with age in the former, and fat fraction values increase in the latter.

PET-CT studies have shown that the prevalence of FDG-detected BAT is highest in infancy and childhood and declines into late adulthood (Pfannenberg et al., 2010, Yoneshiro et al., 2011b). A similar pattern is seen in the MR properties of supraclavicular BAT on water-fat MRI, where FF and T2* are lowest in neonates and infants and highest in the elderly (Franz et al., 2015). When considered across the life cycle, a number of studies report a linear relationship between age and both FDG-detected BAT prevalence (Brendle et al., 2018, Pfannenberg et al., 2010, Cypess et al., 2009).

To date, there have been no direct comparisons between BAT in the neonatal period/early infancy, and BAT in adulthood on FDG-PET-CT or MRI. Neonates and young infants often require sedation or anaesthesia to maintain sufficient immobility for optimal image acquisition and, as many of the medications used to achieve this (e.g. general anaesthesia, benzodiazepines) are recognised to have a direct effect on BAT (Plattner et al., 1997, Gelfand et al., 2005, Cousins et al., 2017), imaging from this age group is typically excluded from these studies. Gupta et al. reported radiodensity consistent with supraclavicular BAT in infants from as young as 2 days old. He described hyperdensity on CT alone in the anatomical regions of supraclavicular BAT during the first year of life in 9.3% infants studied and, within the root of the neck in another 18.5% of contrast-enhanced scans (Gupta et al., 2011).

The majority of studies reporting the presence/absence of FDG-detected BAT in children, adolescents and adults were undertaken in individuals undergoing PET imaging for clinical indications, and were undertaken before the publication of the BARCIST 1.0 guidelines (Chen et al., 2016). These studies were not undertaken to quantify BAT per se, and used differing protocols for image acquisition and differing methods of analysis and quantification, therefore comparison between studies and age groups in particular is difficult.

The prevalence of FDG-detected BAT in children has been reported from 15 – 77% (Yeung et al., 2003, Gilsanz et al., 2012a), and is lowest in children who have been warmed to 24˚C (Zukotynski et al., 2009, Zukotynski et al., 2010) and/or given diazepam pre-medication (Cousins et al., 2017) and highest in children free from

malignant disease and scanned at cooler ambient temperatures (21 – 22˚C) (Gilsanz et al., 2012a, Chalfant et al., 2012). Reported prevalence in similar retrospective studies of adult cohorts is much lower, between approximately 5 – 15% (Hany et al., 2002, Brendle et al., 2018, Cohade et al., 2003) although these figures are likely to have been highly influenced by the environmental conditions preceding clinical imaging.

However, FDG-detected BAT is identified much more frequently in adults in healthy volunteer BAT dedicated studies, particularly in subjects exposed to exogenous BAT stimuli (e.g. cold, thyroid releasing hormone, $B_3$ agonists) (Thuzar et al., 2018, Begaye et al., 2018, Heinen et al., 2018, Salem et al., 2016, Broeders et al., 2015b, Cypess et al., 2015). Nonetheless, given the restrictions on FDG-PET-CT there are no groups of healthy volunteer children or adolescents examined in a similar manner to compare them with. Likewise, FF within the supraclavicular region is the lowest (indicative of the highest BAT activity) in the neonatal period, rises rapidly from c.20% to 50 – 60% in the first 6 months (Ponrartana et al., 2016) and has been reported as high as 90% in elderly adults (Franz et al., 2015), similar to values obtained from subcutaneous WAT (Stauss et al., 2008).

Most human BAT studies seeking to describe BAT throughout the life cycle have included research subjects from mid-childhood to late adulthood. In recent years, a small number of studies have attempted to examine BAT exclusively in childhood and adolescence using PET-CT (Drubach et al., 2011, Deng et al., 2015, Gilsanz et al., 2012b). These suggest that the relationship between BAT and age is likely to be more

complex than the simple linear relationship described initially. When measures of BAT are stratified by age (Drubach et al., 2011), sub-grouped by pubertal status (Deng et al., 2015, Gilsanz et al., 2012b), or considered with adjustment for confounding variables with multivariate analyses (Gilsanz et al., 2012b), it appears that additional peaks in avidity for FDG in supraclavicular BAT are witnessed beyond the peak observed infancy.

For example, using the ratio of BAT/liver FDG uptake on PET-CT, Drubach quantified BAT activation in 172 children with a history of paediatric malignancy (aged from 5.3 to 20.8 years) and stratified this outcome measure by age. The greatest activation was observed in the 13 – 15 year age group), and additional regression modelling (accounting for multiple scans within the same patient) indicated a significant non-linear age-based relationship as summarised in Figure 1.11 (Drubach et al., 2011).

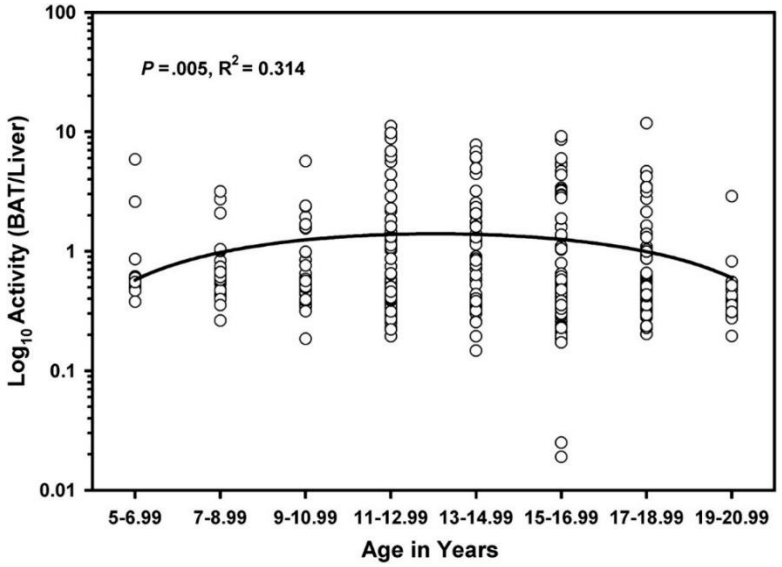



**Figure 1.11 Correlation between BAT activity and age. The best-fit second-order polynomial function is shown (line), which peaked at age 13.0 years.** Reproduced with permission from Drubach et al. 2011 with permission from Elsevier (see Appendix for details).

Similarly, at a different paediatric centre, Gilsanz retrospectively reviewed FDG-PET-CT scans of children aged 4 – 20 years who had been successfully treated for paediatric malignancy but considered disease-free at the time of the scan. Children with FDG uptake suggestive of metabolically active BAT were, on average older than those without (15 years old as compared to 8 – 10 years), as expected, these children were also, taller and more muscular and sexually developed. Moreover, measures of BAT volume in this group were significantly higher during the last two stages of puberty (Tanner stages 4 and 5), findings which persisted even after adjustment for sex, BMI percentile, season and prior corticosteroid treatment (Gilsanz et al., 2012b).

In a similar, but somewhat smaller study, Chalfant et al. reported the average age in children with visualised BAT to also be around 15 years old, those without FDG uptake were on average younger (c.13 years) although, this difference was not found to reach statistical significance. Likewise, Gelfand identified higher uptake grades of FDG uptake in children aged over ten years (Gelfand et al., 2005), indicative of higher BAT activity in the older age group (although the comparative younger group was unbalanced for sex).

Estimation of FF within the supraclavicular region using MRI also indicates that BAT differs between pubertal and pre-pubertal children. Deng et al. compared the FF of the adipose tissue within the supraclavicular fossa between lean and obese healthy volunteer children (aged 9 – 15 years) whilst adjusting for both gender and pubertal status. In support of the PET-CT findings outlined above, pubertal status was found to have a clear effect on FF, T2* and also measures of tissue perfusion derived from

diffusion-weighted MRI (D* and $f_p$), once again signposting pubertal status as a determinant of BAT in early life (Deng et al., 2015).

Only one study, to date, has sought to determine the relationship between age and BAT using FF as a measure of BAT exclusively in infancy and childhood, whilst a strong correlation was observed (r = 0.79) between age and FF in the infant group, no such linear relationship was observed in the group of 39 children (Hu et al., 2013). No further analysis beyond simple linear regression was reported for these children, and the raw data was not shown, so whether an alternative non-linear age-FF relationship was present is unknown.

Taken together, these findings suggest the occurrence of a secondary peak in activity/prevalence in terms of glucose uptake coincident with the time of pubertal onset and/or rapid growth. Evidence from chemical-shift MRI is also accumulating that supports a relationship between age and BAT in early life (Hu et al., 2013, Deng et al., 2015, Franz et al., 2015).

### 1.12.2 Relationship between BAT and sex in early life

The effect of sex on BAT in children is reported frequently (Fukuchi et al., 2003, Drubach et al., 2011, Hu et al., 2011, Deng et al., 2015, Gilsanz et al., 2012b, Gilsanz et al., 2012a, Rockstroh et al., 2015, Cousins et al., 2017, Hui et al., 2017, Brendle et al., 2018, Chalfant et al., 2012, Ponrartana et al., 2012, Gilsanz et al., 2011, Gelfand et al., 2005, Okuyama et al., 2003). However, few studies have been adequately powered to draw firm conclusions from these investigations. Conversely, in adults, it is well

established that, prior to the menopause at least, BAT is more prevalent in females as compared to males (Kim et al., 2008, Brendle et al., 2018, Truong et al., 2004) but, a similar sexual dimorphism has not been observed in children.

However, at the time of writing, only two studies have examined sex as their primary research outcome, each using different methods of BAT assessment, in different age groups (Gilsanz et al., 2012b, Malpique et al., 2018). Some studies have investigated sex as part of their secondary analyses, including sex comparisons of FDG-detected BAT on PET imaging (Drubach et al., 2011, Hu et al., 2011, Gilsanz et al., 2012b, Cousins et al., 2017, Hui et al., 2017, Brendle et al., 2018, Chalfant et al., 2012, Ponrartana et al., 2012, Gilsanz et al., 2012a, Gilsanz et al., 2011, Gelfand et al., 2005); Technetium-99 (Fukuchi et al., 2003) and MIBG (Okuyama et al., 2003) uptake in BAT on scintigraphy; BAT fat fraction, volume and T2* on MRI (Deng et al., 2015, Hui et al., 2017, Ponrartana et al., 2016) and also at tissue level via histology and presence of UCP1 (Rockstroh et al., 2015). The majority of these have found no statistically significant difference between girls and boys. Despite the lack of statistical significance, of 12 studies where the effect of sex has been examined, higher FDG-detected BAT prevalence on PET imaging, lower FF and greater BAT volume on MRI in boys has been observed in 9 of these studies. Furthermore, when multivariate analyses have been undertaken to account for other confounders of BAT activity (Deng et al., 2015, Gilsanz et al., 2012b), this data also suggests higher BAT activity in boys as compared to girls in early life.

A large retrospective analysis of 139 paediatric patients aged 9 – 21 years old was undertaken to ascertain the effects of diazepam premedication and pre-scan warming on reducing FDG uptake in BAT. Although not quite reaching statistical significance ($p = 0.08$), FDG uptake was more frequently observed in boys (30.5%) as compared to girls (17.5%). Furthermore, diazepam was found to be more effective in suppressing FDG uptake in BAT in females, reducing the frequency of BAT uptake in girls by 73% as compared to 44% in boys (Cousins et al., 2017), further evidence indicative of sexual dimorphism in the regulation of BAT during childhood.

### 1.12.3 Relationship between BAT and height, weight and body composition

Whilst a number of studies have endeavoured to determine whether height and/or weight are determinants of BAT prevalence or activity (Gilsanz et al., 2011, Gilsanz et al., 2012a, Gilsanz et al., 2012b, Chalfant et al., 2012, Ponrartana et al., 2012, Hu et al., 2013, Ponrartana et al., 2016, Malpique et al., 2018), at present there is little good evidence to support the existence of any significant independent relationships between these variables and any currently used measures of BAT status. All but one study have considered absolute, rather than standardised, measurements of height and weight. As the majority of these studies involve participants from early childhood into adolescence/young adulthood, considering percentiles, Z scores or standard deviation scores is more appropriate. These measures standardise for age and sex and enable more meaningful comparisons between studies and correlations between variables.

One study reported a positive correlation between BAT volume and absolute weight, and absolute height, a relationship which is likely to merely reflect increasing body size (Ponrartana et al., 2012). The same authors, in a separate study also identified absolute infant length as an independent positive predictor of FF on MRI, suggesting that infants who are longer have less active BAT than those who are shorter (Ponrartana et al., 2016). Given that this study group ranged in age from 0 to 6 months, the apparent effects of length observed here may be heavily confounded by the influence of age and the well-known practical difficulties of obtaining accurate length measurements in non-ambulant children.

Two similar studies examined the relationship between absolute height and weight with FDG-detected BAT on PET imaging (Gilsanz et al., 2011, Gilsanz et al., 2012b). The boys from one cohort who had visible BAT were significantly taller than those without, however, they were also older (Gilsanz et al., 2011), and both boys and girls in the second cohort with visible BAT were also taller, but were noted to be 5 – 6 years older (Gilsanz et al., 2012b). Similar findings were observed with weight in both studies but did not quite reach statistical significance. Nonetheless, these results highlight the importance of standardising for age at the time of measurement or adjusting for its effect during analysis.

The relationship between anthropometric measures standardised for age and sex and BAT to my knowledge has been considered in just one study, in which positive correlations between weight percentile and MRI fat fraction and T2* were identified ($r = 0.59$ and $r = 0.50$ respectively). This suggests that, as weight increases, BAT activity

decreases irrespective of age. Interestingly, this relationship was demonstrated in 39 children aged between 9 – 19 years but was not apparent in the smaller group of infants (Hu et al., 2013).

Many studies have shown a negative relationship between indicators of adiposity and BAT in the adult population, including BMI (Saito et al., 2009, Ouellet et al., 2011, Pfannenberg et al., 2010, Zingaretti et al., 2009, van Marken Lichtenbelt et al., 2009), visceral and subcutaneous adipose tissue volumes (Saito et al., 2009) and total body fat (Saito et al., 2009, van Marken Lichtenbelt et al., 2009). The existence of a relationship between adiposity in children and BAT dysfunction is not quite so clear and is confounded by the difficulties in accurately quantifying adiposity in children.

Absolute BMI is not regarded as a useful measure of body composition in children, although it still referred to (Gilsanz et al., 2011, Zukotynski et al., 2010, Zukotynski et al., 2009), and has been used inappropriately in some recent BAT studies to define obese and healthy weight status (Hui et al., 2017). BMI is often more appropriately presented as percentiles adjusted for age and sex, although, as previously discussed in section 1.2, BMI percentiles are not derived from a single source of reference data, and thresholds for lean, overweight and obesity can be variable. Therefore comparing studies using such classifications must be undertaken with caution, and BMI percentiles should be interpreted in the context of their reference population.

At the time of writing, there is no published data reporting evidence for the existence of a significant relationship between BMI percentile and FDG-detected BAT prevalence

of BAT activity on PET imaging in children or adolescents. The most comprehensive assessment of adiposity and BAT in children was made in 2018; visceral adiposity, subcutaneous adiposity and ectopic deposition of fat within the liver were determined from CT and compared to FDG-detected BAT prevalence. This study failed to identify a significant relationship between BAT and any measures of adiposity; however, these measures were not standardised for age or body size, given that these children ranged from 5 – 17 years such an omission makes these conclusions less reliable (Brendle et al., 2018).

Drubach et al. identified a weak negative correlation (r = -0.3) between BAT activity (derived from PET imaging using a ratio of BAT: liver FDG uptake in children) and BMI percentile (Drubach et al., 2011), and Rockstroh et al. (2015) reported UCP1 positive adipocytes in 10.3% of samples from lean children, but complete absence of UCP1 in the adipose tissue samples from overweight and obese children (Rockstroh et al., 2015). Fat-fraction and T2* in supraclavicular BAT on MRI are higher in obese as compared to lean children, indicative of less active BAT with increased white adiposity (Deng et al., 2015, Hu et al., 2013), (Drubach et al., 2011). A positive linear relationship between adiposity and cervical-supraclavicular-axillary FF (indicative of rising BAT activity with increasing leanness) was recently reported in children (Andersson et al., 2019).

It is of note that an analogous MR study comparing lean and obese children did not find similar differences. Whilst, T2* was similarly higher in the obese group, both fat fraction and BAT volume were not (Hui et al., 2017). However, obesity was defined as

an absolute BMI greater than 25 in a study population aged between 10 and 25 years. Review of the RCPCH BMI growth charts used in the UK (RCPCH, 2013) highlights the inaccuracies of such a definition in children. For example, a male child of 10 years old with an absolute BMI of 19.5 to 22 is considered overweight, and it is therefore possible that children included in the healthy weight group for this study may have been overweight or obese. Using BMI percentile, not absolute BMI should be the gold standard in growing individuals.

The negative relationship between adiposity and BAT prevalence observed in the adult literature has been used to support the hypothesis that BAT dysfunction may predispose to obesity. Consequently, it has been proposed that activation of dysfunctional BAT may be utilised as a therapeutic strategy, improving glucose and lipid clearance and avoiding the detrimental, excessive deposition of WAT associated with obesity (Chondronikola et al., 2014). If this relationship is causal, one may expect that BAT dysfunction would predate clinically apparent obesity and may predict long term excessive adiposity.

As yet there is no evidence to say that BAT status in childhood is linked to later body composition, and there are no studies that have defined BAT status and followed changes in body composition over time in healthy childhood or adolescence. There is, however, one small study that suggests BAT status may predict longitudinal weight gain and fat deposition. A small group of children with no visible BAT on FDG-PET imaging at diagnosis (undertaken for oncological investigation) were followed up with a repeat PET scan after 4 – 5 months. Those with visible BAT at follow up gained less

weight, less visceral and less subcutaneous WAT than those who remained devoid of FDG-detected BAT (Chalfant et al., 2012).

The discrepancy between the findings of the PET-based versus MRI based assessment of BAT may in part relate to the distinct populations' studied with each method. Those undergoing PET imaging were predominantly those with a history of underlying malignant pathology, while the children undergoing MRI were more frequently healthy volunteers.

### 1.12.4 The effect of ambient temperature and pre-PET scan warming measures

FDG-detected supraclavicular BAT in children is responsive to small changes in ambient temperature. For example, Zukotynski et al. demonstrated a significant reduction in FDG uptake in two separate studies of children/adolescents undergoing PET-CT for clinical purposes (oncological investigation). When subjects were maintained at 24˚C for 30 minutes pre FDG dosing, and a further hour during the uptake phase, FDG uptake was reduced to 5% (Zukotynski et al., 2009) and 9% (Zukotynski et al., 2010) respectively, as compared to around 30% when ambient temperature was maintained at 21˚C. Interestingly, in the first study, the children who demonstrated significant FDG uptake despite pre-scan warming were imaged on days when the outdoor temperature was below freezing (Zukotynski et al., 2009). Furthermore, this effect of pre-scan warming was greater in the winter months as compared to the rest of the year, presumably due to exposure to colder outdoor temperatures prior to the scans (Zukotynski et al., 2010).

These findings are similar to those observed in adults (Garcia et al., 2010, Garcia et al., 2006, Christensen et al., 2006, Skillen et al., 2012). Data from adult cohorts have also demonstrated that FDG-uptake in BAT can be affected by ambient temperature in the hours and days preceding FDG dosing (Kim et al., 2008) and, additional warming procedures (such as avoiding air conditioning, using the car heater and wearing warms long sleeved/trousered clothes on the day of scan) can reduce FDG uptake in BAT even more (Skillen et al., 2012). Many of these measures, in addition to environmental temperature control in the clinical setting are now recommended in clinical practice to reduce false positives or obscuration of the metabolically active tissue of clinical interest (Stauss et al., 2008, Surasi et al., 2014).

This suggests that the effects of ambient temperature on glucose uptake in BAT in adults may last for hours or even days (Kim et al., 2008), though the effect of pre-warming measures in children, and the time course of the BAT response to changes in ambient room temperature specifically in infants, children or adolescents is yet to be reported.

### 1.12.5 The effect of season and outdoor temperature

The highest prevalence of BAT in adults throughout the year (in the northern hemisphere) using FDG uptake occurs between November and March, when outdoor temperatures are at their lowest (i.e. the winter season) (Cohade et al., 2003, Au-Yong et al., 2009, Cypess et al., 2009). A seasonal effect on BAT is also present in children and adolescents, with the highest supraclavicular FDG uptake observed most frequently during the winter (Gilsanz et al., 2012a, Gilsanz et al., 2012b, Chalfant et

al., 2012, Hu et al., 2011) but has also been reported in the summer (Zukotynski et al., 2010).

Where warming prior to scan has been used as a means of reducing unwanted FDG uptake in clinical scans, this has been found to be more effective during winter. An increase in injection room temperature from 21˚C to 24˚C during the winter achieved a reduction of unwanted FDG uptake in BAT from 28% to 3% of scans (Zukotynski et al., 2010). Despite the evidence for a strong effect of indoor temperature on BAT activity, there are no studies that have specifically examined the relationship between outdoor temperature and FDG uptake in BAT in infants, children or adolescents. Although there is some recent data from adults to suggest that outdoor temperature is negatively correlated with BAT prevalence (Huang et al., 2012), BAT mass and also glucose uptake within the tissue itself (Ouellet et al., 2011).

### 1.12.6 The impact of sedation, anxiolytics, opiates and anaesthesia

Even before the use of PET and MRI for BAT assessment, functional impairment of NST was observed during paediatric anaesthesia with fentanyl and propofol, indicative of BAT dysfunction (Plattner et al., 1997). Opiates have been shown to significantly reduce the uptake of FDG in BAT in both children and adolescents when administered before imaging (Gelfand et al., 2005). The benzodiazepine diazepam, when used in high dose is also effective in suppressing FDG uptake in BAT (Gelfand et al., 2005), particularly in young girls when used in conjunction with pre-scan warming measures (Cousins et al., 2017).

The mechanisms underlying suppression of BAT by benzodiazepines and opiates is unknown but may involve their central anxiolytic effects on the sympathetic nervous system. Moreover, benzodiazepine receptors have been found in small quantities in rodent interscapular BAT (Gonzalez Solveyra et al., 1988, Hirsch, 1984), though this has not yet been reported in humans. Propranolol has been widely used in adults to reduce FDG uptake in BAT (Parysow et al., 2007, Soderlund et al., 2007), by blockade of β-adrenoreceptors within BAT. To the best of my knowledge at this time, such an effect in young children has not been explored, but administration of propanolol to a small group of adolescents indicates suppression of FDG uptake in BAT.

### 1.12.7 BAT function during childhood ill-health

A large proportion of BAT studies in childhood have utilised the PET scans of children undergoing the diagnosis, treatment or follow-up from malignancy. Children with active malignant disease are unlikely to have normal metabolic physiology, and it is well established that many cancers can have direct and indirect secondary effects on metabolic health (Green et al., 2008, Tisdale, 1997, Picton, 1998, Stallings et al., 1989, Kien and Camitta, 1987).

Three small studies of disease status and BAT activity report conflicting outcomes, Bianchi et al. compared BAT excised from the peri-renal adipose tissue depot in a small number of children undergoing surgery for malignant and non-malignant disease. BAT activity, quantified as the binding of GDP was higher in the group with malignant disease by over three-fold (Bianchi et al., 1989).

In contrast, FDG-detected BAT was identified less frequently in children with active lymphoma, as compared to the same children when considered disease-free. Following successful treatment (regimen details not specified), children were almost ten times more likely to be defined as having BAT visible, with FDG uptake seen on almost 80% of scans at disease-free follow-up. Even after adjustment for BMI percentile and season, disease status remained a significant predictor of BAT status, and although at follow-up these children were older and heavier, addition of age and weight to their multivariate model made no statistical difference these results (Gilsanz et al., 2012a).

Similar findings were also reported at disease-free follow-up in a separate group of children who had no evidence of metabolically active BAT at the time of their cancer diagnosis. Once defined cancer free, 19 of the 32 children demonstrated significant BAT activity of FDG PET-CT (Chalfant et al., 2012). Whether these findings represent suppression of FDG uptake BAT by lymphoma/malignancy, or enhanced capacity of BAT for glucose uptake following treatment, is not known and few other studies have sought to assess BAT in a disease free, or healthy population for comparison.

The conflicting findings of these studies may be due to the differential effect of specific malignant diseases or may be due to the effects of the specific cancer treatments rather than underlying disease pathology. To date, only the role of glucocorticoids in the treatment of paediatric lymphoma has been investigated, with two studies concluding no effect on BAT prevalence in children (Chalfant et al., 2012, Gilsanz et al., 2012a). The number of participants in these studies were small, and despite the

authors' supposition that there was no difference in BAT depiction following corticosteroid administration, their p value was close to significance at 0.06. The wider evidence for the influence role of glucocorticoids on BAT homeostasis is also inconsistent. Whilst some investigators propose an inhibitory role (Barclay et al., 2015, Thuzar et al., 2018) more recent human based investigations suggest the reverse (Scotney et al., 2017, Robinson et al., 2016, Ramage et al., 2016).

Treatment regimens for the common childhood cancers such as leukaemia, lymphoma and solid tumours are aggressive, comprising a combination of multiple cycles of chemotherapy, radiotherapy, surgery and/or high dose steroids. Outcomes following treatment in childhood are improving, and tend to be better than those observed in adulthood. However, long-term effects of these regimens are being increasingly recognised, for example, subfertility following radiation in the lower abdomen, pelvis or testis, or chemotherapy (Brougham and Wallace, 2005). Effects on the neuroendocrine axis following chemo-radiation resulting abnormalities in growth, hormone production (Nandagopal et al., 2008) and puberty (Cicognani et al., 2003), and cardiotoxicity of anthracycline-based chemotherapy regimes (Steinherz et al., 1991). The long term effects on metabolic health and specifically BAT development in humans are unknown and require further investigation.

Another interesting patient group recently examined for BAT are neonates born following hypoxia. Therapeutic cooling is now considered an effective treatment following perinatal hypoxic brain injury, reducing the incidence of death and neurodisability (Rutherford et al., 2010, Azzopardi et al., 2014). A recent study

compared BAT in a group of infants requiring therapeutic cooling following moderate to severe hypoxic ischaemic encephalopathy with a term healthy group born without evidence of significant hypoxia. After 48 hours of cooling to a rectal temperature of 33 – 34˚C, infants in the hypoxic ischaemic encephalopathy-cooled group had lipid depleted supraclavicular adipose tissue on water-fat MRI. Both supraclavicular FF and supraclavicular BAT volume were found to be reduced as compared to the same anatomical depot in healthy controls. In addition, little effect was observed in subcutaneous adipose tissue suggestive of a BAT specific effect (Hu et al., 2014).

This study was not able to determine whether lipid depletion was a reflection of prior BAT activation induced by therapeutic hypothermia/hypoxia or was indicative of ongoing increased BAT metabolic activity. Whether there are long term and possibly permanent effects on BAT development, metabolism and body composition for these children is unclear.

**1.13 Aims and hypotheses**

The literature regarding BAT development and function in early life is lacking. The majority of data on BAT in children are derived from retrospective clinically indicated studies using glucose uptake on static FDG-PET-CT as a marker of BAT activity, volume or prevalence, with their inherent limitations which should not be disregarded. Whilst these studies signpost towards some of the possible determinants of BAT physiology in early life. Given the possible confounding effects of underlying pathology and treatment, variations in environmental conditions at the time of assessment, the lack of standardisation in the protocols for FDG-PET-CT and repeated reporting on the

same children; robust conclusions cannot be drawn from this literature. Furthermore, review of this literature raises many unanswered questions, some of which will be further investigated in the studies presented in this thesis.

The main aims of this thesis are

Using the temperature of the skin overlying supraclavicular BAT as a proxy measure of BAT thermogenic activity:

i) to determine whether age, sex, BMI percentile, season or ambient room temperature are determinants of BAT activity in young children (Chapter 3)

ii) to evaluate the impact of dietary intake, physical activity and eating behaviour on supraclavicular skin temperature and the thermogenic response to cold exposure in young children (Chapter 3)

iii) to assess the feasibility of using infrared thermography in young children and develop a cooling protocol suitable for use in this population that would optimise detection of the cold-induced thermal response (Chapters 3 to 5).

The experimental studies described in this thesis are presented as “published works”, each study is described in context to the specific thesis aims in the relevant chapter preface and conclusion. Study hypotheses are outlined in the relevant preface and manuscript. Whilst the published papers are included in journal format in the Appendix, for clarity, consistency of terminology and accuracy, the manuscripts are presented in thesis format in each chapter. For clarity of later discussion figures and

tables (including the online journal content) have been re-numbered sequentially and annotated according to location rather than the numbering assigned at the time of publication. Data considered informative or important but not included in the final publication due to the constraints of journal space are included in the relevant Appendix for each study.

# CHAPTER TWO

## General materials and methods

## 2.1 Overview of studies

Five studies are presented in this thesis. In each study, supraclavicular skin temperature was evaluated using infrared thermography. This measurement was used as a proxy measure of BAT activity. Studies I, II, IV and V aimed to activate BAT with active localised cooling. Study III sought to stimulate BAT with mild psychological stress. The experimental protocols for each study are summarised in the associated manuscript in Chapters three, four and five and a detailed description of the materials and methods for each of the measurements taken throughout these protocols, as well as the statistical analyses and safety precautions for each study, are outlined below in Chapter two.

## 2.2 Ethical approval

All Studies (I to V) were reviewed and approved by the University of Nottingham Medical School Ethics Committee, and conformed to the Declaration of Helsinki 2008.

In Studies I and II participants were recruited from local primary schools, and the purpose and nature of the studies were explained to parents by way of an information leaflet, plus a verbal explanation by a study investigator if requested. Written consent was obtained from parents/carers, and additional verbal assent was received from the child on the day of the study. Any child who was unable to give verbal assent, or did not want to participate, was not required to take part in the study. Nevertheless, all children whose parents had given consent also agreed to take part in the study. Parents and children were aware that they could withdraw at any stage, and that all

information regarding their participation would be held anonymously and kept confidential.

In Studies III to V young adult participants were recruited via poster advertisements placed around the Nottingham University Campuses. A full explanation of the nature of the study and the procedures required was given to each participant at least 24 hours prior to the first study session, in addition to a study information leaflet. Subjects who participated in Study III were offered a small inconvenience allowance of £15 to compensate for their time and travel. All participants were aware that they could withdraw at any time.

**2.3 Participants**

The volunteers in Studies I and II were young children, of primary school age (6 – 11 years). No details were requested regarding their health, medications or metabolic status.

The volunteers in all other studies were non-obese healthy, Caucasian men and/or women who were students or staff at the University of Nottingham. A short medical history was taken from each participant to ensure they were not suffering from any medical condition that would preclude them from taking part in the study (e.g. diabetes, Raynaud's, pregnancy), or taking any prescribed or recreational medication that would affect BAT activity.

## 2.4 Cooling protocols

### 2.4.1 Acclimatisation and clothing

The adult participants in Studies III to V undertook a formal period of acclimatisation with a period of rest in standardised clothing (as detailed in the individual chapters) for at least 30 minutes, either laying semi-supine on an examination couch (Study V), hospital bed (Study IV) or seated in a chair (Study III). This period was to allow the supraclavicular skin temperature to stabilise, assessment of supraclavicular skin temperature was not possible in contemporaneous real-time using the thermographic equipment available at the time of these studies.

Previous pilot data from a co-supervised BMedSci research project had shown that supraclavicular temperature was highly variable in the period immediately after removing clothes and during the transition from natural, spontaneous movement to sitting immobile. However, the precise magnitude of this variability and its effect on subsequent BAT activation was not evident until the completion of the studies presented within this thesis. The role of the acclimatisation period upon subsequent cold-induced changes in supraclavicular skin temperature has been subsequently formally studied as part of another PhD student research project that ran from 2016 to 2019, in that project, A. Lazaridi determined that in healthy adult volunteers a 30 minute rest period was superior to 5 minutes, and resulted in a significantly lower baseline measurement and had greater sensitivity to detect a rise in supraclavicular skin temperature after cold stimulation, although the variability within this period was not explicitly reported (Lazaridi, 2019). Although the supraclavicular region have not been explicitly examined by these authors, it is noted that Ring and Ammer (2000)

recommend a minimum of 10 minutes prior to thermography of human skin, and Morins et al reported that the time to reach stability in skin temperature is dependent on the region studied, and is also different in men and women. They concluded that for whole-body imaging a minimum of 10 minutes was considered acceptable (Marins et al., 2014, Marins et al., 2015)

Due to the constraints of time within the school day, a formal acclimatisation period was not undertaken prior to the acquisition of baseline measurements in Study I and Study II. However, all children were present in the imaging room wearing a cotton vest for around 10 – 15 minutes prior to the start of imaging (i.e. time taken to check consent, set up equipment and explain the procedure to the child).

In Studies I and II, the clothing worn during thermal imaging was not wholly standardised due to the requirements outlined in the study ethics. Children were not allowed to dress or undress with the research team. Instead, they were asked to remove their school shirt in the classroom with the supervision of their class teacher and change this for a standardised cotton study vest provided by the research team. This was worn alongside the school uniform they attended in that day. 'School uniform' was variable and included trousers, jogging bottoms, skirts or shorts of varying fabric weight.

In Studies III to V, in an empty room, or behind privacy screens, the young adult volunteers were asked to change into standardised clothing. In Study III and Study IV, this consisted of a set of surgical scrubs, with a short-sleeved cotton top, and

drawstring full-length cotton trousers, but in Study V the short-sleeved top was replaced with a sleeveless cotton vest to allow easy access for blood-pressure monitoring. Participants were asked to keep their underwear and socks in place. The insulative effect of this clothing was estimated to be 0.35 and 0.31 Clo, respectively.

### 2.4.2 Ambient room temperature

Only Study IV was undertaken in a temperature-controlled laboratory (Blood Flow Laboratory E6, University of Nottingham Medical School), set at either 23˚C or 18˚C. Given its location within a large heated hospital setting the ambient room temperature in the Academic Child Health Imaging Suite on B floor (Study V) and E floor (Study III) were reasonably stable, but not amenable to manipulation. Room temperature was recorded and documented at the start of each imaging session for all studies with the Extech Moisture Meter MO297 (Extech Instruments).

There was no facility to control the ambient room temperature within the school environment. Therefore the conditions for Studies I and II were variable. Given the recommendations of Ammer and Ring (Ammer and Ring, 2013), only children who were imaged at a room temperature above 20˚C were included in the studies of BAT presented in this thesis. These authors suggest that for most clinical applications, a range of 18 – 25˚C is adequate for thermography. Similarly Quesada et al recommend an ambient temperature of 18 – 26˚C at a humidity of around 60% for the reliable assessment of human skin temperature (Quesada et al., 2017). However, as there are no specific recommendations for thermography of BAT in children, and given the findings of Study IV, an arbitrary threshold of 20˚C was chosen for Study II.

### 2.4.3 Hand cooling

In Studies I, II and IV, single hand immersion in cool tap water was used as a mild cold stimulus to activate BAT. This methodology was used in the initial work undertaken within the Division of Child Health, Obstetrics and Gynaecology (COG), University of Nottingham and preceded the studies presented in this thesis (Symonds et al., 2012a). In this thesis, this cooling protocol was reproduced with a few modifications to optimise image acquisition and reproducibility. To avoid excess movement during the acquisition of thermal images, participants were asked to place their left hand in a small empty bucket (radius: 12 cm, capacity c.6 – 10 L), and the bucket was placed at a height that meant the hand was placed comfortably inside without touching the bottom or sides. To institute cooling, water at c.20˚ ± 0.1˚C from a second bucket was poured gently over the hand into the empty bucket until the water was at the level of the ulnar styloid prominence.

The temperature of the water used for Study I was determined by the availability of tap water in the first school we visited. The coldest water that could be obtained in the room allocated to us was 20.1˚C. Therefore this temperature was used throughout Studies I and II. Once fully covered by water, the left hand was immersed for a total of 5 minutes. To confirm the effect of cooling, the temperature of the hand was assessed by IRT both at baseline and immediately after the hand was removed from the water. The temperature of the skin on the dorsal aspect of the hand dropped by a mean (SD) of 8.41 ± 1.99˚C in Study I, and by a mean (SEM) of 8.85 ± 0.3˚C and 8.0 ± 0.57˚C in the boys and girls (respectively) taking part in Study II. There were no complaints of discomfort during hand immersion.

### 2.4.4 Prolonged hand cooling

In Study IV, an extended period of hand cooling (30 minutes) was used to determine the time course of the BAT response to mild cold in the context of changes in energy expenditure and ambient temperature. The cooling procedure outlined above, where the left hand was immersed in cool water to the level of the ulnar styloid, was used. Preceding feasibility studies identified that the temperature of the water rose significantly with prolonged immersion, due to the heat extracted from the hand by the water. Therefore, to maintain the magnitude of the cold stimulus, in Study IV the water temperature was checked every 5 minutes, and if it had risen by more than 0.2˚C ice water was added in small aliquots (c. 50 – 100ml) until the overall water temperature had returned to 20˚C. The water level (at the ulnar styloid prominence) was also maintained by the removal of water volumes equal to that added using a 200ml beaker. Participants were encouraged to report discomfort during cooling, although this did not occur.

### 2.4.5 Forearm cooling with the Blanketrol® II

In Study V, to achieve a more consistent and maintained cool stimulus, cooling of the whole forearm was achieved using the Blanketrol® II unit attached to a 12.5 by 18 inch cooling blanket (Maxi-Therm Lite® Infant) with the Manual Control Mode set to 14˚C. This is a cooling unit filled with sterile/distilled water and circulating water flows over the cooling element within the reservoir. The cooled water then flows through the connecting hoses over a temperature sensor and into a water-perfused blanket. After circulating through the blanket, water is returned back to the unit and then back to the reservoir to be re-cooled.

The Blanketrol® II was used in line with the manufacturer's instructions for Manual Control Mode. In brief, the unit was filled with water to the level of the strainer at the bottom of the water-fill opening. The blanket was connected to one return and one outlet. With the power off, and the blanket lying flat on the examination couch a System Test routine was conducted to ensure the blanket and machine were functioning correctly prior to being attached to the subject. With the machine off, and all jewellery removed, the blanket was wrapped circumferentially around the participants left forearm. The fingers distal to the interphalangeal joints were left exposed to allow continuous inspection of skin colour and integrity throughout active cooling. The blanket was held in place with light pressure from a circumferentially wrapped crepe bandage. Care was made to ensure that this was not so tight as to restrict blood flow, but tight enough to maintain contact between the skin and the blanket. Tympanic membrane temperature was checked every 10 minutes during active cooling, and core temperature did not drop below 36˚C in any participant. Participants were asked to report any discomfort during cooling (but there were no such complaints). The temperatures of the dorsal aspect of the arm and hand were measured at the end of cooling using thermography.

### 2.5 Mild mental stress protocol

#### 2.5.1 Mental arithmetic test

In Study III, participants were asked to complete a short mental arithmetic (MA) task. This test has previously been shown to result in mild psychological stress (Memon et al., 2013) and consisted of 20 simple two-step arithmetic questions (e.g. 52+5−18 =?) presented on PowerPoint slides on a personal computer in front of the participant.

Each question was to be answered within 6 seconds and was immediately followed by the next question (dictated by the slide transition time). Participants were told that the test was easy and that it was expected that they would get most of the answers correct. They were asked to say their answers out loud, and the study investigator immediately communicated whether their answer was correct or incorrect. When two questions were correctly answered in succession, the subject was told that the next answer was incorrect irrespective of the answer given. This test has previously and successfully been used to elicit mild psychological stress, demonstrating increases in systolic blood pressure and heart rate in line with sympathetic stimulation (Memon et al., 2013).

### 2.5.2 Corresponding control period

The participants in Study III also undertook testing on a subsequent day. During this session, participants watched a 2 minute relaxation video (raindrops on a window) on the same personal computer in place of the MA test.

### 2.5.3 Measurement of salivary cortisol

Cortisol was used as a biological marker of a stress reaction. During a stress reaction, the hypothalamic-pituitary-adrenal (HPA) axis activity is increased, the stressor activates corticotrophin-releasing hormone and vasopressin secretion, and these hormones stimulate the pituitary gland to release adrenocorticotrophic hormone (ACTH), which, in turn, stimulates secretion of cortisol from the adrenals. Most cortisol within the plasma is bound to binding proteins, and just 3 – 5% remains free and metabolically active. Unlike blood cortisol, salivary cortisol levels reflect the

biologically active component and salivary cortisol correlates highly with free cortisol in the plasma. Salivary sampling avoids the stress reaction associated with venepuncture and blood sampling and is considered a simple, safe and non-invasive method (Hanrahan et al., 2006, Keil, 2012).

Cortisol increases at times of acute stress (Dickerson and Kemeny, 2004), and the salivary cortisol response to the MA test was used in Study III to assess the effectiveness of the test beyond that of a cardiovascular response (Memon et al., 2013). Saliva samples were obtained using Salivettes® and analysed using the Salimetrics salivary cortisol ELISA kit. In brief, each sample was collected with a SalivBio Oral Swab (Salimetrics; Starstedt, Leicester, UK) , which is a synthetic swab specifically designed to improve volume collection and increase participant compliance, and it is also validated for use with salivary cortisol. Participants removed the swab from the collection tube and placed it in their mouth. The swab was chewed for 2 minutes until it was saturated, and then it was placed into the basket within the collection tube which was then sealed with a lid. All samples were labelled with an anonymous identifier and sample time and stored on ice until the end of the study session. Samples were then stored in an upright position at −80˚C pending analysis. Participants rinsed their mouths with a small amount of water immediately after sample collection, in preparation for subsequent sampling. No samples were visibly contaminated with blood, and a blood contamination kit was not used.

Analysis of the saliva sample was undertaken using the Salimetrics expanded-range, high-sensitivity salivary cortisol enzyme immunoassay kit as per the manufacturer's

instructions. This assay is a competitive immunoassay kit. Cortisol in the study samples and the kit standards compete with cortisol conjugated to horseradish peroxidase for the antibody binding sites on the microtitre plate. Bound cortisol is measured by the reaction of the horseradish peroxidase to the substrate tetramethylbenzidine (TMB), which gives a blue colour. Once the reaction is stopped with an acidic solution, a yellow colour forms. The optical density is read on a standard plate reader at 450nm. The amount of cortisol present in the sample is inversely proportional to the detection of the cortisol-enzyme conjugate.

Once samples had been collected from the whole study group, the swabs were thawed on ice, vortexed and centrifuged at 1500 x g for 15 minutes to remove mucins and particular matter that may interfere with the assay. All samples were processed on the same day and were subjected to the same number of freeze-thaw cycles. Reagents were prepared according to the kit protocol. Twenty-four µl of standards, control and saliva, were added to the appropriate wells, 25 µl of Assay Diluent was also added to two wells to serve as a zero, and into each non-specific binding well. Then 200 µl of dilute enzyme conjugate was added to each well and mixed on a plate rotator for 5 minutes at 500 rpm. After incubation at room temperature for 1 hour, the plate was washed four times with 1X wash buffer, after each wash, the plate was blotted on paper towel. 200 µl of TMB substrate solution was then added to each well, mixed at 500rpm for 5 minutes and incubated in the dark for 25 minutes. 50 µl of stop solution was added to each well, after mixing for 3 minutes (500 rpm). The plate was immediately read at 450 nm on a plate reader (Benchmark Microplate Reader, BioRad, Hercules, California, USA). The concentrations of the saliva samples and standards

were determined using a four-parameter non-linear regression curve fit using Microplate Manager Software, Biorad, Hercules, California, USA. The overall intra-assay coefficient of variation was < 10%.

**2.6 Infrared thermography**

The electromagnetic spectrum is composed of electromagnetic radiation waves and is often presented in order of wavelength, from longest to shortest. Only a small portion of the spectrum is visible as light (between 390 – 700 nm). Between microwaves and visible light are infrared (IR) waves, these are further classified as near (1.0 – 5 μm), middle (8 – 25 μm) or far-infrared (wavelength of 25 – 1000 μm). Far infrared waves are furthest away from visible light, are thermal and give off heat. All objects that are not at absolute zero (absolute zero is the temperature where all molecular motion ceases and corresponds to −273 Celsius or −460 Fahrenheit or zero degrees Kelvin) emit infrared radiation. Any object with a temperature emits infrared radiation, and thermography can be used to detect this.

A blackbody is a theoretical object that emits a maximum amount of energy at all temperatures in all wavelengths, it is a perfect emitter and a perfect absorber. There are three main laws that concern infrared radiation. These are based on the performance of the blackbody.

i) The Stefan-Boltzmann law defines the formula to determine the amount of energy emitted by an object due to its absolute temperature. The amount

of energy radiated by an object is proportional to the object's temperature in Kelvin raised to the $4^{th}$ power.

Where:

$$\text{Total amount of radiated energy} = 5.67 \times 10^{-8} \times T^4$$

$5.67 \times 10^{-8}$ is the Stefan-Boltzmann constant
T is temperature in Kelvin degrees

ii) Wien's law determines the wavelength at which a maximum amount of energy is emitted by an object at any specific temperature. As most objects emit many wavelengths, this law is useful in thermography to help decide which wavelength device should be selected for maximum accuracy.

Where:

$$\lambda \text{ max} = 2898 / \text{T.Kelvin}$$

When using thermography to detect skin temperature, temperatures often lie between 33 to 37˚C, so λ max is therefore c.9 microns, such that a long wave camera (8 – 15 microns) is the most accurate.

iii) Planck's law describes the relationship between temperature, radiated energy and wavelength. The law is complex and a full explanation is beyond the scope of this thesis; however, it forms the basis of how temperature values are obtained from measurements of infrared radiation from a thermal camera.

The infrared camera not only senses radiant energy emitted directly from an object due to its temperature, but also the energy reflected off the object from its background and the energy transmitted through the object of interest from behind. Although most objects (assuming they are thermally opaque) have no transmission, most do reflect significant amounts of radiant energy. Modern cameras allow for this during the camera set-up and require the operator to input a value for background reflected temperature.

One further property that must be considered during thermography is emissivity. This is the rate at which an object emits energy compared to that of a blackbody at a given temperature and wavelength. The thermal properties of an object can only be assessed during thermography if the emissivity of the object is known. Emissivity is determined by an object's material composition, surface (c. 0.025 mm) condition, temperature, the wavelength it is viewed at and the geometry of the area that is viewed. Emissivity may be measured using a thermal camera or may be determined from published emissivity charts. The emissivity of human skin is 0.98 and is one of the highest natural emitters; therefore, for all the work undertaken in the studies presented in this thesis, emissivity was set at 0.98. In contrast aluminium foil, one of the lowest emitters (emissivity of 0.04) was used during camera set-up to calculate reflected background radiant energy.

A microprocessor within the thermal camera uses the Stefan-Boltzmann formula and Planck's law to calculate the temperature of an object from the radiant energy emitted

from the immediate surface of the object, producing a two-dimensional map of the three-dimensional temperature distribution (Jones and Plassmann, 2002)

There has been rapid development in infrared detection technology since the 1970s; for example, the original single-detector systems have been replaced by large arrays of detectors, which are usually uncooled focal plane arrays (FPA). These arrays come in various sizes with different numbers of detectors, the more detectors the greater the thermal resolution. The radiometric camera used in the Division of COG for the University of Nottingham's early work (the FLIR B60) had a FPA of 180 x 180, generating images with a thermal resolution of 32,400 pixels. The more recent cameras used in Studies I to V, the FLIR B425 and FLIR E60 have a FPA size of 320 x 240, with more than twice the number of detectors and much greater resolution. The camera in use for BAT assessment at the time of thesis submission has a thermal resolution of 161,472 pixels, with a resolution almost five times that of the FLIR B60.

Detected radiant energy is converted to a false-colour image within the camera for immediate viewing, or in the post-processing software as thermograms. These thermograms can then be analysed qualitatively by looking at thermal patterns, or quantitatively to determine the temperature of specific regions of interest (ROI). The quality of the thermal image is integral to accurate quantitative analysis and is dependent on ensuring that all the required parameters are set correctly and consistently (e.g. emissivity, reflected temperature, ambient temperature and humidity) and that the image is focussed adequately on the ROI (Tattersall, 2016, Ring et al., 2004).

### 2.6.1 Acquisition of thermal images

The procedures used in Studies I to V for thermal image acquisition were based upon the Standard Procedures for Infrared Imaging (Ammer and Ring, 2013) and the recommendations of the Glamorgan Protocol (Ammer, 2008) alongside the procedure developed within the Division of COG, the University of Nottingham prior to the start of my studies.

Neither of the documents referred to above discusses imaging of the supraclavicular region. However, the recommendations for subject preparation, imaging environment and camera set-up were followed where feasible and appropriate with the aim of keeping the variability to a minimum.

Two thermal cameras were used in the studies outlined in this thesis, the FLIR B425 and the FLIR E60, and some preliminary work was undertaken using the FLIR B60. All cameras were set up and used as per manufacturer's instructions and following the specific camera user guide.

In brief, the camera was mounted upon a tripod and connected to a power supply (either battery, or mains depending on availability and environmental circumstances), turned on, and the lens cap removed. Care was taken to ensure that imaging was undertaken away from any other source of infrared radiation or airflow. The camera was left on for a minimum of 30 minutes before any images were taken as the failure to do so can result in normal detector noise during imaging, and significant detector drift with subsequent non-uniformity correction (Quesada et al., 2017, Tattersall,

2016). The camera was placed in 'Auto Mode' to determine the upper and lower temperature values used on the camera display. The image was reviewed to ensure that no pixels within the supraclavicular region were black or white and that the overall image of the participant was made up of at least 90% of the colours in the active palette. Imaging was undertaken in all studies in a rainbow palette. The camera was focussed manually (FLIR B425 by using the focus up and down buttons, and the E60 by using the manual rotation of the focus ring) to ensure that the line of the contour of the shoulder was sharp and details of the eyelashes were visible. Whilst the FLIR B425 had the option of an automatic focus, this was not used alone to focus the camera as it could not be relied upon to produce an image with optimal detail in both the left and right supraclavicular regions. It is also of note that the manual control of the focus ring on the E60 was much easier than the up/down buttons of the FLIR B425 and could be undertaken without as much movement of the camera. During sessions of prolonged imaging, the focus was noted to drift with both cameras, images were checked periodically, and the focus was adjusted as needed; this was more evident on the FLIR B425, especially when images were taken using the automatic capture feature.

The angle at which the camera is placed can affect the amount of radiant energy visible to the sensor and can consequently affect the temperature calculations. The maximum amount of energy detected by the sensor occurs when positioned perpendicularly to the surface of interest. Given the morphology of the supraclavicular region as a three-dimensional structure, optimal positioning of the camera in relation to the supraclavicular region was not immediately apparent and has since been

debated (Law et al., 2017). For my studies, the camera was placed with the lens at the level of, and perpendicular to, the sternal notch. The thermograms, therefore, encompassed the neck and whole upper thorax. As the angle between the lens and the ROI becomes smaller than 90˚ the amount of radiated energy captured decreases, however, it is generally accepted that an accurate quantitative temperature calculation can be obtained when the thermal camera is within 45˚ either side of the perpendicular.

Positioning the camera lens perpendicularly to the sternal notch enabled simultaneous imaging of the left and right posterior triangles of the neck, the area in which Bonnot (1908) described the location and anatomy of supraclavicular BAT (Figure 1.7) and encompassing the triangular hotspot observed by Symonds et al (2012a) and Lee et al (2011) as demonstrated in Figure 2.1.

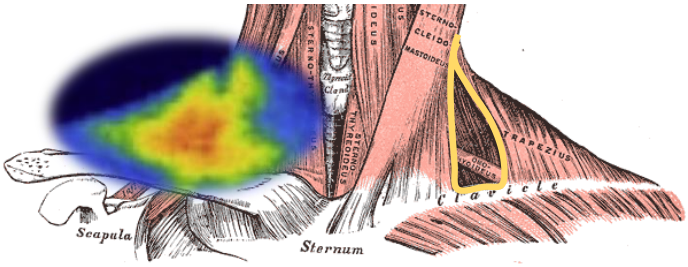



**Figure 2.1 The left posterior triangle of the neck**. Bound by the clavicle inferiorly, and by the anterior border of the sternocleidomastoid muscle and posterior border of the trapezius superiorly (indicated by the orange line). Image reproduced from Grays Anatomy plate number 386 (no longer under copyright) with the right supraclavicular hotspot reproduced from Figure 4.D in Symonds et al (2012a) superimposed (with permission; see Appendix for details).

To maximise the resolution/number of pixels in the supraclavicular region, the camera was placed so that the field of view encompassed the full width of the upper torso, so that the shoulder-to-shoulder width was at least two-thirds of the overall image width. The distance from the lens of the camera to the sternum was recorded and entered into the camera during set-up. Where this was not possible (e.g. Study I, where imaging was undertaken within the constraints of the school environment), the camera was placed at a fixed distance of 1 m from the participant.

The ambient temperature and humidity of the room was measured to one decimal place using the Extech Moisture Meter MO297 (Extech Instruments). The reflective background temperature was also measured at the start of each imaging session. Participants were asked to hold up a square piece of cardboard covered with aluminium foil in front of their sternum. A spot measure of temperature at the centre of the foil-covered square was recorded, and this measurement was repeated three times, then the mean of the three measurements was entered into the camera as the reflective temperature during camera set-up. In addition, the distance from the camera lens to the participant's sternal notch, the ambient room temperature and humidity and the emissivity of skin (0.98) were also entered into the camera set-up menu at this time.

Images were taken manually with the FLIR E60 using the trigger (Study V). In the studies using the FLIR B425, where the cooling protocol was short, images were taken at intervals manually using the capture button. Where the cooling protocol was long (Study IV), images were obtained using the automatic capture feature. All images were

saved directly to a memory card and uploaded onto a personal computer for quality review and thermographic analysis.

To ensure that images could be compared between time points, it was imperative to keep participants sitting as still as possible. Several methods were used to optimise this and varied between the studies as the methodology evolved. Maintaining even short periods of immobility for children was extremely difficult. To assist, children were seated on an appropriately sized chair, with their feet resting flat on the floor. The chair was placed directly in front of a wall to allow the child to rest the back of their head against it to maintain a neutral position.

The thermal camera was connected to a large TV screen and once the child was seated with their shoulders relaxed and their head in the neutral position, markers were placed onto the screen at the shoulder tips, the sternum and at the mandibular prominence of the chin. Very young children in Study I were asked to watch an innocuous DVD (The Blue Planet) and to try to sit still. If movement did occur, children were asked to reposition themselves using the screen markers just before the next image was taken using the screen as a mirror. A similar method was used in Study II (without the use of a DVD).

An adaptation of this method was also used for Study III, where adult participants were imaged over a longer duration. The screen and markers were used but away from the participant and viewed only by the researcher. Participants were not required to sit completely still. Some movement was incurred during salivary sampling

and participants were also allowed to read a newspaper or magazine during periods of inactivity. The participant was seated upright with their head resting against the wall and behind a privacy screen away from the researcher and equipment to reduce any anxiety of being watched. Unlike the children, these participants could therefore not reposition themselves, but did so under verbal direction of the research investigator.

Studies IV and V were undertaken with the participants semi-reclined on a hospital bed (Study IV) or examination couch (Study V) this enabled them to be still throughout imaging, but did not produce images with as good exposure of the supraclavicular region.

A technical summary of the different cameras in use in the Division of COG, the University of Nottingham for the assessment of supraclavicular BAT from 2011 to 2019 is shown for reference in Table 2.1 below.

**Table 2.1 Technical summary of the FLIR cameras used in the Division of Child Health, Obstetrics and Gynaecology, the University of Nottingham for the assessment of supraclavicular skin temperature as a proxy measure of brown adipose tissue activity between 2011 and 2019.**

| Camera model | Thermal sensitivity | Thermal resolution | FOV | Accuracy | Range (µm) | Detector type |
|---|---|---|---|---|---|---|
| B60 | < 0.07˚C | 180 x 180 | 25˚ X 25˚ /0.1m | 2% | 7.5 – 13 µm | FPA, uncooled microbolometer |
| B425 | < 0.05˚C | 320 x 240 | 25˚ X 19˚ /0.4m | 2% | 7.5 – 13 µm | FPA, uncooled microbolometer |

| | | | | | | |
|---|---|---|---|---|---|---|
| E60 | < 0.05˚C | 320 x 240 | 25˚ X 19˚ /0.1m | 2% | 7.5 – 13 µm | FPA, uncooled microbolometer |
| T540 | < 40 mK | 464 x 348 | 24˚ X 18˚ /0.15m | 2% | 7.5 – 14 µm | FPA, uncooled microbolometer |

Abbreviations: FOV – field of view; FPA – focal plane array

**2.6.2 Thermal image analysis**

The procedure for analysing supraclavicular thermograms has evolved during the time taken to complete the studies presented in this thesis and beyond. Over the last 5 – 6 years, the availability of new software had a dramatic impact on how images have been analysed within the Division of COG, the University of Nottingham. In parallel progress has also been made in adapting this commercially available FLIR software and also in devising in-house software specific for analysing supraclavicular BAT. Therefore, the methods of thermal image analysis for each of my studies vary slightly, representing this evolution. Irrespective of these minor method variations, the underlying principle whereby a thermal camera is used to quantify the radiant heat emitted from the surface of the skin overlying supraclavicular BAT remains the same.

In all my studies thermal images were firstly displayed in the proprietary FLIR software available at the time of analysis (including QuickReport, ThermaCAM Researcher Pro, ResearchIR, ResearchIR Max and FLIR Tools+) allowing the thermograms to be inspected visually for an assessment of quality.

Firstly, the metadata were cross-referenced with the written records of ambient temperature, humidity, reflective temperature, emissivity and camera distance to ensure no errors had been made during camera set-up. Although these parameters

were recorded to one decimal place, the set-up menu on the FLIR E60 camera would only accept integers. Therefore, when the images from this camera were uploaded into the post-processing software, these parameters were revised to one decimal place in the software settings and the images were re-saved for further quantitative analysis. For all analyses, the colour palette was set to the highest-resolution rainbow setting available in the FLIR software and the span of the visible temperatures was set to ensure that at least 90% of the available colours within the palate were visible on the thermograms of the participant (background not included).

All images were visually reviewed to ensure that no artefacts were obscuring the supraclavicular region for example, strands of hair or jewellery overlying the supraclavicular region. The thermograms for each participant were visually checked for evidence of significant movement, scrolling through from the first image to the last in order of acquisition. To allow accurate comparison of a single ROI at different time points, the positioning of the subject or object being imaged must remain constant (Ammer and Ring, 2013). Therefore any sets of images where the movement was significant were excluded from further analysis. In the studies where images were analysed using the manual method of ROI isolation (detailed in section 2.6.2.1), the size of each supraclavicular ROI was calculated in terms of pixel area.

Given that the camera was maintained in a fixed position, and landmarks were used to place the ROI, large changes in the pixel area were assumed to be as a result of movement. Preliminary work undertaken during thermographic training clearly identified that movement of the shoulders, neck and upper torso can affect the size

of the supraclavicular region. Therefore, thermograms where the area of the supraclavicular ROI increased or decreased by more than 10% from the size of the ROI in the first image of the series, were not considered suitable for quantitative analysis.

#### 2.6.2.1 Manual ROI placement using FLIR software

The first thermographic studies of supraclavicular BAT undertaken within the Division of COG, the University of Nottingham were analysed using FLIR Quick Report V 1.2 (FLIR Systems AB, Danderyd, Sweden). This was rudimentary software and allowed the isolation of only simple ROIs (e.g. circle, square, oval, etc.), or spot measurements. These initial measurements of $T_{SCR}$ were made using a rectangular ROI to encompass the upper thorax and neck, using anatomical landmarks of the shoulder tips laterally, the mandible superiorly, and the nipple line inferiorly (Symonds et al., 2012a). This was modified slightly during the preliminary work for Study I so that the inferior border was revised to be at the level of the sternal notch rather than the horizontal nipple line, as this was not visible in these participants whilst wearing the standardised cotton vest (Figure 2.2A). The radiometric temperature data were exported into Excel as a CSV file (Figure 2.2B), where each cell within the CSV file contained a numerical value of temperature in ˚C representing a single pixel from the original thermal image. A thermal ROI was designated as the upper $10^{th}$ percentile of temperatures within the rectangular ROI (demonstrated as the green cells in Figure 2.2B), and a summary measure of supraclavicular temperature was defined as the mean of this thermal ROI.

This method gave a crude assessment of the temperature of the hottest part of the supraclavicular region; however, it was clear when starting to analyse the images from

Study I with this method that the proportion of the rectangular ROI actually containing the subject being imaged was quite variable and depended on the size, age, habitus and position of the head of the participant.

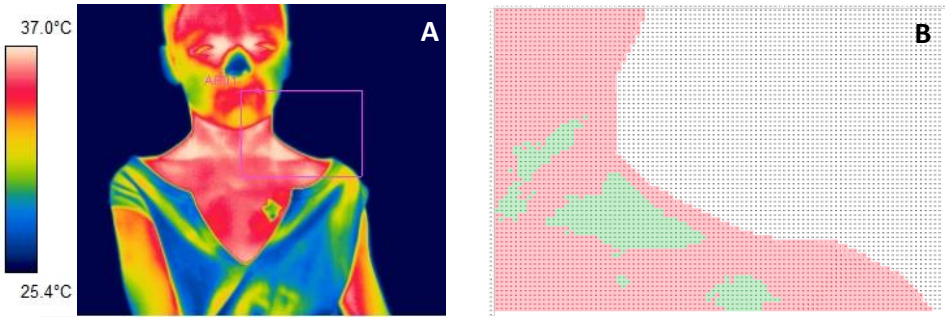



**Figure 2.2 Thermograms visualised in a high-resolution rainbow palette in FLIR ThermaCAM pro 2.1 and the output of the temperature data displayed in Excel.** A) A thermogram of a male child with the manually placed rectangular region of interest (ROI) placed over the supraclavicular region (the purple rectangle) using the landmarks outlined by Symonds et al (2012a). B) A representative image of the CSV output in Excel when the rectangular region of interest is exported from the FLIR software. Each cell represents an individual pixel from the thermogram. For illustrative purposes, the pixels from the participant's body are colour-coded pink, and the upper 10$^{th}$ percentile of temperatures within the rectangular ROI is identified as green (the thermal ROI).

Also, it was evident that this method was designating pixels to the thermal ROI that lay outside the borders of the posterior triangle of the neck (as observed in the Figure 2.2B) and may represent other structures (e.g. superficial veins or lymph nodes), and not exclusively reflect BAT. Hot spots generated by superficial vasculature are well recognised in thermography. Using a high resolution thermal camera it has been reported that IRT of the hot spot overlying the carotid arterio-venous complex can even yield accurate heart rate data by detecting small fluctuations in temperature associated with blood flow (Cardone et al., 2015).

In a randomly selected subset of 30 children from Study I, the first image from each child was analysed using ImageJ (Schneider et al., 2012) to determine the proportion of the rectangular ROI as defined by Symonds et al (2012a) that was actually the participant. This ranged from 35% up to 54% (with a mean of 44%). A similar degree of variability in supraclavicular region size relative to the rectangular ROI was seen in the thermograms obtained in an early adult pilot study obtained as part of a co-supervised BMedSci project (n = 16), where the SCR was found to be between 45% and 85% of the size of the overall rectangular ROI.

Acquisition of ThermaCAM Researcher Pro 2.1 (FLIR Systems AB, Danderyd, Sweden) software with a polygon ROI function enabled more accurate isolation of the supraclavicular region. Using this, I developed the method of supraclavicular ROI isolation further. Using the polygon tool, the left and right supraclavicular regions were drawn around manually, aiming to encompass the posterior triangle of the neck without the inclusion of structures unrelated to supraclavicular BAT.

To reduce the variability and optimise repeatability of ROI placement, the supraclavicular regions were isolated using anatomical landmarks visible within the thermograms. These consisted of the sternal notch inferiorly, the acromioclavicular joint laterally, and the course of the sternocleidomastoid down to the sternal notch in the midline medially. The sternal notch was not easily identifiable in all children. Therefore the midpoint at the level of the larynx was identified using the placement of two identically sized rectangles placed across the width of the neck. A vertical line was then drawn through this midpoint to represent the midline of the participant and

the sternal notch estimated to lie on this line at the level of the clavicular head (Figure 2.3).

The image was then enlarged to 200% of its original size and the cursor used to manually trace along the lateral contour of the shoulder to the acromioclavicular joint, then along the course of the clavicle in a straight line to the sternal notch in the midline, and along the course of the sternocleidomastoid muscle as shown in Figure 2.3. Once in place, the image was enlarged further to 400% and the course of the line along the lateral aspect checked and adjusted to ensure the ROI was lying exclusively over the skin.

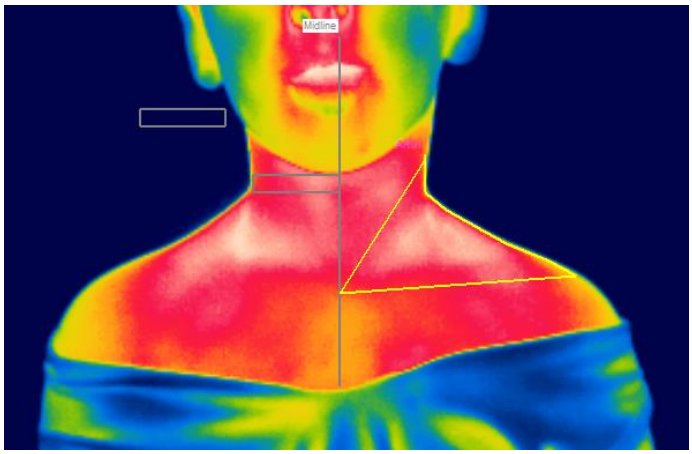



**Figure 2.3 Example of the left supraclavicular region of interest isolated manually using FLIR software (ThermaCAM Researcher Pro 2.1 or ResearchIR Max).** The supraclavicular region is bound by the yellow outline, and the vertical grey line demonstrates the midline. Two rectangles are shown, one to the right of the participant's midline, and the other moved away after identification of the midline to allow placement of the supraclavicular ROI.

The repeatability of the supraclavicular ROI defined in this manner was excellent. As variation in ROI size is associated with variability in temperature readings, particularly

when the ROI is small (Ammer, 2005, Seixas et al., 2018), the intra-rater reliability of supraclavicular polygonal ROI placement was assessed using the same subset of 30 images from Study I described above. To assess the reliability of this method, images were analysed as detailed above on two occasions five days apart. Relative reliability was assessed by Intraclass Correlation Coefficient (ICC) measures (using a two-way, mixed-effects, absolute agreement, and single measurement model), and absolute reliability was assessed using Bland Altman agreement measures. The ICC coefficients (and 95% confidence intervals (CI)) for ROI size, sum total temperature and mean temperature were 0.94 (95% CI 0.87 – 0.97), 0.94 (95% CI 0.88 – 0.97) and 0.98 (95% CI 0.96 – 0.99). The Bland Altman plots for each of these measures also indicate good reliability with minimal mean biases and narrow limits of agreement (Figure 2.4).

**A**

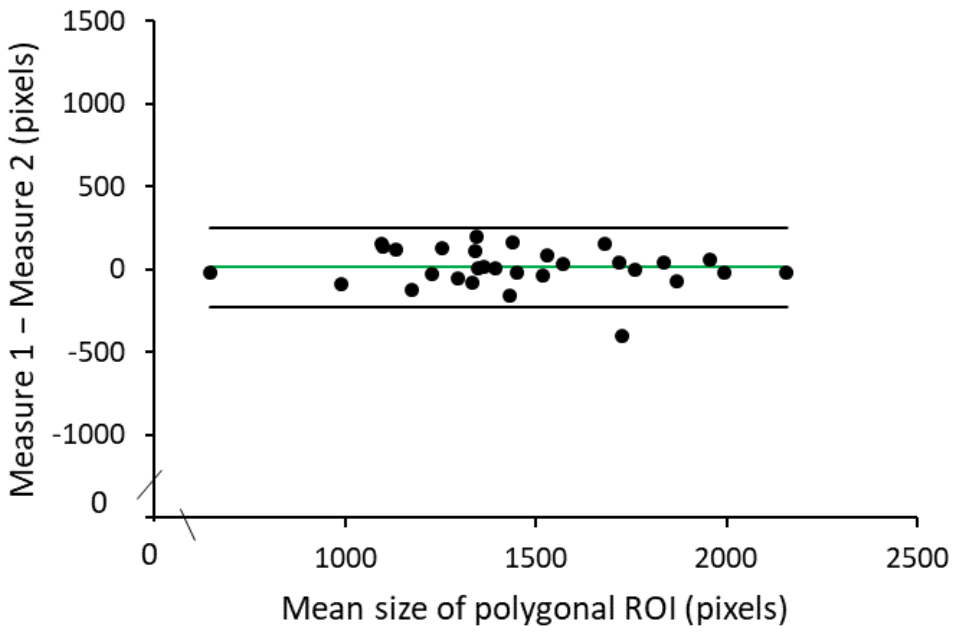
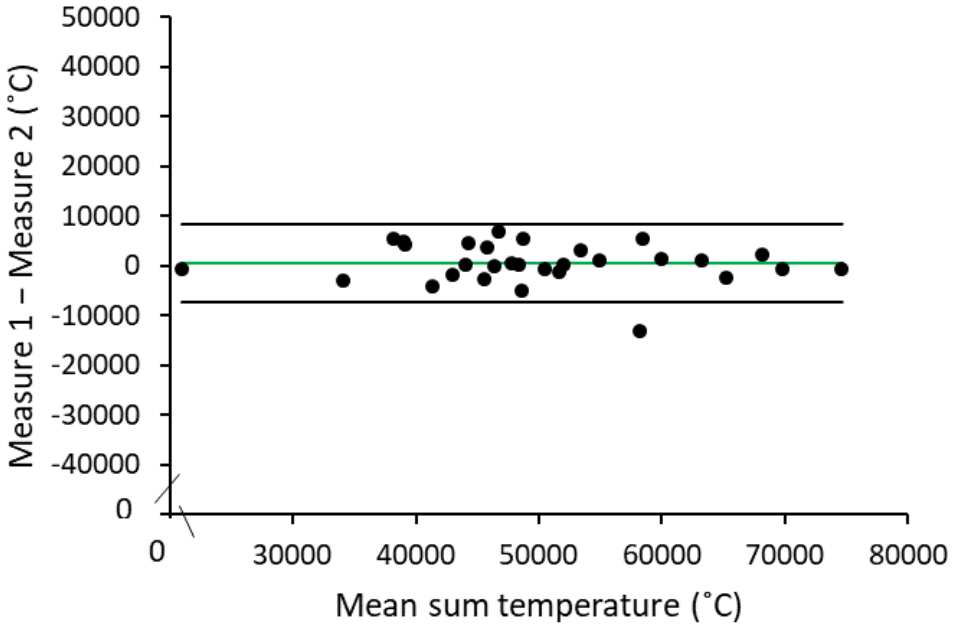



**Figure 2.4A Bland-Altman plot using the size in pixel area of the polygonal supraclavicular region of interest (ROI) isolated using manual placement with FLIR ThermaCAM Pro 2.1.** Measure2 was made 5 days after Measure1. Mean bias (shown

as a green line) = 11 pixels, upper limit of agreement = 246 and lower limit of agreement = −223 pixels indicated by black lines

**B**




**C**

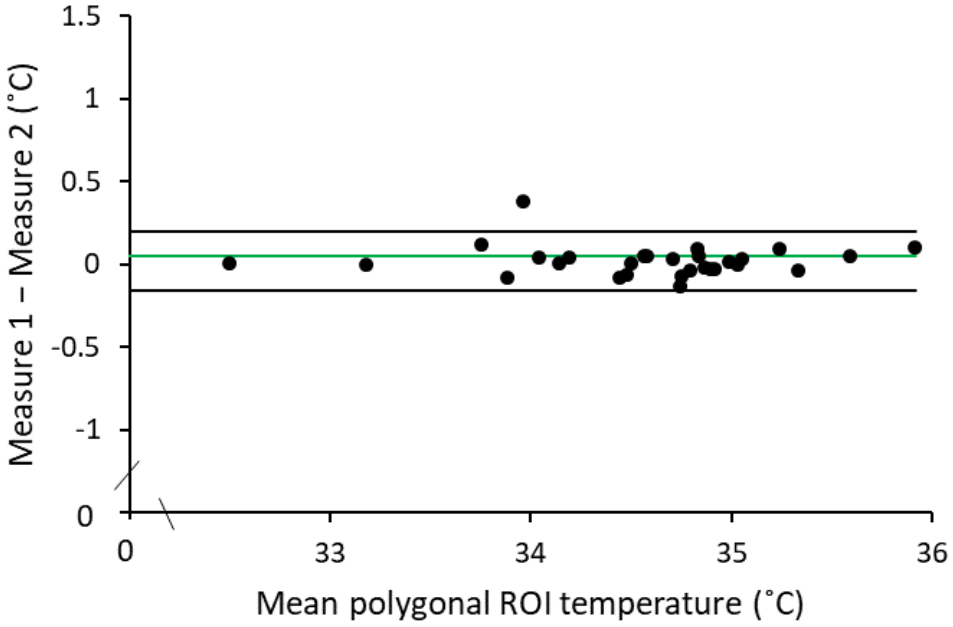


**Figure 2.4B and C Bland-Altman plot using the sum temperature and mean temperature of the polygonal supraclavicular region of interest (ROI) isolated using manual placement with FLIR ThermaCAM Pro 2.1.** Measure2 was made 5 days after Measure1. B) Mean bias = 485.26˚C, upper limit of agreement = 8369.23˚C and lower limit of agreement = − 7398.71˚C. C) Mean bias = 0.02˚C, upper limit of agreement =0.2˚C and lower limit of agreement = − 0.15˚C. The mean bias is indicated by a green line and the limits of agreement indicated by black lines.

The inter-rater reliability of this manual procedure was explored as part of a wider collaborative project, but the data or findings were still not available to me at the time of thesis submission. This manual method of supraclavicular ROI placement was extremely labour intensive and time consuming and was rapidly superseded by a semi-automated method of ROI placement developed by J Law (Law, Pending submission) detailed in section 2.6.2.3.

The polygonal supraclavicular ROI isolated using these anatomical landmarks was significantly smaller than the rectangular ROI used in the Symonds et al. (21012a) study and preliminary work for this thesis. To encompass a similar hotspot predominantly within the borders of the posterior triangle of the neck visible within the thermograms, an approximation was made based on a subjective comparison of the thermal patterns observed in the thermograms and, the thermal hotspot ROI detected in the CSV radiometric temperature data output. The upper 25$^{th}$ percentile of temperature values within the supraclavicular polygonal ROI was chosen as this most similarly represented the triangular-shaped hotspot collocating to the posterior triangle of the neck observed in thermograms (Figure A3.1 in Appendix to Study I). This thermal ROI also selected a set of pixels that were principally contiguous (see Figure A3.1A in the Appendix to Study I) and clustered over the anatomical position of

supraclavicular BAT described by Bonnot (1908) (Figure A2.1). Proportions isolated using the upper 5$^{th}$ to the 50$^{th}$ percentiles were also explored, and in the absence of any paired FDG-PET-CT and thermal data at the time the 25$^{th}$ percentile was chosen for the analysis of Study I.

The distribution of the pixel data within the upper 25$^{th}$ percentile in each polygonal supraclavicular ROI of each image was explored, and when plotted as histograms these data were positively skewed. The calculation of this skewness confirmed a moderately positive skew (mean skew 0.60, 95% CI 0.47 – 0.73). Therefore, the median value within the upper 25$^{th}$ percentile (or overall 87.5$^{th}$ percentile value of the polygonal supraclavicular ROI) was chosen as the summary measure for $T_{SCR}$.

Study III represented the first group of adults imaged with thermography to assess BAT using a polygonal supraclavicular ROI, and at this time IRT of the SCR had not been validated against any other measure of BAT nor had the anatomical co-location of this ROI been formally explored. Qualitative preliminary analysis of the SCR in the images acquired from adults identified that the thermal patterns observed in older participants were very different from those seen in children. In nearly all children a distinct large localised hot spot was evident in the SCR in the same anatomical position. In the adults imaged as part of Study III, this thermal pattern was not observed as consistently. When classified as the upper 25$^{th}$ percentile, the thermal ROI was not a discrete region as seen in the children and was highly variable in terms of its location within the polygonal ROI. Therefore for Study III, the upper 5$^{th}$ percentile was utilised instead, as this produced a more focal thermal ROI.

The optimum summary measure for supraclavicular temperature was explored in more detail within the Division of COG, the University of Nottingham by another researcher using an analysis of paired FDG-PET-CT and thermographic data obtained from healthy volunteer adults (Law, Pending submission). Using this data Law and colleagues demonstrated that the 95$^{th}$ percentile (the median of the upper 10$^{th}$ percentile) and the uptake of radiolabelled glucose correlated positively with the change in relative $T_{SCR}$ in response to cold stimulation, and that there was a significant spatial overlap between maximal MR(gluc) and maximal supraclavicular temperature during the cooling period explored.

Consequently the use of the 95$^{th}$ percentile within a polygonal supraclavicular ROI was adopted as standard procedure for supraclavicular BAT assessment within COG (Standard Operating Procedure V3.0 Automated analysis of thermal images) and was used for the analysis and preparation of manuscripts for Studies II, and V.

#### 2.6.2.2 Calculating the summary measure of supraclavicular skin temperature

The CSV file containing the radiometric data of the ROI was either analysed in Excel using a Macro, or analysed in R (A Language and Environment for Statistical Computing, V3.4.3 (R Core team)) with a custom written script. I wrote the Macro in Visual Basic, and the R script (with the assistance of Dr A Prayle) to identify the thermal ROI within the anatomical supraclavicular ROI. The details of the thermal ROI used for each study are referred to in each study manuscript.

#### 2.6.2.3 Semi-automated ROI placement using custom MATLAB script

A departmental semi-automated method for polygonal ROI placement over the supraclavicular region was developed by J Law (Law et al., 2018) and became standard procedure for BAT assessment from May 2016 within the Division of COG, the University of Nottingham. It was utilised to analyse the images obtained in Studies II, and V to bring this data into line with standard departmental practice.

Using the custom written script in MATLAB (adapted from a script by Tattersall (2015), thermal images were exported into the MATLAB environment, where they were visible in a Portable Network Graphic format in an unspecified rainbow palette (figure 2.5A). An individualised body threshold temperature was set to ensure that the background behind the participant was completely black (thus not contributing any thermal data to the ROI). This varied between participants but was kept the same for each individual. The size of the image was maximised and markers were placed at the five apices of the polygonal region of interest, notably the most lateral visible aspects of the sternocleidomastoid and the acromioclavicular joint on the left and right sides, and a single marker placed just below the sternal notch (Figure 2.5B).

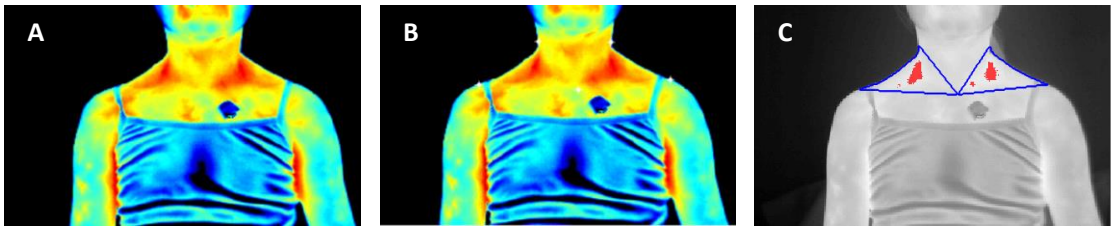



**Figure 2.5 Procedure for thermal image analysis of supraclavicular brown adipose tissue in MATLAB.** A) Representative thermal image as displayed in Portable Network Graphic format within MATLAB, with the individualised body threshold temperature set to ensure a completely black background. B) The positioning of the five markers to isolate the borders of the supraclavicular region of interest (ROI), shown as white dots with cross-hairs. C) The supraclavicular anatomical ROI identified using the custom processing script in MATLAB demonstrated by the blue triangular outline, and the thermal ROI demonstrated by the red pixel area (upper 10$^{th}$ percentile of values).

A "processing" script was then run that produced an image of the polygonal anatomical ROI (bound within a blue line) and the thermal ROI (displayed as red pixels) as shown in Figure 2.5C and an Excel worksheet containing the summary data for each image analysed (filename, left and right 95$^{th}$ percentile supraclavicular temperature).

## 2.7 Non-BAT skin temperature measurement

### 2.7.1 Skin temperature measurement using iButton devices

Skin temperature at other sites away from the supraclavicular region was measured using iButton Thermacron® temperature data loggers (model no. DS1219H-F50; Maxim, Sunnyvale, California, USA). These small wireless data loggers consist of a silicon chip encased in a stainless-steel can. The can consists of a base and a lid, and the silicon chip sits on top of the base. For my studies, the iButtons were placed with their base flush to the skin surface and were maintained in position with two pieces of surgical tape (Micropore™ Surgical tape, 2.5cm wide) placed at right angles to each other. The iButtons were activated to begin sampling using the 1-Wire interface and a

personal computer, detached then secured in position on the skin of the participant. Following the first study undertaken with these devices (Study I), it became clear that iButtons should be in situ for a minimum of 15 minutes to allow the metal casing to equilibrate with the skin and ambient temperature. This was undertaken as standard in all studies except for Study I.

The manufacturer's information advises that the DS1219H measures in 1/8˚C increments to ±1˚C accuracy; therefore to maximise the consistency of measurements between individual data loggers all iButtons were examined simultaneously in a water bath at a fixed temperature to allow calculation of a calibration formula for each button (Table 2.2).

**Table 2.2 Calibration formulae used for the set of iButtons used in Studies I to V.** These individual calibration formulae were used in all studies described in this thesis.

| iButton unique identifier | Calibration formula |
|---|---|
| 67B821 | 1.009 +0.06 |
| 605c21 | 1.010 + 0.158 |
| 664f21 | 1.005 + 0.492 |
| 678421 | 1.005 + 0.288 |
| 5c3421 | 1.004 + 0.434 |
| 5de321 | 1.003 + 0.359 |
| 5eab21 | 1.005 + 0.080 |
| 63bc21 | 0.995 + 0.491 |
| 646721 | 1.000 + 0.495 |
| 5df321 | 1.014 – 0.014 |

To calculate mean skin temperature, iButtons were placed at seven sites as follows; central forehead, dorsum of the hand, dorsal aspect of the mid -forearm, chest at the level of the second intercostal space midclavicular line, mid-anterior thigh, mid-point of the tibia and dorsal aspect of the foot. When used in a cooling study, iButtons were placed on the opposite side to the cold stimulus.

Mean skin temperature ($T_{MSK}$) was calculated using the weighting formula of Hardy and Du Bois (Hardy and Oppel, 1938). Several such formulae exist, using measurements from 4 to 15 skin sites, with different weighting coefficients. Each has advantages and disadvantages in terms of practicality, repeatability and consistency. The optimal method is generally considered to be one that uses a large number of skin sites. The 15-point method of Winslow has been reported to be the best (Mitchell and Wyndham, 1969). However, for participant comfort, this method was not felt to be feasible for use in a semi-reclined supine position (i.e. measurements were required on the back, neck and underside of the calf). Therefore, Hardy and DuBois's modified version of Winslow's formula was chosen as a practical alternative (Hardy and Oppel, 1938).

$$T_{MSK} = 0.07\ t_{head} + 0.14\ t_{arm} + 0.05\ t_{hand} + 0.07\ t_{foot} + 0.13\ t_{leg} + 0.19\ t_{thigh} + 0.35\ t_{trunk}$$

As the minimum sampling rate for the DS1219H was one sample per minute, this was used unless specified otherwise. Each iButton was synced to the clock on a personal computer and activated together to ensure measurements at different sites were made simultaneously.

### 2.7.2 Skin temperature measurement using thermography

In Study II skin temperature over the mandibular prominence was measured using the mean temperature of an 86-pixel ellipse (using FLIR's ResearchIR software) before and after hand immersion in cool water, to determine whether the changes in skin temperature observed in the SCR were localised or reflective of a more systemic response. Similar measurements of hand and forearm temperature were made in Study V.

### 2.7.3 Tympanic membrane temperature

Tympanic membrane temperature was used to estimate core temperature in Studies I, II, IV and V using a Braun ThermoScan Pro 4000 infra-red thermometer (Welch Allyn, Skaneateles Falls, New York, USA). Measurements were taken in triplicate, and an average of the three readings used for statistical analysis where appropriate. Tympanic temperature was used to screen for intercurrent illness and monitor for hypothermia during cooling. There were no participants in any of the study who had signs of fever, and nor did any individuals tympanic temperature fall below 36˚C during cooling.

## 2.8 Anthropometrics

### 2.8.1 Height and body weight

Height was measured to the nearest 0.1 cm using a stadiometer (Leicester height measure; Child Growth Foundation, Sutton Coldfield, United Kingdom). Participants stood in a vertical plane against the stadiometer with their heels towards the wall, toes were pointing forward and their knees together. With each participant's head in

the Frankfort horizontal plane, the headboard measuring plate was brought down to reach the crown of the head, forming a right angle with the stadiometer scale. The participant's height was recorded to the nearest 0.1 cm on a data-collection proforma, and this procedure was repeated a further two times. The average of the three readings was used in subsequent data analyses.

Weight was measured to the nearest 0.1 kg with calibrated portable digital scales placed on a firm level surface. All participants were weighed without shoes. In the studies undertaken in local primary schools, children were weighed in their school uniform, in the laboratory-based studies, participants were weighed in standardised clothing as outlined in the experimental study protocols. Participants were asked to stand in the middle of the platform, looking straight ahead. The digital readout was recorded to the nearest 0.1 kg, then the procedure was repeated a further two times, and an average of the three measurements was used for statistical data analyses.

**2.8.2 Body mass index**

Height and weight were measured as described above. Body mass index was calculated as follows:

$$\text{BMI} = \text{weight (kg)} / \text{height}^2 \text{ (m)}$$

Normal weight, overweight and obesity, are classified using absolute cut-offs in adults (e.g. BMI > 30 is classified as obese) and these standard classifications were used in the Studies III, IV and V. Age- and sex-specific BMI percentiles were calculated for children in Studies I and II, using the NHS healthy weight BMI calculator (NHS Choices),

which uses the UK90 reference data in line with the BMI growth charts issued by the RCPCH.

### 2.8.3 Bioelectrical impedance

Bioelectrical impedance analysis (BIA) is frequently used to estimate body composition. It measures the opposition to a small electrical current as it travels through total body water. The conductance of the electrical current is greater through fat-free mass than fat mass as the latter contains very little water. Body water volume can be estimated from the impedance index ($ht^2/R$) and is often used to estimate fat-free mass, so fat mass can then be estimated using known body weight.

BIA measurements were made using a hand-to-foot, single-frequency (50 kHz) battery-operated bioimpedance analyser (BIM4; ImpediMed P/L, Capalaba, Austria) in the supine position. The BIM4 consists of two injecting and two sensing electrodes, the current electrodes were placed on the foot over the distal point of the second metatarsal, and on the hand on the distal portion of the second metacarpal. The sensing electrodes were placed on the anterior ankle between the tibial and fibular malleoli and at the writs between the radial and ulnar styloid. Electrodes were attached to the skin using 5500 Diagnostic Tab Electrodes (Coviden, Tullamore, Ireland).

Arms and legs were positioned at 30 degrees from the midline to ensure they were not in contact with the body or each other. If difficulties in maintaining electrode contact were encountered, the patch electrodes were removed, underlying skin was

cleaned with an alcohol wipe and the electrodes were re-sited. The BIA monitor proprietary algorithms calculated impedance, which was used alongside anthropometric data, age and sex to predict body composition. Values were obtained for total body water, fat mass and fat-free mass. BIA was used in Studies IV and V, but technical issues were experienced with the monitor resulting in an incomplete assessment for Study V.

While quick, simple, non-invasive and relatively inexpensive BIA has a number of limitations that should be acknowledged, the BIA method relies upon regression equations which are usually held by the manufacturers and not made publicly available due to their commercial value. The validity of BIA is influenced by gender, age, ethnicity and hydration status. Moreover, BIA overestimates body fat percentage in those who are very lean and underestimates it in those who are obese. It is generally accepted that BIA is most useful for assessing body composition in large populations and less useful for individuals, particularly in detecting short-term changes. While BIA may be suitable for use in adults, most monitors are not recommended for use in children under 7 years old, limiting their use in the assessment of paediatric body composition.

### 2.8.4 Subcutaneous adipose tissue thickness

MRI of the neck and upper thorax was performed using a 3T scanner (GE Discovery MR750 3.0T, GE medical Systems) with a T1-weighted axial plane with the following variables (TR 500, TE 13.6, matrix 256 x 256, slice thickness 5mm and interslice thickness 3mm). SCAT was defined as the distance between the anterior edge of the

subcutaneous fat and the subcutaneous fascia at the level of the first thoracic vertebrae (T1) and measurements were made in triplicate using OsiriX version 5.6.

### 2.9 Metabolic and cardiovascular

#### 2.9.1 Indirect calorimetry

Indirect calorimetry is the gold standard for measuring metabolic rate and energy expenditure. It uses respirometry as an indirect measure of heat production (energy expenditure) based on the principle that the final common pathway of all cellular fuels is oxidation, which in turn produces carbon dioxide and water. Using continuous measures of gas exchange, calorimetry estimates whole-body oxygen consumption and carbon dioxide release. Energy expenditure can be calculated from oxygen consumption ($VO_2$) and carbon dioxide ($CO_2$) release, using the modified Weir equation (Weir, 1949) (1), but the urinary nitrogen component is often excluded as its total contribution to EE is minimal. The abbreviated formula (2) is more commonly used and forms the basis of the assessment of energy expenditure in this thesis.

$$\text{Energy expenditure } \left(\frac{\text{kcal}}{\text{day}}\right) = ([\text{VO2x3.91}] + [\text{VCO2x1.11}] + [\mu\text{N2x2.17}]) \text{ x } 1440 \quad (1)$$

$$\text{Energy expenditure } \left(\frac{\text{kcal}}{\text{day}}\right) = 1.44(3.94\text{VO2} + 1.11\text{CO2}) \quad (2)$$

In Study IV continuous recordings of oxygen consumption and carbon dioxide production were made using a mask collection method (Oro-nasal reusable face mask, V7450 series, Hans Rudolph Inc., Shawnee, USA) with the Europa gas exchange monitor (GEM; Europa Scientific Ltd., Crewe, UK). Measurements were made in a

quiet laboratory throughout the morning. Baseline measurements were taken only once resting energy expenditure looked to be stable, and individuals had been resting for at least 15 minutes. Participants were all asked to fast from midnight (fasted for 8 to 10 hours) and to avoid alcohol and strenuous exercise in the preceding 24 hours.

In brief, the GEM analyser was connected to a personal computer and cylinder gas supply ($N_2$, $O_2$ and $CO_2$) and allowed to warm up for a minimum of 20 minutes before calibration. The GEM analyser was then calibrated using the GEM Nutrition software $O_2$, and $CO_2$ readings were checked to ensure that they fell within limits outlined in the departmental standard operating procedure. The face mask was secured over the nose and mouth using the headgear as per manufacturer's instructions. To allow adequate exposure of the neck and upper thorax, the tubing was rotated 180˚ up over the shoulder and was secured to the head of the bed. Continuous measurements were made over 60 minutes, 30 minutes at baseline, and during 30 minutes of cooling. An average of the last 15 minutes of each period was used in the final analysis. Energy expenditure was calculated automatically by the GEM Nutrition software and exported as a CSV file onto a personal computer for later analysis.

### 2.9.2 Dietary intake, activity and eating behaviour

Questionnaires regarding dietary intake, activity levels and eating behaviour were completed by all parents/carers of children taking part in Study II. To determine whether the parental responses were subject to contamination by social bias parents were first asked to complete 10 true or false questions regarding personal attitudes and traits, which constituted a short form of the modified Marlowe-Crowne Social

Desirability Scale (MCSDS) (Strahan and Gerbasi, 1972). Significant contamination by socially desirable responding was considered if there was a strong significant correlation between the MCSDS score and the outcome variable of interest. These data are summarised in Table A3.2 in the Appendix to Study II.

Dietary intake was quantified using a standardised food frequency questionnaire, consisting of 151 foods, (adapted from Wardle et al (2001). Parents were asked to indicate how often their child consumed each item on a scale of 1 to 8 (1 – more than once a day; 2 – once a day; 3 – more than once a week; 4 – once a week; 5 – more than once a month; 6 – once a month; 7 – less than once a month; 8 – never tried it). The responses for items were then grouped by food group (carbohydrate, dairy, vegetable, fruit, protein, sweet snack and savoury snack), and a total summed score for each food group was calculated for each parental questionnaire. Where more than 25% of parental responses for a food item were 8 (i.e. never tried), this food was excluded as per standard use of this questionnaire.

Cronbach's alpha was calculated for each food group to assess the reliability of the parental responses, where reliability was low, the foods included within the food group were reviewed, foods were removed one by one to determine if reliability could be improved.

The food groups (and individual items included within these groups) used in the final analyses presented in this thesis for food frequency are summarised in Table A3.1 in the Appendix to Study II.

### 2.9.3 Blood pressure and heart rate

Blood pressure was measured at intervals in Study V using the Omron M3 digital automatic blood pressure monitor (Omron Healthcare UK Ltd, Milton Keynes, UK) with an appropriately sized upper-arm cuff. A single measurement was made, and the systolic, diastolic pressures and heart rate were recorded. Attempts were made to measure blood pressure using a continuous measurement from the ring finger using the Finapres® blood pressure monitor in Study IV. This failed due to vasoconstriction of the fingers during cooling of the contralateral hand when the ambient temperature was low.

## 2.10 Safety precautions

Given the non-invasive nature of these studies, there were few safety concerns. A medically qualified researcher undertook all studies, and a short medical history was taken from all adult participants to ensure they were all healthy volunteers. Tympanic temperature was monitored at intervals of 10 minutes in all studies involving cooling, although this did not drop below 36˚C in any individual in any of the studies.

Where participants fasted, all imaging sessions were undertaken in the early morning to avoid prolonged fasting and hypoglycaemia. All studies were completed before midday. A capillary blood glucose analyser and concentrated sugar drink were available in the imaging suite but were not required.

Children in Studies I and II attended in pairs, having changed into their cotton vests under the supervision of their teacher in the classroom. Children were imaged in a

room with an open door close to their classroom and school teacher, and there were two members of the research team undertaking thermal imaging of the children at all times.

**2.11 Statistical analysis and data presentation**

The distribution of each data set was inspected visually for distribution and tested for normality using the Kolmogorov-Smirnov normality test. Data are presented either mean ± standard deviation (SD) or mean ± standard error (SE) unless otherwise stated and as detailed in each manuscript.

Comparisons between two means were undertaken using Student's paired and unpaired t-tests. Comparisons between percentages were undertaken using the Chi-squared test ($\chi^2$). The degree of association between variables was assessed by calculation of the Pearson product-moment correlation coefficients. The presence of a simple linear relationship between two variables was assessed by linear regression analyses, and standard multiple regression analysis using a simultaneous entry method (where all the predictor variables were entered at the same time) was undertaken to identify determinants of supraclavicular skin temperature.

A one-way repeated measures ANOVA with Dunnet's post hoc multiple comparisons test was used to evaluate the effect of cooling over multiple time points.

A two-way mixed ANOVA was used to determine whether there was an interaction between between-subjects and within-subjects factors. Where a statistically significant interaction effect was identified, a post hoc analysis of simple main effects

or pairwise comparisons were made (detailed for each study in the respective manuscript). All data were checked to ensure that they met the five assumptions required for the two-way ANOVA. Outliers were assessed by inspection of a boxplot, normality was assessed using Shapiro-Wilk's normality test for each cell of the design, and homogeneity of variances was assessed by Levene's test. Mauchly's test of sphericity indicated that the assumption of sphericity was met. There were no outliers, residuals were normally distributed, and there was homogeneity of variances and covariances. Similarly, a two-way analysis of covariance analysis (ANCOVA) was subsequently used to identify interaction effects after controlling for the effect of BMI percentile as a covariate. Where this analysis has been used, data were found not to violate the assumptions required for testing (homoscedasticity, homogeneity of regression slopes, homogeneity of variances as assessed by Levene's test, that there were no outliers, that there were no leverage or influential points as assessed by leverage values and Cook's distance, and that the Studentized residuals were normally distributed as assessed by Shapiro-Wilk's test).

A two-way repeated measures ANOVA was used to identify a significant interaction effect between two within-subjects factors on supraclavicular temperature. All data were checked so that it met the assumptions required for the two-way repeated measures ANOVA. Where a statistically significant interaction was identified, an analysis of the simple main effects was undertaken (detailed within the respective study manuscript). Analysis of the Studentized residuals confirmed normality, as assessed by the Shapiro-Wilk test. There were no outliers, as assessed by having no

studentized residuals greater than ± 3 standard deviations. There was sphericity for the interaction term (assessed by Mauchly's test of sphericity).

A P value of $< 0.05$ was considered as statistically significant unless otherwise stated. Adjustments to the significance threshold were made to allow for multiple comparisons in Study II (during calculation of the Pearson correlation coefficient, false discovery rate was controlled using the corrected method of Benjamini and Yekutieli (Benjamini and Yekutieli, 2001) – with an FDR of 5%), and in Study V (using a simple Bonferroni correction, $P < 0.025$).

Study I represents the first large study of supraclavicular BAT in children aged 6 to 11 years. Sample size calculation based on the small group of children aged 3 to 8 years in Symonds et al. (2012a) study indicated that the minimum number children required to detect the rise in supraclavicular skin temperature after hand cooling was five. The data from Study I were used to calculate the sample size required in Study II, where a sample size of 30 (15 girls and 15 boys) was calculated to detect a 25% difference in $\Delta T_{SCR}$ in response to cold, where right $\Delta T_{SCR} = 0.28 \pm 0.064$ ˚C; $\beta = 0.2$; $\alpha = 0.05$).

To detect a strong correlation ($r > 0.5$) between two variables it was calculated that 29 children would be required. Therefore it is recognised that Study II was underpowered for correlational analysis with adjustment made for multiple comparisons. Studies III, IV and V were considered exploratory pilot studies, no data using supraclavicular temperature as a proxy measure of BAT activity nor the specific

BAT activation protocols trialled in these studies had been used before; therefore, a priori sample-size calculations were not possible for these studies.

Data were analysed using a combination of GraphPad Prism (V. 60c – 7.04, GraphPad software, La Jolla, California, USA) and SPSS (V.19 – 24, IBM, Armonk, New York, USA), using the most contemporary version available at the time of data analysis.

# CHAPTER TWO

## General materials and methods

## 2.1 Overview of studies

Five studies are presented in this thesis. In each study, supraclavicular skin temperature was evaluated using infrared thermography. This measurement was used as a proxy measure of BAT activity. Studies I, II, IV and V aimed to activate BAT with active localised cooling. Study III sought to stimulate BAT with mild psychological stress. The experimental protocols for each study are summarised in the associated manuscript in Chapters three, four and five and a detailed description of the materials and methods for each of the measurements taken throughout these protocols, as well as the statistical analyses and safety precautions for each study, are outlined below in Chapter two.

## 2.2 Ethical approval

All Studies (I to V) were reviewed and approved by the University of Nottingham Medical School Ethics Committee, and conformed to the Declaration of Helsinki 2008.

In Studies I and II participants were recruited from local primary schools, and the purpose and nature of the studies were explained to parents by way of an information leaflet, plus a verbal explanation by a study investigator if requested. Written consent was obtained from parents/carers, and additional verbal assent was received from the child on the day of the study. Any child who was unable to give verbal assent, or did not want to participate, was not required to take part in the study. Nevertheless, all children whose parents had given consent also agreed to take part in the study. Parents and children were aware that they could withdraw at any stage, and that all

information regarding their participation would be held anonymously and kept confidential.

In Studies III to V young adult participants were recruited via poster advertisements placed around the Nottingham University Campuses. A full explanation of the nature of the study and the procedures required was given to each participant at least 24 hours prior to the first study session, in addition to a study information leaflet. Subjects who participated in Study III were offered a small inconvenience allowance of £15 to compensate for their time and travel. All participants were aware that they could withdraw at any time.

**2.3 Participants**

The volunteers in Studies I and II were young children, of primary school age (6 – 11 years). No details were requested regarding their health, medications or metabolic status.

The volunteers in all other studies were non-obese healthy, Caucasian men and/or women who were students or staff at the University of Nottingham. A short medical history was taken from each participant to ensure they were not suffering from any medical condition that would preclude them from taking part in the study (e.g. diabetes, Raynaud's, pregnancy), or taking any prescribed or recreational medication that would affect BAT activity.

## 2.4 Cooling protocols

### 2.4.1 Acclimatisation and clothing

The adult participants in Studies III to V undertook a formal period of acclimatisation with a period of rest in standardised clothing (as detailed in the individual chapters) for at least 30 minutes, either laying semi-supine on an examination couch (Study V), hospital bed (Study IV) or seated in a chair (Study III). This period was to allow the supraclavicular skin temperature to stabilise, assessment of supraclavicular skin temperature was not possible in contemporaneous real-time using the thermographic equipment available at the time of these studies.

Previous pilot data from a co-supervised BMedSci research project had shown that supraclavicular temperature was highly variable in the period immediately after removing clothes and during the transition from natural, spontaneous movement to sitting immobile. However, the precise magnitude of this variability and its effect on subsequent BAT activation was not evident until the completion of the studies presented within this thesis. The role of the acclimatisation period upon subsequent cold-induced changes in supraclavicular skin temperature has been subsequently formally studied as part of another PhD student research project that ran from 2016 to 2019, in that project, A. Lazaridi determined that in healthy adult volunteers a 30 minute rest period was superior to 5 minutes, and resulted in a significantly lower baseline measurement and had greater sensitivity to detect a rise in supraclavicular skin temperature after cold stimulation, although the variability within this period was not explicitly reported (Lazaridi, 2019). Although the supraclavicular region have not been explicitly examined by these authors, it is noted that Ring and Ammer (2000)

recommend a minimum of 10 minutes prior to thermography of human skin, and Morins et al reported that the time to reach stability in skin temperature is dependent on the region studied, and is also different in men and women. They concluded that for whole-body imaging a minimum of 10 minutes was considered acceptable (Marins et al., 2014, Marins et al., 2015)

Due to the constraints of time within the school day, a formal acclimatisation period was not undertaken prior to the acquisition of baseline measurements in Study I and Study II. However, all children were present in the imaging room wearing a cotton vest for around 10 – 15 minutes prior to the start of imaging (i.e. time taken to check consent, set up equipment and explain the procedure to the child).

In Studies I and II, the clothing worn during thermal imaging was not wholly standardised due to the requirements outlined in the study ethics. Children were not allowed to dress or undress with the research team. Instead, they were asked to remove their school shirt in the classroom with the supervision of their class teacher and change this for a standardised cotton study vest provided by the research team. This was worn alongside the school uniform they attended in that day. 'School uniform' was variable and included trousers, jogging bottoms, skirts or shorts of varying fabric weight.

In Studies III to V, in an empty room, or behind privacy screens, the young adult volunteers were asked to change into standardised clothing. In Study III and Study IV, this consisted of a set of surgical scrubs, with a short-sleeved cotton top, and

drawstring full-length cotton trousers, but in Study V the short-sleeved top was replaced with a sleeveless cotton vest to allow easy access for blood-pressure monitoring. Participants were asked to keep their underwear and socks in place. The insulative effect of this clothing was estimated to be 0.35 and 0.31 Clo, respectively.

### 2.4.2 Ambient room temperature

Only Study IV was undertaken in a temperature-controlled laboratory (Blood Flow Laboratory E6, University of Nottingham Medical School), set at either 23˚C or 18˚C. Given its location within a large heated hospital setting the ambient room temperature in the Academic Child Health Imaging Suite on B floor (Study V) and E floor (Study III) were reasonably stable, but not amenable to manipulation. Room temperature was recorded and documented at the start of each imaging session for all studies with the Extech Moisture Meter MO297 (Extech Instruments).

There was no facility to control the ambient room temperature within the school environment. Therefore the conditions for Studies I and II were variable. Given the recommendations of Ammer and Ring (Ammer and Ring, 2013), only children who were imaged at a room temperature above 20˚C were included in the studies of BAT presented in this thesis. These authors suggest that for most clinical applications, a range of 18 – 25˚C is adequate for thermography. Similarly Quesada et al recommend an ambient temperature of 18 – 26˚C at a humidity of around 60% for the reliable assessment of human skin temperature (Quesada et al., 2017). However, as there are no specific recommendations for thermography of BAT in children, and given the findings of Study IV, an arbitrary threshold of 20˚C was chosen for Study II.

### 2.4.3 Hand cooling

In Studies I, II and IV, single hand immersion in cool tap water was used as a mild cold stimulus to activate BAT. This methodology was used in the initial work undertaken within the Division of Child Health, Obstetrics and Gynaecology (COG), University of Nottingham and preceded the studies presented in this thesis (Symonds et al., 2012a). In this thesis, this cooling protocol was reproduced with a few modifications to optimise image acquisition and reproducibility. To avoid excess movement during the acquisition of thermal images, participants were asked to place their left hand in a small empty bucket (radius: 12 cm, capacity c.6 – 10 L), and the bucket was placed at a height that meant the hand was placed comfortably inside without touching the bottom or sides. To institute cooling, water at c.20˚ ± 0.1˚C from a second bucket was poured gently over the hand into the empty bucket until the water was at the level of the ulnar styloid prominence.

The temperature of the water used for Study I was determined by the availability of tap water in the first school we visited. The coldest water that could be obtained in the room allocated to us was 20.1˚C. Therefore this temperature was used throughout Studies I and II. Once fully covered by water, the left hand was immersed for a total of 5 minutes. To confirm the effect of cooling, the temperature of the hand was assessed by IRT both at baseline and immediately after the hand was removed from the water. The temperature of the skin on the dorsal aspect of the hand dropped by a mean (SD) of 8.41 ± 1.99˚C in Study I, and by a mean (SEM) of 8.85 ± 0.3˚C and 8.0 ± 0.57˚C in the boys and girls (respectively) taking part in Study II. There were no complaints of discomfort during hand immersion.

### 2.4.4 Prolonged hand cooling

In Study IV, an extended period of hand cooling (30 minutes) was used to determine the time course of the BAT response to mild cold in the context of changes in energy expenditure and ambient temperature. The cooling procedure outlined above, where the left hand was immersed in cool water to the level of the ulnar styloid, was used. Preceding feasibility studies identified that the temperature of the water rose significantly with prolonged immersion, due to the heat extracted from the hand by the water. Therefore, to maintain the magnitude of the cold stimulus, in Study IV the water temperature was checked every 5 minutes, and if it had risen by more than 0.2˚C ice water was added in small aliquots (c. 50 – 100ml) until the overall water temperature had returned to 20˚C. The water level (at the ulnar styloid prominence) was also maintained by the removal of water volumes equal to that added using a 200ml beaker. Participants were encouraged to report discomfort during cooling, although this did not occur.

### 2.4.5 Forearm cooling with the Blanketrol® II

In Study V, to achieve a more consistent and maintained cool stimulus, cooling of the whole forearm was achieved using the Blanketrol® II unit attached to a 12.5 by 18 inch cooling blanket (Maxi-Therm Lite® Infant) with the Manual Control Mode set to 14˚C. This is a cooling unit filled with sterile/distilled water and circulating water flows over the cooling element within the reservoir. The cooled water then flows through the connecting hoses over a temperature sensor and into a water-perfused blanket. After circulating through the blanket, water is returned back to the unit and then back to the reservoir to be re-cooled.

The Blanketrol® II was used in line with the manufacturer's instructions for Manual Control Mode. In brief, the unit was filled with water to the level of the strainer at the bottom of the water-fill opening. The blanket was connected to one return and one outlet. With the power off, and the blanket lying flat on the examination couch a System Test routine was conducted to ensure the blanket and machine were functioning correctly prior to being attached to the subject. With the machine off, and all jewellery removed, the blanket was wrapped circumferentially around the participants left forearm. The fingers distal to the interphalangeal joints were left exposed to allow continuous inspection of skin colour and integrity throughout active cooling. The blanket was held in place with light pressure from a circumferentially wrapped crepe bandage. Care was made to ensure that this was not so tight as to restrict blood flow, but tight enough to maintain contact between the skin and the blanket. Tympanic membrane temperature was checked every 10 minutes during active cooling, and core temperature did not drop below 36˚C in any participant. Participants were asked to report any discomfort during cooling (but there were no such complaints). The temperatures of the dorsal aspect of the arm and hand were measured at the end of cooling using thermography.

### 2.5 Mild mental stress protocol

#### 2.5.1 Mental arithmetic test

In Study III, participants were asked to complete a short mental arithmetic (MA) task. This test has previously been shown to result in mild psychological stress (Memon et al., 2013) and consisted of 20 simple two-step arithmetic questions (e.g. 52+5−18 =?) presented on PowerPoint slides on a personal computer in front of the participant.

Each question was to be answered within 6 seconds and was immediately followed by the next question (dictated by the slide transition time). Participants were told that the test was easy and that it was expected that they would get most of the answers correct. They were asked to say their answers out loud, and the study investigator immediately communicated whether their answer was correct or incorrect. When two questions were correctly answered in succession, the subject was told that the next answer was incorrect irrespective of the answer given. This test has previously and successfully been used to elicit mild psychological stress, demonstrating increases in systolic blood pressure and heart rate in line with sympathetic stimulation (Memon et al., 2013).

### 2.5.2 Corresponding control period

The participants in Study III also undertook testing on a subsequent day. During this session, participants watched a 2 minute relaxation video (raindrops on a window) on the same personal computer in place of the MA test.

### 2.5.3 Measurement of salivary cortisol

Cortisol was used as a biological marker of a stress reaction. During a stress reaction, the hypothalamic-pituitary-adrenal (HPA) axis activity is increased, the stressor activates corticotrophin-releasing hormone and vasopressin secretion, and these hormones stimulate the pituitary gland to release adrenocorticotrophic hormone (ACTH), which, in turn, stimulates secretion of cortisol from the adrenals. Most cortisol within the plasma is bound to binding proteins, and just 3 – 5% remains free and metabolically active. Unlike blood cortisol, salivary cortisol levels reflect the

biologically active component and salivary cortisol correlates highly with free cortisol in the plasma. Salivary sampling avoids the stress reaction associated with venepuncture and blood sampling and is considered a simple, safe and non-invasive method (Hanrahan et al., 2006, Keil, 2012).

Cortisol increases at times of acute stress (Dickerson and Kemeny, 2004), and the salivary cortisol response to the MA test was used in Study III to assess the effectiveness of the test beyond that of a cardiovascular response (Memon et al., 2013). Saliva samples were obtained using Salivettes® and analysed using the Salimetrics salivary cortisol ELISA kit. In brief, each sample was collected with a SalivBio Oral Swab (Salimetrics; Starstedt, Leicester, UK) , which is a synthetic swab specifically designed to improve volume collection and increase participant compliance, and it is also validated for use with salivary cortisol. Participants removed the swab from the collection tube and placed it in their mouth. The swab was chewed for 2 minutes until it was saturated, and then it was placed into the basket within the collection tube which was then sealed with a lid. All samples were labelled with an anonymous identifier and sample time and stored on ice until the end of the study session. Samples were then stored in an upright position at −80˚C pending analysis. Participants rinsed their mouths with a small amount of water immediately after sample collection, in preparation for subsequent sampling. No samples were visibly contaminated with blood, and a blood contamination kit was not used.

Analysis of the saliva sample was undertaken using the Salimetrics expanded-range, high-sensitivity salivary cortisol enzyme immunoassay kit as per the manufacturer's

instructions. This assay is a competitive immunoassay kit. Cortisol in the study samples and the kit standards compete with cortisol conjugated to horseradish peroxidase for the antibody binding sites on the microtitre plate. Bound cortisol is measured by the reaction of the horseradish peroxidase to the substrate tetramethylbenzidine (TMB), which gives a blue colour. Once the reaction is stopped with an acidic solution, a yellow colour forms. The optical density is read on a standard plate reader at 450nm. The amount of cortisol present in the sample is inversely proportional to the detection of the cortisol-enzyme conjugate.

Once samples had been collected from the whole study group, the swabs were thawed on ice, vortexed and centrifuged at 1500 x g for 15 minutes to remove mucins and particular matter that may interfere with the assay. All samples were processed on the same day and were subjected to the same number of freeze-thaw cycles. Reagents were prepared according to the kit protocol. Twenty-four µl of standards, control and saliva, were added to the appropriate wells, 25 µl of Assay Diluent was also added to two wells to serve as a zero, and into each non-specific binding well. Then 200 µl of dilute enzyme conjugate was added to each well and mixed on a plate rotator for 5 minutes at 500 rpm. After incubation at room temperature for 1 hour, the plate was washed four times with 1X wash buffer, after each wash, the plate was blotted on paper towel. 200 µl of TMB substrate solution was then added to each well, mixed at 500rpm for 5 minutes and incubated in the dark for 25 minutes. 50 µl of stop solution was added to each well, after mixing for 3 minutes (500 rpm). The plate was immediately read at 450 nm on a plate reader (Benchmark Microplate Reader, BioRad, Hercules, California, USA). The concentrations of the saliva samples and standards

were determined using a four-parameter non-linear regression curve fit using Microplate Manager Software, Biorad, Hercules, California, USA. The overall intra-assay coefficient of variation was < 10%.

**2.6 Infrared thermography**

The electromagnetic spectrum is composed of electromagnetic radiation waves and is often presented in order of wavelength, from longest to shortest. Only a small portion of the spectrum is visible as light (between 390 – 700 nm). Between microwaves and visible light are infrared (IR) waves, these are further classified as near (1.0 – 5 μm), middle (8 – 25 μm) or far-infrared (wavelength of 25 – 1000 μm). Far infrared waves are furthest away from visible light, are thermal and give off heat. All objects that are not at absolute zero (absolute zero is the temperature where all molecular motion ceases and corresponds to −273 Celsius or −460 Fahrenheit or zero degrees Kelvin) emit infrared radiation. Any object with a temperature emits infrared radiation, and thermography can be used to detect this.

A blackbody is a theoretical object that emits a maximum amount of energy at all temperatures in all wavelengths, it is a perfect emitter and a perfect absorber. There are three main laws that concern infrared radiation. These are based on the performance of the blackbody.

i) The Stefan-Boltzmann law defines the formula to determine the amount of energy emitted by an object due to its absolute temperature. The amount

of energy radiated by an object is proportional to the object's temperature in Kelvin raised to the $4^{th}$ power.

Where:

$$\text{Total amount of radiated energy} = 5.67 \times 10^{-8} \times T^4$$

$5.67 \times 10^{-8}$ is the Stefan-Boltzmann constant
T is temperature in Kelvin degrees

ii) Wien's law determines the wavelength at which a maximum amount of energy is emitted by an object at any specific temperature. As most objects emit many wavelengths, this law is useful in thermography to help decide which wavelength device should be selected for maximum accuracy.

Where:

$$\lambda \text{ max} = 2898 / \text{T.Kelvin}$$

When using thermography to detect skin temperature, temperatures often lie between 33 to 37˚C, so λ max is therefore c.9 microns, such that a long wave camera (8 – 15 microns) is the most accurate.

iii) Planck's law describes the relationship between temperature, radiated energy and wavelength. The law is complex and a full explanation is beyond the scope of this thesis; however, it forms the basis of how temperature values are obtained from measurements of infrared radiation from a thermal camera.

The infrared camera not only senses radiant energy emitted directly from an object due to its temperature, but also the energy reflected off the object from its background and the energy transmitted through the object of interest from behind. Although most objects (assuming they are thermally opaque) have no transmission, most do reflect significant amounts of radiant energy. Modern cameras allow for this during the camera set-up and require the operator to input a value for background reflected temperature.

One further property that must be considered during thermography is emissivity. This is the rate at which an object emits energy compared to that of a blackbody at a given temperature and wavelength. The thermal properties of an object can only be assessed during thermography if the emissivity of the object is known. Emissivity is determined by an object's material composition, surface (c. 0.025 mm) condition, temperature, the wavelength it is viewed at and the geometry of the area that is viewed. Emissivity may be measured using a thermal camera or may be determined from published emissivity charts. The emissivity of human skin is 0.98 and is one of the highest natural emitters; therefore, for all the work undertaken in the studies presented in this thesis, emissivity was set at 0.98. In contrast aluminium foil, one of the lowest emitters (emissivity of 0.04) was used during camera set-up to calculate reflected background radiant energy.

A microprocessor within the thermal camera uses the Stefan-Boltzmann formula and Planck's law to calculate the temperature of an object from the radiant energy emitted

from the immediate surface of the object, producing a two-dimensional map of the three-dimensional temperature distribution (Jones and Plassmann, 2002)

There has been rapid development in infrared detection technology since the 1970s; for example, the original single-detector systems have been replaced by large arrays of detectors, which are usually uncooled focal plane arrays (FPA). These arrays come in various sizes with different numbers of detectors, the more detectors the greater the thermal resolution. The radiometric camera used in the Division of COG for the University of Nottingham's early work (the FLIR B60) had a FPA of 180 x 180, generating images with a thermal resolution of 32,400 pixels. The more recent cameras used in Studies I to V, the FLIR B425 and FLIR E60 have a FPA size of 320 x 240, with more than twice the number of detectors and much greater resolution. The camera in use for BAT assessment at the time of thesis submission has a thermal resolution of 161,472 pixels, with a resolution almost five times that of the FLIR B60.

Detected radiant energy is converted to a false-colour image within the camera for immediate viewing, or in the post-processing software as thermograms. These thermograms can then be analysed qualitatively by looking at thermal patterns, or quantitatively to determine the temperature of specific regions of interest (ROI). The quality of the thermal image is integral to accurate quantitative analysis and is dependent on ensuring that all the required parameters are set correctly and consistently (e.g. emissivity, reflected temperature, ambient temperature and humidity) and that the image is focussed adequately on the ROI (Tattersall, 2016, Ring et al., 2004).

### 2.6.1 Acquisition of thermal images

The procedures used in Studies I to V for thermal image acquisition were based upon the Standard Procedures for Infrared Imaging (Ammer and Ring, 2013) and the recommendations of the Glamorgan Protocol (Ammer, 2008) alongside the procedure developed within the Division of COG, the University of Nottingham prior to the start of my studies.

Neither of the documents referred to above discusses imaging of the supraclavicular region. However, the recommendations for subject preparation, imaging environment and camera set-up were followed where feasible and appropriate with the aim of keeping the variability to a minimum.

Two thermal cameras were used in the studies outlined in this thesis, the FLIR B425 and the FLIR E60, and some preliminary work was undertaken using the FLIR B60. All cameras were set up and used as per manufacturer's instructions and following the specific camera user guide.

In brief, the camera was mounted upon a tripod and connected to a power supply (either battery, or mains depending on availability and environmental circumstances), turned on, and the lens cap removed. Care was taken to ensure that imaging was undertaken away from any other source of infrared radiation or airflow. The camera was left on for a minimum of 30 minutes before any images were taken as the failure to do so can result in normal detector noise during imaging, and significant detector drift with subsequent non-uniformity correction (Quesada et al., 2017, Tattersall,

2016). The camera was placed in 'Auto Mode' to determine the upper and lower temperature values used on the camera display. The image was reviewed to ensure that no pixels within the supraclavicular region were black or white and that the overall image of the participant was made up of at least 90% of the colours in the active palette. Imaging was undertaken in all studies in a rainbow palette. The camera was focussed manually (FLIR B425 by using the focus up and down buttons, and the E60 by using the manual rotation of the focus ring) to ensure that the line of the contour of the shoulder was sharp and details of the eyelashes were visible. Whilst the FLIR B425 had the option of an automatic focus, this was not used alone to focus the camera as it could not be relied upon to produce an image with optimal detail in both the left and right supraclavicular regions. It is also of note that the manual control of the focus ring on the E60 was much easier than the up/down buttons of the FLIR B425 and could be undertaken without as much movement of the camera. During sessions of prolonged imaging, the focus was noted to drift with both cameras, images were checked periodically, and the focus was adjusted as needed; this was more evident on the FLIR B425, especially when images were taken using the automatic capture feature.

The angle at which the camera is placed can affect the amount of radiant energy visible to the sensor and can consequently affect the temperature calculations. The maximum amount of energy detected by the sensor occurs when positioned perpendicularly to the surface of interest. Given the morphology of the supraclavicular region as a three-dimensional structure, optimal positioning of the camera in relation to the supraclavicular region was not immediately apparent and has since been

debated (Law et al., 2017). For my studies, the camera was placed with the lens at the level of, and perpendicular to, the sternal notch. The thermograms, therefore, encompassed the neck and whole upper thorax. As the angle between the lens and the ROI becomes smaller than 90˚ the amount of radiated energy captured decreases, however, it is generally accepted that an accurate quantitative temperature calculation can be obtained when the thermal camera is within 45˚ either side of the perpendicular.

Positioning the camera lens perpendicularly to the sternal notch enabled simultaneous imaging of the left and right posterior triangles of the neck, the area in which Bonnot (1908) described the location and anatomy of supraclavicular BAT (Figure 1.7) and encompassing the triangular hotspot observed by Symonds et al (2012a) and Lee et al (2011) as demonstrated in Figure 2.1.

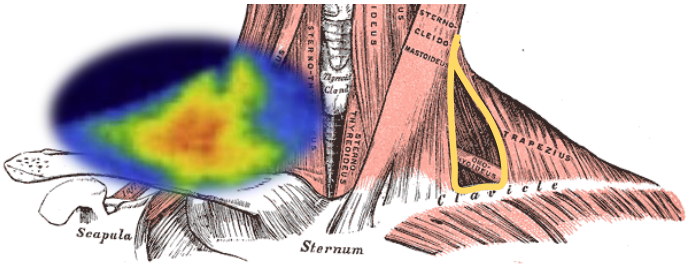



**Figure 2.1 The left posterior triangle of the neck**. Bound by the clavicle inferiorly, and by the anterior border of the sternocleidomastoid muscle and posterior border of the trapezius superiorly (indicated by the orange line). Image reproduced from Grays Anatomy plate number 386 (no longer under copyright) with the right supraclavicular hotspot reproduced from Figure 4.D in Symonds et al (2012a) superimposed (with permission; see Appendix for details).

To maximise the resolution/number of pixels in the supraclavicular region, the camera was placed so that the field of view encompassed the full width of the upper torso, so that the shoulder-to-shoulder width was at least two-thirds of the overall image width. The distance from the lens of the camera to the sternum was recorded and entered into the camera during set-up. Where this was not possible (e.g. Study I, where imaging was undertaken within the constraints of the school environment), the camera was placed at a fixed distance of 1 m from the participant.

The ambient temperature and humidity of the room was measured to one decimal place using the Extech Moisture Meter MO297 (Extech Instruments). The reflective background temperature was also measured at the start of each imaging session. Participants were asked to hold up a square piece of cardboard covered with aluminium foil in front of their sternum. A spot measure of temperature at the centre of the foil-covered square was recorded, and this measurement was repeated three times, then the mean of the three measurements was entered into the camera as the reflective temperature during camera set-up. In addition, the distance from the camera lens to the participant's sternal notch, the ambient room temperature and humidity and the emissivity of skin (0.98) were also entered into the camera set-up menu at this time.

Images were taken manually with the FLIR E60 using the trigger (Study V). In the studies using the FLIR B425, where the cooling protocol was short, images were taken at intervals manually using the capture button. Where the cooling protocol was long (Study IV), images were obtained using the automatic capture feature. All images were

saved directly to a memory card and uploaded onto a personal computer for quality review and thermographic analysis.

To ensure that images could be compared between time points, it was imperative to keep participants sitting as still as possible. Several methods were used to optimise this and varied between the studies as the methodology evolved. Maintaining even short periods of immobility for children was extremely difficult. To assist, children were seated on an appropriately sized chair, with their feet resting flat on the floor. The chair was placed directly in front of a wall to allow the child to rest the back of their head against it to maintain a neutral position.

The thermal camera was connected to a large TV screen and once the child was seated with their shoulders relaxed and their head in the neutral position, markers were placed onto the screen at the shoulder tips, the sternum and at the mandibular prominence of the chin. Very young children in Study I were asked to watch an innocuous DVD (The Blue Planet) and to try to sit still. If movement did occur, children were asked to reposition themselves using the screen markers just before the next image was taken using the screen as a mirror. A similar method was used in Study II (without the use of a DVD).

An adaptation of this method was also used for Study III, where adult participants were imaged over a longer duration. The screen and markers were used but away from the participant and viewed only by the researcher. Participants were not required to sit completely still. Some movement was incurred during salivary sampling

and participants were also allowed to read a newspaper or magazine during periods of inactivity. The participant was seated upright with their head resting against the wall and behind a privacy screen away from the researcher and equipment to reduce any anxiety of being watched. Unlike the children, these participants could therefore not reposition themselves, but did so under verbal direction of the research investigator.

Studies IV and V were undertaken with the participants semi-reclined on a hospital bed (Study IV) or examination couch (Study V) this enabled them to be still throughout imaging, but did not produce images with as good exposure of the supraclavicular region.

A technical summary of the different cameras in use in the Division of COG, the University of Nottingham for the assessment of supraclavicular BAT from 2011 to 2019 is shown for reference in Table 2.1 below.

**Table 2.1 Technical summary of the FLIR cameras used in the Division of Child Health, Obstetrics and Gynaecology, the University of Nottingham for the assessment of supraclavicular skin temperature as a proxy measure of brown adipose tissue activity between 2011 and 2019.**

| Camera model | Thermal sensitivity | Thermal resolution | FOV | Accuracy | Range (µm) | Detector type |
|---|---|---|---|---|---|---|
| B60 | < 0.07˚C | 180 x 180 | 25˚ X 25˚ /0.1m | 2% | 7.5 – 13 µm | FPA, uncooled microbolometer |
| B425 | < 0.05˚C | 320 x 240 | 25˚ X 19˚ /0.4m | 2% | 7.5 – 13 µm | FPA, uncooled microbolometer |

| | | | | | | |
|---|---|---|---|---|---|---|
| E60 | < 0.05˚C | 320 x 240 | 25˚ X 19˚ /0.1m | 2% | 7.5 – 13 µm | FPA, uncooled microbolometer |
| T540 | < 40 mK | 464 x 348 | 24˚ X 18˚ /0.15m | 2% | 7.5 – 14 µm | FPA, uncooled microbolometer |

Abbreviations: FOV – field of view; FPA – focal plane array

**2.6.2 Thermal image analysis**

The procedure for analysing supraclavicular thermograms has evolved during the time taken to complete the studies presented in this thesis and beyond. Over the last 5 – 6 years, the availability of new software had a dramatic impact on how images have been analysed within the Division of COG, the University of Nottingham. In parallel progress has also been made in adapting this commercially available FLIR software and also in devising in-house software specific for analysing supraclavicular BAT. Therefore, the methods of thermal image analysis for each of my studies vary slightly, representing this evolution. Irrespective of these minor method variations, the underlying principle whereby a thermal camera is used to quantify the radiant heat emitted from the surface of the skin overlying supraclavicular BAT remains the same.

In all my studies thermal images were firstly displayed in the proprietary FLIR software available at the time of analysis (including QuickReport, ThermaCAM Researcher Pro, ResearchIR, ResearchIR Max and FLIR Tools+) allowing the thermograms to be inspected visually for an assessment of quality.

Firstly, the metadata were cross-referenced with the written records of ambient temperature, humidity, reflective temperature, emissivity and camera distance to ensure no errors had been made during camera set-up. Although these parameters

were recorded to one decimal place, the set-up menu on the FLIR E60 camera would only accept integers. Therefore, when the images from this camera were uploaded into the post-processing software, these parameters were revised to one decimal place in the software settings and the images were re-saved for further quantitative analysis. For all analyses, the colour palette was set to the highest-resolution rainbow setting available in the FLIR software and the span of the visible temperatures was set to ensure that at least 90% of the available colours within the palate were visible on the thermograms of the participant (background not included).

All images were visually reviewed to ensure that no artefacts were obscuring the supraclavicular region for example, strands of hair or jewellery overlying the supraclavicular region. The thermograms for each participant were visually checked for evidence of significant movement, scrolling through from the first image to the last in order of acquisition. To allow accurate comparison of a single ROI at different time points, the positioning of the subject or object being imaged must remain constant (Ammer and Ring, 2013). Therefore any sets of images where the movement was significant were excluded from further analysis. In the studies where images were analysed using the manual method of ROI isolation (detailed in section 2.6.2.1), the size of each supraclavicular ROI was calculated in terms of pixel area.

Given that the camera was maintained in a fixed position, and landmarks were used to place the ROI, large changes in the pixel area were assumed to be as a result of movement. Preliminary work undertaken during thermographic training clearly identified that movement of the shoulders, neck and upper torso can affect the size

of the supraclavicular region. Therefore, thermograms where the area of the supraclavicular ROI increased or decreased by more than 10% from the size of the ROI in the first image of the series, were not considered suitable for quantitative analysis.

#### 2.6.2.1 Manual ROI placement using FLIR software

The first thermographic studies of supraclavicular BAT undertaken within the Division of COG, the University of Nottingham were analysed using FLIR Quick Report V 1.2 (FLIR Systems AB, Danderyd, Sweden). This was rudimentary software and allowed the isolation of only simple ROIs (e.g. circle, square, oval, etc.), or spot measurements. These initial measurements of $T_{SCR}$ were made using a rectangular ROI to encompass the upper thorax and neck, using anatomical landmarks of the shoulder tips laterally, the mandible superiorly, and the nipple line inferiorly (Symonds et al., 2012a). This was modified slightly during the preliminary work for Study I so that the inferior border was revised to be at the level of the sternal notch rather than the horizontal nipple line, as this was not visible in these participants whilst wearing the standardised cotton vest (Figure 2.2A). The radiometric temperature data were exported into Excel as a CSV file (Figure 2.2B), where each cell within the CSV file contained a numerical value of temperature in ˚C representing a single pixel from the original thermal image. A thermal ROI was designated as the upper $10^{th}$ percentile of temperatures within the rectangular ROI (demonstrated as the green cells in Figure 2.2B), and a summary measure of supraclavicular temperature was defined as the mean of this thermal ROI.

This method gave a crude assessment of the temperature of the hottest part of the supraclavicular region; however, it was clear when starting to analyse the images from

Study I with this method that the proportion of the rectangular ROI actually containing the subject being imaged was quite variable and depended on the size, age, habitus and position of the head of the participant.

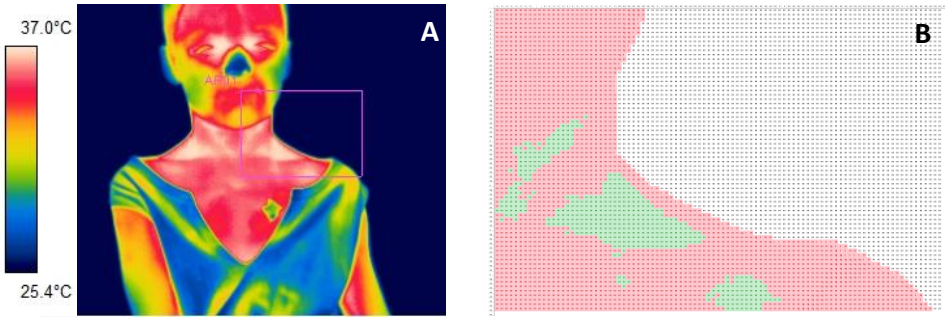



**Figure 2.2 Thermograms visualised in a high-resolution rainbow palette in FLIR ThermaCAM pro 2.1 and the output of the temperature data displayed in Excel.** A) A thermogram of a male child with the manually placed rectangular region of interest (ROI) placed over the supraclavicular region (the purple rectangle) using the landmarks outlined by Symonds et al (2012a). B) A representative image of the CSV output in Excel when the rectangular region of interest is exported from the FLIR software. Each cell represents an individual pixel from the thermogram. For illustrative purposes, the pixels from the participant's body are colour-coded pink, and the upper 10$^{th}$ percentile of temperatures within the rectangular ROI is identified as green (the thermal ROI).

Also, it was evident that this method was designating pixels to the thermal ROI that lay outside the borders of the posterior triangle of the neck (as observed in the Figure 2.2B) and may represent other structures (e.g. superficial veins or lymph nodes), and not exclusively reflect BAT. Hot spots generated by superficial vasculature are well recognised in thermography. Using a high resolution thermal camera it has been reported that IRT of the hot spot overlying the carotid arterio-venous complex can even yield accurate heart rate data by detecting small fluctuations in temperature associated with blood flow (Cardone et al., 2015).

In a randomly selected subset of 30 children from Study I, the first image from each child was analysed using ImageJ (Schneider et al., 2012) to determine the proportion of the rectangular ROI as defined by Symonds et al (2012a) that was actually the participant. This ranged from 35% up to 54% (with a mean of 44%). A similar degree of variability in supraclavicular region size relative to the rectangular ROI was seen in the thermograms obtained in an early adult pilot study obtained as part of a co-supervised BMedSci project (n = 16), where the SCR was found to be between 45% and 85% of the size of the overall rectangular ROI.

Acquisition of ThermaCAM Researcher Pro 2.1 (FLIR Systems AB, Danderyd, Sweden) software with a polygon ROI function enabled more accurate isolation of the supraclavicular region. Using this, I developed the method of supraclavicular ROI isolation further. Using the polygon tool, the left and right supraclavicular regions were drawn around manually, aiming to encompass the posterior triangle of the neck without the inclusion of structures unrelated to supraclavicular BAT.

To reduce the variability and optimise repeatability of ROI placement, the supraclavicular regions were isolated using anatomical landmarks visible within the thermograms. These consisted of the sternal notch inferiorly, the acromioclavicular joint laterally, and the course of the sternocleidomastoid down to the sternal notch in the midline medially. The sternal notch was not easily identifiable in all children. Therefore the midpoint at the level of the larynx was identified using the placement of two identically sized rectangles placed across the width of the neck. A vertical line was then drawn through this midpoint to represent the midline of the participant and

the sternal notch estimated to lie on this line at the level of the clavicular head (Figure 2.3).

The image was then enlarged to 200% of its original size and the cursor used to manually trace along the lateral contour of the shoulder to the acromioclavicular joint, then along the course of the clavicle in a straight line to the sternal notch in the midline, and along the course of the sternocleidomastoid muscle as shown in Figure 2.3. Once in place, the image was enlarged further to 400% and the course of the line along the lateral aspect checked and adjusted to ensure the ROI was lying exclusively over the skin.

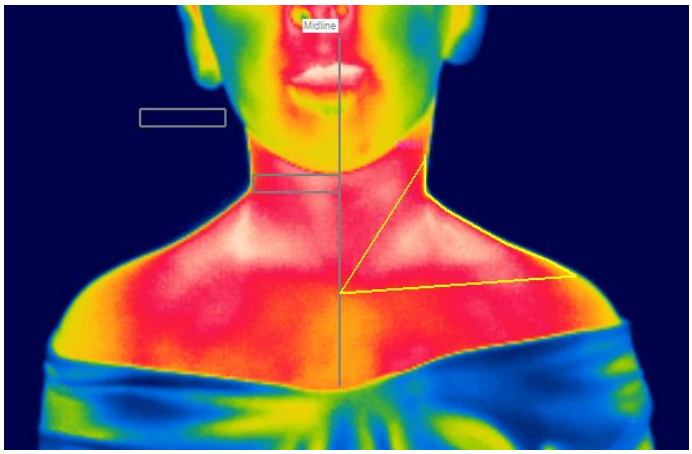



**Figure 2.3 Example of the left supraclavicular region of interest isolated manually using FLIR software (ThermaCAM Researcher Pro 2.1 or ResearchIR Max).** The supraclavicular region is bound by the yellow outline, and the vertical grey line demonstrates the midline. Two rectangles are shown, one to the right of the participant's midline, and the other moved away after identification of the midline to allow placement of the supraclavicular ROI.

The repeatability of the supraclavicular ROI defined in this manner was excellent. As variation in ROI size is associated with variability in temperature readings, particularly

when the ROI is small (Ammer, 2005, Seixas et al., 2018), the intra-rater reliability of supraclavicular polygonal ROI placement was assessed using the same subset of 30 images from Study I described above. To assess the reliability of this method, images were analysed as detailed above on two occasions five days apart. Relative reliability was assessed by Intraclass Correlation Coefficient (ICC) measures (using a two-way, mixed-effects, absolute agreement, and single measurement model), and absolute reliability was assessed using Bland Altman agreement measures. The ICC coefficients (and 95% confidence intervals (CI)) for ROI size, sum total temperature and mean temperature were 0.94 (95% CI 0.87 – 0.97), 0.94 (95% CI 0.88 – 0.97) and 0.98 (95% CI 0.96 – 0.99). The Bland Altman plots for each of these measures also indicate good reliability with minimal mean biases and narrow limits of agreement (Figure 2.4).

**A**

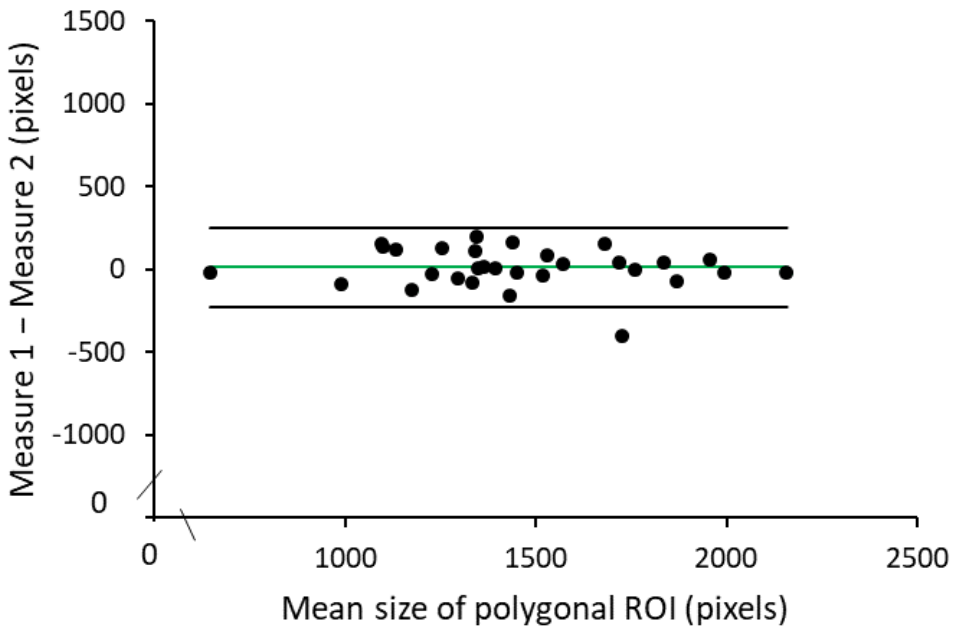
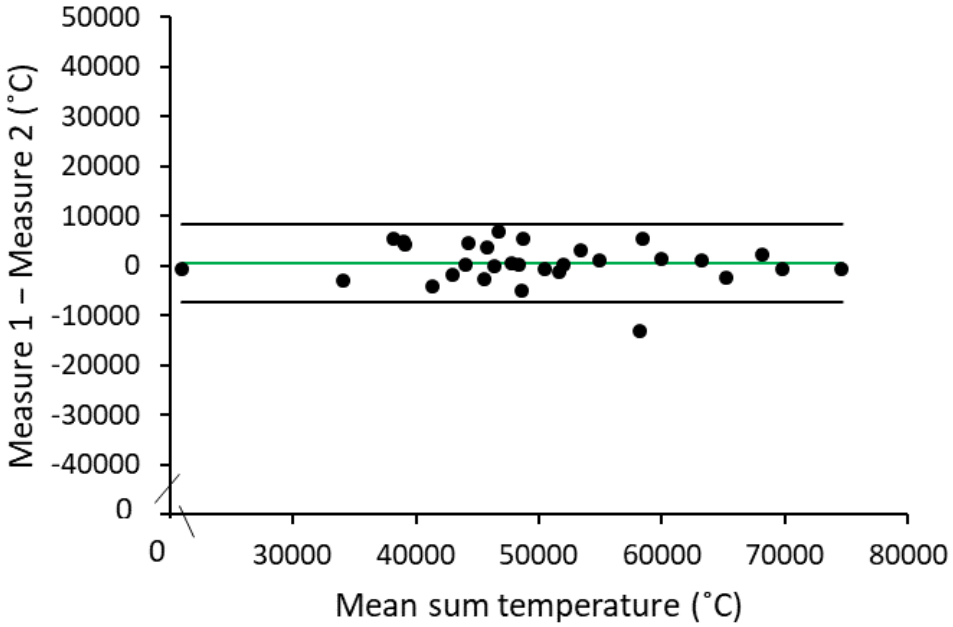



**Figure 2.4A Bland-Altman plot using the size in pixel area of the polygonal supraclavicular region of interest (ROI) isolated using manual placement with FLIR ThermaCAM Pro 2.1.** Measure2 was made 5 days after Measure1. Mean bias (shown

as a green line) = 11 pixels, upper limit of agreement = 246 and lower limit of agreement = −223 pixels indicated by black lines

**B**




**C**

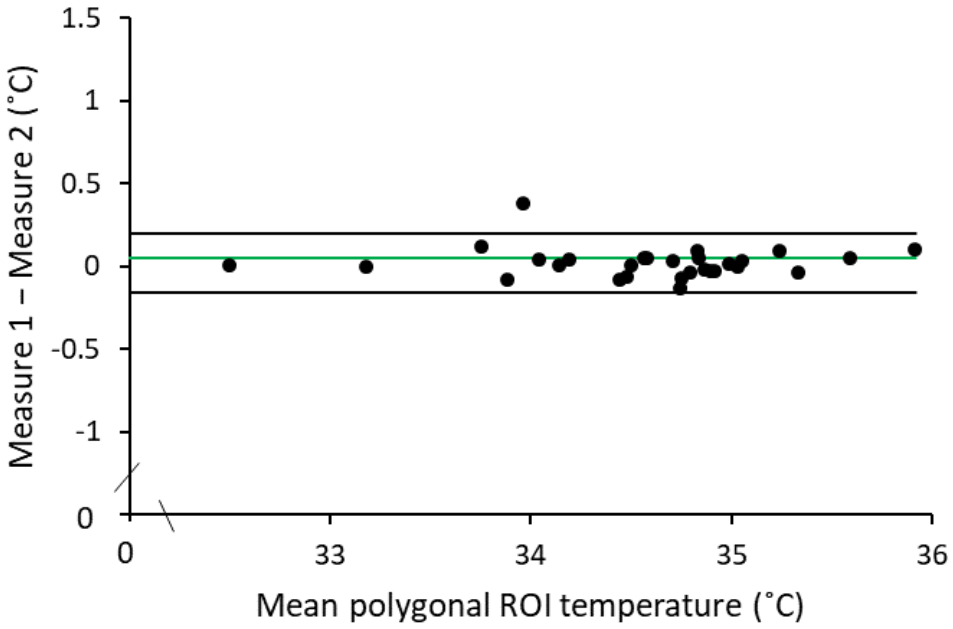


**Figure 2.4B and C Bland-Altman plot using the sum temperature and mean temperature of the polygonal supraclavicular region of interest (ROI) isolated using manual placement with FLIR ThermaCAM Pro 2.1.** Measure2 was made 5 days after Measure1. B) Mean bias = 485.26˚C, upper limit of agreement = 8369.23˚C and lower limit of agreement = − 7398.71˚C. C) Mean bias = 0.02˚C, upper limit of agreement =0.2˚C and lower limit of agreement = − 0.15˚C. The mean bias is indicated by a green line and the limits of agreement indicated by black lines.

The inter-rater reliability of this manual procedure was explored as part of a wider collaborative project, but the data or findings were still not available to me at the time of thesis submission. This manual method of supraclavicular ROI placement was extremely labour intensive and time consuming and was rapidly superseded by a semi-automated method of ROI placement developed by J Law (Law, Pending submission) detailed in section 2.6.2.3.

The polygonal supraclavicular ROI isolated using these anatomical landmarks was significantly smaller than the rectangular ROI used in the Symonds et al. (21012a) study and preliminary work for this thesis. To encompass a similar hotspot predominantly within the borders of the posterior triangle of the neck visible within the thermograms, an approximation was made based on a subjective comparison of the thermal patterns observed in the thermograms and, the thermal hotspot ROI detected in the CSV radiometric temperature data output. The upper 25$^{th}$ percentile of temperature values within the supraclavicular polygonal ROI was chosen as this most similarly represented the triangular-shaped hotspot collocating to the posterior triangle of the neck observed in thermograms (Figure A3.1 in Appendix to Study I). This thermal ROI also selected a set of pixels that were principally contiguous (see Figure A3.1A in the Appendix to Study I) and clustered over the anatomical position of

supraclavicular BAT described by Bonnot (1908) (Figure A2.1). Proportions isolated using the upper 5$^{th}$ to the 50$^{th}$ percentiles were also explored, and in the absence of any paired FDG-PET-CT and thermal data at the time the 25$^{th}$ percentile was chosen for the analysis of Study I.

The distribution of the pixel data within the upper 25$^{th}$ percentile in each polygonal supraclavicular ROI of each image was explored, and when plotted as histograms these data were positively skewed. The calculation of this skewness confirmed a moderately positive skew (mean skew 0.60, 95% CI 0.47 – 0.73). Therefore, the median value within the upper 25$^{th}$ percentile (or overall 87.5$^{th}$ percentile value of the polygonal supraclavicular ROI) was chosen as the summary measure for $T_{SCR}$.

Study III represented the first group of adults imaged with thermography to assess BAT using a polygonal supraclavicular ROI, and at this time IRT of the SCR had not been validated against any other measure of BAT nor had the anatomical co-location of this ROI been formally explored. Qualitative preliminary analysis of the SCR in the images acquired from adults identified that the thermal patterns observed in older participants were very different from those seen in children. In nearly all children a distinct large localised hot spot was evident in the SCR in the same anatomical position. In the adults imaged as part of Study III, this thermal pattern was not observed as consistently. When classified as the upper 25$^{th}$ percentile, the thermal ROI was not a discrete region as seen in the children and was highly variable in terms of its location within the polygonal ROI. Therefore for Study III, the upper 5$^{th}$ percentile was utilised instead, as this produced a more focal thermal ROI.

The optimum summary measure for supraclavicular temperature was explored in more detail within the Division of COG, the University of Nottingham by another researcher using an analysis of paired FDG-PET-CT and thermographic data obtained from healthy volunteer adults (Law, Pending submission). Using this data Law and colleagues demonstrated that the 95$^{th}$ percentile (the median of the upper 10$^{th}$ percentile) and the uptake of radiolabelled glucose correlated positively with the change in relative $T_{SCR}$ in response to cold stimulation, and that there was a significant spatial overlap between maximal MR(gluc) and maximal supraclavicular temperature during the cooling period explored.

Consequently the use of the 95$^{th}$ percentile within a polygonal supraclavicular ROI was adopted as standard procedure for supraclavicular BAT assessment within COG (Standard Operating Procedure V3.0 Automated analysis of thermal images) and was used for the analysis and preparation of manuscripts for Studies II, and V.

#### 2.6.2.2 Calculating the summary measure of supraclavicular skin temperature

The CSV file containing the radiometric data of the ROI was either analysed in Excel using a Macro, or analysed in R (A Language and Environment for Statistical Computing, V3.4.3 (R Core team)) with a custom written script. I wrote the Macro in Visual Basic, and the R script (with the assistance of Dr A Prayle) to identify the thermal ROI within the anatomical supraclavicular ROI. The details of the thermal ROI used for each study are referred to in each study manuscript.

#### 2.6.2.3 Semi-automated ROI placement using custom MATLAB script

A departmental semi-automated method for polygonal ROI placement over the supraclavicular region was developed by J Law (Law et al., 2018) and became standard procedure for BAT assessment from May 2016 within the Division of COG, the University of Nottingham. It was utilised to analyse the images obtained in Studies II, and V to bring this data into line with standard departmental practice.

Using the custom written script in MATLAB (adapted from a script by Tattersall (2015), thermal images were exported into the MATLAB environment, where they were visible in a Portable Network Graphic format in an unspecified rainbow palette (figure 2.5A). An individualised body threshold temperature was set to ensure that the background behind the participant was completely black (thus not contributing any thermal data to the ROI). This varied between participants but was kept the same for each individual. The size of the image was maximised and markers were placed at the five apices of the polygonal region of interest, notably the most lateral visible aspects of the sternocleidomastoid and the acromioclavicular joint on the left and right sides, and a single marker placed just below the sternal notch (Figure 2.5B).

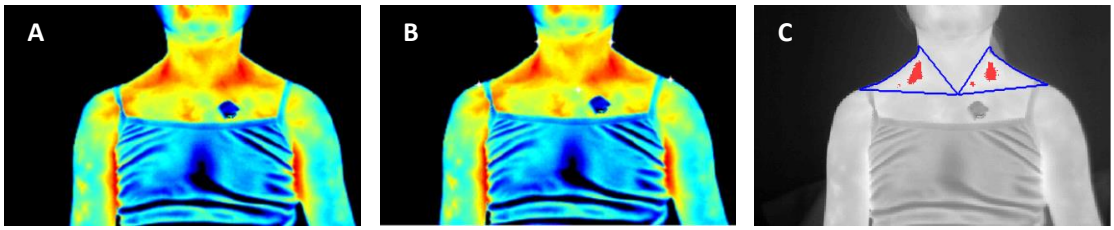



**Figure 2.5 Procedure for thermal image analysis of supraclavicular brown adipose tissue in MATLAB.** A) Representative thermal image as displayed in Portable Network Graphic format within MATLAB, with the individualised body threshold temperature set to ensure a completely black background. B) The positioning of the five markers to isolate the borders of the supraclavicular region of interest (ROI), shown as white dots with cross-hairs. C) The supraclavicular anatomical ROI identified using the custom processing script in MATLAB demonstrated by the blue triangular outline, and the thermal ROI demonstrated by the red pixel area (upper 10$^{th}$ percentile of values).

A "processing" script was then run that produced an image of the polygonal anatomical ROI (bound within a blue line) and the thermal ROI (displayed as red pixels) as shown in Figure 2.5C and an Excel worksheet containing the summary data for each image analysed (filename, left and right 95$^{th}$ percentile supraclavicular temperature).

## 2.7 Non-BAT skin temperature measurement

### 2.7.1 Skin temperature measurement using iButton devices

Skin temperature at other sites away from the supraclavicular region was measured using iButton Thermacron® temperature data loggers (model no. DS1219H-F50; Maxim, Sunnyvale, California, USA). These small wireless data loggers consist of a silicon chip encased in a stainless-steel can. The can consists of a base and a lid, and the silicon chip sits on top of the base. For my studies, the iButtons were placed with their base flush to the skin surface and were maintained in position with two pieces of surgical tape (Micropore™ Surgical tape, 2.5cm wide) placed at right angles to each other. The iButtons were activated to begin sampling using the 1-Wire interface and a

personal computer, detached then secured in position on the skin of the participant. Following the first study undertaken with these devices (Study I), it became clear that iButtons should be in situ for a minimum of 15 minutes to allow the metal casing to equilibrate with the skin and ambient temperature. This was undertaken as standard in all studies except for Study I.

The manufacturer's information advises that the DS1219H measures in 1/8˚C increments to ±1˚C accuracy; therefore to maximise the consistency of measurements between individual data loggers all iButtons were examined simultaneously in a water bath at a fixed temperature to allow calculation of a calibration formula for each button (Table 2.2).

**Table 2.2 Calibration formulae used for the set of iButtons used in Studies I to V.** These individual calibration formulae were used in all studies described in this thesis.

| iButton unique identifier | Calibration formula |
|---|---|
| 67B821 | 1.009 +0.06 |
| 605c21 | 1.010 + 0.158 |
| 664f21 | 1.005 + 0.492 |
| 678421 | 1.005 + 0.288 |
| 5c3421 | 1.004 + 0.434 |
| 5de321 | 1.003 + 0.359 |
| 5eab21 | 1.005 + 0.080 |
| 63bc21 | 0.995 + 0.491 |
| 646721 | 1.000 + 0.495 |
| 5df321 | 1.014 – 0.014 |

To calculate mean skin temperature, iButtons were placed at seven sites as follows; central forehead, dorsum of the hand, dorsal aspect of the mid -forearm, chest at the level of the second intercostal space midclavicular line, mid-anterior thigh, mid-point of the tibia and dorsal aspect of the foot. When used in a cooling study, iButtons were placed on the opposite side to the cold stimulus.

Mean skin temperature ($T_{MSK}$) was calculated using the weighting formula of Hardy and Du Bois (Hardy and Oppel, 1938). Several such formulae exist, using measurements from 4 to 15 skin sites, with different weighting coefficients. Each has advantages and disadvantages in terms of practicality, repeatability and consistency. The optimal method is generally considered to be one that uses a large number of skin sites. The 15-point method of Winslow has been reported to be the best (Mitchell and Wyndham, 1969). However, for participant comfort, this method was not felt to be feasible for use in a semi-reclined supine position (i.e. measurements were required on the back, neck and underside of the calf). Therefore, Hardy and DuBois's modified version of Winslow's formula was chosen as a practical alternative (Hardy and Oppel, 1938).

$$T_{MSK} = 0.07\ t_{head} + 0.14\ t_{arm} + 0.05\ t_{hand} + 0.07\ t_{foot} + 0.13\ t_{leg} + 0.19\ t_{thigh} + 0.35\ t_{trunk}$$

As the minimum sampling rate for the DS1219H was one sample per minute, this was used unless specified otherwise. Each iButton was synced to the clock on a personal computer and activated together to ensure measurements at different sites were made simultaneously.

### 2.7.2 Skin temperature measurement using thermography

In Study II skin temperature over the mandibular prominence was measured using the mean temperature of an 86-pixel ellipse (using FLIR's ResearchIR software) before and after hand immersion in cool water, to determine whether the changes in skin temperature observed in the SCR were localised or reflective of a more systemic response. Similar measurements of hand and forearm temperature were made in Study V.

### 2.7.3 Tympanic membrane temperature

Tympanic membrane temperature was used to estimate core temperature in Studies I, II, IV and V using a Braun ThermoScan Pro 4000 infra-red thermometer (Welch Allyn, Skaneateles Falls, New York, USA). Measurements were taken in triplicate, and an average of the three readings used for statistical analysis where appropriate. Tympanic temperature was used to screen for intercurrent illness and monitor for hypothermia during cooling. There were no participants in any of the study who had signs of fever, and nor did any individuals tympanic temperature fall below 36˚C during cooling.

## 2.8 Anthropometrics

### 2.8.1 Height and body weight

Height was measured to the nearest 0.1 cm using a stadiometer (Leicester height measure; Child Growth Foundation, Sutton Coldfield, United Kingdom). Participants stood in a vertical plane against the stadiometer with their heels towards the wall, toes were pointing forward and their knees together. With each participant's head in

the Frankfort horizontal plane, the headboard measuring plate was brought down to reach the crown of the head, forming a right angle with the stadiometer scale. The participant's height was recorded to the nearest 0.1 cm on a data-collection proforma, and this procedure was repeated a further two times. The average of the three readings was used in subsequent data analyses.

Weight was measured to the nearest 0.1 kg with calibrated portable digital scales placed on a firm level surface. All participants were weighed without shoes. In the studies undertaken in local primary schools, children were weighed in their school uniform, in the laboratory-based studies, participants were weighed in standardised clothing as outlined in the experimental study protocols. Participants were asked to stand in the middle of the platform, looking straight ahead. The digital readout was recorded to the nearest 0.1 kg, then the procedure was repeated a further two times, and an average of the three measurements was used for statistical data analyses.

**2.8.2 Body mass index**

Height and weight were measured as described above. Body mass index was calculated as follows:

$$\text{BMI} = \text{weight (kg)} / \text{height}^2 \text{ (m)}$$

Normal weight, overweight and obesity, are classified using absolute cut-offs in adults (e.g. BMI > 30 is classified as obese) and these standard classifications were used in the Studies III, IV and V. Age- and sex-specific BMI percentiles were calculated for children in Studies I and II, using the NHS healthy weight BMI calculator (NHS Choices),

which uses the UK90 reference data in line with the BMI growth charts issued by the RCPCH.

### 2.8.3 Bioelectrical impedance

Bioelectrical impedance analysis (BIA) is frequently used to estimate body composition. It measures the opposition to a small electrical current as it travels through total body water. The conductance of the electrical current is greater through fat-free mass than fat mass as the latter contains very little water. Body water volume can be estimated from the impedance index ($ht^2/R$) and is often used to estimate fat-free mass, so fat mass can then be estimated using known body weight.

BIA measurements were made using a hand-to-foot, single-frequency (50 kHz) battery-operated bioimpedance analyser (BIM4; ImpediMed P/L, Capalaba, Austria) in the supine position. The BIM4 consists of two injecting and two sensing electrodes, the current electrodes were placed on the foot over the distal point of the second metatarsal, and on the hand on the distal portion of the second metacarpal. The sensing electrodes were placed on the anterior ankle between the tibial and fibular malleoli and at the writs between the radial and ulnar styloid. Electrodes were attached to the skin using 5500 Diagnostic Tab Electrodes (Coviden, Tullamore, Ireland).

Arms and legs were positioned at 30 degrees from the midline to ensure they were not in contact with the body or each other. If difficulties in maintaining electrode contact were encountered, the patch electrodes were removed, underlying skin was

cleaned with an alcohol wipe and the electrodes were re-sited. The BIA monitor proprietary algorithms calculated impedance, which was used alongside anthropometric data, age and sex to predict body composition. Values were obtained for total body water, fat mass and fat-free mass. BIA was used in Studies IV and V, but technical issues were experienced with the monitor resulting in an incomplete assessment for Study V.

While quick, simple, non-invasive and relatively inexpensive BIA has a number of limitations that should be acknowledged, the BIA method relies upon regression equations which are usually held by the manufacturers and not made publicly available due to their commercial value. The validity of BIA is influenced by gender, age, ethnicity and hydration status. Moreover, BIA overestimates body fat percentage in those who are very lean and underestimates it in those who are obese. It is generally accepted that BIA is most useful for assessing body composition in large populations and less useful for individuals, particularly in detecting short-term changes. While BIA may be suitable for use in adults, most monitors are not recommended for use in children under 7 years old, limiting their use in the assessment of paediatric body composition.

### 2.8.4 Subcutaneous adipose tissue thickness

MRI of the neck and upper thorax was performed using a 3T scanner (GE Discovery MR750 3.0T, GE medical Systems) with a T1-weighted axial plane with the following variables (TR 500, TE 13.6, matrix 256 x 256, slice thickness 5mm and interslice thickness 3mm). SCAT was defined as the distance between the anterior edge of the

subcutaneous fat and the subcutaneous fascia at the level of the first thoracic vertebrae (T1) and measurements were made in triplicate using OsiriX version 5.6.

### 2.9 Metabolic and cardiovascular

#### 2.9.1 Indirect calorimetry

Indirect calorimetry is the gold standard for measuring metabolic rate and energy expenditure. It uses respirometry as an indirect measure of heat production (energy expenditure) based on the principle that the final common pathway of all cellular fuels is oxidation, which in turn produces carbon dioxide and water. Using continuous measures of gas exchange, calorimetry estimates whole-body oxygen consumption and carbon dioxide release. Energy expenditure can be calculated from oxygen consumption ($VO_2$) and carbon dioxide ($CO_2$) release, using the modified Weir equation (Weir, 1949) (1), but the urinary nitrogen component is often excluded as its total contribution to EE is minimal. The abbreviated formula (2) is more commonly used and forms the basis of the assessment of energy expenditure in this thesis.

$$\text{Energy expenditure } \left(\frac{\text{kcal}}{\text{day}}\right) = ([\text{VO2x3.91}] + [\text{VCO2x1.11}] + [\mu\text{N2x2.17}]) \text{ x } 1440 \quad (1)$$

$$\text{Energy expenditure } \left(\frac{\text{kcal}}{\text{day}}\right) = 1.44(3.94\text{VO2} + 1.11\text{CO2}) \quad (2)$$

In Study IV continuous recordings of oxygen consumption and carbon dioxide production were made using a mask collection method (Oro-nasal reusable face mask, V7450 series, Hans Rudolph Inc., Shawnee, USA) with the Europa gas exchange monitor (GEM; Europa Scientific Ltd., Crewe, UK). Measurements were made in a

quiet laboratory throughout the morning. Baseline measurements were taken only once resting energy expenditure looked to be stable, and individuals had been resting for at least 15 minutes. Participants were all asked to fast from midnight (fasted for 8 to 10 hours) and to avoid alcohol and strenuous exercise in the preceding 24 hours.

In brief, the GEM analyser was connected to a personal computer and cylinder gas supply ($N_2$, $O_2$ and $CO_2$) and allowed to warm up for a minimum of 20 minutes before calibration. The GEM analyser was then calibrated using the GEM Nutrition software $O_2$, and $CO_2$ readings were checked to ensure that they fell within limits outlined in the departmental standard operating procedure. The face mask was secured over the nose and mouth using the headgear as per manufacturer's instructions. To allow adequate exposure of the neck and upper thorax, the tubing was rotated 180˚ up over the shoulder and was secured to the head of the bed. Continuous measurements were made over 60 minutes, 30 minutes at baseline, and during 30 minutes of cooling. An average of the last 15 minutes of each period was used in the final analysis. Energy expenditure was calculated automatically by the GEM Nutrition software and exported as a CSV file onto a personal computer for later analysis.

### 2.9.2 Dietary intake, activity and eating behaviour

Questionnaires regarding dietary intake, activity levels and eating behaviour were completed by all parents/carers of children taking part in Study II. To determine whether the parental responses were subject to contamination by social bias parents were first asked to complete 10 true or false questions regarding personal attitudes and traits, which constituted a short form of the modified Marlowe-Crowne Social

Desirability Scale (MCSDS) (Strahan and Gerbasi, 1972). Significant contamination by socially desirable responding was considered if there was a strong significant correlation between the MCSDS score and the outcome variable of interest. These data are summarised in Table A3.2 in the Appendix to Study II.

Dietary intake was quantified using a standardised food frequency questionnaire, consisting of 151 foods, (adapted from Wardle et al (2001). Parents were asked to indicate how often their child consumed each item on a scale of 1 to 8 (1 – more than once a day; 2 – once a day; 3 – more than once a week; 4 – once a week; 5 – more than once a month; 6 – once a month; 7 – less than once a month; 8 – never tried it). The responses for items were then grouped by food group (carbohydrate, dairy, vegetable, fruit, protein, sweet snack and savoury snack), and a total summed score for each food group was calculated for each parental questionnaire. Where more than 25% of parental responses for a food item were 8 (i.e. never tried), this food was excluded as per standard use of this questionnaire.

Cronbach's alpha was calculated for each food group to assess the reliability of the parental responses, where reliability was low, the foods included within the food group were reviewed, foods were removed one by one to determine if reliability could be improved.

The food groups (and individual items included within these groups) used in the final analyses presented in this thesis for food frequency are summarised in Table A3.1 in the Appendix to Study II.

### 2.9.3 Blood pressure and heart rate

Blood pressure was measured at intervals in Study V using the Omron M3 digital automatic blood pressure monitor (Omron Healthcare UK Ltd, Milton Keynes, UK) with an appropriately sized upper-arm cuff. A single measurement was made, and the systolic, diastolic pressures and heart rate were recorded. Attempts were made to measure blood pressure using a continuous measurement from the ring finger using the Finapres® blood pressure monitor in Study IV. This failed due to vasoconstriction of the fingers during cooling of the contralateral hand when the ambient temperature was low.

## 2.10 Safety precautions

Given the non-invasive nature of these studies, there were few safety concerns. A medically qualified researcher undertook all studies, and a short medical history was taken from all adult participants to ensure they were all healthy volunteers. Tympanic temperature was monitored at intervals of 10 minutes in all studies involving cooling, although this did not drop below 36˚C in any individual in any of the studies.

Where participants fasted, all imaging sessions were undertaken in the early morning to avoid prolonged fasting and hypoglycaemia. All studies were completed before midday. A capillary blood glucose analyser and concentrated sugar drink were available in the imaging suite but were not required.

Children in Studies I and II attended in pairs, having changed into their cotton vests under the supervision of their teacher in the classroom. Children were imaged in a

room with an open door close to their classroom and school teacher, and there were two members of the research team undertaking thermal imaging of the children at all times.

**2.11 Statistical analysis and data presentation**

The distribution of each data set was inspected visually for distribution and tested for normality using the Kolmogorov-Smirnov normality test. Data are presented either mean ± standard deviation (SD) or mean ± standard error (SE) unless otherwise stated and as detailed in each manuscript.

Comparisons between two means were undertaken using Student's paired and unpaired t-tests. Comparisons between percentages were undertaken using the Chi-squared test ($\chi^2$). The degree of association between variables was assessed by calculation of the Pearson product-moment correlation coefficients. The presence of a simple linear relationship between two variables was assessed by linear regression analyses, and standard multiple regression analysis using a simultaneous entry method (where all the predictor variables were entered at the same time) was undertaken to identify determinants of supraclavicular skin temperature.

A one-way repeated measures ANOVA with Dunnet's post hoc multiple comparisons test was used to evaluate the effect of cooling over multiple time points.

A two-way mixed ANOVA was used to determine whether there was an interaction between between-subjects and within-subjects factors. Where a statistically significant interaction effect was identified, a post hoc analysis of simple main effects

or pairwise comparisons were made (detailed for each study in the respective manuscript). All data were checked to ensure that they met the five assumptions required for the two-way ANOVA. Outliers were assessed by inspection of a boxplot, normality was assessed using Shapiro-Wilk's normality test for each cell of the design, and homogeneity of variances was assessed by Levene's test. Mauchly's test of sphericity indicated that the assumption of sphericity was met. There were no outliers, residuals were normally distributed, and there was homogeneity of variances and covariances. Similarly, a two-way analysis of covariance analysis (ANCOVA) was subsequently used to identify interaction effects after controlling for the effect of BMI percentile as a covariate. Where this analysis has been used, data were found not to violate the assumptions required for testing (homoscedasticity, homogeneity of regression slopes, homogeneity of variances as assessed by Levene's test, that there were no outliers, that there were no leverage or influential points as assessed by leverage values and Cook's distance, and that the Studentized residuals were normally distributed as assessed by Shapiro-Wilk's test).

A two-way repeated measures ANOVA was used to identify a significant interaction effect between two within-subjects factors on supraclavicular temperature. All data were checked so that it met the assumptions required for the two-way repeated measures ANOVA. Where a statistically significant interaction was identified, an analysis of the simple main effects was undertaken (detailed within the respective study manuscript). Analysis of the Studentized residuals confirmed normality, as assessed by the Shapiro-Wilk test. There were no outliers, as assessed by having no

studentized residuals greater than ± 3 standard deviations. There was sphericity for the interaction term (assessed by Mauchly's test of sphericity).

A P value of $< 0.05$ was considered as statistically significant unless otherwise stated. Adjustments to the significance threshold were made to allow for multiple comparisons in Study II (during calculation of the Pearson correlation coefficient, false discovery rate was controlled using the corrected method of Benjamini and Yekutieli (Benjamini and Yekutieli, 2001) – with an FDR of 5%), and in Study V (using a simple Bonferroni correction, $P < 0.025$).

Study I represents the first large study of supraclavicular BAT in children aged 6 to 11 years. Sample size calculation based on the small group of children aged 3 to 8 years in Symonds et al. (2012a) study indicated that the minimum number children required to detect the rise in supraclavicular skin temperature after hand cooling was five. The data from Study I were used to calculate the sample size required in Study II, where a sample size of 30 (15 girls and 15 boys) was calculated to detect a 25% difference in $\Delta T_{SCR}$ in response to cold, where right $\Delta T_{SCR} = 0.28 \pm 0.064$ ˚C; $\beta = 0.2$; $\alpha = 0.05$).

To detect a strong correlation ($r > 0.5$) between two variables it was calculated that 29 children would be required. Therefore it is recognised that Study II was underpowered for correlational analysis with adjustment made for multiple comparisons. Studies III, IV and V were considered exploratory pilot studies, no data using supraclavicular temperature as a proxy measure of BAT activity nor the specific

BAT activation protocols trialled in these studies had been used before; therefore, a priori sample-size calculations were not possible for these studies.

Data were analysed using a combination of GraphPad Prism (V. 60c – 7.04, GraphPad software, La Jolla, California, USA) and SPSS (V.19 – 24, IBM, Armonk, New York, USA), using the most contemporary version available at the time of data analysis.

# CHAPTER THREE

---

## Exploring the determinants of supraclavicular skin temperature in early life using infrared thermography

### Study I

### Study II

### 3.1 Preface

The following two studies were designed to explore the determinants of BAT function in childhood, using thermography to quantify the changes in $T_{SCR}$ as a proxy measure of BAT activity. Each followed a similar experimental protocol, observing baseline $T_{SCR}$ under free-living conditions and the subsequent response to a mild cold stimulus. These studies were designed to expand upon the findings of Symonds et al. in 2012 where triangular shaped hot spots were observed in the supraclavicular region of all children, and cooling of one hand in a bucket of domestic tap water was associated with a small rise in the skin temperature overlying the anatomical location of supraclavicular BAT (Symonds et al., 2012a). Five minutes after cold exposure, children aged 3 – 8 years demonstrated the highest thermogenic response of 0.62 ± 0.08˚C. In the older children aged 13 – 18 years, this response was much lower at 0.25 ± 0.08˚C, children aged between 8 and 13 years were not studied.

The initial aims of the two studies (Study I and Study II) presented in this thesis are to explore the cold-induced thermogenic response in a larger group of young children and, to determine whether age, sex, BMI, season and ambient room temperature are associated with $T_{SCR}$. At the time of Study I's conception, data published regarding BAT in children was scant and predominantly focussed on children with oncological diagnoses. Over 6 years later, at the time of writing this thesis, the significant lack of data regarding the developmental physiology of BAT in healthy children is still evident. Therefore, in the context of the small amount of existing data obtained in early life, and also extrapolating from the data acquired from adult populations, it is hypothesised that BAT activity/supraclavicular skin temperature:

i) declines with age
ii) is higher in males as compared to females
iii) declines with increasing BMI percentile
iv) is higher in winter as compared to summer
v) varies with ambient room temperature.

After the first phase of Study I in the winter months, it was not possible to follow-up these children in the summer months for repeat imaging. Therefore seasonal comparisons were abandoned.

Given the findings of Study I, Study II was conceived to confirm the relationship between BMI percentile and $T_{SCR}$ in a second group of children and to explore the relationship between food intake, sedentary behaviour and eating behaviour on childhood BAT. Although Study I did not demonstrate a statistically significant effect of sex on $T_{SCR}$, at the time of Study II's conception evidence was emerging that some sex-dependent differences in BAT exist (Deng et al., 2015, Gilsanz et al., 2012). Therefore, Study II was also designed to explore this in further detail.

### 3.2 Study I

**Body mass index is a determinant of brown adipose tissue function in healthy children (published in *J Pediatr* 2014; 164:318 – 322)**

#### 3.2.1 Abstract

**Objective** To determine whether body mass index (BMI) percentile and ethnicity influence skin temperature overlying brown adipose tissue (BAT) depots in the supraclavicular region in healthy children.

**Study design** Infrared thermography measured supraclavicular region temperature ($T_{SCR}$) at baseline and after exposure to a mild cool stimulus (single hand immersion in water at 20.1˚C) for 5 minutes in children aged 6 – 11 years (n = 55). The studies were undertaken in a normal school environment.

**Results** BMI percentile and ethnicity were significant predictors of baseline $T_{SCR}$ with an inverse relationship between BMI percentile persisting after adjustment for ethnicity. Twenty-four children demonstrated a significant rise in $T_{SCR}$ after exposure to the cool stimulus.

**Conclusion** We have demonstrated a negative relationship between BMI percentile and both baseline $T_{SCR}$, co-locating with the primary region of BAT, and the change in $T_{SCR}$ response to cool stimulus. Future studies aimed at determining the primary factors regulating BAT function in healthy children should be targeted at the goal of maintaining a healthy BMI trajectory during childhood.

### 3.2.2 Introduction

Brown adipose tissue is a highly metabolic, thermogenic tissue characterised by the unique uncoupling protein UCP1 (Cypess et al., 2009), which was previously considered to disappear during infancy but is now known to persist into adulthood (Cypess et al., 2009, Virtanen et al., 2009, Saito et al., 2009). It has been estimated that only 40 – 50 g of BAT maximally stimulated could contribute up to 20% of daily energy expenditure (Cannon and Nedergaard, 2004). In children and adults subject to cold exposure, significant UCP1-positive adipose tissue depots have been demonstrated in the pericardial region (Sacks et al., 2009), supraclavicular region (Wu et al., 2012) and mediastinal and perirenal regions (Nedergaard et al., 2007, van Marken Lichtenbelt et al., 2009), using tissue biopsy and/or radiolabelled $^{18}$F-fluorodeoxy glucose positron-emission tomography with computed tomography (PET-CT).

The precise roles of BAT in human metabolism and energy balance have yet to be fully elucidated, especially for children. Nonetheless, a clear link exists between obesity and BAT dysfunction in adults (Wijers et al., 2010, Vijgen et al., 2011). Understanding the developmental physiology of BAT is crucial in determining whether this is a causative association, although some major limitations of PET-CT imaging prevent its use as a gold standard imaging technique in healthy children. We have recently demonstrated the feasibility of using infrared thermography as a safe, reproducible and robust technique for measuring the temperature of the skin overlying BAT depots in the supraclavicular region and quantifying thermogenesis induced by a mild cold

stimulus (Symonds et al., 2012a). This technique has demonstrated that BAT function is greatest in young children, although its primary regulators remain to be determined.

The main objective of the present study was to perform infrared thermography in a cohort of healthy children while in their normal school environment to test the hypothesis that a high body mass index (BMI) percentile is associated with a lower supraclavicular temperature. Because infrared thermography permits measurements in real time, we performed measurements under both basal and stimulated conditions; the latter is the norm for other modalities of BAT function in which it is not feasible to directly follow dynamic changes in function . Secondary objectives included evaluating whether age, sex, ethnicity and ambient temperature are additional independent predictors of supraclavicular skin temperature.

### 3.2.3 Methods

Sixty-eight children aged 6 – 11 years were recruited from two inner-city schools in Nottingham, United Kingdom, between November 2011 and January 2012. There were no major exclusion criteria. Parents and children were given an information leaflet at school inviting any child who wished to do so to participate in the study, to ensure a representative sample of healthy volunteer children. The children expressing interest in the study were enrolled after receipt of written informed parental consent. Additional verbal assent was obtained from each child on the day of study. Before participant recruitment, the study was approved by the University of Nottingham Medical School Ethics Committee.

The study was undertaken in the school environment, in a specifically designated area that provided adequate privacy for thermal imaging and assessment of BMI. To ensure adequate exposure of the neck and upper thorax for thermal imaging, the children were provided with standard cotton T-shirts to wear on their allocated day of study. The images of the children who did not attend in suitable clothing (n = 10) were not processed and were not used for the quantification of $T_{SCR}$ owing to inadequate exposure of the SCR to the thermal imager.

Children attended the study in pairs and before imaging were introduced to the research team and familiarised with the equipment and study protocol. Date of birth and sex were recorded along with an assessment of ethnicity based on skin colour, with each child classed as Caucasian or non-Caucasian. Because we did not have ethical approval to ascertain the detailed ethnicity of parents and grandparents, no further information was available for this aspect of the investigation.

Children were dressed in their standard school uniform and their study T-shirt. Measurements of height and weight without shoes were performed following standard protocols. Height was measured to the nearest 0.1 cm using a stadiometer (Leicester height measure; Child Growth Foundation, Sutton Coldfield, United Kingdom) and weight was measured to the nearest 0.1 kg with portable digital scales using standard methodology. Because BMI percentile for children standardise BMI for age and sex, BMI was calculated for each child as weight (in kg)/ height$^2$ ($m^2$) and individual sex- and age-specific percentiles were determined using an online calculator (NHS Choices).

The experimental protocol included a 7 minute baseline period, followed by exposure to a mild cold stimulus for another 5 minutes as established previously (Symonds et al., 2012a), producing a decrease in hand temperature of 8.41 ± 1.99˚C. The stimulus was immersion of the left hand in cool water. Images were obtained at 1 minute intervals with a thermal imaging camera (FLIR B425; FLIR Systems, Danderyd, Sweden) with a range limit of -20˚C to 120˚C. The child was positioned to provide an optimal view of the head, neck and upper thorax seated 0.8 – 0.9 m from the thermal imaging camera with the arms adducted, right hand placed in the lap and left hand placed in an empty 6 L receptacle. Before imaging, ambient room temperature, relative humidity and perpendicular distance from the camera were recorded, and the camera was set up accordingly.

After acquisition of adequate baseline images, cool water (20.1˚C) was poured into the bucket such that the whole hand was immersed to the level of the ulnar and radial styloid process. Immersion was maintained for a total of 5 minutes; the child was free to remove his or her hand at any point during the study. Tympanic membrane temperature was measured immediately before and on cessation of thermal imaging in triplicate using a Braun Thermoscan Pro 4000 (Welch Allyn, Skaeanteles Falls, New York, USA).

The infrared thermography images were downloaded onto a personal computer and analysed using FLIR ThermaCAM Researcher Pro 2.1 (FLIR Systems AB, Danderyd, Sweden). A region of interest was defined for the left and right SCR overlying known regions of BAT using the anatomic landmarks for the border of the posterior triangle

of the neck (sternocleidomastoid, trapezius and clavicle) as described previously. $T_{SCR}$ was calculated as the median value of the hottest 25% of the defined region of interest (i.e. the 87.5$^{th}$ percentile value of the SCR). Skin surface temperature was determined from data obtained using iButtons (model DS1921H-F50; Maxim, Sunnyvale, California) applied to a region not known to contain BAT on the chest wall, below the sternal notch.

Baseline $T_{SCR}$ was calculated as a mean of the values measured at -2, -1, and 0 minutes before exposure to the cool stimulus. The peak $T_{SCR}$ reached during the 5 minute period of hand immersion was recorded and the change from baseline was defined as $\Delta T_{SCR}$. Given that previous studies using PET-CT have shown that not all individuals have detectable BAT at thermoneutrality (Cypess et al., 2009, Virtanen et al., 2009, Saito et al., 2009), a priori we designated a rise of 2 SD of baseline $T_{SCR}$ variability (0.09 ˚C) as a likely biologically significant increase (maximal $\Delta T_{SCR}$).

During the initial descriptive analysis it became clear that 3 subjects were extreme outliers on the basis of both body weight and baseline $T_{SCR}$ (i.e. 2 SDs from those children included in the analysis). These children, 2 Caucasian females and 1 Caucasian male, performed the study on different data collection days, were significantly obsese (>98$^{th}$ percentile calculated BMI), close in age (7 years, 1 month to 7 years, 3 months), and had a $T_{SCR}$ > 2.5 SD below the mean value for their BMI group. These children were excluded from subsequent analysis; thus data from 55 children were analysed.

Data were entered using a simultaneous entry method and assessed for normality using the Kolmogorov-Smirnov normality test, and are presented as mean ± SD unless

stated otherwise. Comparisons between left and right $T_{SCR}$ were done using the paired t-test. Pearson product-moment correlation coefficients were calculated to determine the correlation between BMI percentile and $T_{SCR}$ or $\Delta T_{SCR}$. Multiple linear regression analyses were performed to assess associations of $T_{SCR}$ with age, sex, ambient temperature and ethnicity in addition to BMI percentile. This was undertaken to elucidate the possible relationships taking into account the age, sex, ethnicity and BMI range of the children participating in the study. Given the relatively small number of children who were classified as obese, multiple regression analysis permitted exploration of relationships between variables. Variables were selected a priori and were based on previous findings and the hypotheses of this study. Sex and ethnicity were entered as dummy variables. Data were analysed using SPSS 19.0 (IBM, Armonk, New York), with statistical significance set at $P < 0.05$.

### 3.2.4 Results

The study sample consisted of children with a mean age of 101.1 ± 18.2 months and a mean BMI percentile of 58.8 ± 28.0, 6 of whom were overweight (defined as BMI ≥ 85$^{th}$ percentile) and 5 of whom were obese (defined as BMI ≥ 95$^{th}$ percentile (Barlow and Expert, 2007, Cole et al., 1995)). Characteristics of the final study population and conditions are summarised in Table 3.1.

**Table 3.1 Demographic and anthropometric variables in healthy children aged 6 – 11 years (n = 55)**

| Variable | Value |
|---|---|
| Age, mo, mean ± SD (range) | 101.1 ± 18.2 (72 – 134) |
| BMI percentile, mean ± SD (range) | 58.8 ± 28.0 (0.4 – 99) |
| Sex, males: females, n | 25:30 |
| Ethnicity, Caucasian: non-Caucasian, n | 36:19 |
| Sternum temperature, ˚C, mean ± SD (range)* | 33.13 ± 0.91 (32.83 – 35.53) |
| Ambient temperature, ˚C, mean ± SD (range) | 21.80 ± 0.7 (19.6 – 23.8) |
| Δ Tympanic membrane temperature, ˚C, mean ± SD | 0.11 ± 0.12 |

*n = 47 for whom iButton data were available.

A small difference in baseline $T_{SCR}$ between left and right depots was demonstrated (Table 3.2), and so these were considered separately for subsequent analyses.

**Table 3.2 $T_{SCR}$ at baseline and in response to a cool stimulus (placing a hand in cool water at 20.1˚C for 5 minutes) in healthy children aged 6 – 11 years (n = 55)**

| Variable | Mean ± SD |
|---|---|
| Left baseline $T_{SCR}$, ˚C | 35.43 ± 0.41* |
| Right baseline $T_{SCR}$, ˚C | 35.36 ± 0.40 |
| Left peak $\Delta T_{SCR}$, ˚C | 0.11 ± 0.12* |
| Right peak $\Delta T_{SCR}$, ˚C | 0.12 ± 0.12 |

* Significant difference between left and right $T_{SCR}$ $P < 0.05$

An inverse relationship between baseline $T_{SCR}$ and BMI percentile was observed regardless of the SCR studied (Table 3.3). This difference in $T_{SCR}$ is further illustrated in Figure 3.1 for age-matched children.

**Table 3.3 Multiple regression analyses for left and right baseline $T_{SCR}$ as dependent variables and age, BMI percentile, ethnicity, sex and ambient temperature as independent variables (n = 55)**

| | Left $T_{SCR}$ | | | | Right $T_{SCR}$ | | | |
|---|---|---|---|---|---|---|---|---|
| **Variable** | **B** | **SE** | **β** | **P** | **B** | **SE** | **β** | **P** |
| **Constant** | 31.392 | 1.70 | - | < 0.01 | 31.327 | 1.717 | - | < 0.01 |
| **Age** | 0.001 | 0.003 | 0.06 | NS | 0.000 | 0.003 | -0.009 | NS |
| **BMI percentile** | -0.006 | 0.002 | -0.393 | 0.004 | -0.005 | 0.002 | -0.337 | 0.016 |
| **Ethnicity*** | 0.266 | 0.106 | 0.311 | 0.016 | 0.250 | 0.108 | 0.298 | 0.024 |
| **Sex** $^{\Psi}$ | -0.036 | 0.105 | -0.044 | NS | -0.007 | 0.106 | -0.009 | NS |
| **Ambient room temperature** | 0.156 | 0.078 | 0.2768 | 0.051 | 0.161 | 0.079 | 0.282 | 0.046 |

Left $T_{SCR}$: $R^2 = 0.26$ (significant model P = 0.009); right $T_{SCR}$: $R^2 = 0.25$ (significant model P = 0.028)
* Caucasian compared with non-Caucasian
$^{\Psi}$ Females compared with males
NS, non-significant

As with baseline data, $\Delta T_{SCR}$ was significantly negatively correlated with BMI percentile (Figure 3.2). This relationship was independent of body temperature and the degree of hand cooling achieved by the stimulus (e.g. BMI versus hand cooling: $R^2 = 0.078$; P not significant).

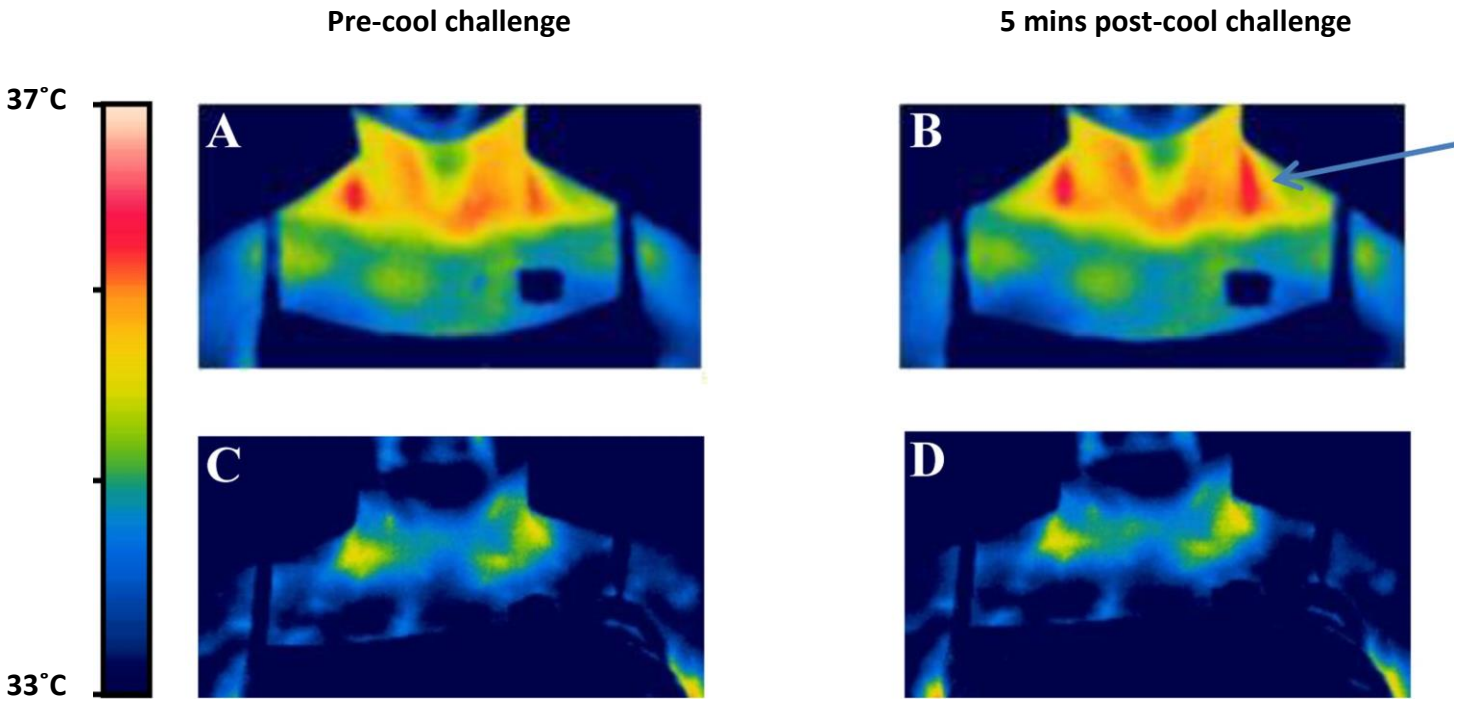



**Figure 3.1 Anterior thermal images of the neck and upper thorax in A, B a 7 year of normal BMI (25$^{th}$ percentile) and C, D a 7 year old of high BMI (98$^{th}$ percentile).** Showing representative examples of the active SCR before (A and C) and 5 minutes after (B and D) immersion of a hand into cool tap water at 20.1˚C. The arrow indicates, by way of example, the area of interest in the left SCR.

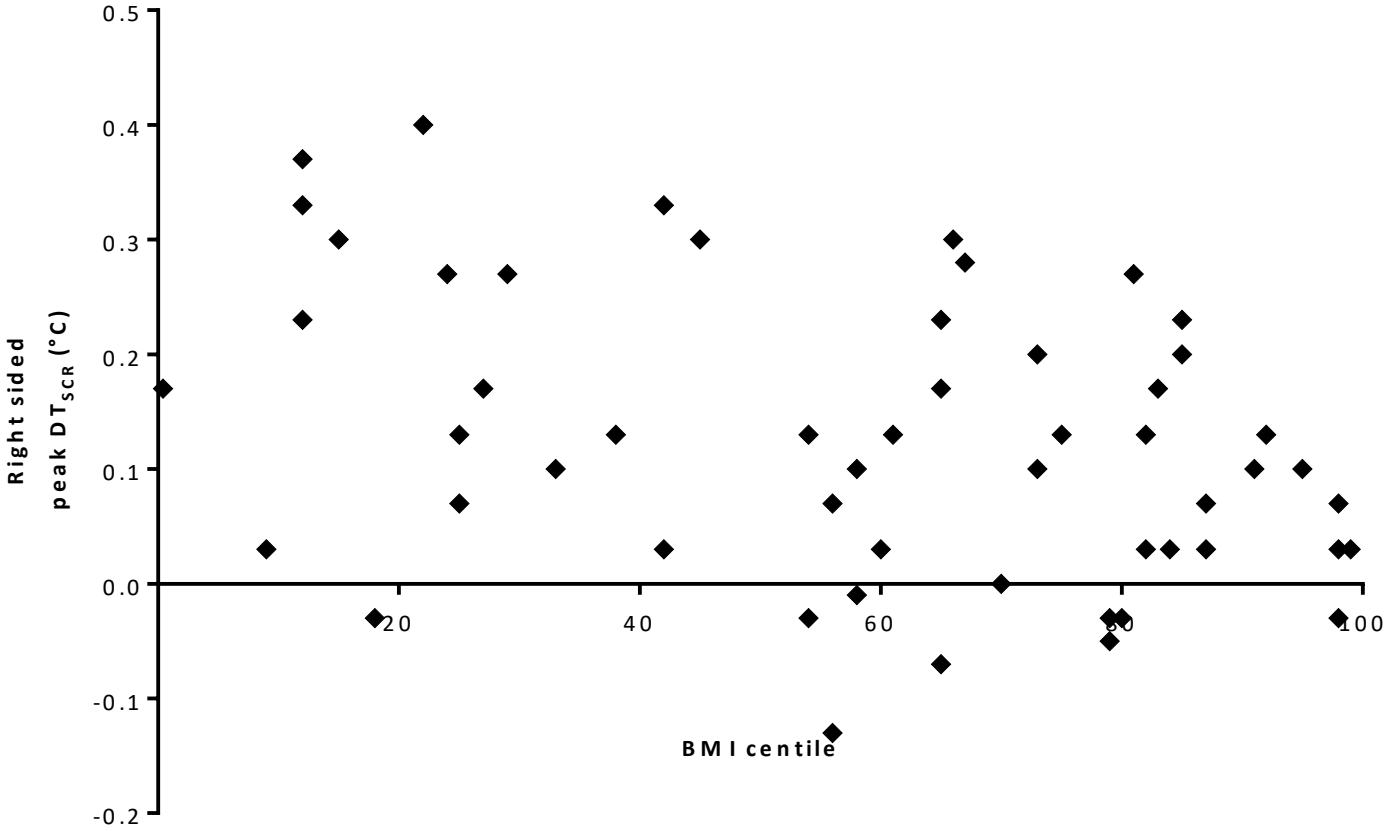



**Figure 3.2 Relationship between right-sided $\Delta T_{SCR}$ measured by infrared thermography in response to immersion of a hand into cool tap water at 20.1˚C and BMI percentile in healthy volunteer children aged 6 – 11 years (n = 55); r = -0.384 (95% CI -0.59 to -0.13); P = 0.004).**

Multiple regression analysis identified BMI percentile as a significant predictor of $\Delta T_{SCR}$; however, this relationship was confined to the right SCR, and there was no influence of sex, ethnicity or ambient temperature (Table 3.4).

**Table 3.4 Multiple regression analyses for left and right $\Delta T_{SCR}$ as dependent variables age, BMI percentile, ethnicity, sex and ambient temperature as independent variables (n = 55)**

| | Left $\Delta T_{SCR}$ | | | | Right $\Delta T_{SCR}$ | | | |
|---|---|---|---|---|---|---|---|---|
| **Variable** | **B** | **SE** | **β** | **P** | **B** | **SE** | **β** | **P** |
| **Constant** | -0.567 | 0.541 | - | NS | -0.104 | 0.520 | - | NS |
| **Age** | -0.001 | 0.001 | -0.164 | NS | -0.002 | 0.001 | -0.282 | 0.043 |
| **BMI percentile** | -0.001 | 0.001 | 0.19 | NS | -0.002 | 0.001 | -0.369 | 0.008 |
| **Ethnicity*** | 0.026 | 0.034 | 0.103 | NS | 0.028 | 0.032 | 0.110 | NS |
| **Sex$^{\Psi}$** | 0.046 | 0.033 | 0.190 | NS | 0.029 | 0.032 | 0.118 | NS |
| **Ambient room temperature** | -0.022 | 0.025 | -0.128 | NS | 0.017 | 0.024 | 0.100 | NS |

Left $\Delta T_{SCR}$: $R^2 = 0.14$ (Non-significant model P = 0.18); right $\Delta T_{SCR}$: $R^2 = 0.25$ (significant model P = 0.014)
* Caucasian compared with non-Caucasian
$^{\Psi}$ Females compared with males
NS, non-significant

Twenty-four children exceeded the predetermined threshold for maximal $T_{SCR}$ increase in the left side, right side or both sides over the study period (maximal $\Delta T_{SCR}$ ≥ 0.18˚C). In these maximal responders, while sternal temperature was maintained

(Δ sternal temperature, 0.09 ± 0.31˚C; n = 20 with available iButton data), $T_{SCR}$ response was greatest to the cool challenge, and similar maximal increases in left and right $T_{SCR}$ (left $\Delta T_{SCR}$: 0.26 ± 0.07˚C after; right $\Delta T_{SCR}$: 0.28 ± 0.06˚C after 3 ± 1 minutes) were seen.

### 3.2.5 Discussion

The major finding of the present study is that we detected distinct "hotspots" within the SCR of all children (Figure A3.1 in the Appendix to Study I) studied which co-locate with the main location of BAT in humans (Cypess et al., 2009, Virtanen et al., 2009, Saito et al., 2009) and are strongly influenced by BMI and ethnicity. Importantly, differential effects of these factors on $T_{SCR}$ were found within the BMI range of healthy children. Our finding of a negative relationship between BMI percentile and $T_{SCR}$ in children is in accordance with comparable findings of BAT function assessed by PET-CT in adult populations (Cypess et al., 2009, Virtanen et al., 2009, Saito et al., 2009). Importantly, we have been able to study contemporary children across the normal range of BMI percentiles rather than by BMI category (Cypess et al., 2009, van Marken Lichtenbelt and Schrauwen, 2011).

That we found evidence of BAT in all children is also in marked contrast to an earlier study reported by Drubach et al (Drubach et al., 2011), which was confined to paediatric oncology patients aged 5 – 21 years within a hospital environment and was able to detect BAT in fewer than 50% of subjects with PET-CT. This differs from the present study, in which healthy children aged 6 – 11 years were all studied in a school setting and every subject irrespective of BMI, ethnicity, and sex, exhibited clear

evidence of BAT, as indicated by a distinct thermogenic area of raised $T_{SCR}$ at baseline. These findings are in accordance with the suggestion of Lee et al. that although all humans have significant amounts of BAT in the SCR, PET-CT is relatively insensitive for routine studies at thermoneutrality (Lee et al., 2010).

One potential limitation of the thermal imaging technique is that the transfer of heat from BAT within the SCR maybe restricted by the depth of subcutaneous fat above this depot. To date, there are no data indicating whether such a response may be reduced in individuals with high BMI, although our initial studies in adults suggest that this is not a major factor in determining the $T_{SCR}$ measured by infrared thermography (unpublished data).

We have shown differences in $T_{SCR}$ in healthy children across the BMI percentile range. This would be expected to directly relate to differences in whole body heat production, given that only small amounts of BAT may make a substantial difference in daily energy expenditure; for example, ~ 40 – 50 g of BAT is estimated to contribute between 5% (van Marken Lichtenbelt and Schrauwen, 2011) and 20% (Ouellet et al., 2012) in adults, which has now been directly quantified indirectly in adults (Cypess et al., 2013). It is plausible that BAT development and activity differ with BMI as classical brown adipocytes are derived from skeletal muscle precursors (Seale et al., 2008) and a positive relationship between muscular volume and BAT activity has been shown in children (Gilsanz et al., 2011). The contribution of BAT to both basal and stimulated heat production is fundamental to our understanding of how differences in BAT activity contribute to both the maintenance and return to a normal body weight.

Studies in sheep in which BAT is also found within a region analogous to the SCR (Symonds et al., 2012c) have also established that the declining abundance of BAT with early postnatal age is accompanied by a widening of the thermoneutral range and a concomitant reduction in basal oxygen consumption that parallels a decline in plasma thyroid hormones (Symonds et al., 1989). Changes in thyroid function are essential for the activation of BAT across a range of species (Hall et al., 2010, Symonds et al., 2011); small differences in thyroid function have been linked to adult obesity (Knudsen et al., 2005), and lean body mass is a determinant of thyroid size (Wesche et al., 1998).

The present study did not include blood sampling, because we did not wish to restrict the number of children volunteering to participate. As a result, we are unable to directly assess how endocrine factors contributed to differences in BAT function between subjects. However there is now a clear need to establish whether endocrine, dietary and thermal interventions can enhance BAT activity (Symonds et al., 2012b). In addition, there is increasing evidence in large mammals, including humans, that such depots are “beige” rather than brown (Wu et al., 2012), although the exact time course of this process remains to be examined in humans. Consequently, it is possible that repeated thermal imaging of subgroups of children may enable quantification of these processes in much more detail.

The impact of ethnicity on body composition and endocrine status has received relatively little attention during early life, and previous studies have measured only resting energy expenditure rather than thermogenesis (Kaplan et al., 1996, Morrison

et al., 1996). A recent small study based in South Africa found no difference in the detection of BAT by PET-CT between adult African and Caucasian cancer patients, but observed that BAT was detectable in the neck region of a small number of Asian patients (Perkins et al., 2013). Clearly, more detailed studies of the potential factors that might explain ethnic influences on BAT function are warranted, especially because most studies reported to date indicate that non-Caucasians are at greater risk of diabetes (Shai et al., 2006) and that African-Americans are at greater risk of the metabolic syndrome (Deboer, 2011), both of which are common consequences of obesity. The extent to which BAT function in childhood may predict and/or results in adult ill-heath remain unknown and requires investigation, but we suggest that reduced BAT activity may directly contribute to obesity.

### 3.3 Study II

**The sexual dimorphism of brown adipose tissue function (published in *J Pediatr* 2019; 210:166-172)**

#### 3.3.1 Abstract

**Objective** To determine whether brown adipose tissue (BAT) activity in school-age children differs between the sexes and to explore the impact of dietary intake, sedentary behaviour, and picky/fussy eating.

**Study design** Children aged 8.5 – 11.8 years of age (n = 36) underwent infrared thermography to determine the temperature of the skin overlying the main superficial BAT depot in the supraclavicular region before and after 5 minutes of mild cold exposure (single hand immersion in cool tap water at about 20˚C). The relationships between the supraclavicular region temperature and parental reports of food consumption, eating behaviour, and inactivity were explored.

**Results** The supraclavicular region temperature was higher in boys (n = 16) at baseline, and after cold exposure. Boys displayed a greater thermogenic response to cold. Strong negative correlations were observed between the supraclavicular region temperature and body mass index percentile, and differences in supraclavicular region temperature between girls and boys persisted after adjustment for body mass index percentile. A negative linear relationship was observed between protein and vegetable intake and supraclavicular region temperature in girls only, but did not persist after adjustment for multiple comparisons. There was no difference in the

adjusted supraclavicular region temperature between active or inactive children, or picky and non-picky eaters.

**Conclusions** These findings indicate sexual dimorphism in BAT thermogenic activity and a sex-specific impact of diet. Future studies should aim to quantify the contribution of BAT to childhood energy expenditure, energy imbalance, and any role in the origins of childhood obesity.

### 3.3.2 Introduction

Globally, over 124 million school-age children are now classified as overweight or obese (Collaboration, 2017) and, as a consequence, are at risk of significant cardio-metabolic disease in adulthood (Tirosh et al., 2011, Eriksson et al., 2003). The individual components of childhood energy balance are poorly understood, and the impact of brown adipose tissue (BAT) on energy expenditure, has yet to be quantified.

BAT persists outside the neonatal period into childhood and beyond. Increasing evidence suggests that this highly metabolic, thermogenic tissue contributes to energy expenditure by oxidising lipids and glucose (Saito, 2013, Carpentier et al., 2018, Chondronikola et al., 2014, Zingaretti et al., 2009). This is achieved by the dissipation of chemical energy as heat through the action of mitochondrial UCP1. Histological evidence of BAT has been demonstrated in children in the neck, upper thorax, mediastinum (Heaton, 1972, Lean et al., 1986), and in the adipose tissue surrounding the heart (Ojha et al., 2016) and kidneys (Heaton, 1972, Rockstroh et al., 2015) as well as subcutaneously (Rockstroh et al., 2015). It is estimated that just 63 g of adult BAT

could combust the energy equivalent of 4.1 kg of white adipose tissue over the course of a year (Virtanen et al., 2009). As the prevalence and activity of BAT are higher throughout infancy (Lean et al., 1986) and childhood (Gilsanz et al., 2012), the relative contribution of BAT to bio-energetic metabolism may be even greater in infants and children than in adulthood.

Although associations between dietary intake and sedentary behaviours, such as TV viewing, on white adipose tissue (i.e. obesity) have been widely reported, their effects on BAT has not. Methods for measurement of supraclavicular skin temperature using thermal imaging present an ethically acceptable, non-invasive, repeatable method for BAT assessment in children and have been repeatedly shown to reflect measurements of BAT activity as assessed on positron emission tomography/computed tomography (PET-CT) scanning (Law et al., 2018, Jang et al., 2014, Boon et al., 2014).

Sexual dimorphism in both BAT mass and activity has been comprehensively reviewed in adults (Bloor and Symonds, 2014, Valencak et al., 2017) and, despite similar distribution of depots throughout the body, pre-menopausal women appear to have more BAT than men (Cypess et al., 2009, Pfannenberg et al., 2010) implicating a role for hormonal regulation. Data in infants and children are less clear (Rockstroh et al., 2015, Gilsanz et al., 2012, Ponrartana et al., 2012, Gilsanz et al., 2011, Zukotynski et al., 2009, Deng et al., 2015, Drubach et al., 2011, Chalfant et al., 2012). Gilsanz et al. report a higher BAT mass, increased BAT activity and more rapid increase in BAT during the pubertal growth spurt in boys, as compared to girls (Gilsanz et al., 2012). Although glucose is utilised during BAT thermogenesis, the primary substrates for brown

adipocytes at the cellular level are fatty acids. The functional assessment of BAT beyond that of glucose uptake is integral to understanding how BAT may be regulated and its contribution to energy expenditure in early life.

Given the potential importance of BAT activity in metabolic health, our aim was to determine whether the sexual dimorphism observed in adults exists between girls and boys at baseline and in response to a brief mild cold stimulus (Robinson et al., 2014, Symonds et al., 2012a) when infrared themography of supraclavicular skin temperature is utilised as a measure of BAT thermogenic activity. In addition, as diet and habitual physical activity influence metabolic health, we sought to identify whether parental reports of dietary intake, picky eating behaviour, and TV viewing were associated with differences in BAT activity in a sex-specific manner.

### 3.3.3 Methods

This study was approved by the University of Nottingham's School of Medicine Ethics Committee (E10012013 SCS ACH TREAT). Participants were recruited from two Nottingham City schools over a period of 3 weeks, and data collection was undertaken between April and June 2013. There were no specific eligibility criteria other than the requirement for parental written consent and receipt of children's verbal consent for anthropometry and imaging. Parents/guardians gave informed written consent for participation in this study, and all children gave additional verbal assent. Thirty-six children were imaged under free-living conditions within a primary school environment.

Infrared thermography of the neck and upper thorax was undertaken as previously described (Robinson et al., 2014). In brief, the reflective temperature, ambient room temperature and humidity were measured prior to each imaging session and entered into the thermal camera according to manufacturer's instructions. Supraclavicular temperature is also related to ambient temperature (Robinson et al., 2014), and ambient room temperatures were stable during the study (Table 3.5). Each child sat 0.8 m away from the thermal camera (FLIR B425FLIR Systems AB, Danderyd, Sweden) for 5 minutes wearing a sleeveless cotton vest. BAT in children responds to very mild cold stimulation (Robinson et al., 2014, Symonds et al., 2012a) and participants next immersed their left hand in cool tap water (c.20 ˚C) for 5 minutes, producing a similar decrease in hand temperature in girls and boys (Table 3.5).

**Table 3.5 Demographic and anthropometric variables in healthy girls and boys aged 8 – 11 years (n = 36)**

| | Value (SEM) | | |
|---|---|---|---|
| **Variable** | **Boys (n = 16)** | **Girls(n = 20)** | **P value** |
| Age (decimal years) | 9.9 (0.24) | 8.5 (0.23) | 0.62 |
| Height (cm) | 138.8 (2.0) | 139.0 (1.7) | 0.94 |
| Weight (kg) | 31.81 (1.33) | 34.89 (1.72) | 0.12 |
| BMI percentile | 48.36 (8.00) | 59.57 (6.63) | 0.28 |
| Ambient temperature (°C) | 22.01 (0.20) | 22.10 (0.14) | 0.71 |
| $T_{SCR}$ pre cold exposure (°C) | 36.02 (-0.14) | 35.63 (-0.12) | 0.03 |
| $T_{SCR}$ post cold exposure (°C) | 36.17 (-0.14) | 35.62 (-0.12) | 0.004 |
| $T_{mp}$ pre cold exposure (°C) | 32.96 (-0.25) | 33.13 (-0.31) | 0.65 |
| $T_{mp}$ post cold exposure (°C) | 33.36 (-0.22) | 33.09 (-0.27) | 0.46 |
| Hand temperature drop (°C, n = 28) (F: n = 16; M: n = 12) | -8.85 (-0.30) | -8.00 (-0.57) | 0.20 |
| TV watching (hrs)* | 2.12 (0.26) | 2.20 (0.24) | 0.84 |
| Picky eater (yes) | 8/16 | 11/20 | 0.76 |
| Food consumption score (Likert-item group sum)[#] | | | |
| Protein | 61.69 (2.67) | 63.60 (2.13) | 0.57 |
| Vegetable | 84.94 (4.66) | 86.45 (2.85) | 0.77 |

[#] food consumption score: higher value = lower consumption

$T_{SCR}$: supraclavicular region skin temperature; $T_{mp}$: mandibular prominence temperature

*Contaminated by socially desirable responding

Images were taken at intervals throughout the study with comparable subject positioning. Thermograms obtained 1 minute prior to hand immersion, and 5 minutes post-hand immersion, were analysed to calculate supraclavicular region temperature. Values were defined as baseline supraclavicular region temperature and cold exposed supraclavicular region temperature respectively, and the thermogenic response to cold as the change in supraclavicular region temperature (calculated as cold exposed supraclavicular region temperature minus baseline supraclavicular region temperature). For the purposes of image analysis, the supraclavicular region was defined as the region of skin visible between the acromioclavicular joint, sternal notch and contour of the shoulder. Only thermograms where both left and right SCRs were completely exposed and unobstructed by clothing or hair, and where clavicles were positioned perpendicular to the camera lens, were regarded as acceptable for analysis.

The radiometric data obtained from thermograms were converted to temperature data within MATLAB (2017b, Mathworks, Natick, MA, USA) using a script adapted from Tattersall (2015). The thermal image was displayed on a graphical user interface, allowing identification of 5 points representing the apices of the SCR as defined above. Supraclavicular region temperature was calculated as the 95th percentile temperature value of the supraclavicular region of interest (Law et al., 2018, Symonds et al., 2012a, Scotney et al., 2017).

To determine baseline temperature of the skin not overlying BAT, a region away from the proximity of supraclavicular BAT visible in all children's thermograms was chosen

as a comparator. This anatomical region, the centre of the anterior mandibular protuberance, was identified visually using FLIR's proprietary software, ResearchIR version 4 (FLIR Systems AB, Danderyd, Sweden). The mean temperature value of an 86-pixel area ellipse ($T_{mp}$) was calculated pre- and post-cold exposure (using the same thermograms as for the calculation of supraclavicular region temperature). To confirm, and quantify, the degree of hand cooling, the temperature of the left hand prior to, and immediately after, cooling was calculated for each subject using the mean value of an individualised maximally-sized ellipse fitted to the anatomical area bound by the metacarpophalangeal joints and radial-ulnar styloid processes on the dorsum of the hand. Nine of the 36 children analysed for this study did not have thermograms of the left hand both prior to, and following, hand immersion. The mandibular prominence temperature and hand temperature were calculated using the standard ellipse region-of-interest tool in ResearcherIR version 4 (FLIR Systems AB, Danderyd, Sweden).

The parents of each child completed questionnaires regarding their child's food intake, and were asked to rate their child's frequency of consumption of 151 foods (adapted from Wardle et al (Wardle et al., 2001)) from 1 to 8 (1 'more than once a day' to 7 'less than once a month' and where 8 represented 'never' eaten). Responses were grouped into 7 standard food categories as described previously (Townsend and Pitchford, 2012) and summed to create a score for each food group for each child. Each food group consisted of between 9 and 20 items (summarised in the Appendix to Study II Table A3.1).

Where consumption of a food was rated as 'never' in more than 25% of children, that food was excluded from grouped analysis (Wardle et al., 2001). The remaining foods were grouped into the following categories: i) carbohydrate; ii) dairy; iii) fruit; iv) protein; v) savoury; vi) sweet and vii) vegetable. Cronbach's alpha was calculated for each group as a measure of the internal consistency of the scale. Reliability was acceptable (Cronbach's alpha > 0.7 (Nunally, 1978)) for all groups except dairy (0.54) for the food consumption questionnaires. 'Food consumption score', as a sum for each food group, was calculated for each child and compared to indices of supraclavicular region temperature (i.e. baseline supraclavicular region temperature, cold exposed supraclavicular region temperature and the change in supraclavicular region temperature) derived from thermograms as described above.

To identify children with fussy eating behaviour, parents were asked if they would classify their child as a "picky eater". Parents were also asked to estimate their child's duration of TV exposure per day to the nearest half an hour. Those children reported as watching ≥2 hours a day were classed as sedentary, and those watching <2 hours TV a day as active.

To ensure responses were not contaminated by socially-desirable responding, parents also completed a short form of the Marlowe–Crowne Social Desirability Scale (MCSDS) (Strahan and Gerbasi, 1972). Analysis of the MCSDS identified that food consumption scores were not contaminated by socially desirable responding. However, MCSDS scores were significantly correlated with the estimated number of hours of TV watched indicating contamination (Table A3.2 in the Appendix to Study II).

Height was measured to the nearest 0.1cm using a stadiometer (Leicester height measure; Child Growth Foundation, Sutton Coldfield, United Kingdom), and weight to the nearest 0.1kg using a standard, calibrated weighing scale. BMI percentile was calculated to adjust for sex and age using the National Health Service Choices BMI calculator (NHS Choices). Height, weight and BMI percentile for the children in this study are summarised in Table 3.5.

### 3.3.4 Statistics

Data were analysed using SPSS V.24 (IBM, Armonk, New York). Data are mean ± SE and normally distributed (as assessed by the Shapiro-Wilk normality test) unless stated otherwise. Comparisons between left and right supraclavicular region temperature were performed using the paired t-test. Percentages were compared using the chi-squared test. Pearson's product-moment correlation coefficients were calculated to determine the correlation between supraclavicular region temperature and food exposure scores and supraclavicular region temperature and BMI percentile. A two-way mixed ANOVA was conducted to examine the effects of sex and cold exposure on supraclavicular region temperature. Post-hoc comparisons were undertaken using the t-test. ANCOVA was performed to determine the effect of sex and cold exposure on supraclavicular region temperature after controlling for BMI percentile. A two-way ANCOVA was conducted to examine the effects of sex and sedentary behaviour, and sex and picky eating behaviour, on supraclavicular region temperature after controlling for BMI percentile.

A sample size of 30 (15 boys and 15 girls) was calculated to detect a 25% difference in the supraclavicular skin temperature response (i.e. change in supraclavicular region temperature) to cold exposure, based on previously published data from healthy children of comparative age (i.e. right-sided change in supraclavicular region temperature 0.28 ± 0.064˚C (mean ± SD), $\beta = 0.2$, $\alpha = 0.05$).

P values of <0.05 (2 tailed) were considered statistically significant. To account for multiple testing during calculation of Pearson's correlation coefficient, the false discovery rate (FDR) was controlled using the corrected method of Benjamini and Yekutieli (Benjamini and Yekutieli, 2001) with the desired FDR of 5%. Full details of the statistical analysis are included in section 2.11.

### 3.3.5 Results

The skin temperature overlying supraclavicular BAT was higher in boys at baseline, following cold exposure, and there was a greater change in temperature response to cold exposure which was significant in boys but not girls (Figure 3.3). Sex had a statistically significant effect on the supraclavicular region temperature response to cold exposure (right supraclavicular region temperature: $F(1,34) = 6.37$, $P = 0.016$, partial $\eta^2 = 0.16$; left supraclavicular region temperature, $F(1,34) = 6.41$, $P = 0.016$, partial $\eta^2 = 0.16$).

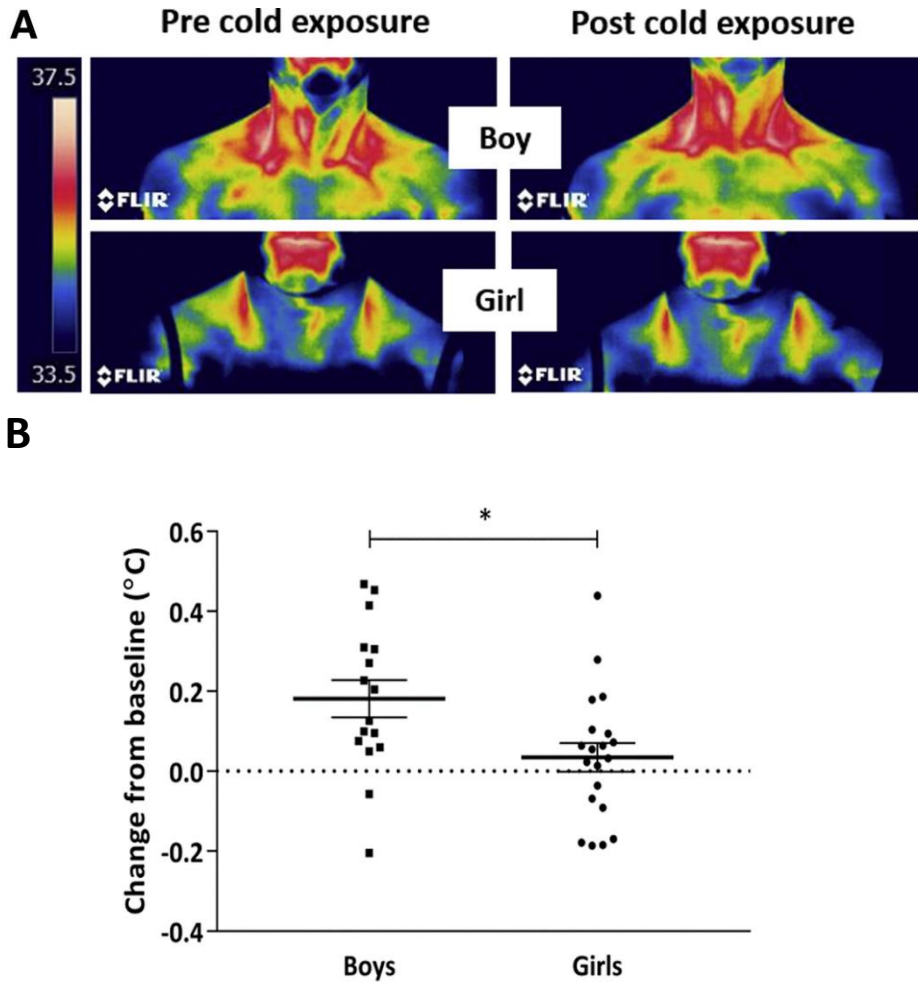



**Figure 3.3 Change in supraclavicular skin temperature following 5 minutes single hand immersion in cool water**. A) representative anterior thermal images of a girl and boy (matched for age and BMI percentile) at baseline and following cold exposure and B) left-sided change in supraclavicular temperature following 5 minutes cold exposure in healthy girls and boys aged 8 – 11 years (n = 36). Post-hoc pair-wise comparisons - Right supraclavicular region temperature: F (1, 15) = 11.38, P = 0.004, partial $\eta^2$ = 0.43; left supraclavicular region temperature: F (1, 15) = 15.16, P = 0.007, partial $\eta^2$ = 0.50, *P < 0.05. FLIR™, forward looking infrared.

Because a significant negative linear relationship was observed between supraclavicular region temperature and BMI percentile (r = -0.71 to -0.53, P < 0.01), even after correction for multiple comparisons (Table A3.3A and B in the Appendix to Study II) adjustment was made for this in subsequent analyses.

The adjusted cold exposed supraclavicular region temperature was statistically higher in boys than girls (right supraclavicular region temperature mean difference: 0.41˚C [95% CI 0.14 to 0.68˚C]; left supraclavicular region temperature mean difference: 0.41˚C [95% CI 0.12 to 0.70˚C]); however, the similar trend in baseline supraclavicular region temperature did not maintain statistical significance, right supraclavicular region temperature: $F(1,33) = 3.48$ , $P = 0.07$, partial $\eta^2 = 0.10$; left $T_{SCR}$: $F(1,33) = 3.46$, $P = 0.07$, partial $\eta^2 = 0.10$. However, the thermogenic response to cold exposure (the change in supraclavicular region temperature) remained greater in boys (right supraclavicular region temperature mean difference: 0.14˚C [95% CI 0.02 to 0.26˚C]; left change in supraclavicular region temperature mean difference: 0.17˚C [95% CI 0.02 to 0.25˚C]). The adjusted means for supraclavicular region temperature at baseline, following cold exposure and for the change in supraclavicular region temperature, are summarised in Table 3.6.

**Table 3.6 Unadjusted means (SEM) for left and right supraclavicular skin temperatures ($T_{SCR}$) and means (SEM) adjusted for BMI percentile in healthy girls and boys before and after 5 minutes of cold exposure (n = 36)**

| | | Supraclavicular skin temperature (˚C) | | | | | |
|---|---|---|---|---|---|---|---|
| | | Baseline | | Cold exposure | | $\Delta T_{SCR}$ | |
| | | Boys | Girls | Boys | Girls | Boys | Girls |
| Unadjusted means (SEM) | Left $T_{SCR}$ | 35.88$^{*\$}$ (0.13) | 35.47$^{\$}$ (0.13) | 36.06$^{*\$\#}$ (0.14) | 35.51$^{\$}$ (0.13) | 0.18$^{*\$}$ (0.05) | 0.03$^{\$}$ (0.04) |
| | Right $T_{SCR}$ | 36.02$^{*}$ (0.14) | 35.63 (0.12) | 36.17$^{*\#}$ (0.14) | 35.62 (0.12) | 0.15$^{*}$ (0.04) | -0.002 (0.04) |
| Adjusted means (SEM)¥ | Left $T_{SCR}$ | 35.81 (0.11) | 35.53 (0.10) | 35.98 (0.11) | 35.57 (0.10) | 0.17 (0.04) | 0.04 (0.04) |
| | Right $T_{SCR}$ | 35.95 (0.11) | 35.68 (0.10) | 36.10 (0.10) | 35.68 (0.09) | 0.14 (0.04) | 0.02 (0.04) |

¥ANCOVA, BMI percentile; $^{*}P < 0.05$, boys compared to girls; $^{\$}P < 0.05$, left compared to right; $^{\#}P < 0.05$, baseline compared to cold exposed

A significant negative linear relationship between supraclavicular region temperature and parental report of vegetable and protein consumption was observed in girls. However, these relationships were no longer statistically significant following adjustment for multiple testing in our study sample. There were no associations between supraclavicular region temperature and food consumption in any category in boys (Table 3.7) and no difference in vegetable and protein consumption scores between girls and boys (Table 3.5).

Sixty-one percent of children were reported to watch 2 or more hours of television per day, but there was no significant difference between boys and girls (Table 3.5).

There was no effect of sex and sedentary behaviour (classified as ≥2 hours of television per day) on supraclavicular region temperature after controlling for the effect of BMI percentile and no statistically significant two-way interaction between sex and sedentary behaviour, while controlling for BMI percentile (Table 3.8).

Therefore, an analysis of the main effects of sedentary behaviour and sex was performed. There was no statistically significant difference in unweighted marginal adjusted means for the main effect of sedentary behaviour on left, or right, supraclavicular region temperature at baseline, or following cold exposure (baseline, right supraclavicular region temperature mean difference, -0.25˚C [95% CI -0.54 to 0.05˚C, P = 0.09]; left supraclavicular region temperature mean difference: -0.12˚C [95% CI -0.43 to 0.19˚C, P = 0.44]; after cold exposure,: right supraclavicular region temperature mean difference: -0.18˚C [95% CI -0.46 to 0.10˚C, P = 0.19]; left supraclavicular region temperature mean difference, -0.10˚C [95% CI -0.39 to 0.22˚C, P = 0.58].

**Table 3.7 Relationship between supraclavicular region temperature ($T_{SCR}$) measured by infrared thermography and food consumption score in healthy volunteer boys and girls aged 8 – 11 years before and after 5 minutes cold exposure (n = 36).**

| | | Boys | | | | | | Girls | | | | | |
|---|---|---|---|---|---|---|---|---|---|---|---|---|---|
| | | Left | | | Right | | | Left | | | Right | | |
| | | Pre $T_{SCR}$ | Post $T_{SCR}$ | $\Delta T_{SCR}$ | Pre $T_{SCR}$ | Post $T_{SCR}$ | $\Delta T_{SCR}$ | Pre $T_{SCR}$ | Post $T_{SCR}$ | $\Delta T_{SCR}$ | Pre $T_{SCR}$ | Post $T_{SCR}$ | $\Delta T_{SCR}$ |
| Correlation to consumption score (Pearson's correlation coefficient) | **Carbohydrate** | -0.05 | -0.02 | 0.10 | -0.09 | -0.09 | 0.00 | 0.21 | 0.16 | -0.19 | 0.20 | 0.20 | 0.01 |
| | **Dairy** | -0.23 | -0.25 | -0.09 | -0.29 | -0.31 | -0.04 | 0.11 | 0.13 | 0.06 | 0.09 | 0.16 | 0.19 |
| | **Fruit** | -0.33 | -0.25 | 0.21 | -0.25 | -0.26 | -0.01 | -0.07 | -0.07 | 0.00 | -0.09 | -0.08 | 0.03 |
| | **Protein** | -0.02 | -0.08 | -0.19 | 0.07 | -0.03 | -0.31 | 0.48* | 0.48* | 0.00 | 0.47* | 0.51* | 0.09 |
| | **Savoury** | -0.19 | -0.26 | -0.23 | -0.20 | -0.27 | -0.24 | 0.32 | 0.28 | -0.12 | 0.39 | 0.39 | -0.01 |
| | **Sweet** | -0.39 | -0.42 | -0.12 | -0.43 | -0.46 | -0.07 | -0.19 | -0.15 | 0.13 | -0.12 | -0.08 | 0.14 |
| | **Vegetable** | 0.11 | 0.13 | 0.06 | -0.01 | 0.03 | 0.14 | 0.53* | 0.46* | -0.23 | 0.52* | 0.48* | -0.13 |

*$P < 0.05$ $\Delta T_{SCR}$ – change in $T_{SCR}$ after 5 minutes cold exposure

**Table 3.8 Means (SEM) for left and right supraclavicular region temperature ($T_{SCR}$), unadjusted and adjusted for BMI percentile, in sedentary and active healthy children at baseline, and following 5 minutes cold exposure (n = 36).** (ANCOVA: baseline left $T_{SCR}$ F = 0.25, partial $\eta^2$ = 0.008, P = 0.62, right $T_{SCR}$ F = 1.66, partial $\eta^2$= 0.051, P = 0.28; cold stimulated left $T_{SCR}$ F = 0.04, partial $\eta^2$ = 0.001, P =0.84 cold stimulated right $T_{SCR}$ F = 0.06, partial $\eta^2$ = 0.002, P = 0.81)

| | | Left $T_{SCR}$ (˚C) | | | | Right $T_{SCR}$ (˚C) | | | |
|---|---|---|---|---|---|---|---|---|---|
| | | Boys | | Girls | | Boys | | Girls | |
| | | Sedentary (n = 10) | Active (n = 6) | Sedentary (n = 12) | Active (n = 8) | Sedentary (n = 10) | Active (n = 6) | Sedentary (n = 12) | Active (n = 8) |
| Baseline $T_{SCR}$ | Mean | 35.82 | 35.97 | 35.50 | 35.44 | 35.88 | 36.26 | 35.64 | 35.60 |
| | SE | 0.20 | 0.11 | 0.20 | 0.13 | 0.20 | 0.11 | 0.17 | 0.18 |
| | Mean adjusted | 35.73 | 35.93 | 35.51 | 35.56 | 35.79 | 36.22 | 35.66 | 35.72 |
| | SE | 0.14 | 0.18 | 0.13 | 0.16 | 0.13 | 0.17 | 0.12 | 0.15 |
| Cold exposed $T_{SCR}$ | Mean | 36.06 | 36.06 | 35.51 | 35.51 | 36.11 | 36.27 | 35.61 | 35.65 |
| | SE | 0.22 | 0.09 | 0.20 | 0.13 | 0.22 | 0.08 | 0.17 | 0.16 |
| | Mean adjusted | 35.96 | 36.01 | 35.53 | 35.64 | 36.01 | 36.23 | 35.63 | 35.78 |
| | SE | 0.14 | 0.18 | 0.12 | 0.15 | 0.13 | 0.16 | 0.11 | 0.14 |

Fifty-three per cent of children were reported to be picky eaters by their parents. There was no significant difference between the eating behaviour of girls or boys (Table 3.5). A two-way ANCOVA was conducted to examine the effects of sex and picky eating behaviour on supraclavicular region temperature, while adjusting for the effect of BMI percentile and there was no statistically significant two-way interaction between sex and picky eating behaviour while controlling for BMI percentile (Table 3.9).

Therefore, an analysis of the main effects of picky eating behaviour and sex was performed. The main effect of eating behaviour showed no statistically significant difference in unweighted marginal adjusted means of the left or right $T_{SCR}$ at baseline or following cold exposure (Baseline right supraclavicular region temperature, mean difference: 0.04˚C [95% CI -0.26 to 0.34˚C, P = 0.79]; left supraclavicular region tempereature mean difference, -0.07˚C [95% CI -0.38 to 0.23˚C, P = 0.63]; after cold exposure, right $T_{SCR}$ mean difference: 0.01˚C [95% CI -0.27 to 0.29˚C, P = 0.93]; left $T_{SCR}$ mean difference, -0.01˚C [95% CI -0.31 to 0.29˚C, P = 0.96]).

**Table 3.9 Means (SEM) for the left and right supraclavicular skin temperature, unadjusted and adjusted for BMI percentile, in children classified as picky or non-picky eaters at baseline and following 5 minutes cold exposure (n = 36).** ANCOVA: baseline left $T_{SCR}$ F = 0.11, partial $\eta^2$ = 0.004, P = 0.77, right $T_{SCR}$ F = 0.01, partial $\eta^2$ = 0.0004, P = 0.92; cold stimulated left $T_{SCR}$ F = 0.12, partial $\eta^2$ = 0.004, P = 0.73, cold stimulated right $T_{SCR}$ F = 0.13, partial $\eta^2$ = 0.004, P = 0.72

| | | Left $T_{SCR}$ (˚C) | | | | Right $T_{SCR}$ (˚C) | | | |
|---|---|---|---|---|---|---|---|---|---|
| | | Boys | | Girls | | Boys | | Girls | |
| | | Picky (n = 8) | Not picky (n = 8) | Picky (n = 11) | Not picky (n = 9) | Picky (n = 8) | Not picky (n = 8) | Picky (n = 11) | Not picky (n = 9) |
| Baseline $T_{SCR}$ | Mean | 35.96 | 35.79 | 35.49 | 35.46 | 36.07 | 35.98 | 35.57 | 35.69 |
| | SE | 0.19 | 0.19 | 0.16 | 0.20 | 0.22 | 0.18 | 0.17 | 0.17 |
| | Mean adjusted | 35.82 | 35.80 | 35.59 | 35.46 | 35.93 | 35.98 | 35.67 | 35.70 |
| | SE | 0.16 | 0.16 | 0.14 | 0.15 | 0.16 | 0.16 | 0.13 | 0.15 |
| Cold exposed $T_{SCR}$ | Mean | 36.12 | 36.00 | 35.49 | 35.53 | 36.27 | 36.07 | 35.55 | 35.71 |
| | SE | 0.20 | 0.19 | 0.16 | 0.21 | 0.22 | 0.17 | 0.16 | 0.18 |
| | Mean adjusted | 35.96 | 36.00 | 35.60 | 35.54 | 36.12 | 36.08 | 35.66 | 35.72 |
| | SE | 0.16 | 0.15 | 0.13 | 0.14 | 0.15 | 0.14 | 0.12 | 0.14 |

### 3.3.6 Discussion

We found a sexual dimorphism in the skin temperature overlying supraclavicular BAT in young children which may be related to dietary intake. Boys exhibit higher BAT activity under resting and cold-stimulated conditions than girls of a similar age and BMI, indicating that boys may have not only higher basal BAT activity under free-living conditions but also BAT that is more responsive to cold stimulation.

Previous investigations of the impact of sex on BAT in healthy young children are currently limited, with the majority of studies confined to clinical imaging in the context of paediatric malignancy. Furthermore, as the purpose of such scanning is to determine disease recurrence/progression, these scans are undertaken under environmental conditions designed to minimise BAT uptake of radio-labelled flurodeoxyglucose (i.e. warm room temperatures) and do not measure BAT activity in response to physiological BAT substrates. Despite these limitations a small number of studies support our findings. Gilsanz et al found no sex-specific differences in the numbers defined as BAT positive on PET-CT (57% girls vs 60% boys), however multiple regression analysis identified an independent effect of sex on BAT volume after adjustment for pubertal stage, BMI, season and exposure to previous glucocorticoid treatment (Gilsanz et al., 2012). Chalfant et al identified BAT in 65% of boys and only 50% of girls (using PET-CT following successfully treated malignancy) and, although not statistically significant, their study was not specifically powered to explore sex-differences (Chalfant et al., 2012).

Similarly, Drubach et al reported no difference in overall BAT activity in boys and girls on PET-CT. However, when stratified by age group, median BAT activity was 2.4 times higher in boys than girls aged between 11 and 13 years (Drubach et al., 2011). Deng et al identified sex as a significant covariate of the MRI properties of BAT in 28 young healthy children aged 9 – 15 years, reporting increased markers of tissue perfusion (ADC - apparent tissue diffusion coefficient and D* - perfusion coefficient) on diffusion-weighted imaging, and a higher T2* using Dixon MRI (Deng et al., 2015) findings, suggestive of higher BAT activity in boys in this age group. Even fewer studies have directly examined childhood BAT histologically, but those that have report either no sex-specific differences (Rockstroh et al., 2015), or did not look for them (Ojha et al., 2016, Rockstroh et al., 2015).

Differences between pre-pubertal girls and boys which are contrary to our findings have been reported (Malpique et al., 2018). However, these differences were principally identified when “area” of the supraclavicular region was used as a thermal index. This measure, defined as the number of pixels over an arbitrary threshold of 35.2˚C, has yet to be validated against other assessments of BAT, such as PET-CT in the same way as supraclavicular region temperature.

The children taking part in this study were between the ages of 8.5 and 11.8 years. The UK median age of pubertal onset is 11.3 (RCOG, 2013) and 11.6 years for girls and boys respectively, meaning our study population may be a heterogeneous group in terms of pubertal stage. It is, therefore, likely that they exhibited a wide range of gonadotrophin and sex steroid hormones which could explain, in part, variation in

basal and cold-stimulated supraclavicular region temperature. Given our study was undertaken in the primary school environment, physical assessment of pubertal stage was not considered appropriate. Future study under laboratory conditions utilising self-reported pubertal stage in combination with non-invasive measures of sex steroid hormones (e.g. saliva or urinary assays) presents a practical and ethical solution to the assessment of supraclavicular region temperature in relation to pubertal status for future studies.

Our univariate analyses suggest BAT thermogenesis may also be influenced by dietary intake in a sex-specific manner. In girls, higher vegetable and protein consumption was associated with a lower supraclavicular region temperature (lower BAT activity). However, the sample size of our study was limited and it was underpowered to detect significant relationships between supraclavicular region temperature and food consumption after correction for multiple testing. Parental reports of dietary intake may be subject to bias. Hours of screen time are commonly used as a simple assessment of sedentary behaviour (Pearson and Biddle, 2011) but may falsely classify some children as active, and may also be associated with dietary intake (Fletcher et al., 2015), use of accelerometry in future studies could provide a comprehensive assessment of movement duration and intensity.

The insulative effect of overlying subcutaneous adipose tissue (SCAT) has not been quantified. Gatidis et al suggest SCAT significantly impacts supraclavicular region temperature; however, their measurements were defined as the minimal distance between the vascular compartment and the skin of the neck (Gatidis et al., 2016)

(rather than the white fat layer that lies immediately below the dermis). Biopsy of adipose tissue surrounding the supraclavicular vasculature clearly demonstrates UCP1 (Lee et al., 2018) indicative of capacity for thermogenesis. Therefore, the assumption that this layer is purely insulative is too simplistic. Because the white fat layer immediately below the skin in the posterior triangle of the skin is minimal in healthy subjects in our studies we have been unable to obtain reproducible and robust measures with either ultrasound or magnetic resonance imaging. We have however identified that the relationship between supraclavicular region temperature and BMI persists in a non-obese group following adjustment for SCAT in close proximity to the supraclavicuar region (dorsal aspect at T1) (See Chapter 5, section 5.2.4.2). The dynamic response of supraclavicular region temperature correlates well with FDG uptake in BAT on PET-CT in a non-obese adult cohort with proven FDG detected BAT (Law et al., 2018), the children in this study were similarly non-obese, and all had a BMI percentile of the 85th percentile or less. These findings suggest that the insulative effect of SCAT is minimal, in a non-obese population at least.

Given the contribution of BAT to energy balance and metabolic health, further exploration of these findings will provide a better understanding of how BAT may be activated, and recruited, in early life. This study helps to delineate how BAT dysfunction may predispose to childhood obesity.

### 3.4 Studies I and II conclusions

Study I identified BMI percentile as a negative predictor of baseline supraclavicular skin temperature and right-sided $\Delta T_{SCR}$ in both univariate (Figure A3.2E, Figure A3.3E and A3.5E in the Appendix to Study I) and multivariate analyses (Table 3.3 and Table 3.4). Although diffierences were seen between the left and right side these were not consistent between the two studies.

Similar findings regarding the relationship with BMI percentile were also observed in Study II; children with higher BMI percentiles had lower $T_{SCRs}$, indicative of lower supraclavicular BAT activity (Table A3.3A and B in the Appendix to Study II). In the final multivariate regression model of Study I, ambient room temperature and ethnicity were also identified as significant predictors of baseline $T_{SCR}$ (Table 3.3), and age was also identified as a predictor of right-sided $\Delta T_{SCR}$ (Table 3.4).

These findings are in line with those observed in adults using thermography (Muros-Molina et al., 2019), thermometry (El Hadi et al., 2016), PET-CT (Matsushita et al., 2014, Brendle et al., 2018, Pfannenberg et al., 2010, Ouellet et al., 2011, Saito et al., 2009) and MRI (Deng et al., 2018) to assess BAT, where the majority of studies report that leanness is associated with higher BAT activity and that severe obesity is frequently associated with no detectable BAT (Vijgen et al., 2011). Likewise, a retrospective study of paediatric patients requiring FDG-PET-CT for clinical indications also indicated a weak negative relationship between BMI percentile and FDG uptake/BAT activity (Drubach et al., 2011), and the findings of MRI based studies also

suggest that the relative proportions of BAT are greater in lean children as compared to those who are obese (Hui et al., 2017, Deng et al., 2015).

However, overall, the relationship between BMI percentile/adiposity and BAT has not been well evaluated in children. Some studies conclude that there is no relationship (Chalfant et al., 2012, Brendle et al., 2018). However, many of these fail to use BMI adjusted for age/sex (Gilsanz et al., 2011, Brendle et al., 2018) or appear to be insufficiently powered to make firm conclusions.

At present, no prospective BAT dedicated studies of healthy children have investigated the relationship between body composition and BAT. It is often suggested that the relationship between BAT and BMI/excess adiposity is a causal one, and that BAT dysfunction leads to obesity due to a subsequent reduction in energy expenditure. While logical, clear evidence for this is lacking, particularly in children. To date, there have been no longitudinal studies where BAT function has been tracked in healthy children over time and examined in relation to future body composition or adiposity. Studies of clinically obese adults undergoing bariatric surgery indicate that post-surgical weight loss is associated with an increase in BAT detection (Vijgen et al., 2012). Although this evidence is supportive, this still does not confirm that BAT dysfunction is the cause of obesity.

It is well established that the origins of obesity lie in early life (Gillman, 2005, Barker, 2007). If energy imbalance associated with BAT dysfunction were to cause excess adiposity, reduced BAT thermogenesis is likely to be detectable prior to the onset of

clinically apparent overweight or obesity. Our understanding of normal physiological human BAT development is poor, as is our knowledge of how and when BAT may become dysfunctional. Simple longitudinal assessment of BAT in early childhood, alongside comprehensive measures of body composition, may help to identify whether the relationship between supraclavicular temperature (as a proxy measure of BAT activity) and BMI percentile observed in Studies I and II represents a causal one.

Ambient room temperature was also identified as a predictor of baseline $T_{SCR}$ in the multiple regression model and a trend towards a positive linear relationship with $T_{SCR}$ was apparent in the initial univariate analyses (Figure A3.2B, Figure A3.4B in the Appendix to Study I), as expected supraclavicular temperature rose alongside ambient room temperature, but no significant elationship between the thermogenic response to cold and room temperature was observed, suggesting that this did not impact BAT activation. The relationship between $T_{SCR}$ and ambient room temperature may actually be more complex, particularly when participants are imaged at much higher or lower room temperatures, and may reflect not only the direct effect of ambient conditions on heat flow to the environment, but also the reactivity of cutaneous vasculature and underlying BAT activity.

Studying more children at a broader range of room temperatures both below, within and above thermoneutrality may help to quantify this relationship more accurately and allow for any confounders to be adjusted for in future studies. In the meantime, the findings of this study merely highlight the need to carefully control ambient

conditions where possible, especially where groups are to be compared or individuals are to be tracked over time.

Study II identified a significant difference in baseline supraclavicular temperature and $\Delta T_{SCR}$ between boys and girls (after adjustment for BMI percentile as a confounder). Boys had a higher baseline $T_{SCR}$ and demonstrated a more significant thermogenic response to cold exposure than girls. Interestingly this was not seen in Study I (Figure A3.6 in the Appendix to Study I, Table 3.3 and Table 3.4). However, despite the similarities of the experimental protocol, the study setting and the nature of the participants, some of the children in Study I were younger (range: 6 – 11 years) than those in Study II (range: 8.5 – 11 years). The data from Study I was revisited with this in mind. When considering only children 8.5 years (102 months) and over, and adjusting for the effect of BMI percentile, the response to cold stimulation was greater in boys (Figure A3.7 in the Appendix to Study I) in a pattern and magnitude similar to that seen in Study II. No differences in baseline $T_{SCR}$ were observed.

There is additional evidence to support the hypothesis that this sex difference could be driven by the age-dependent changes in endocrine physiology occurring prior to, or at the onset of, puberty. Hormonal changes occur before the physical manifestations of puberty become apparent due to rising concentrations of gonadal steroids (e.g. thelarche and pubarche). In girls, increases in the sex hormone precursor, dehydroepiandrosterone sulphate (DHEAS), are observed up to 30 months before thelarche, and increases in oestrogen, androstenedione and testosterone become apparent during the preceding year (Biro et al., 2014).

The study of human brown adipocytes in vitro is in its infancy, and the effects of pubertal hormonal changes on brown adipocytes in childhood are unknown. DHEAS administration inhibits the proliferation of a human brown adipocyte cell line (Rice et al., 2010), and oestrogen regulates UCP1 expression in rodent brown adipocytes in vitro (Suzuki et al., 2018). When oestrogen was administered at an early stage of adipogenesis, the cellular responsiveness to stimulation was enhanced, whereas when administered during the late stage, UCP1 expression in was downregulated (Suzuki et al., 2018) indicating that developmental stage maybe crucial.

Girls enter puberty between 8 and 13 years old, and boys between 10 to 15 years. Therefore, many of the children in Study II, particularly the girls, are likely to have been peri-pubertal. Furthermore, the hormonal changes observed prior to puberty are different in girls and boys and may explain why boys aged 8.5 – 11 years in the study had higher $T_{SCR}$ and $\Delta T_{SCR}$ (indicative of higher BAT activity) than girls.

Sex steroid hormones modulate BAT activity in rodents, and oestrogen has been shown to have a thermogenic effect (Martínez de morentin et al., 2014). Blockade of follicle-stimulating hormone (FSH) in mice stimulates UCP1 in both brown and beige fat depots, leading to a reduction in body fat (Liu et al., 2017). Whether childhood human BAT expresses FSH receptors is unknown, but the findings of this rodent study raise the possibility that FSH itself may inhibit BAT activity. In children, it is possible that the peri-pubertal increase of FSH (that occurs before the rise of oestrogen and testosterone) mediates the decline in BAT activity observed between infancy and puberty. Moreover, serum FSH is higher in girls than boys over the same period

(Koenis et al., 2013). This may account for the sex differences observed in Study I and II in the 8.5 – 11 year age group.

Although FSH is higher in menstruating females than males, FDG detected BAT is reported more frequently in adult females, suggesting that the pre-pubertal influence of FSH may be minor compared to the thermogenic effect of oestrogen in adulthood. Taken together, these important endocrine differences between sexes could also explain why adult females are more likely to have demonstrable BAT on PET-CT than males (Cypess et al., 2009, Pfannenberg et al., 2010).

Other differences between the Study I and Study II data, aside from those of sex are notable. On initial inspection it appears that the average baseline $T_{SCR}$ was higher in Study II, and $\Delta T_{SCR}$ was also marginally higher (Table 3.10). However, comparisons of $T_{SCR}$ between Study I and II are difficult due to minor variations in the methods of the thermographic analysis used for each study. These methods have evolved in the 5 years between the two studies and are discussed in detail in Chapter 2. In brief, in Study I, the left and right ROIs were isolated manually and independently using the proprietary FLIR software, and $T_{SCR}$ was calculated as the value of the 87.5$^{th}$ percentile ($T_{SCR87.5}^{F}$). In Study II, in line with standard departmental practice in 2018, an ROI including both the left and right SCR was isolated using a semi-automated method using a custom MATLAB script and $T_{SCR}$ was calculated as the value of the 95$^{th}$ percentile ($T_{SCR95}^{M}$). Furthermore, Study I considers the maximum supraclvicular temperature reached during the 5 minutes exposure to cold whereas Study II utilises a fixed time point ($T_{SCR}$ at 5 minutes)

**Table 3.10 Supraclavicular temperature values for Study I and Study II**. Values obtained using manual isolation of the supraclavicular ROI using FLIR's proprietary software ($^{F}$) and using a semi-automated MATLAB custom script ($^{M}$), using either the 87.5$^{th}$ percentile or the 95$^{th}$ percentile. Data presented in the journal manuscripts is highlighted in bold. $\Delta T_{SCR}$ was calculated as $T_{SCR}$ at 5 minutes minus baseline $T_{SCR}$ to allow comparison between the methodology of image analysis.

| | **Left baseline $T_{SCR}$ (˚C)** | **Right baseline $T_{SCR}$ (˚C)** | **$\Delta T_{SCR}$ (L;R) (˚C)** |
|---|---|---|---|
| **Study I** | | | |
| $T_{SCR87.5}^{F}$ | **35.43** | **35.36** | 0.02; 0.03 |
| $T_{SCR87.5}^{M}$ | 35.46 | 35.36 | 0.03; 0.03 |
| $T_{SCR95}^{M}$ | 35.66 | 35.57 | 0.04; 0.06 |
| **Study II** ($T_{SCR95}^{M}$) | | | |
| Girls | **35.47** | **35.63** | **0.03; -0.02** |
| Boys | **35.88** | **36.02** | **0.18; 0.15** |
| All | 35.65 | 35.80 | 0.10; 0.06 |

As expected, the values derived from the 95$^{th}$ percentile (Study II) were higher than those derived from the 87.5$^{th}$ percentile (Study I). When the semi-automated MATLAB and manual FLIR methods were compared using the same data set, both methods produced similar values for baseline $T_{SCR87.5}$. There was a strong correlation between $T_{SCR87.5}^{M}$ and $T_{SCR87.5}^{F}$ (Table A3.1 in the Appendix to Study I), and Bland-Altman plots revealed a minimal mean bias and narrow 95% limits of agreement when the manual and semi-automated methods were compared (Figure A3.8 in the Appendix to Study I). This indicates that the choice of method/software to calculate $T_{SCR}$ has little impact. However, when $T_{SCR95}^{M}$ was used to analyse the full set of Study I thermograms, and the multiple regression analysis re-run on the resultant data set in an identical manner to that of Robinson et al 2014 paper, there were some slight differences in the overall findings reported (Table A3.2 and Table A3.3 in the Appendix to Study I). While significant predictors of baseline $T_{SCR}$ remained the same (BMI percentile, ambient

room temperature and ethnicity), the size of β and P value were reduced, suggesting that the strength of these relationships were not considered as strong. Furthermore, BMI percentile and age were no longer statistically significant predictors of right-sided $\Delta T_{SCR}$. One explanation for this may be that the ROI determined by the 95$^{th}$ percentile is "less dynamic" than the 87.5$^{th}$ percentile, and is, therefore, less sensitive in detecting changes in skin temperature, particularly in children who may have high levels of basal activity.

While the 95$^{th}$ percentile has been validated using FDG-PET-CT in response to cold stimulation, this was in a small group of eight adult males who had been pre-selected for having BAT visible on FDG-PET (Law et al., 2018). This is in contrast to both Studies I and II, which consisted of young children with unknown BAT status. A more comprehensive study of what summary measure is most sensitive to detecting BAT activation in all age groups is needed going forward.

Both Study I and Study II identified differences between measurements taken on the left and right, however, this was not consistent between the two studies calling into question whether this has any physiological basis or implication. Of the 19 studies that used IRT to assess supraclavicular BAT that I reviewed in Table 1.1 only Jang et al. (2014) compared left and the right supraclavicular skin tempature, they reported that that skin temperature on the left SCR was higher than the right in an adult group of study participants. Moreover, measurements of BAT volume derived from FDG-PET-CT were not statistically different between the two sides despite the left being almost 4cm$^3$ greater ( left: 47.4 cm$^3$ ± 17.3 and right: 43.4 ± 17.1 cm$^3$) suggesting that this was

not due to inherent differences in BAT mass. This may merely reflect generalised minor thermal asymetrety of skin temperatures that is commonly observed throughout the body.

Early attempts to establish reference values for skin temperature using thermography by Uematsu (1986 and 1988), Goodman (1987) and Niu (2001) as cited by Vardasca (Vardasca et al., 2012) identified subtle thermal asymmetry (<0.5˚C) thoughout the body as a normative finding, further suggesting that the differences observed in my studies may be unrelated to BAT function.

The mean group change in $T_{SCR}$ after/during 5 minutes exposure to a mild cold stimulus was small in both studies (0.02 – 0.1˚C) and, even when the maximal change over the 5 minute duration was considered this change in Study I was still small (c.0.12 – 13˚C), and much smaller than that observed in the preliminary work undertaken by our research group (Symonds et al., 2012a), although there was no comparative age group included in this preliminary work (i.e. 9 to 12 years). The lack of thermal response to cold stimulation in this age group may reflect the age-related decline in BAT activity in early life that has been reported by others (Rogers, 2015). Evidence is emerging that BAT function reaches a nadir by mid-childhood, then transiently increases during adolescence coincident with the time of significant hormonal change and skeletal muscle increase (Gilsanz et al., 2011, Drubach et al., 2011).

However, given that $T_{SCR}$ or $\Delta T_{SCR}$ have yet to be validated as measures of BAT activity in children, other options for the lack of response to cold stimulation seen in these

two studies must also be considered. While the use of $\Delta T_{SCR}$ as a proxy measure of BAT activity is tempting, its use in isolation could be misleading, especially in children in whom baseline BAT activity or volume may be high. Change in $T_{SCR}$ from baseline alone will not identify the child with large volumes of supraclavicular BAT that are already near maximally active, nor distinguish this child from the child with no functional BAT at all. Using the thermogenic response to cold stimulation alone as a marker of BAT positivity is therefore problematic and it's limitations should be acknowledged accordingly (particularly, for example when data used for subsequent sample size or power calculation of future studies). Although, during the initial univariate analysis of Study I no linear relationship was evident between baseline $T_{SCR}$ and the supraclavicular thermal response to cold stimulation (Figure A3.2F and Figure A3.4F in the Appendix to Study I). A hypothetical plot based on the above scenario, including children with dysfunctional or absent BAT and children with near maximally active BAT, may be expected to look more bell-shaped than linear. Generation of age-specific normal ranges of $T_{SCR}$ large population based studies may assist in interpreting $\Delta T_{SCR}$ in the context or normal or abnormal baseline $T_{SCR.}$

It was clear from imaging two moderately sized groups of young children that many external factors could have affected baseline BAT activity. The presence of the research team within the school environment generated a lot of interest, enthusiasm and excitement. Some children attending for imaging were clearly excited to take part, and given that BAT activation is driven by the sympathetic nervous system (Bartness et al., 2010) this may have affected the basal levels of BAT activation even prior to cold exposure.

Furthermore, the mean average ambient temperature in the classrooms during Study I and II were 21.8˚C and 22.0˚C, respectively. There is little data on what constitutes the thermoneutral zone for clothed primary school children at rest. Extrapolating from data in adults, at similar clothing insulation levels (c.0.4 Clo) the lower critical ambient temperature is estimated to be around 25˚C, and for children without clothing at least 31˚C (Kingma et al., 2012). It is, therefore, likely that my studies were undertaken outside the thermoneutral zone for most children and consequently these children will have been subject to cold stimulation even before hand-immersion in cool water. This hypothesis is supported by the report of Zukotynski et al who identified FDG detectable BAT in 31% of their paediatric study population when imaged at 21˚C. This may, in turn, have had an effect on BAT activity during baseline, and affected both $T_{SCR}$ and $\Delta T_{SCR}$ in these studies.

Studies I and II were both undertaken in the school environment. We were allocated an empty classroom and a water supply but did not have access to any means of cooling water for hand immersion. When we attended the first school, the coldest water we could obtain was 20˚C. This was, therefore, used as the cold stimulus for the remainder of the study for consistency. However, Symonds et al. (2012a) used cooler water, and it may be that 20˚C was not a sufficient stimulus to cause significant BAT activation in all children in our study. Studies III to V, presented in the remainder of this thesis, sought to explore the impact of excitement, ambient room temperature and magnitude and duration of cold exposure on $T_{SCR}$ to allow the cooling protocol for BAT activation in children to be refined.

# CHAPTER FOUR

---

## The influence of mild anticipatory psychological stress on supraclavicular skin temperature in lean, healthy females

## Study III

### 4.1 Preface

Brown adipose tissue activity is under sympathetic nervous system control (Bartness et al., 2010, Himms-Hagen et al., 1990) and is responsive to β adrenergic stimulation (Cypess et al., 2015, Loh et al., 2019). Medications such as diazepam and propranolol can be used prior to clinical PET-CT scans to significantly reduce FDG uptake in human BAT in children and adults (Cousins et al., 2017, Soderlund et al., 2007, Jacobsson et al., 2005), suggesting that even under basal, physiological conditions without significant cold exposure, emotional stress, anxiety and anticipation may result in BAT stimulation. Both drugs are also widely used in clinical practice for their anxiolytic effects and, despite different mechanisms of action, are likely to attenuate sympathetically mediated BAT activation.

In contrast to the children imaged in the preliminary pilot study (who were previously known to the research team, had seen the equipment before, and were imaged within their home environment with parents present) the children who took part in Studies I and II were unfamiliar with the research team and study protocol. This may have led to a degree of anxiety or psychological stress in some children despite best efforts to make the children feel at ease. Children attending imaging during my sessions did not appear unduly stressed, and many were visibly excited to take part. The timing of Study I also coincided with the end of the winter term and the beginning of the Christmas holidays, so the general levels of excitement within school were reasonably high. Therefore, the emotional and psychological states of the children taking part in my studies is likely to have been very different from those taking part in the home-based pilot study of Symonds et al. (2012a).

Study III was designed to explore whether these differences in emotional and psychological state may have significantly impacted basal supraclavicular temperature and the subsequent response to cold stimulation. I, therefore, aimed to identify whether mild psychological stress can impact upon supraclavicular skin temperature and to explore whether any increase in $T_{SCR}$ observed is confined to the region of supraclavicular BAT (thus reflecting BAT activation) or is merely reflective of a more widespread thermogenic response.

In this study the hypothesis is that mild psychological stress results in an isolated thermogenic supraclavicular response detected by an increase in $T_{SCR}$ without evidence of increasing in mean skin temperature.

Purposefully subjecting young children to psychological stressors would be ethically challenging to justify and, therefore, the study was undertaken with young, adult participants instead. The methods for this study were, however, kept non-invasive and child friendly, to allow for elements of this study to be translated directly and reproduced in future child-based studies.

## 4.2 Study III

**The influence of mild anticipatory stress on supraclavicular temperature in lean health females (published in *Experimental Physiology* 2016; 101(4), pp.549-557)**

### 4.2.1 Abstract

Brown adipose tissue (BAT) has been implicated in the pathogenesis of obesity, type 2 diabetes and the metabolic syndrome and is a potential therapeutic target. Brown adipose tissue can have a significant impact on energy balance and glucose homeostasis through the action of uncoupling protein 1, dissipating chemical energy as heat following neuroendocrine stimulation. We hypothesised that psychological stress, which is known to promote cortisol secretion, would simultaneously activate BAT at thermoneutrality. Brown adipose tissue activity was measured using infrared thermography to determine changes in the temperature of the skin overlying supraclavicular BAT ($T_{SCR}$). A mild psychological stress was induced in five healthy, lean female, Caucasian volunteers using a short mental arithmetic (MA) test. The $T_{SCR}$ was compared with a repeated assessment, in which the MA test was replaced with a period of relaxation. Although MA did not elicit an acute stress response, anticipation of MA testing led to an increase in salivary cortisol, indicative of an anticipatory stress response that was associated with a trend towards higher absolute and relative $T_{SCR}$. A positive correlation between $T_{SCR}$ and cortisol was found during the anticipatory phase, a relationship that was enhanced by increased cortisol linked to MA. Our findings suggest that subtle changes in the level of psychological stress can stimulate BAT, findings that may account for high variability and inconsistency reported in BAT prevalence and activity measured by other modalities. Consistent assessment of this

uniquely metabolic tissue is fundamental to the discovery of potential therapeutic strategies against metabolic disease.

### 4.2.2 Introduction

There is increasing evidence that brown adipose tissue (BAT) has an important physiological role beyond that of thermoregulation in new-born infants and rodents (Ouellet et al., 2012, Cypess et al., 2014, Sidossis and Kajimura, 2015). Adult humans have significant amounts of BAT (Cypess et al., 2009, van Marken Lichtenbelt et al., 2009, Virtanen et al., 2009), and as it is a highly metabolic tissue with the capacity to oxidise both glucose and lipid, attention has turned to its involvement in the pathogenesis of obesity, type 2 diabetes and the metabolic syndrome (Nedergaard and Cannon, 2010).

Brown adipose tissue is characterised by the presence of uncoupling protein 1 (UCP1). This unique mitochondrial protein uncouples the respiratory chain from the production of ATP, allowing the dissipation of excess chemical energy as heat (Cannon and Nedergaard, 2004). In adult humans, UCP1-containing adipose tissues have been identified in the neck and upper thorax (Virtanen et al., 2009, Zingaretti et al., 2009, Jespersen et al., 2013), around the kidneys (Svensson et al., 2014) and heart (Sacks et al., 2009), and UCP1 also appears to be inducible in depots classically considered white (Sidossis et al., 2015). Importantly, when the amount of BAT is reduced or dysfunctional, excess adiposity can occur (Feldmann et al., 2009, Vijgen et al., 2011). Several studies have demonstrated not only lower BAT activity in obese individuals compared with those who are lean, but also reduced UCP1 (Carey et al., 2014) and a

negative association between BAT activity and body mass index (Saito et al., 2009, Pfannenberg et al., 2010, Robinson et al., 2014).

Brown adipose tissue is under control of the sympathetic nervous system and is activated directly by catecholamines through β-adrenoreceptor signalling (Cannon and Nedergaard, 2004). In humans, this response can be mimicked using pharmacological stimulation with the $\beta_3$-adrenergic agonist mirabegron (Cypess et al., 2015). In addition, there is indirect evidence of active BAT in basal conditions from the observation that active noradrenaline uptake within the supraclavicular BAT in warm conditions is correlated with core body temperature (Hwang et al., 2015). The presence of BAT has largely been determined from the increased uptake of radiolabelled glucose during positron emission tomography-computed tomography (PET-CT) during cold exposure of fasted subjects (van Marken Lichtenbelt et al., 2009, Virtanen et al., 2009). However, the extent to which BAT activity can be promoted in more normal physiological conditions has been less well studied, because this cannot be readily achieved using PET-CT, alternative approaches are therefore needed to explore the regulation of BAT and investigate the effects of potential therapeutic agents.

Infrared thermography is able to assess BAT thermogenic function in adults and children by measuring changes in skin temperature overlying the main BAT depot in humans (Symonds et al., 2012a, Lee et al., 2011) that has now been shown to appear similar to that shown by PET-CT (Salem et al., 2016). Furthermore, owing to the low variability in measurements between subjects (Symonds et al., 2012a) it can be used

to undertake studies in comparatively small subject groups. Infrared thermography therefore has the potential to elucidate the mechanisms by which BAT activation occurs and thus optimise metabolic health. However, thermography can be affected by cutaneous vasoconstriction, which can be modulated by the sympathetic nervous system, in addition to changes in ambient temperature (Greaney et al., 2015).

Flurodeoxyglucose (FDG) uptake in BAT has also been shown to be affected by the psychological state prior to scanning, such that simple relaxation measures (exposure to audio-visual intervention) resulted in a significant reduction in BAT activity (Vogel et al., 2012). The aim of our study was, therefore, to determine whether mild psychological stress would acutely promote supraclavicular BAT activity detectable using dynamic thermal imaging in subjects maintained within a warm environment. We hypothesised that exposure to a short mental arithmetic (MA) test would elicit an acute stress response, thereby activating BAT thermogenesis.

### 4.2.3 Methods

Following University of Nottingham School of Medicine Ethics Committee approval, five lean Caucasian females aged between 21 and 29 years gave written informed consent to participate in the study. The study conformed to the standards set by the *Declaration of Helsinki*. The experimental protocol and study equipment were demonstrated to each participant at least 24 h before the initial study session to ensure familiarisation. All subjects were fasted from midnight. Study sessions commenced between 08.00 and 09.00 h, and thermography commenced at least 60 min after waking. We aimed to induce mild psychological stress using a short MA test, and anticipated that in addition to our intervention the first visit would engender more

stress than the second. By keeping the order of interventions identical between participants, we increased the internal consistency of the results, maximising the power to detect a difference due to stress.

At the start of the first study session, subjects were informed that they would be undertaking a short 2 min MA test (Memon et al., 2013), during which they would receive real-time verbal feedback regarding their performance. Subjects were unaware, however, that those answering more than two successive questions incorrectly would be told that their next answer was incorrect regardless of the answer given. The second study session was undertaken at least 48 h after the first and was identical in every respect to the MA session, except that the MA test was replaced with a 2 min relaxation video (R). Participants were aware of this from the beginning of the second study session.

Both study sessions consisted of an acclimation period of 30 min, during which subjects were asked to sit comfortably at rest with their supraclavicular region exposed. Thereafter, a 30 min baseline period was recorded, in which supraclavicular skin temperature and mean skin temperature were measured and samples of saliva taken for cortisol measurement. On completion of baseline measurements, 2 min of either MA or R was undertaken, followed by a further period of 50 min consisting of thermography and salivary sampling as summarised in Figure 4.1.

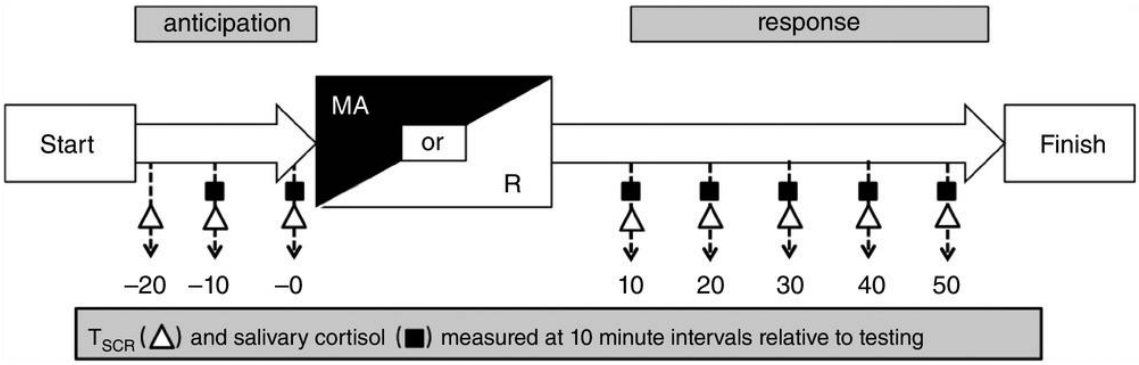



**Figure 4.1 Summary of the study protocol, demonstrating the timing of thermal imaging and salivary cortisol assessment relative to mental arithmetic (MA) testing or exposure to the audiovisual relaxation film (R), which were conducted at the same time on different days.**

Abbreviations: $T_{SCR}$ – supraclavicular temperature

The temperature of the skin overlying supraclavicular BAT ($T_{SCR}$) was measured using infrared thermography (FLIR B425; FLIR systems, Danderyd, Sweden) and used as an indicator of BAT activity as described previously (Symonds et al., 2012a, Robinson et al., 2014). A region of interest was defined as that bounded by the left sternocleidomastoid muscle, clavicle and lateral contour of the neck using ThermaCAM Researcher Pro 2.10 (FLIR Systems AB, Täby, Sweden). These were then exported into Excel (Microsoft, Redmond, WA, USA) to calculate the 97.5$^{th}$ percentile temperature value of the region of interest. Images were taken in triplicate at each designated time point and at intervals before and after MA or R testing. The $T_{SCR}$ at each time point was calculated as the average value derived from the triplicate images. Baseline was defined as the mean temperature of the 10 min preceding MA or R. Mean skin temperature ($T_{MSK}$) was evaluated using measurements of skin temperature obtained from wireless data loggers (iButton, model no. DS1219H-F50; Sunnyvale, CA, USA) placed at seven body sites (i.e. forehead, trunk, arm, hand, lower

leg, thigh and foot) and calculated using the Hardy-Du Bois formula (Hardy et al., 1938). The $T_{SCR}$ was adjusted for the local effect of ambient temperature by calculating the difference between $T_{SCR}$ and $T_{MSK}$.

Salivary cortisol samples were taken using small cotton swabs (Salivette; Stastedt, Leicester, UK) 10 min before and immediately before MA or R and at 10, 20, 30, 40 and 50 min post intervention. These were stored at -80˚C until analysis using a commercially available enzyme-linked immunosorbent assay kit designed for saliva samples (kit no. 1-2003; Salimetrics Europe Ltd). A total of 70 samples were analysed and intra-assay precisions were < 10%.

### 4.2.4 Statistical analysis

Data were assessed for normality using the Kolmogorov-Smirnov normality test and are presented as means ± SEM unless otherwise stated. Comparisons between data obtained during MA and R testing at single time points were made using Student's paired t test. Pearson product-moment correlation coefficients were calculated to determine the correlation between salivary cortisol levels and $T_{SCR}$. To determine the effect of MA and R over time, two-way repeated measures ANOVA was undertaken with Sidak's post hoc multiple comparisons test.

### 4.2.5 Results

All subjects were lean Caucasian females with an average height, weight and body mass index of 1.70 ± 0.04 m, 65.6 ± 5.05 kg and 22.2 ± 0.95 kg $m^2$, respectively. Ambient room temperature did not differ between the MA and R study sessions and was on average 22.8 ± 0.2˚C. A summary of these anthropometric measures and room conditions is shown in Table 4.1.

**Table 4.1 Summary of the anthropometric measures of the study participants and room temperature on each study day**

| Participant no. | Height (m) | Weight (kg) | Body mass index ($kg/m^2$) | Age (year, months) | Ambient room temperature for MA testing (˚C) | Ambient room temperature for R (˚C) |
|---|---|---|---|---|---|---|
| 1 | 1.85 | 83.7 | 22.5 | 29 y 2 mo | 22.5 | 23.0 |
| 2 | 1.70 | 59.1 | 23.4 | 26 y 7 mo | 23.4 | 23.3 |
| 3 | 1.65 | 53.9 | 23.1 | 21 y 9 mo | 23.1 | 22.9 |
| 4 | 1.72 | 64.3 | 22.9 | 24 y 10 mo | 22.9 | 22.9 |
| 5 | 1.67 | 66.9 | 23.0 | 23 y 2 mo | 23.0 | 22.1 |

Abbreviations: MA, mental arithmetic; and R, audiovisual relaxation.

#### 4.2.5.1 Salivary cortisol response

Anticipation of MA was associated with significantly higher salivary cortisol concentrations at 10 min prior to the test compared with the same period before the relaxation film (i.e. 0.62 ± 0.17 versus 0.25 ± 0.05 μg/dL P = 0.004), confirming that anticipation alone was sufficient to act as a mild psychological stressor. After administration of either MA or R, salivary cortisol decreased (Figure 4.2). Although there was a continued trend towards higher levels immediately prior to MA (baseline – 0.41 ± 0.11 versus 0.21 ± 0.05 μg/dL), this difference was no longer statistically significant (P = 0.09).

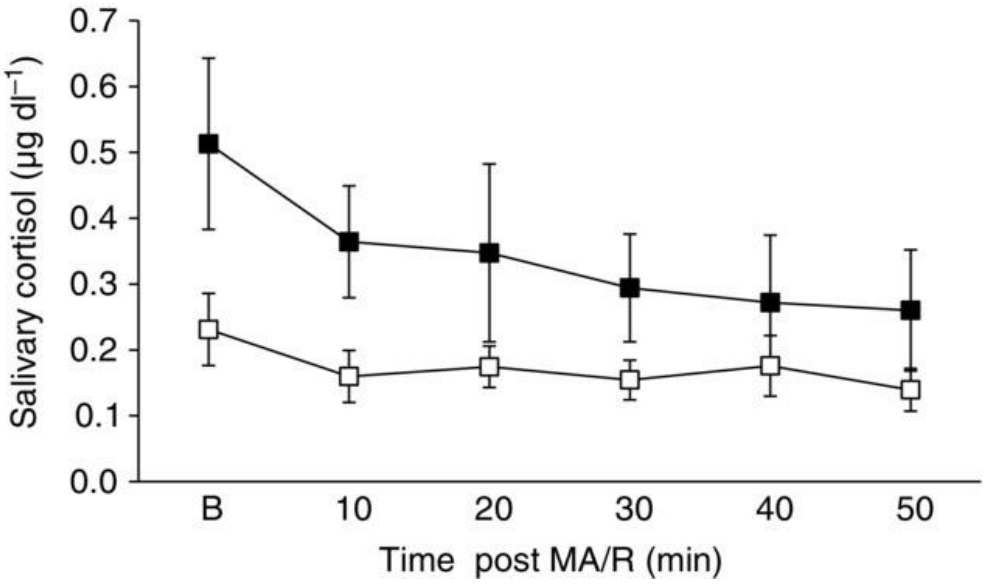



**Figure 4.2 Salivary cortisol concentrations (in micrograms per decilitre) at baseline (B) and after mental arithmetic testing (MA) or exposure to audiovisual relaxation film, in lean, Caucasian female subjects (n = 5)**

Data are shown as mean ± SEM. Filled squares, MA; and open squares, R.

#### 4.2.5.2 Anticipation of MA is associated with increased supraclavicular temperature

A trend for a higher absolute value of $T_{SCR}$ before MA (compared with R) was also observed at 20 min before the MA test ($T_{SCR}$ 34.9 ± 0.2 versus 34.6 ± 0.1°C, respectively, P = 0.09). Furthermore, after adjustment for ambient temperature by calculating the difference between $T_{SCR}$ and $T_{MSK}$ ($T_{Diff} = T_{SCR} – T_{MSK}$), a significantly greater $T_{Diff}$ was observed at both 20 and 10 min prior to MA testing (Fig. 4.3), indicating that anticipation of MA testing was associated with a relatively higher $T_{SCR}$.

#### 4.2.5.3 Supraclavicular temperature increases following MA and R and is associated with baseline $T_{SCR}$ and salivary cortisol concentration

Unexpectedly, $T_{SCR}$ rose significantly from baseline in the subjects attending for R (Figure 4.4). Two-way repeated-measures ANOVA identified a significant effect of time, with no effect of psychological stress. Sidak's *post hoc* multiple comparisons test revealed that the effects of time were observed at 30, 40 and 50 min and were limited to the R session. (Figure 4.4C and D). In contrast to the changes in $T_{SCR}$, values of $T_{MSK}$ were seen to decrease significantly over time in both study sessions by 30 min in the response period, suggestive of a reduction in overall body skin temperature (Fig. 4.4E and F). Figures 4.4A and B further demonstrates representative changes in $T_{SCR}$ visualised as thermograms between baseline and post-MA or post-R testing at 50 min, with no change with MA but an increase in R.

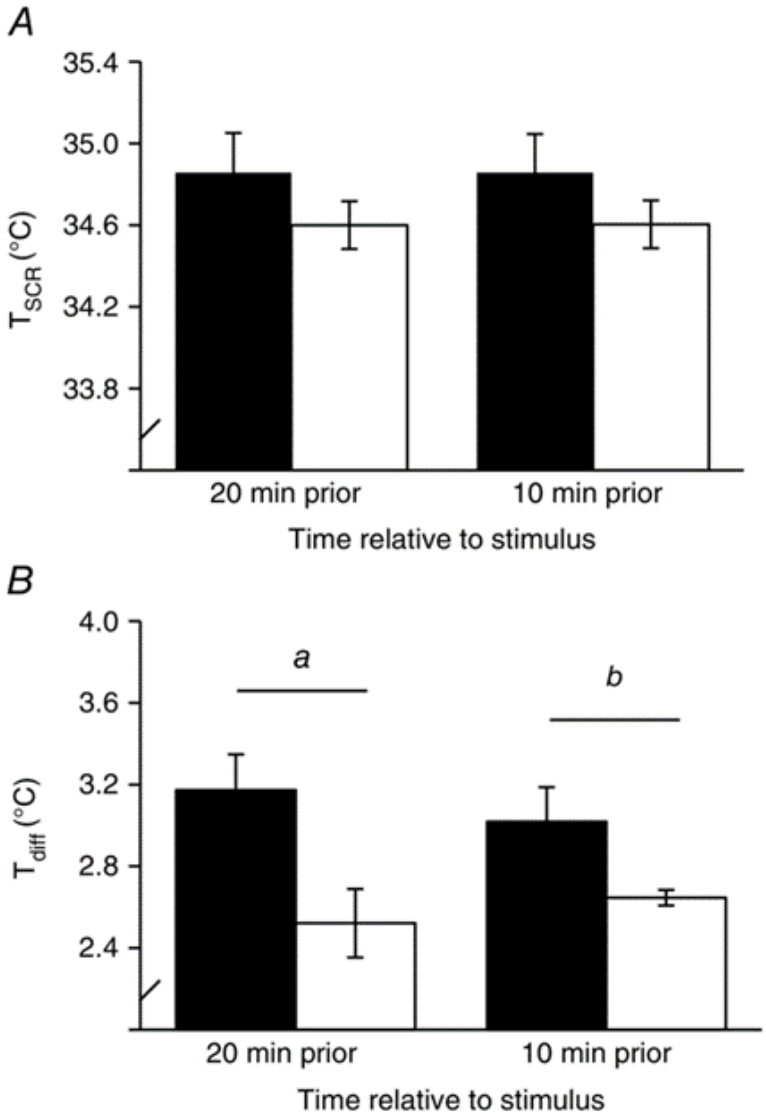



**Figure 4.3 Supraclavicular temperature ($T_{SCR}$) A) and temperature difference between the supraclavicular region and mean skin temperature ($T_{Diff} = T_{SCR} – T_{MSK}$;B) 20 and 10 min prior to mental arithmetic testing (filled bars) and the audiovisual relaxation film (open bars) in lean, Caucasian white female subjects (n = 5)**

*a*, P = 0.048; and *b*, p = 0.041. Data are shown as means ± SEM.

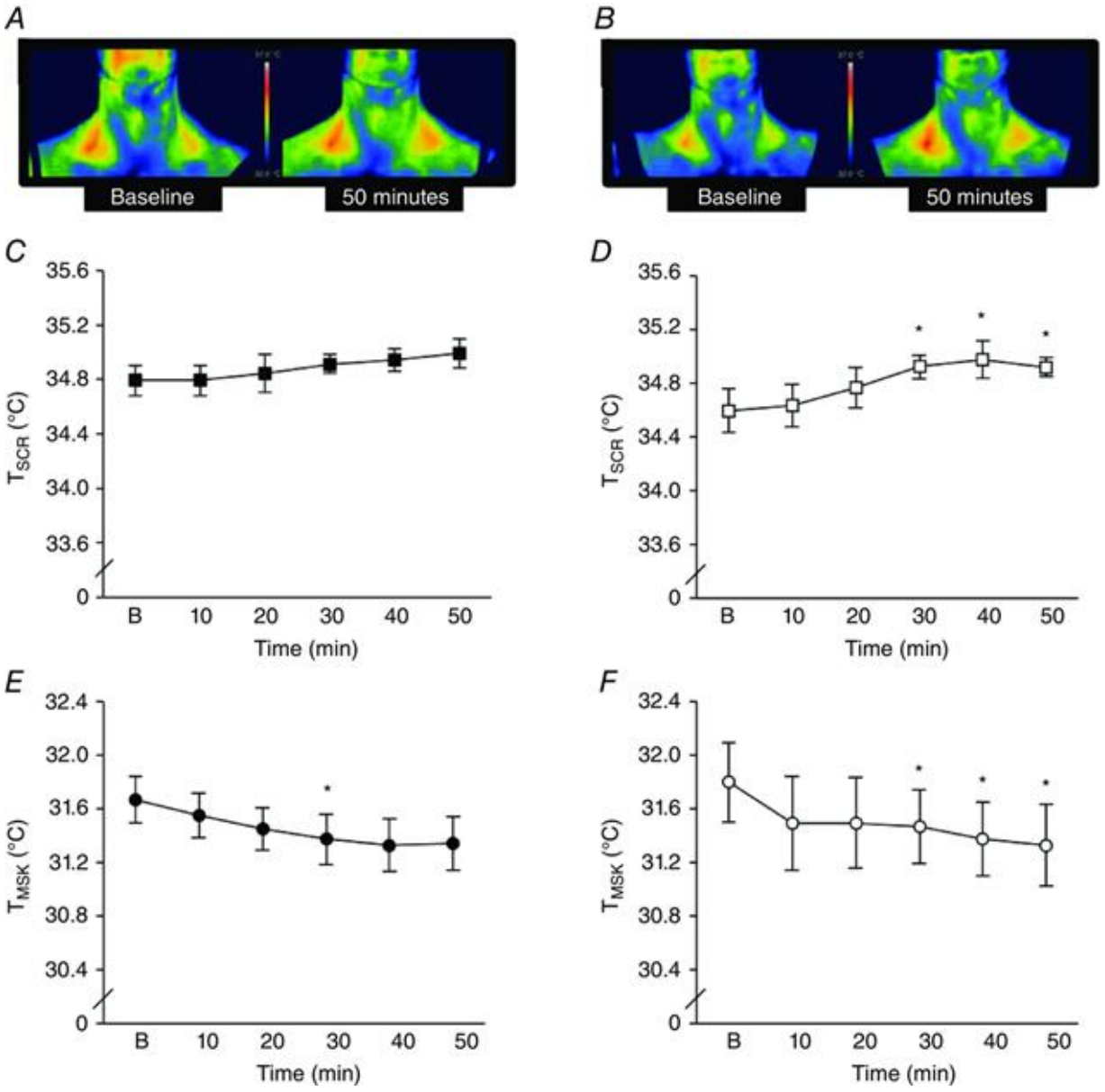



**Figure 4.4 Mean changes in supraclavicular and reference point skin temperature**
A, representative anterior thermograms of the supraclavicular region during baseline and 50 min after a 2 min mental arithmetic test. B, representative anterior thermograms of the supraclavicular region during baseline and 50 min after watching a 2 min relaxation film. C and D demonstrate the changes in supraclavicular temperature ($T_{SCR}$) from baseline until 50 min after mental arithmetic testing (C) or exposure to the relaxation video (D). E and F demonstrate the changes in mean skin temperature ($T_{MSK}$) from baseline until 50 min after mental arithmetic testing (E) or exposure to the relaxation video (F). Filled symbols, mental arithmetic testing; and open symbols, relaxation video. Squares represent $T_{SCR}$ and circles $T_{MSK}$. *$P < 0.05$ following two-way repeated-measures ANOVA. Data are shown as mean values ± SEM, n = 5.

Furthermore, when the maximal change in $T_{SCR}$ ($\Delta T_{SCRmax}$) was considered, although small, significant increases in $T_{SCR}$ were observed after both the MA and R testing and no significant difference was observed between the two sets of experimental conditions ($\Delta T_{SCRmax}$ R 0.54 ± 0.15°C versus ($\Delta T_{SCRmax}$ MA 0.44 ± 0.05°C, P = 0.5). A negative correlation was observed between baseline $T_{SCR}$ and $\Delta T_{SCRmax}$ (Pearson's r = −0.72, P = 0.017), indicating that the degree of maximal temperature change over time was inversely related to the baseline starting value of $T_{SCR}$ (Figure 4.5).

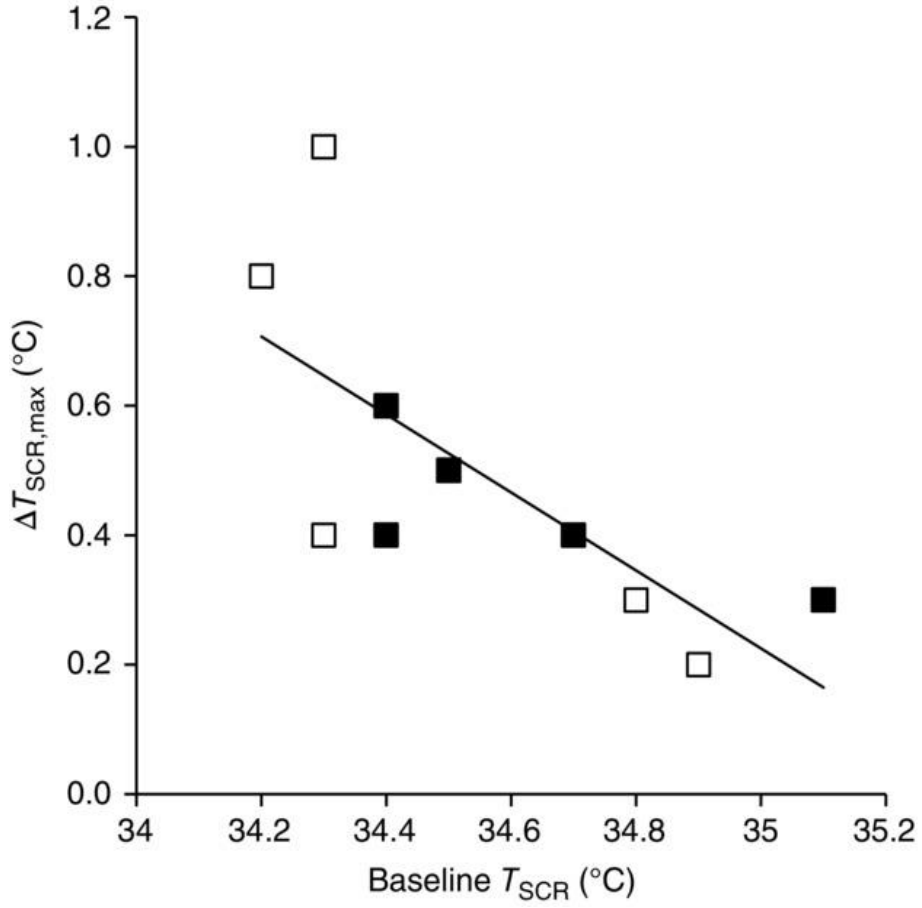



**Figure 4.5 Relationship between minimal baseline supraclavicular temperature ($T_{SCR}$) and maximal change in supraclavicular temperature ($\Delta T_{SCRmax}$) throughout the duration of the study periods (Pearson's correlation coefficient r = −0.72, P = 0.017) in lean, Caucasian female subjects (n = 5)**

Filled squares, mental arithmetic testing; and open squares, relaxation video.

A significant positive correlation was observed between paired measures of $T_{SCR}$ and salivary cortisol at 10 min prior to MA testing, but not prior to R (Figure 4.6).

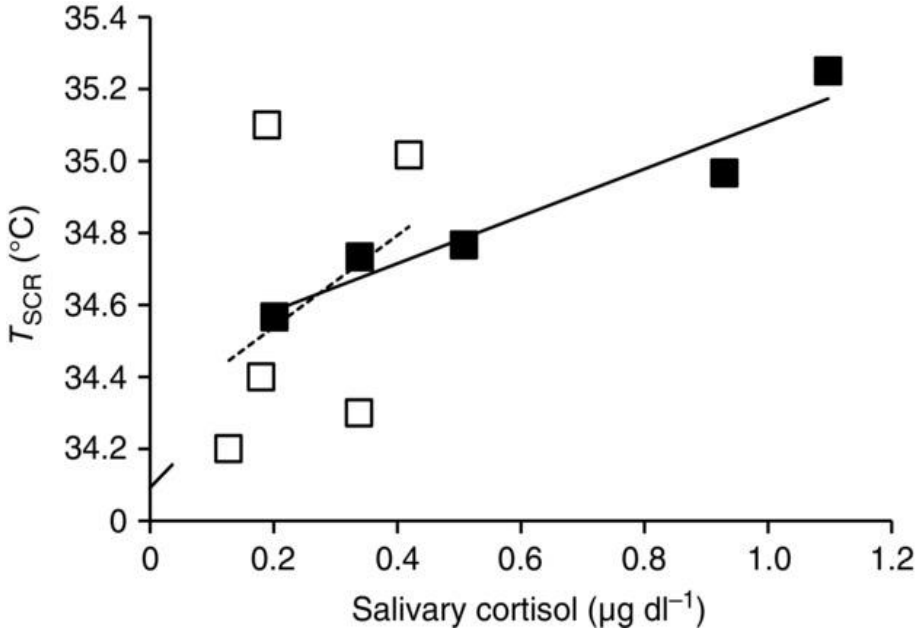



**Figure 4.6 Relationship between supraclavicular temperature ($T_{SCR}$) and salivary cortisol during the baseline period prior to mental arithmetic testing (Pearson's correlation coefficient, r = 0.97, P = 0.008) and prior to the audiovisual relaxation film (Pearson's correlation coefficient, r = 0.14, P = 0.188) in lean, Caucasian female subjects (n = 5)**

Filled squares, mental arithmetic testing; and open squares, relaxation video.

### 4.2.6 Discussion

We have shown that mild anticipatory psychological stress, induced by the expectation of MA testing increased supraclavicular skin temperature, which is indicative of increased BAT activity (Jang et al., 2014, Salem et al., 2016). This finding is, therefore, supportive of a significant impact of anxiety on BAT, as suggested previously from studies in both humans (Hwang et al., 2015) and rodents (Lkhagvasuren et al., 2011, Mohammed et al., 2014). Furthermore, we have shown that, irrespective of the cause, elevated cortisol is strongly correlated with supraclavicular temperature. This finding is in accord with the previously suggested role of the hypothalamic-pituitary-adrenal

axis in sensing energy balance and caloric flow (Kirschbaum et al., 1997). It has also been recently shown in rodents that the dorsomedial hypothalamic node bifurcates stress signalling to the sympathetic outflow to promote BAT thermogenesis and to the endocrine outflow, thereby promoting stress hormone release (including corticoids) through the hypothalamic-pituitary-adrenal axis (Kataoka et al., 2014).

In our study, MA testing per se did not elicit the acute stress response we had expected. However, all but one subject was educated to postgraduate level and scored highly on the MA test, suggesting that it was not sufficiently challenging. Interestingly, we also observed an increase in $T_{SCR}$ over the 50 min following MA and R, whilst the maximal change from baseline did not differ between the two experimental conditions. Consequently, these effects appear to be more pronounced following R. The $T_{SCR}$ when first recorded was also lower prior to R, and salivary cortisol measures did not increase in line with MA-induced acute stress response, further BAT stimulation must have occurred by an alternative mechanism. It should be noted that for successful thermography the subjects must remain still, such that despite being undertaken fully clothed in a warm, comfortable room, subjects may gradually cool down owing to a reduction in non-exercise activity thermogenesis.

In support of this theory is the reduction in mean skin temperature we observed particularly in the R intervention. The MA group, with their higher $T_{SCR}$ at baseline, seemed better able to maintain their overall body temperature, such that BAT thermogenesis recruited during the anticipatory phase was sufficient to offset any reduction in non-exercise activity thermogenesis or represents maximally stimulated

BAT at baseline. Further studies conducted at cooler ambient temperatures could now be undertaken to investigate this further.

Although the effect of catecholamines on BAT thermogenesis has been well characterised in rodents (Cannon and Nedergaard, 2004) and has been observed in humans with pathological adrenergic excess (Nagano et al., 2015) and in subjects exposed to therapeutic intervention (Cypess et al., 2015), our understanding of the endocrine control of human BAT in the physiological state is less well understood. A role for anxiety or anticipatory stress has also been suggested from the finding that administration of anxiolytic medications such as propranolol, diminishes the 'unwanted' BAT glucose uptake in patients undergoing clinical PET-CT scanning (Gelfand et al., 2005, Jacobsson et al., 2005), as does exposure to relaxing audiovisual imagery (Vogel et al., 2012). A potential role for cortisol in BAT function has not been previously shown in adults in vivo. The increase in cortisol observed in our study most probably represents the overall neuroendocrine response to acute stress (hypothalamic-pituitary-adrenal activation), including a concomitant increase in systemic circulating catecholamines. Our novel observation that cortisol was positively correlated with $T_{SCR}$, in conjunction with in vitro studies in humans (Barclay et al., 2015), highlights the effect of cortisol on human BAT as an interesting avenue for future investigation.

Rodent studies, both in vitro (Soumano et al., 2000, Viengchareun et al., 2001) and in vivo, have reported that glucocorticoids have an inhibitory effect in classical BAT, suppressing thermogenesis (Strack et al., 1995), although these must be interpreted with caution because they were not undertaken at thermoneutrality (Celi et al., 2015).

It should be noted that endocrine factors suggested to stimulate BAT function in rodents may not necessarily have the same role in humans.

Cortisol is, however, known to have an important role in promoting maximal BAT function around the time of birth, although whether this is a direct effect or mediated by changes in thyroid hormones remains to be established fully (Mostyn et al., 2003). Direct effects of exogenous administration on human BAT activity have yet to be shown but hypercortisolaemia, induced by exogenous administration of hydrocortisone, results in a significant increase in energy expenditure (Brillon et al., 1995). Whether this is mediated by BAT remains to be elucidated, although we have recently shown that a 14 h infusion of hydrocortisone into adult men of normal weight stimulates BAT function (Scotney et al., 2017). Dexamethasone stimulates the proliferation, differentiation and function of human brown adipocytes in vitro (Barclay et al., 2015). This suggests that metabolic manifestations of Cushing's syndrome could be related, in part, to the effect of hypercortisolaemia on BAT, such as the characteristic region excess adiposity (e.g. buffalo hump) represents hyperproliferation of BAT, as recently suggested from the response to trauma in subcutaneous adipose tissue following severe burns (Sidossis et al., 2015).

In conclusion, our findings have important implications in the study of BAT during supposedly basal conditions because it is clear that subtle changes in psychological stress, including anticipation, can stimulate the production of heat from BAT within the supraclavicular depot. This may explain why functional measurements of BAT measured using PET-CT are not directly confirmed by comparable changes in BAT temperature (Jang et al., 2014) and further highlights the need for caution when

interpreting such results. Our findings, if repeated in larger subject groups, could, therefore, enable novel interventions linked to mild stress in order to promote BAT function.

### 4.3 Study III: conclusions in 2019

Following the publication of this study, no studies have gone on to examine the specific effects of psychological stress on BAT in more detail. The effects of glucocorticoids on BAT continue to be a topic of debate, and two notable human double-blind crossover studied have endeavoured to examine how glucocorticoids may acutely modulate BAT function using a combination of FDG uptake, supraclavicular skin temperature and indirect calorimetry (Scotney et al., 2017, Ramage et al., 2016).

Scotney et al. demonstrated the stimulatory effects of acute glucocorticoid administration on adult supraclavicular BAT. Following overnight intravenous infusion of hydrocortisone, basal $T_{SCR}$ increased alongside an increase in plasma cortisol, non-esterified fatty acids, glucose and insulin. Furthermore, maximal supraclavicular skin temperatures during β stimulation with isoprenaline were higher after receiving hydrocortisone as compared to placebo (Scotney et al., 2017). Similarly, Ramage et al. reported BAT stimulation after the acute administration of prednisolone. Interestingly, although data regarding cortisol was not reported in this study, activation occurred independently of any changes in plasma catecholamine concentrations. FDG uptake was increased and $T_{SCR}$ and energy expenditure were higher during whole body cooling as compared to placebo (Ramage et al., 2016). Interestingly, this group did not observe an increase in $T_{SCR}$ following hand immersion in cool water in this small group of participants (n = 8). However, their measure of $T_{SCR}$ was determined using a different

method to that used in the studies presented in this thesis ("mean average temperature of a circular ROI") which may have been less sensitive to small changes in skin temperature.

In the studies described above, the plasma cortisol concentrations associated with exogenous glucocorticoid administration far exceeded those observed in Study III, and are significantly higher than those observed during the physiological acute stress response observed in the laboratory setting (Kirschbaum et al., 1993). Therefore, it may be argued that the responses in $T_{SCR}$ in my study may be more representative of physiological changes and the studies of Scotney and Ramage more reflective of pathological states or the effects of treatment. The normal physiological response to acute stress comprises several neuroendocrine changes that include both the stimulation of the sympathetic nervous system and changes within the hypothalamic-pituitary-adrenal axis, which are likely to act in parallel on BAT. Therefore, the effects of cortisol and adrenergic stimulation may act synergistically.

The basis of the acute stress response is to elicit behavioural and physical adaptations, which allow an individual to survive under life-threatening conditions (Gray, 1987, Cannon, 1916). Under normal circumstances, these adaptations are beneficial, allowing an organism to defend itself or run away (e.g. 'flight or fight'). As to what the physiological benefit of BAT activation may be in the survival context is unclear. Enhancing metabolic inefficiency seems counterintuitive when many of the other adaptations occur to allow mobilisation of energy stores. BAT activation during acute stress may, therefore, merely represent a by-product of sympathetic nervous system activation without physiological purpose.

As FDG uptake in BAT during scans undertaken to identify glucose uptake into tumour tissue can be problematic, there has been some recent research into non-pharmacological methods of reducing patient anxiety during the uptake phase of PET-CT. Listening to 30 minutes of meditative music after injection of FDG was shown to reduce heart rate, cardiac sympathetic activity and reduce patient perceived anxiety (Lee et al., 2017). While not formally quantified, the authors of this study also reported a concomitant reduction in BAT visible on PET in these subjects too. The source and degree of anxiety or psychological stress suffered by patients undergoing clinically indicated FDG-PET-CT is likely to differ from that of healthy volunteer research subjects, yet some of the factors affecting basal levels of anxiety will be the same. For example, unfamiliarity with the research equipment or experimental protocol, concern about invasive procedures and diagnostic uncertainty.

Simple additions to any experimental protocol for BAT assessment regardless of method used may keep BAT activation secondary to acute stress to a minimum, thus reducing between-subjects variability and optimising any response to subsequent stimulation by ensuring baseline activity is as low as possible. For example, participants could attend the research laboratory for a pre-assessment visit where experimental procedures and the study protocol could be explained and demonstrated before the acquisition of study data. An assessment of anxiety at the beginning of each study, using simple non-invasive measures such as heart rate, blood pressure or heart rate variability may identify individuals with high basal levels of anxiety. More formal assessments of anxiety state using non-invasive tools like the Spielberger State-Trait Anxiety Inventory (Spielberger, 1983) may also assist in identifying participants who

are not sufficiently at ease to commence the experimental protocol. The provision of audiovisual relaxation material during the study set up and throughout the experimental protocol is an easy, practical measure that could be implemented in all BAT dedicated studies.

# CHAPTER FIVE

---

## Exploring the physiological response to localised limb cooling and the effect of ambient temperature

### Study IV

### Study V

## 5.1 Preface

In Studies I and II, the response to mild cold exposure in young children (single hand immersion in cool water at 20˚C) was smaller than expected. The maximal $T_{SCR}$ response was between 0.1 – 0.2˚C. Given the sensitivity and accuracy of the thermal cameras being used (FLIR B425, and FLIR E60 respectively) in these studies, and the variability observed during baseline measurements observed previously in Studies I to III (even after allowing sufficient time for stabilisation of $T_{SCR}$), the magnitude of this response to cold exposure is not large enough to detect reproducibly without utilising large numbers of study participants. This hinders the further study of children, as often the number of available participants is limited.

This is especially relevant if this methodology is to be used to study groups of interest in whom the total population is small (e.g. children with clinical diagnoses that may impact upon BAT such as or maturity-onset diabetes of the young or Silver-Russell syndrome). Study III revealed that excitement or anticipatory stress prior to cold exposure in Studies I and II may have accounted partially for the attenuated response to hand cooling I observed in comparison to the response seen in previous studies (Symonds et al., 2012a), although this has yet to be confirmed in a paediatric population. It is not clear whether basal BAT activity in these children was approaching the maximum for reasons other than psychological stress or whether the cool stimulus used in these studies was insufficient to elicit large changes in $T_{SCR}$.

Studies IV and V were designed to determine if the thermogenic response to single hand immersion in cool water could be enhanced by whole-body warming prior to localised cold exposure or could be enhanced by using a longer and/or cooler stimulus.

At the time these studies were undertaken, $T_{SCR}$ had not been validated against any other measure of BAT activity, and these studies were also used to seek further evidence to support that cold-induced changes in $T_{SCR}$ were solely due to BAT activation. I, therefore, to aimed to determine whether the observed $T_{SCR}$ response was associated with other physiological changes indicative of cold-induced thermogenesis (e.g. energy expenditure) and whether there were any indicators of the cold-pressor reflex. The cardiovascular effects of the sympathetically driven cold-pressor response may, in turn, lead to local changes in blood flow and indirectly obscure any changes in skin temperature that occurs secondary to BAT thermogenesis.

Like Study III, the two studies presented in this chapter were designed to use minimally invasive methods that could be directly applied to future studies of children. However, given the nature of the studies as pilot/feasibility studies, these were undertaken in young adult participants in the first instance.

Published data in both children and adults identifies that warming prior to and during PET-PET scanning can effectively suppress FDG uptake in BAT (Christensen et al., 2006, Skillen et al., 2012, Zukotynski et al., 2009, Zukotynski et al., 2010). Zukotynski et al. showed that accommodating children requiring PET scan at 24˚C as opposed to 21˚C reduced the proportions of children with FDG-detectable BAT by three times, down to just 9% (Zukotynski et al., 2010), indicating that basal activity (in terms of glucose uptake at least) can be altered by relatively small changes in room temperature. Therefore, in Study IV I hypothesised that warming participants at an ambient room

temperature of 23˚C results in a greater thermogenic response to hand cooling as compared to hand cooling undertaken in a cool room at 18˚C.

Most BAT dedicated studies are undertaken during cold stimulation. Cooling methods vary by research group and comprise various permutations of air, water or ice cooling of the whole-body or specific body regions (summarised in Chapter 1.11.5). These methods generally utilise more severe methodology that would not be suitable for use with children such as: torso cooling with a water-perfused jacket (Salem et al., 2016), whole-body cooling with a liquid filled body suit or mattress (Ouellet et al., 2012, Boon et al., 2014), foot immersion in ice water (Yoneshiro et al., 2011, Yoneshiro et al., 2016) furthermore, there is still little existing data regarding cooling protocols for BAT activation in children.

Study V was designed to develop a cooling protocol that could deliver more effective cooling than hand cooling in tap water, and which could also be applied to future research studies involving children. Given the high density of cold thermoreceptors in the forearm and hand (Stevens and Choo, 1998), to enhance the degree of cooling the area chosen to be cooled in Study V was extended to include the whole forearm. Also, the degree of cooling was enhanced by reducing the water temperature to 14 – 15˚C, to maximise the cool stimulus yet avoid stimulation of thermal nociceptors and the cold-pressor reflex. Maintaining the water temperature during hand immersion beyond 5 minutes in Study IV was technically difficult. Therefore, in Study V, I examined the feasibility of cooling via a water-perfused cooling blanket placed circumferentially around the whole forearm as an alternative. Study V aimed to

determine the time course and magnitude of changes in supraclavicular skin temperature in response to cooling of the whole forearm. I also aimed to explore whether a relationship between $T_{SCR}$ and adiposity was present young adults in a similar manner to that observed in children in Studies I and II.

Therefore, in the two studies presented in this chapter the hypotheses are that $T_{SCR}$:

i) increases in response to cooling to a greater degree after pre-warming at 23˚C (as compared to 18˚C)
ii) continues to increase with prolonged cold exposure beyond 5 minutes
iii) increases in parallel to an increase in energy expenditure indicative of cold-induced thermogenesis
iv) rises with forearm cooling at 14˚C without evidence of the cold-pressor reflex
v) is associated with participant body composition in line with the findings of Study I and Study II.

## 5.2 Study IV

**The supraclavicular skin temperature response to hand cooling is dependent on ambient room temperature (Published on the Science Repository in the Journal of Diabetes, Metabolism and its complications DOI: 10.31487/j.JDMC.2019.01.02)**

### 5.2.1 Abstract

Purpose: This study investigated the basal activity, and cold-induced thermogenic response, of supraclavicular brown adipose tissue (BAT) under warm (23˚C) and cool (18˚C) ambient conditions using supraclavicular skin temperature ($T_{SCR}$) as a measure of BAT activity. As a highly metabolic, heat-producing tissue, it has been hypothesised that under-active/dysfunctional BAT may underlie a pathological energy imbalance leading to obesity.

Methods: Five lean, healthy participants underwent infrared thermography (IRT) of supraclavicular BAT before, and during, 30 minutes mild cold exposure (single hand immersion in cool water at 20˚C), once at 18˚C and once at 23˚C. Energy expenditure (EE) was measured simultaneously using indirect calorimetry, and mean skin temperature ($T_{MSK}$) was measured in parallel to IRT using wireless data loggers.

Results: Following 30 minutes of hand cooling, $T_{SCR}$ rose significantly from baseline ($\Delta T_{SCR}$) at an ambient temperature of 23˚C ($\Delta T_{SCR}$: 0.17 ± 0.03˚C, $P < 0.01$), and EE rose by 0.22 ± 0.02 kJ/min, $P < 0.001$. At an ambient room temperature of 18˚C, $T_{SCR}$ after hand cooling was similar to baseline, and EE remained unchanged. The $T_{MSK}$ response was indicative of a systemic vasoconstrictive response of similar magnitude in both warm and cool ambient temperatures.

Conclusions: At 18˚C in light clothing, BAT may already be maximally stimulated at baseline, and respond minimally to additional cold exposure. This may indicate near maximal activity at baseline under these conditions. Ambient temperature is recognised as a determinant of glucose uptake in BAT. In this study, we show, that it also modulates the $T_{SCR}$ response to further localised cold stimulation, indicating an effect on BAT thermogenesis.

### 5.2.2 Introduction

Following the recent discovery of functional, metabolically active brown adipose tissue (BAT) in humans (van Marken Lichtenbelt et al., 2009, Cohade et al., 2003, Cypess et al., 2009, Virtanen et al., 2009, Zingaretti et al., 2009), interest lies in elucidating the mechanisms underlying the BAT mediated non-shivering thermogenic (NST) component of the physiological response to acute cold. It is well established that cold-induced activation of uncoupling protein (UCP)1 on the inner mitochondrial membrane of thermogenic brown adipocytes uncouples oxidative phosphorylation from the generation of ATP, and that the excess chemical energy is dissipated as heat (Cannon and Nedergaard, 2004). As a result, fat depots containing an abundance of thermogenic UCP1-containing adipocytes generate heat and expend energy (Bartesaghi et al., 2015, Cypess et al., 2013). It is estimated that cold-induced BAT activation could increase resting energy expenditure by at least 2.5 – 5% (van Marken Lichtenbelt and Schrauwen, 2011).

The most superficial thermogenic BAT depot in humans is found in the neck and upper thorax (Cohade et al., 2003), and supraclavicular skin temperature has been used in conjunction with varying cold stimuli (e.g. localised chest cooling, personalised whole-

body cooling protocols designed to achieve maximal non-shivering thermogenesis(NST)) as a proxy measure of thermogenesis (Law et al., 2018, Jang et al., 2014, Boon et al., 2014, Lee et al., 2016). As a highly metabolic tissue, BAT has a high glucose requirement, and radio-labelled glucose uptake is often used as an indicator of BAT activity. $^{18}$F-fluorodeoxyglucose (FDG) positron emission tomography (PET) is frequently used for clinical purposes, and warming patients prior to scanning is recommended to reduce FDG uptake in BAT (which may obscure the region of clinical interest (Surasi et al., 2014)). Retrospective studies of clinically indicated FDG-PET scans have identified that BAT is less frequently observed in individuals who have been subject to a range of pre-warming procedures (Christensen et al., 2006, Zukotynski et al., 2009, Skillen et al., 2012) and, prospective BAT dedicated studies confirm an acute BAT response to both warming and cooling (Leitner et al., 2018).

Furthermore, the primary substrates of BAT are intracellular lipids (Blondin et al., 2015a), and UCP1 activation is fatty acid-dependent (Bertholet and Kirichok, 2018). Glucose uptake is, therefore, a crude measure of BAT activity, and when quantified as standard uptake values on static FDG-PET-CT (e.g. SUVmean, SUVmax) may be considered semi-quantitative at best (Ong et al., 2018). Importantly, these measures do not quantify thermogenic output.

How exposure to warm ambient conditions before exposure to a cold stimulus affects the subsequent heat production from BAT, has not been explored. In this study, we used direct measurements of supraclavicular skin temperature to investigate the basal activity and cold-induced thermogenic response of supraclavicular brown adipose tissue (BAT) under warm (23˚C) and cool (18˚C) ambient conditions. We hypothesised

that the basal activity of BAT would be lowest under warm conditions and that the response to mild cold exposure would, therefore, be greater.

### 5.2.3 Methods

The study was undertaken following the University of Nottingham School of Medicine Ethics Committee approval (Reference no: D052011) during the months of October and November. All participants gave written informed consent to take part, and the study conformed to the standards set by the Declaration of Helsinki 2008, in place at the time. The study protocol is summarised in Figure 5.1 below.

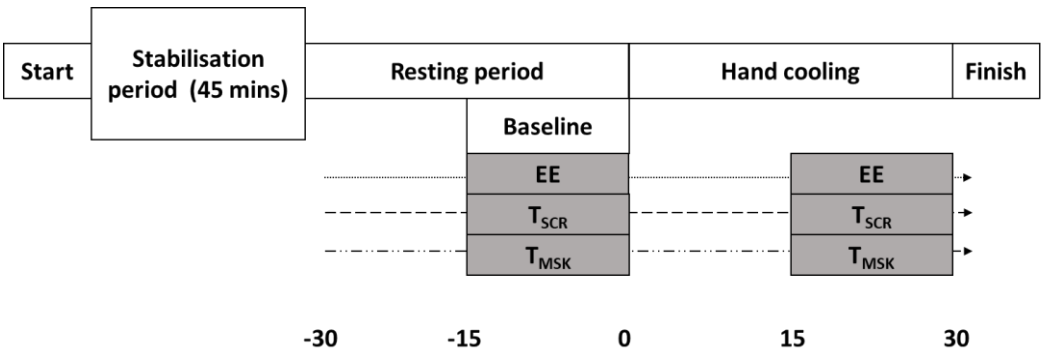



**Figure 5.1 Summary of the study protocol, demonstrating the timing of hand cooling and the assessment of energy expenditure (EE), supraclavicular skin temperature ($T_{SCR}$) and mean skin temperature ($T_{MSK}$) during baseline and cold stimulation.** Study protocol was undertaken by participants in a temperature-controlled laboratory at 18˚C and 23˚C.

#### 5.2.3.1 Participants

Five healthy non-obese male volunteers aged 18 – 36 years with a mean body mass index of 24 ± 0.75 kg/m$^2$, fat mass of 17.1 ± 2.2kg and fat-free mass of 67.4 ± 4.2 kg took part. Each attended twice after an overnight fast (from midnight). Visits were on separate days and were allocated in random order. Experiments were conducted in a quiet, temperature-controlled laboratory with participants in a semi-reclined supine

position. Participants wore standardised clothing consisting of a cotton short sleeved shirt, long cotton trousers and socks (0.35 Clo). Subjects were asked to avoid alcohol and strenuous exercise in the preceding 24 hours. Participants with any condition, disease or drug known to affect metabolic rate or BAT activity were excluded. Height was measured using a stadiometer to the nearest 0.1 cm (Leicester height measure; Child Growth Foundation, Sutton Coldfield, United Kingdom) weight was measured to the nearest 0.1 kg using calibrated portable digital scales, and body composition was determined using bioelectrical impedance using a hand-to-foot, single-frequency (50 kHz) battery-operated bioimpedance analyser (BIM4; ImpediMed P/L, Capalaba, Austria).

#### 5.2.3.2 Cooling protocol

Participants attended the laboratory on two mornings, and the cooling protocol was undertaken at room temperatures of 18˚C and 23˚C. Measurements commenced after a minimum of 45 minutes stabilisation to the room temperature. After a 15 minute basal period, the left hand was immersed in a 9 L bucket of cool water (20˚C) to the level of the ulnar styloid process. Water temperature was checked every 5 minutes, ice water added if it had risen by more than 0.2˚C until temperature was restored to 20˚C, and after mixing, equal volumes of water were removed to maintain the water depth to the level of the ulnar styloid process.

#### 5.2.3.3 Energy expenditure

Indirect calorimetry was performed during baseline and single hand immersion in cool water. Continuous recordings of oxygen consumption and carbon dioxide production were made using a mask collection method (Oro-nasal reusable face mask, V7450

series, Hans Rudolph Inc., Shawnee, USA) with the Europa gas exchange monitor (GEM; Europa Scientific Ltd., Crewe, UK). Resting energy expenditure (REE) was recorded for 30 minutes before, and during, the 30 minutes hand cooling period. Average values for REE during baseline and the 30 minute hand cooling period were calculated from the last 15 minutes of each period.

#### 5.2.3.4 Infrared thermography

Supraclavicular skin temperature was measured using infrared thermography (FLIR B425, thermal resolution 320 x 240 pixels; FLIR Systems, Danderyd, Sweden) as described previously (Robinson et al., 2014, Robinson et al., 2016, Law et al., 2018, Scotney et al., 2017, Symonds et al., 2012a) and used as an indicator of BAT activity. In brief, the camera was positioned so that the lens was perpendicular to the larynx and the field of view included, as a minimum, the full width of the shoulders laterally, the manubriosternal joint inferiorly and angle of the mandible superiorly. The distance from the camera required to achieve this was measured and entered alongside ambient and reflective temperatures into the thermal camera during setup as per the manufacturer's instructions. Images were taken at 1 minute intervals during baseline and cooling. During thermographic image analysis, a region of interest (ROI) was defined as that bounded by the left sternocleidomastoid muscle, clavicle and lateral contour of the neck using ThermaCAM Researcher Pro 2.10 (FLIR systems AB, Taby, Sweden) as described previously (Robinson et al., 2014, Law et al., 2018). ROIs were exported into Excel (Microsoft, Redmond, WA, USA) and a custom written script in R (A Language and Environment for Statistical Computing, version 3.4.3 (R Core Team)) was used to calculate the 87.5th percentile temperature value ($T_{SCR}$).

#### 5.2.3.5 Mean skin temperature

Mean skin temperature ($T_{MSK}$) was evaluated using measurements of skin temperature obtained from wireless data loggers (iButton, model no. DS1219H-F50, resolution 0.125˚C; Maxim, Sunnyvale, CA, USA) placed at seven body sites (i.e. forehead, trunk, arm, hand, lower leg, thigh and foot) and calculated using the Hardy DuBois formula (Hardy et al., 1938). Measurements were taken at 1 minute intervals throughout, in parallel to the acquisition of thermograms as described above.

#### 5.2.3.6 Statistical analysis

All analyses were performed using GraphPad Prism for Windows Version 7 (GraphPad Software, La Jolla California USA). Data are reported as means ± SEM unless otherwise stated. All data were normally distributed as indicated by the Kolmogorov-Smirnov normality test. Comparison between baseline and 30 minute energy expenditure and skin temperature of the thigh was made using a two-tailed paired t-test.

A two-way repeated measures ANOVA was used to determine whether any interaction was present between cold stimulation and ambient room temperature. Where ANOVA analysis revealed a significant F-ratio for the interaction, a post-hoc paired two-tailed t-test was employed to define the simple effect of cold stimulation at each ambient room temperature. A P value $< 0.05$ was considered to be statistically significant; where comparisons were made at both 18˚C and 23˚C, this threshold was adjusted (using a simple Bonferroni correction) to $< 0.025$.

### 5.2.4 Results

$T_{SCR}$ increased following single hand immersion in cool water (20˚C) at an ambient room temperature of 23˚C (Figure 5.2).

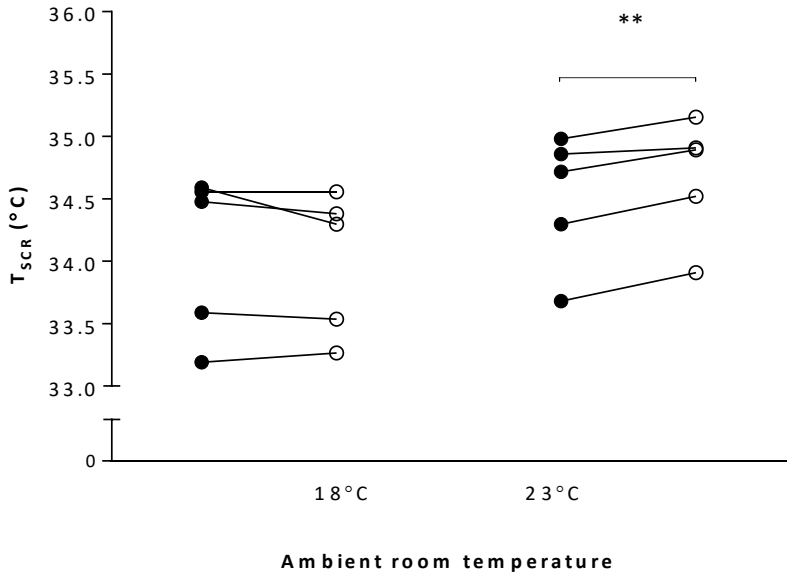



**Figure 5.2 Effect of single hand immersion in cool water on supraclavicular temperature at 18˚C and 23˚C ambient room temperature**. A significant interaction was observed between ambient temperature and thermogenic response to hand cooling (F (1, 4) = 12.22, P = 0.025), ** P < 0.01 following 30 minutes of hand cooling (open circle) compared with baseline (closed circle); n = 5. $T_{SCR}$ – supraclavicular skin temperature.

This was accompanied by a small, statistically significant increase in REE from baseline (baseline EE: 4.76 ± 0.30 kJ/min, ΔREE: 0.22 ± 0.02 kJ/min, P = 0.0008) (Figure 5.3).

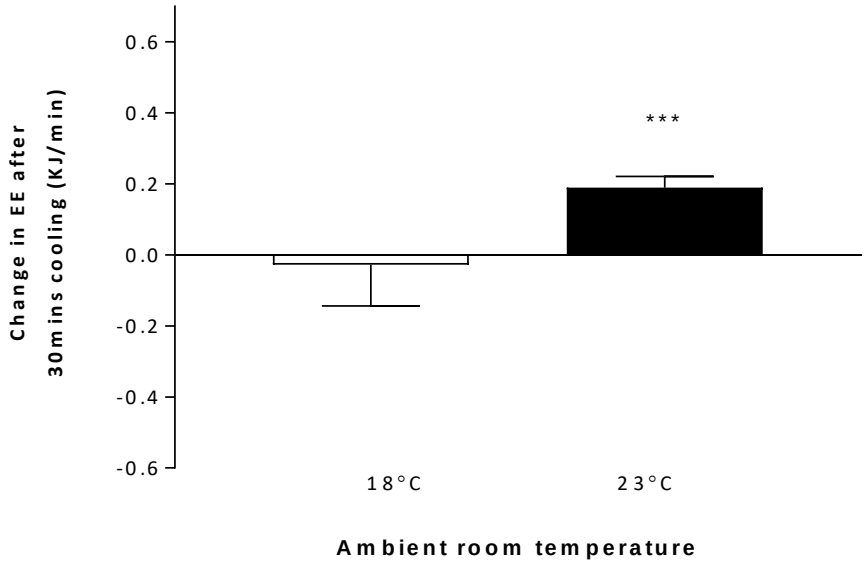



**Figure 5.3 Change in resting energy expenditure after 30 minutes hand cooling at 18˚C and 23˚C**. *** P < 0.001 when compared to baseline, n = 5. EE – energy expenditure.

Neither change was observed in the same group of participants examined at a room temperature of 18˚C. In contrast, skin temperature measurements taken over a central location not overlying BAT (i.e. thigh) remained static at 23˚C (Figure 5.4), suggesting that this rise in temperature was localised to BAT, rather than secondary to a wider systemic thermogenic response.

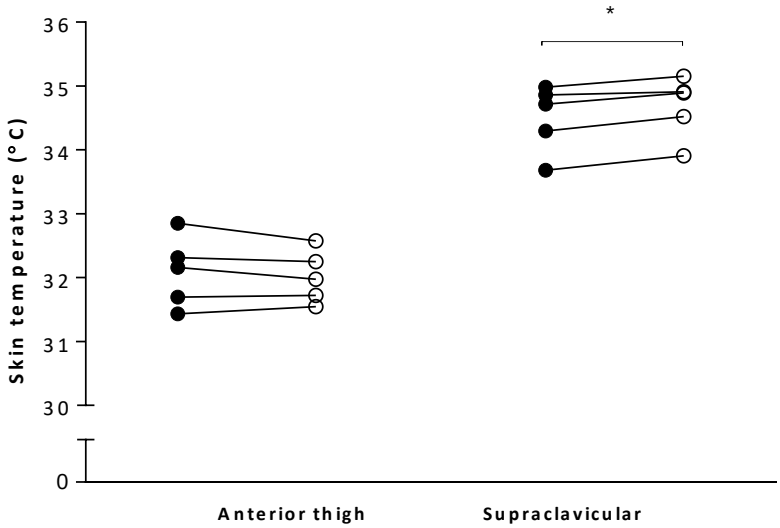



**Figure 5.4 Skin temperature of the anterior thigh and supraclavicular region prior to and following 30 minutes hand cooling (20˚C) at an ambient room temperature of 23˚C.** ** P < 0.01 when compared to baseline, n = 5. Closed circles = baseline, open circles = 30 minutes cooling.

Consistent with the well-described insulative response to acute cold exposure (Castellani and Young, 2016), $T_{MSK}$ fell from baseline throughout the duration of cooling. The degree and pattern of this fall was remarkably similar at both ambient room temperatures (Figure 5.5), suggesting that at both 18˚C and 23˚C hand immersion in cool water acts as an effective cold stimulus of similar magnitude. Skin temperature was, as expected lower at all sites when measured at 18˚C. Moreover, the skin temperature of the non-immersed hand was well above ambient temperature during baseline at 18˚C (mean: 28.01˚C, [95% CI 23.33 to 32.70˚C]) and dropped significantly (−0.61˚C, [95% CI −0.93 to −0.29˚C]) following immersion of the left hand in water at 20˚C. This is consistent with the recognised vasoconstrictor response of the contralateral hand to indirect cooling (Marshall et al., 1990), further supporting the efficacy of the cold stimulus at a cooler room temperature. However, the extent

to which vasoconstriction within the hand and fingers at 18˚C prior to immersion in water may have attenuated subsequent heat extraction during immersion is not certain.

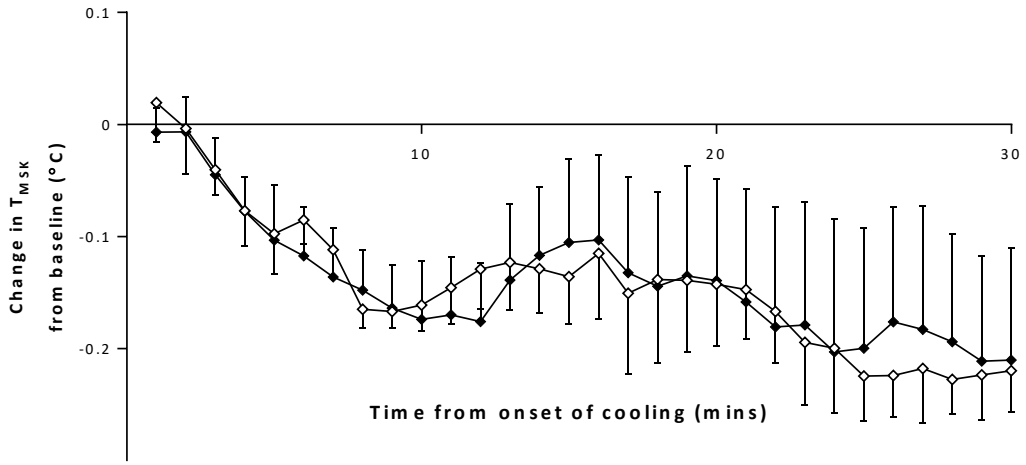



**Figure 5.5 Time course of changes in mean skin temperature after 30 minutes hand cooling at an ambient room temperature of 18˚C and 23˚C.** Closed squares (+SEM) = ambient temperature 23˚C, and open squares (−SEM) = ambient temperature 18˚C, n = 5. $T_{MSK}$ – mean skin temperature.

### 5.2.5 Discussion

The supraclavicular BAT response to acute localised cold exposure under varying ambient conditions has not been reported before. However, the outcomes of a recent study in a similar study cohort of non-obese males at 22 – 23˚C support our findings (Acosta et al., 2018). In that study, acute mild cold exposure prior to the onset of significant involuntary superficial muscle activity (i.e. shivering) resulted in a similar increase in energy expenditure and a similar pattern of reduction in mean skin temperature. However, supraclavicular temperature (measured using a single iButton placed within the "supraclavicular zone" rather than with thermography) was unchanged throughout (Acosta et al., 2018). Gashi et al. also reported an isolated

increase in $T_{SCR}$ during cooling in contrast to a fall in skin temperature at seven other sites, in addition they identified a significant positive linear relationship between $\Delta T_{SCR}$ and cold-induced thermogenesis (Gashi et al., 2019).

Ambient temperature is a determinant of FDG-detected BAT prevalence (Zukotynski et al., 2009, Skillen et al., 2012), and acute cold exposure has been shown to increase BAT activity on PET-CT (Saito et al., 2009). Our findings are in line with this but are the first to show a differential effect of ambient temperature on supraclavicular heat production using thermography in response to cold stimulation, which suggests that supraclavicular BAT can be activated with minimal cold exposure. The REE and $T_{SCR}$ response observed at 23˚C may have been even greater had we also examined our subjects under confirmed thermoneutral conditions. One explanation for our findings is that BAT at a room temperature of 18˚C is already close to its maximal activity. However, REE at baseline was similar at 18˚C and 23˚C (4.76 ± 0.30 kJ/min and 4.88 ± 0.35 kJ/min respectively), indicating that the overall increase in REE in response to acute cold exposure may not be maintained long term. This may reflect a compensatory reduction in energy expenditure from another component of REE or may indicate that cold-induced BAT activation is transient.

Maximising BAT activity by increasing time spent outside of thermoneutrality presents an attractive mechanism for enhancing lipid/glucose metabolism, particularly in the context of diabetes, obesity and their metabolic sequelae. Although the changes in energy expenditure seen following cold stimulation in our study group were small (c. 3 – 5.5% of baseline REE), if these were sustained over a long period they could contribute significantly to energy balance. For example, assuming that 1 kg of body fat

contains 37,000 kJ and a prior neutral energy balance, an increase in EE of 0.22 kJ/min for just 50% of each day would increase daily energy expenditure by 160 kJ, which, if accumulated as WAT over a single year, would equate to around 1.5 kg. However, the bio-energetic significance of BAT remains controversial, and recent studies claim that the contribution of BAT to whole-body energy expenditure is negligible (UDin et al., 2016, Carpentier et al., 2018, Muzik et al., 2013)

As a pilot study, the main limitation of this study was small sample size. Nonetheless, the magnitude of the response to the mild cool stimulus at 23˚C was sufficient to reach statistical significance. How these findings may relate to a larger, more diverse population is unclear and will only be identified by further, more comprehensive studies. Although we did not observe shivering, nor did our subjects report it, EMG measurements would have enabled us to rule out subclinical muscular contraction as the cause for the increase in energy expenditure observed in our subjects. Evidence is also emerging from rodent studies for non-UCP1 dependent mechanisms of non—shivering thermogenesis originating from muscle, whereby mitochondrial proton leak may be generated through UCP3 (Lin et al., 1998) (although the role for UCP3 in humans is considered controversial), increased consumption of ATP via creatine cycling, or thermogenesis achieved via sarcolipin-mediated calcium cycling (Bal et al., 2018).

Supraclavicular thermography measures infrared radiation from the skin surface, this is determined not only by the heat produced from the deeper structures such as BAT but also by an overlying “insulative layer” consisting of the skin, subcutaneous adipose tissue and also a dynamic cutaneous vascular network. At present there are no

methods to control for this. However, given that cold-induced changes in supraclavicular temperature closely approximate to FDG uptake on PET-CT (Law et al., 2018, Lee et al., 2016, Jang et al., 2014), and also to changes in energy expenditure (Gashi et al., 2019) we speculate that these effects are minimal. As chemical-shift water-fat MRI becomes more available for the assessment of BAT, large scale studies in conjunction with perfusion assessment may enable the thermographic evaluation of BAT to be refined.

Our initial findings show that supraclavicular BAT can be activated under warm conditions by a very mild cold stimulus, generating heat in association with an increase in energy expenditure, and that supraclavicular BAT may be maximally stimulated at an ambiet room temperature of c.18˚C. Whether sustained activation of BAT occurs at lower ambient temperatures under free-living conditions, and whether this can directly impact on overall energy balance, is unknown but presents an exciting avenue for further study.

## 5.3 Study V

**Effects of unilateral forearm cooling on supraclavicular skin temperature, and the relationship to body composition in young adults (pending submission)**

### 5.3.1 Abstract

The cold-induced thermogenic properties of supraclavicular brown adipose tissue (BAT) measured by infrared thermography (IRT) correlate with radiolabelled glucose uptake on positron-emission computed-tomography (PET-CT). Data on the real-time kinetics of BAT activation are lacking, and changes in supraclavicular temperature ($T_{SCR}$) may be obscured by vasoconstriction of the cutaneous vasculature during whole-body cooling, or the regional cardiovascular changes of the cold-pressor reflex associated with severe cold stress. Therefore, to circumvent these effects, using a mild cold localised stimulus we assessed the time course and magnitude of changes in IRT derived $T_{SCR}$. Secondary analyses explored the relationship between $T_{SCR}$ and adiposity. Seven healthy subjects (age 30.3 ± 5.1 years, 22.6 ± 3.2 kg/m$^2$, 4 male) were assessed using IRT prior to, and during, 45 minutes of forearm cooling. During cooling $T_{SCR}$ increased by a maximum of 0.42 ± 0.07°C, at c. 31 min. A negative correlation was observed between $T_{SCR}$ and BMI under basal (r = −0.87 [95% CI −0.98 to −0.33], P = 0.01) and stimulated conditions (r = −0.85 [95% CI −0.98 to −0.27], P = 0.02), but no relationships with $\Delta T_{SCR}$ were observed. Moreover, the correlation between $T_{SCR}$ and BMI persisted after adjustment for SCAT (partial correlation coefficient basal $T_{SCR}$: r = −0.80; P = 0.03 stimulated $T_{SCRmax}$: r = −0.83, P = 0.02). Our findings identify that a thermogenic BAT response can be detected with IRT, maximal by 30 minutes of mild

localised forearm cooling. Providing an alternative to the whole-body severe cooling protocols commonly used for BAT activation.

### 5.3.2 Introduction

Brown adipose tissue rapidly produces heat in response to cold through activation of mitochondrial uncoupling protein 1 (UCP1). Activated UCP1 facilitates a proton leak across the inner mitochondrial membrane, uncoupling oxidative phosphorylation from the production of ATP, and in turn, allowing dissipation of the electrochemical gradient as heat (Cannon and Nedergaard, 2004). BAT is, therefore, a highly thermogenic tissue and, with the capacity to metabolise both lipid and glucose, may present a therapeutic target for the prevention and treatment of obesity and its related disorders (Nedergaard and Cannon, 2010).

It is now well established that metabolically active BAT is present in adult humans (Cypess et al., 2009, Virtanen et al., 2009, Zingaretti et al., 2009), though its bio-energetic significance remains uncertain and continues to be debated (Carpentier et al., 2018, UDin et al., 2016, Matsushita et al., 2014, Sanchez-Delgado et al., 2018). The temperature of the skin overlying BAT within the supraclavicular region is increasingly being used as a surrogate measure of BAT activity (Malpique et al., 2018, Scotney et al., 2017, Shorakae et al., 2019), and a number of studies have reported that $T_{SCR}$ correlates well with measures of BAT glucose uptake on both static (Jang et al., 2014, Boon et al., 2014, van der Lans et al., 2016, Chondronikola et al., 2016, Lee et al., 2016) and dynamic PET-CT (Law et al., 2018).

BAT is commonly examined under cold stimulated conditions, and cooling protocols vary by research group. Brown adipose tissue stimulation is most frequently achieved using whole-body cooling (Lee et al., 2011, Jang et al., 2014, van der Lans et al., 2016) where participants are housed within a temperature-controlled laboratory or wear liquid perfused cooling garments. Methods include both fixed temperature cooling protocols, subjecting individuals to room temperatures of 16 – 19˚C for 2 – 3 hours (Yoneshiro et al., 2016) and personalised protocols whereby participants are cooled to just above their individual shivering threshold, with the aim of inducing maximal non-shivering thermogenesis (Martinez-Tellez et al., 2018, van der Lans et al., 2016, Boon et al., 2014, Acosta et al., 2018).

Whole-body cooling has a direct impact upon supraclavicular skin temperature as a result of vasoconstriction of the overlying cutaneous blood vessels. This may subsequently affect the heat flow from underlying BAT to the skin and may explain why some studies using this methodology fail to detect a significant rise in supraclavicular skin temperature with stimuli known to elicit detectable BAT activation on PET-CT (Chondronikola et al., 2016, Jang et al., 2014).

Some cooling protocols also utilise placement of hands and feet onto ice blocks, or into iced-water (Yoneshiro et al., 2011, Yoneshiro et al., 2016). Given the proximity of supraclavicular BAT to the large blood vessels within the neck and upper thorax (Bonnot, 1908, Lee et al., 2018) (e.g. carotid, internal and external jugular vein), the BAT thermogenic response visualised at the skin surface by IRT may be obscured by

large changes in regional blood flow, unrelated to cold-induced BAT thermogenesis (e.g. secondary to the cold-pressor reflex).

Localised cooling using a relatively mild, localised stimulus may circumvent these confounding factors and improve the sensitivity and specificity of $T_{SCR}$ as a measure of BAT activation. Cold thermoreceptors are found in high density in the dermis (Zotterman, 1959) in the hand and forearm (Stevens and Choo, 1998), and are most responsive between 25˚C and 30˚C (Dodt and Zotterman, 1952) and, although we have previously demonstrated a small rise in $T_{SCR}$ following 5 minutes of isolated hand cooling in children, this response was less significant in adults (Symonds et al., 2012a, Muros-Molina et al., 2019).

In this pilot study, we evaluate the feasibility of mild cooling of the whole forearm to elicit BAT thermogenesis via a detectable rise in $T_{SCR}$ using IRT and sought to characterise the time course and magnitude of this rise. Having previously detected a small cold-induced increase in $T_{SCR}$ in children which was inversely related to BMI percentile (Robinson et al., 2014), secondary analyses also aimed to determine whether any thermogenic response observed in adults in this study was similarly related to body composition.

### 5.3.3 Methods

The study was undertaken following University of Nottingham School of Medicine Ethics Committee approval (No. H19042012). All participants gave written informed consent to take part. The study conformed to the standards set by the Declaration of Helsinki 2013, except for study registration in a public database.

#### 5.3.3.1 Study protocol and participants

Following receipt of written informed consent, a targeted medical history was obtained from each participant to ensure they were free of metabolic or endocrine disease and were not taking any medications (other than those required for contraception) or recreational drugs. Given the localised nature of active cooling in this study, participants reporting a diagnosis, or symptoms indicative, of Raynaud's syndrome were excluded from this study. All participants were asked to refrain from alcohol, caffeine and vigorous exercise in the preceding 24 hours and fasted from midnight on the morning of the study. Study sessions were conducted between October 2015 and January 2016.

The experimental protocol commenced after a minimum period of 30 minutes acclimatisation within the laboratory environment to allow the stabilisation of skin temperatures. Participants were seated on a medical examination couch in a semi-reclined (120 degrees) supine position with their head fully supported posteriorly, the right arm resting on their lap, left arm by their side and legs outstretched and uncrossed. Standardised clothing, consisting of cotton trousers and vest (0.31 Clo), allowed adequate exposure of the neck and upper thorax for IRT. Vest straps were taped into position at the acromioclavicular joint to serve as anatomical markers for later thermographic analysis. The camera was positioned such that the lens was perpendicular to the larynx and field of view included, as a minimum, the full width of the shoulders laterally, manubriosternal joint inferiorly and angle of the mandible superiorly. The distance from the camera required to achieve this was measured and entered alongside ambient temperature and reflective temperature into the thermal

camera (FLIR E60) during set-up as per manufacturer's instructions (FLIR Systems, Danderyd, Sweden).

The temperature of the skin overlying supraclavicular BAT was measured using IRT (FLIR E60 2.3 Megapixel Infrared Camera, thermal resolution 320 x 240 pixels, thermal sensitivity < 0.05°C; FLIR Systems, Danderyd, Sweden) and was used as an indicator of BAT activity, as described previously (Law et al., 2018, Robinson et al., 2014, Robinson et al., 2016). The supraclavicular region of interest (ROI) was defined as that bounded by the left sternocleidomastoid muscle, clavicle and lateral contour of the neck using ResearchIR Max 4.4 (FLIR systems AB, Taby, Sweden). These ROIs were exported in CSV format and the 95$^{th}$ percentile temperature value of this region of interest was calculated ($T_{SCR}$) using a custom R script. A single thermal image was taken manually every 30 seconds throughout baseline and active cooling. Baseline $T_{SCR}$ was defined as the average of 15 minutes preceding the onset of active cooling from T: −18 min to T: −3 min, where T: 0 min defined the onset of cooling, and $T_{SCR}$ during cooling was calculated at T: 10, 20, 30, 40 and 45 min, values were calculated as the mean of all images taken in the minute prior to and after the designated time point (e.g. T: 10 = average $T_{SCR}$ of all images taken 9, 10 and 11 minutes after the onset of cooling). The maximal $_{TSCR}$ was defined as the maximum $T_{SCR}$ identified from all thermal images acquired during cooling.

Forearm cooling was achieved using the Blanketrol II circulating water system (Cincinnati Sub-zero product, Cincinnati, USA) set to deliver a continuous cold stimulus of 14°C. The cooling blanket was applied circumferentially around the forearm and

secured using a crepe bandage. The fingers and thumb were left exposed to allow inspection of skin integrity and digital circulation throughout. Participants were asked to report any discomfort and were aware that the study would be terminated in this case. Cooling was commenced after the acquisition of a 30 minute baseline period and was continued for 45 minutes. To confirm cooling was adequate, the skin temperature of the cooled limb was assessed using thermography of the dorsal arm surface. The mean temperature values of circular ROIs placed mid forearm and dorsum of the hand (the size of each ROI was determined by the maximal width of the mid forearm and hand), were obtained from a thermogram taken immediately after cooling had been discontinued and the blanket had been removed. All participants completed the full study session, and none declared any discomfort with cooling or requested early discontinuation.

Mean skin temperature ($T_{MSK}$) was evaluated using measurements of skin temperature obtained from wireless data loggers (iButton sensor DS1219H-F50; Maxim Integrated, Winnersh, UK) which sampled every minute. These were placed on the right side of the body at seven sites as described previously (Robinson et al., 2016, Mitchell and Wyndham, 1969) and $T_{MSK}$ was calculated using the Hardy DuBois formula (Mitchell and Wyndham, 1969).

#### 5.3.3.2 Anthropometric Measurements

Height and weight were measured to the nearest 0.1 cm and 0.1 kg respectively using standard methodology and used to calculate body mass index (BMI: weight/height$^2$).

Blood pressure and heart rate were measured using an automated blood pressure monitor (Omron M2, Omron Healthcare, Kyoto, Japan), and mean arterial blood pressure (MABP) calculated as ((2 × diastolic blood pressure) + systolic blood pressure))/3. To avoid excess movement during thermal imaging, the cuff was placed on the right arm during the acclimatisation period and remained in situ throughout. Core temperature was measured with a tympanic thermometer from the right tympanic membrane (triplicate measurements being taken to permit calculation of a mean average). These measurements were recorded during baseline and at the end of active cooling.

MRI of the neck and upper thorax was performed using a 3T scanner (GE Discovery MR750 3.0T, GE medical Systems) with a T1-weighted axial plane with the following variables (TR 500, TE 13.6, matrix 256 x 256, slice thickness 5mm and interslice thickness 3mm). Subcutaneous adipose tissue thickness (SCAT) was defined as the distance between the anterior edge of the subcutaneous fat and the subcutaneous fascia at the level of the first thoracic vertebrae (T1) and measurements were made in triplicate using OsiriX version 5.6. (Figure 5.6).

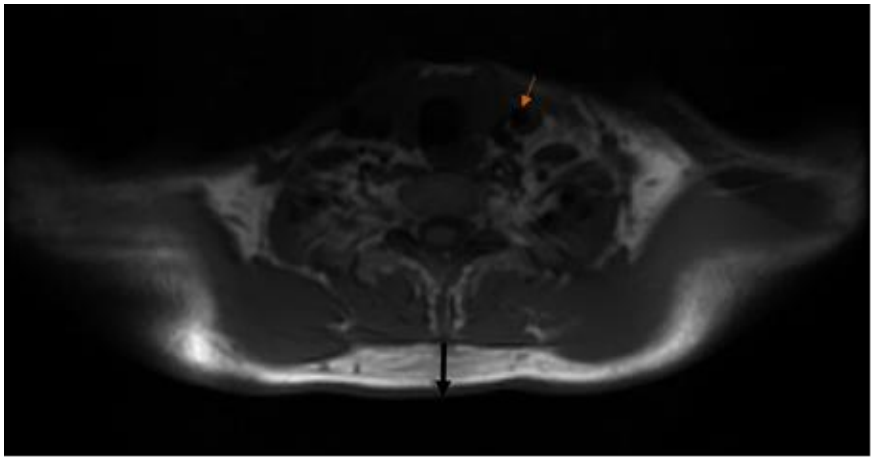


**Figure 5.6 MRI of the upper thorax demonstrating measurements subcutaneous adipose tissue (SCAT).** A representative T1 weighted MRI of the upper thorax, dorsal SCAT measurements taken as indicated by the black arrow. Orange arrow indicates the approximate anatomical boundaries for the measurements of anterior SCAT undertaken by Gatidis and co-workers (2016).

#### 5.3.3.3 Statistical Analysis

Data were analysed using GraphPad Prism version 7.04 for Windows (GraphPad Software, Inc., La Jolla California USA) and SPSS statistical package version 24 (SPSS Inc, Chicago, IL). All data were normally distributed as indicated by the Kolmogorov-Smirnov normality test and are presented as means ± standard error of the mean (SEM) unless otherwise stated.

Comparisons between two groups (e.g. baseline and active cooling) were made using Student's paired t test (two-tailed). One-way repeated measures ANOVA with Dunnett's post hoc multiple comparisons test was used to evaluate the effect of duration of cooling on supraclavicular temperature.

Pearson product-moment correlation coefficients (r) and their 95% confidence intervals (CI) (two-tailed) were calculated to determine the relationship between

continuous variables, and partial correlation coefficients were calculated to determine the relationship between $T_{SCR}$ and BMI while controlling for SCAT.

Intraclass Correlation Coefficient (ICC) estimates for the MRI measurements of SCAT thickness, and their 95% CIs, were calculated based on a mean-rating (*k* = 3), absolute-agreement, 2-way mixed-effects model, and indicated excellent reliability (ICC = 0.998, [95% CI 0.992 – 1.00], P < 0.0001). The coefficient of variation of the triplicate values was 2.1 ± 0.2%.

Using *linest* function (least squares method) in Excel, a line of best fit was fitted to the $T_{MSK}$ time series data and used to calculate an estimated rate of change during baseline and active cooling.

A significance value (P) of < 0.05 was considered to indicate statistical significance.

#### 5.3.3.4 Sample size and power

A priori calculation of sample size and post-hoc power analysis were undertaken using the Gpower computer program where $\alpha = 0.05$ and $\beta = 0.2$ (Faul et al., 2007). A minimum of four participants were required to detect an increase in $T_{SCR}$ following forearm cooling in line with that detected in a previous similar study (mean (SD) increase of 0.17 (0.07) and effect size of 2.42).

For the two-tailed correlational analysis between $T_{SCR}$ and BMI, and $T_{SCR}$ and SCAT power was retrospectively calculated at 83% and 48% respectively.

### 5.3.4 Results

Study conditions, physical characteristics of the participants (n = 7) and MABP, HR and tympanic membrane temperature values at baseline and after 45 minutes of cooling are given in Table 5.1.

**Table 5.1 Participant demographics, anthropometry and room conditions.** Data shown are mean ± SEM.

| Variable | Mean (± SEM) |
|---|---|
| Room temperature (˚C) | 22.9 ± 0.8 |
| Room humidity (%) | 42.6 ± 6.5 |
| Participants (male/female) | 7 (4/3) |
| Age (decimal years) | 30.3 ± 5.1 |
| Height (m) | 1.74 ± 0.1 |
| Weight (kg) | 69.3 ± 14.5 |
| BMI ($kg/m^2$) | 22.6 ± 3.2 |
| SCAT (cm) | 1.77 ± 0.25 |
| Δ MABP (mmHg) | 4.4 ± 2.4 |
| Δ Heart rate (bpm) | 1 ± 4.9 |
| Δ Tympanic membrane temperature (˚C) | 0 ± 0.1 |

Abbreviations: BMI – body mass index; SCAT – subcutaneous adipose tissue thickness; Δ – change from baseline at 45 minutes; MABP – Mean arterial blood pressure.

### 5.3.4.1 Time course and magnitude of the $T_{SCR}$ response to forearm cooling

After 30 minutes of forearm cooling $T_{SCR}$ was significantly increased from baseline (Figure 5.7A). The maximal $T_{SCR\ increase}$ from baseline during cooling was 0.42 ± 0.07°C (Figure 5.7B) up to 34.73 ± 0.28°C, which was reached at an average of 31 min 46 sec ± 9 min 23 secs.

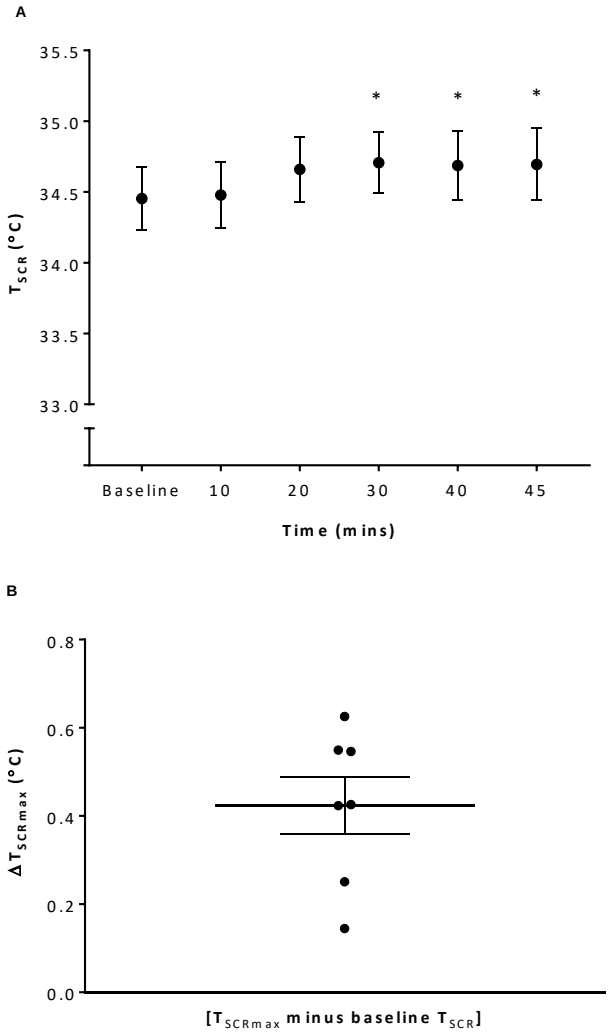



**Figure 5.7 A – B Supraclavicular BAT response to forearm cooling in adults**
A) Supraclavicular skin temperature ($T_{SCR}$) prior to, and during, forearm cooling in adults. Data points are mean ± SEM, n = 7; * P < 0.05 indicates time point comparison to baseline $T_{SCR.}$ B) Maximal change in supraclavicular skin temperature ($\Delta T_{SCRmax}$) during 45 minutes of localised forearm cooling. Individual data points shown (n = 7) with mean ± SEM.

After 10 minutes of forearm cooling mean skin temperature dropped significantly below baseline (Figure 5.8). Stability in $T_{MSK}$ during baseline was not achieved in all participants, leading to a mean decline in $T_{MSK}$ of c. 0.2°C over the last 15 minutes of the baseline period (Figure 5.8). Furthermore, the rate of decline in $T_{MSK}$ was attenuated during active cooling (Figure 5.8) and, the rate of $T_{MSK}$ change during the active cooling period was positively correlated with the maximal $T_{SCR}$ reached during cooling (r = 0.83 [95% CI 0.22 to 0.98], P = 0.02).

Application of the cooling blanket set to 14°C for 45 minutes provided consistent cooling of the hand and forearm to 18.11 ± 0.51°C, and 19.08 ± 0.43°C respectively. Following completion of the active cooling period the left arm was on average c.10 degrees colder than the right. There was no statistically significant change from baseline in MABP, heart rate or tympanic membrane temperature (Table 5.1 and Figure A5.2 in the Appendix to Study V).

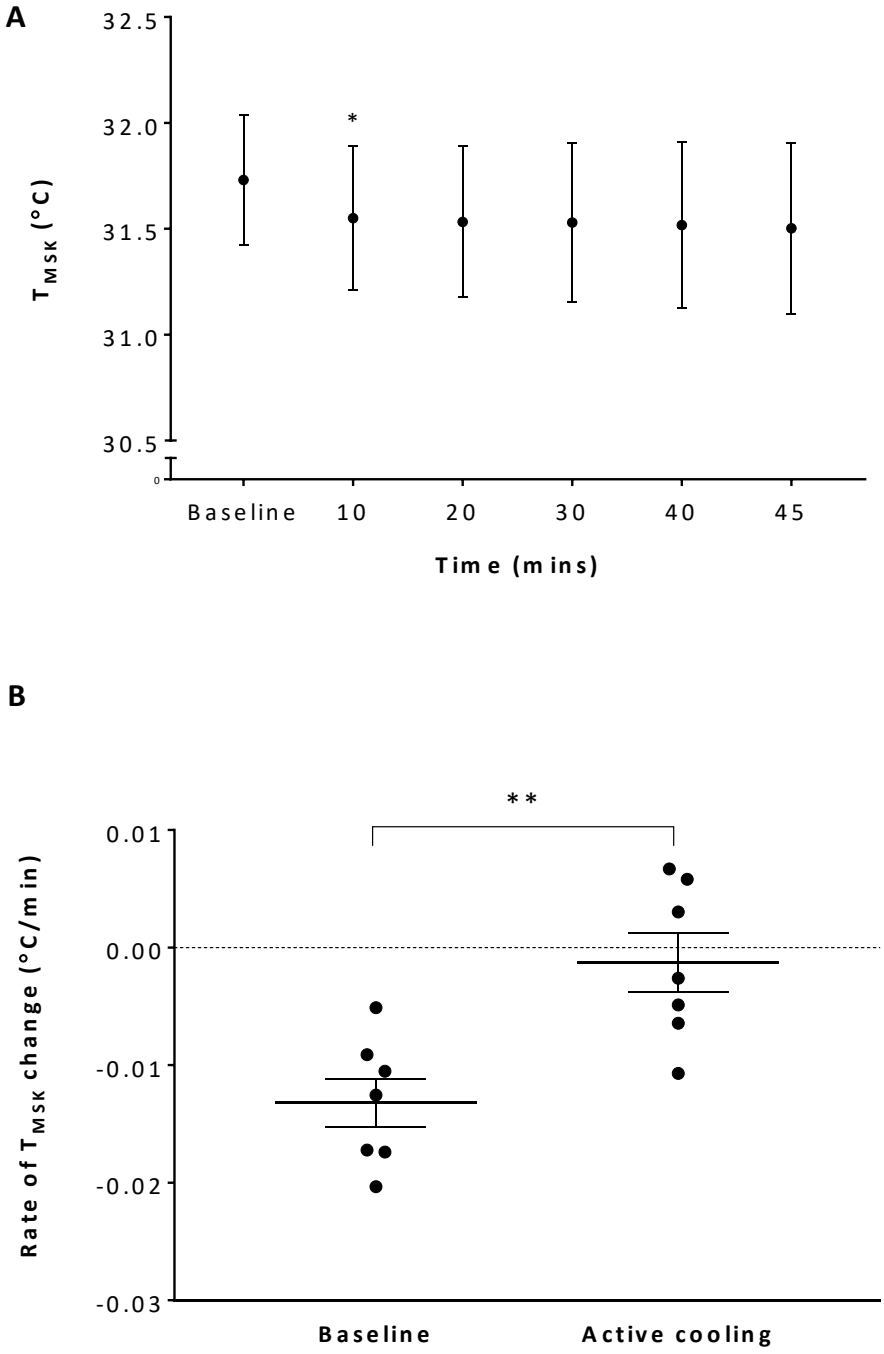



**Figure 5.8 A – B Mean overall skin temperature response to forearm cooling in adults** B) Mean (SEM) changes in $T_{MSK}$ (n = 7). C) Rate of change in $T_{MSK}$ during baseline and active cooling. * $P < 0.05$ indicates time point comparison to baseline $T_{MSK}$ and ** $P < 0.01$ comparison between $T_{MSK}$ rate of change during baseline and active cooling.

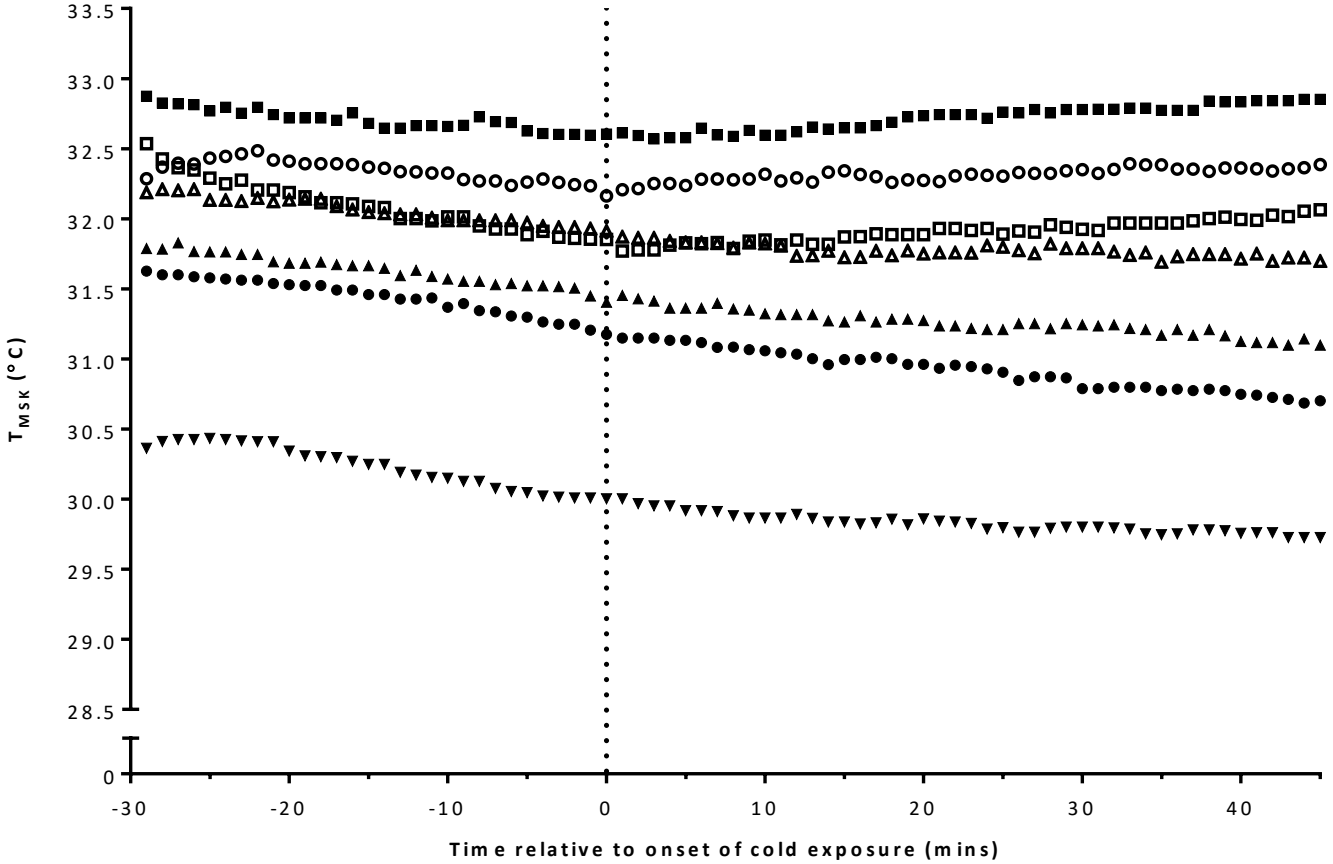



**Figure 5.9 Time course of changes in mean skin temperature ($T_{MSK}$) for each individual participant relative to onset of active forearm cooling using the Blanketrol II set to deliver circulating water at 14˚C.** Each symbol indicates one participant. (n = 7)

#### 5.3.4.2 Relationship between $T_{SCR}$ and body composition

There was a strong negative correlation between BMI and both baseline and stimulated maximal $T_{SCR}$ (Figure 5.10). Pearson's correlation coefficients were −0.87 and −0.85 respectively, $P < 0.05$). There was a trend towards a significant correlation between $T_{SCR}$ and SCAT, although the associated 95% confidence intervals were wide (Figure 5.10).

The negative relationships between BMI and baseline $T_{SCR}$ and $T_{SCRmax}$ were preserved after controlling for SCAT (baseline $T_{SCR}$: partial correlation coefficient: −0.80; $P = 0.03$; $T_{SCRmax}$: partial correlation coefficient: −0.83; $P = 0.02$). However, no significant relationships were observed between $\Delta T_{SCR}$ (defined as maximal $T_{SCR}$ during cooling minus baseline $T_{SCR}$) and BMI ($r = -0.31$ [95% CI −0.86 to 0.58], $P = 0.51$) or SCAT ($r = -0.14$ 95% CI −0.81 to 0.68 $P = 0.76$).

Significant correlations were also observed between baseline $T_{MSK}$ and BMI ($r = -0.87$ [95% CI −0.98 to −0.33], $P = 0.01$) and baseline $T_{MSK}$ and SCAT ($r = -0.80$ [95% −0.97 to −0.11]).

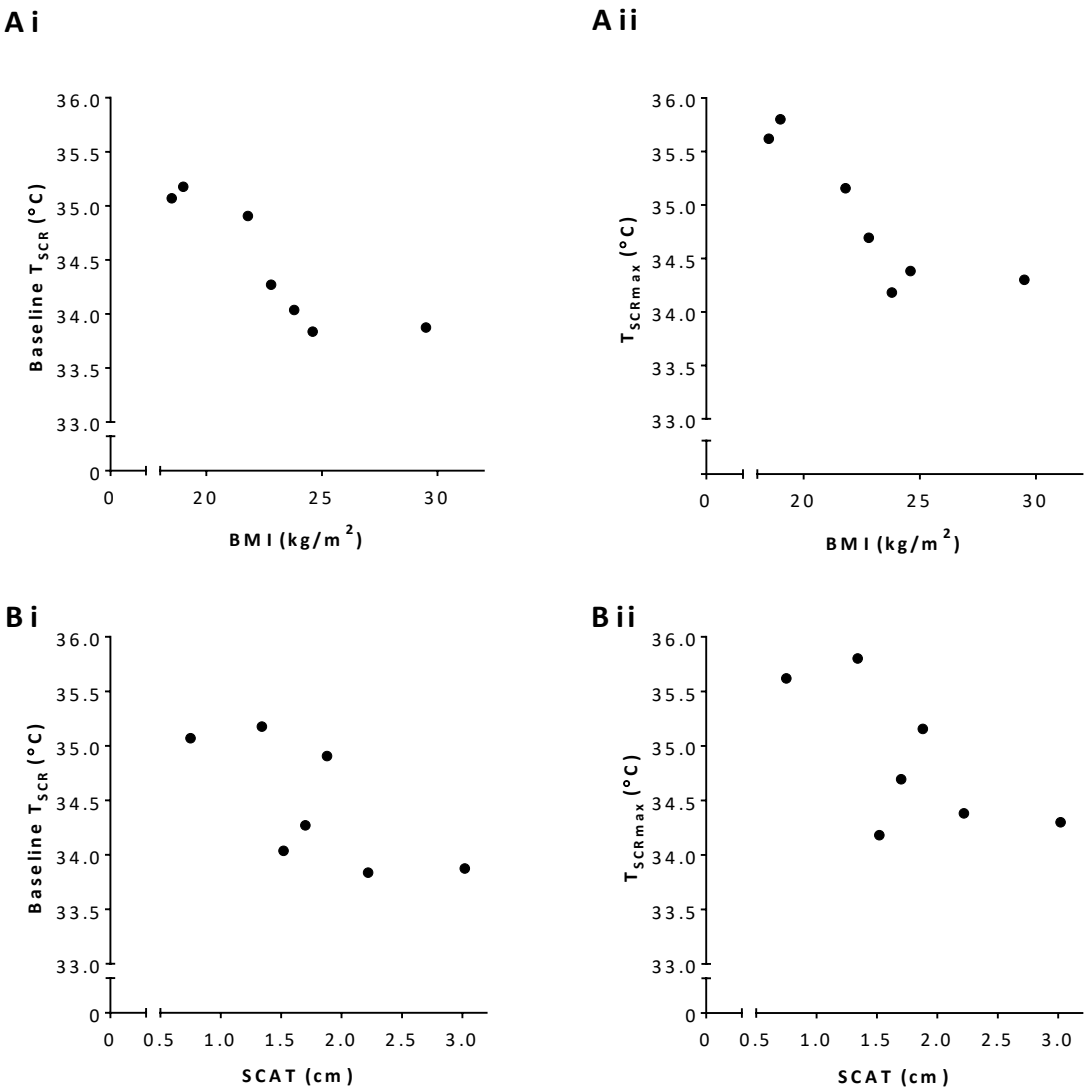



**Figure 5.10 A – C Relationship between supraclavicular skin temperature ($T_{SCR}$) and body mass index (BMI) and subcutaneous adipose tissue thickness (SCAT).** Correlation coefficients between baseline $T_{SCR}$ and Ai) BMI: r = −0.87 (95% CI −0.98 to −0.33), P = 0.01; Bi) SCAT: r = −0.71 (95% CI −0.95 to 0.09), P = 0.07.
Correlation between maximal $T_{SCR}$ during forearm cooling and Aii) BMI: r = −0.85 (95% CI −0.98 to −0.27), P = 0.02; Bii) SCAT: r = −0.67 (95% CI −0.95 to 0.17, P = 0.10. Individual data points shown (n = 7).

### 5.3.5 Discussion

In this study, we show that the skin temperature overlying supraclavicular BAT increases in response to prolonged unilateral forearm cooling in contrast to the vasoconstrictor response observed elsewhere. We describe the magnitude and time course of this response to active localised forearm cooling for the first time (maximal $\Delta T_{SCR}$ of 0.4˚C after 30 minutes), a time course that closely parallels the cold-induced changes in fat-fraction recently reported on chemical-shift water-fat MRI (Oreskovich et al., 2019).

The most frequently used methods of BAT assessment, static FDG PET-CT and water-fat MRI, to date have otherwise yielded little regarding the real-time kinetics of BAT activity in response to stimulation. Due to the combined restrictions imparted by the essential FDG dosing-to-scan interval, and radiotracer half-life, measures from PET are static and considered semi-quantitative at best (Ong et al., 2018). As a result, few imaging studies have explored how human BAT responds to cold stimulation in real-time. However, our findings are also in line with the rapid rise in BAT activity on FDG-PET-CT observed following just 20 minutes of torso cooling in adult humans (Leitner et al., 2018) and the magnitude of the rise in $T_{SCR}$ with cooling was also in accord with others utilising cooling of the chest/torso (Salem et al., 2016, Boon et al., 2014).

Using limb as opposed to torso, or whole-body cooling ensures that the supraclavicular region is not exposed directly to cold and, allows for additional physiological measurement (e.g. mean skin temperature) enabling the supraclavicular BAT response to be observed in the context of overall thermal balance. Using a relative, rather than absolute, value of $T_{SCR}$ may also help to tease out further the

kinetics of BAT activation by reducing between-subject variation, although the most reliable reference point for these calculations has been debated but not yet determined (Law et al., 2017).

Dynamic measures of supraclavicular temperature such as $\Delta T_{SCR}$ have been proposed to be more reflective of BAT activity than those made at a single time point (Gatidis et al., 2016) and have been shown to correlate with MRgluc in subjects with FDG-detected BAT on dynamic PET-CT (Law et al., 2018). However, the expectation that a simple linear relationship between $\Delta T_{SCR}$ and BAT activity exists in a population of adults with unknown BAT status is too simplistic. For example, a person may demonstrate a small $\Delta T_{SCR}$ in response to stimulation but using this measure alone will not distinguish between an individual with BAT dysfunction and one with active BAT in a state of near maximal activation at baseline.

Both thermography and contact thermometry for the assessment of BAT in humans have shown that the temperature of the supraclavicular region is consistently higher than elsewhere (Gashi et al., 2019), and that subjects with FDG-detected BAT have a higher $T_{SCR}$, or are more responsive to cold stimulation than those without (Salem et al., 2016, Chondronikola et al., 2016). Supraclavicular temperature is correlated with quantitative measures of glucose uptake (e.g., SUVmax, MRgluc) and BAT volume derived from PET-CT (Boon et al., 2014, Law et al., 2018, Lee et al., 2016).

The most frequent criticism of using $T_{SCR}$ as a marker of BAT activity is of the insulative effects of overlying SCAT (Gatidis et al., 2016, Ammer, 2017). Particularly when assessing overweight and obese individuals, as adiposity influences skin temperature,

whereby higher body fat percentages are associated with lower skin temperatures at the majority of anatomical sites (Salamunes et al., 2017). We, however, demonstrate that when controlling for SCAT, a correlation between $T_{SCR}$ and BMI remains evident and this is, therefore, supportive of the hypotheses that the relationship between $T_{SCR}$ and adiposity is also related to BAT function, and that BAT dysfunction may predispose to energy imbalance, which in turn may favour excess white adipose tissue deposition and consequent obesity.

Gatidis et al report contradictory findings and conclude that supraclavicular SCAT thickness significantly influences $T_{SCR}$ making detection of activated BAT difficult. However, their measure of SCAT was described as "the minimal distance between the vascular compartment of the neck and skin surface" (highlighted for clarity in Figure 5.6). Early anatomical studies clearly describe the location of BAT within the posterior triangle of the neck, with close approximations to the large vessels (e.g. internal jugular vein and carotid artery) extending below the clavicle into the upper thorax (Bonnot, 1908, Hatai, 1902). Furthermore more recently, UCP1 has been identified in the adipose tissue surrounding the vasculature within the cervical region (Lee et al., 2018), indicating that this region of adipose tissue included in Gatidis' definition of SCAT rather than insulative white adipose tissue may also be thermogenic adipose tissue.

Differences in true SCAT directly overlying supraclavicular BAT are dependent on an individual's body composition but, in our study, were found to be so small as to be unmeasurable in a robust and reproducible manner on our images. In order, to obtain

credible measurements of non-thermogenic subcutaneous white adipose, the dorsal aspect of the back overlying the vertebrae at the level of the first thoracic vertebrae was used instead. A simple, cost-effective and accurate method of measuring the true SCAT directly overlying the supraclavicular region, rather than the deeper adiposity as described by Gatidis et al. could be undertaken using Harpenden callipers (traditionally used to measure skinfold thickness). Such measurements, in combination with measures of BAT activity may enable quantification and comparison of the influence of this insulative layer. Ultimately, a thermal index based on $T_{SCR}$ that considers an individual's supraclavicular skinfold thickness could enable the further refinement of $T_{SCR}$, thereby allowing robust longitudinal assessment of interventions for obesity as well as comparisons between lean and obese subjects.

In accordance with our previous findings in healthy children (Robinson et al., 2016), we also demonstrate that BMI is negatively correlated with the skin temperature overlying supraclavicular BAT, both before and during active cooling. Conversely, in this study there was no relationship between BMI and the cold-induced thermogenic response. Moreover, a similar relationship with BMI was also observed with mean skin temperature suggesting that this may reflect a relationship with skin temperature rather than BAT per se.

BMI has been identified as a determinant of the frequency of FDG-detected BAT on PET-CT (Ouellet et al., 2011), and also fat fraction using water-fat MRI (Brendle et al., 2018), indicative of a relationship with glucose uptake and lipid depletion. Furthermore, a direct comparison between lean and obese individuals reveals higher

PET-detected BAT prevalence and lower supraclavicular fat fraction in lean individuals. Our findings from this study suggest a similar relationship exists between $T_{SCR}$ and BMI and has subsequently been confirmed in a larger group of individuals also studied before and after a short period of cold exposure using thermography (Muros-Molina et al., 2019).

It was notable that during our 30 minute baseline period $T_{MSK}$ fell and did not reach stability, which most likely represents the physiological response to passive cooling (Figure 5.1). The first response to cooling is often behavioural, with an increase in movement. In our study, however, subjects were asked to remain as still as possible, meaning that cutaneous vasoconstriction occurs to reduce further heat loss, resulting in a drop in skin temperature, particularly at the peripheries. Interestingly, following the onset of active cooling, this rate of decline became significantly slower (Figure 5.8C). Given the observed increase in $T_{SCR}$ over a similar time scale, the additional heat produced by BAT thermogenesis appears to maintain thermal balance and avoid the need for maximal vasoconstriction.

In this feasibility study there were no detectable large changes in heart rate or blood pressure indicative of the cold-pressor response, however this was limited by both small sample size and mixed gender, and whilst adequately powered to detect changes in $T_{SCR}$, given the high variability of heart rate and blood pressure between participants in this study robust inferences from this cardiovascular data cannot be made.

In conclusion, we demonstrate that thermogenic BAT can be activated in young adults with a prolonged localised mild cold stimulus, detected by an isolated rise in supraclavicular skin temperature. We highlight the benefits of a mild localised cooling protocol as compared to the more generalised methods currently used for BAT activation, particularly when using $T_{SCR}$ as a marker of BAT activity.

**5.4 Studies IV and V conclusions**

Both Studies IV and V identified an increase in supraclavicular skin temperature indicative of BAT activation (Figure 5.4, Figure, Figure 5.7 and 5.1A in the Appendix to Study IV). This is consistent with other recent reports of a thermogenic supraclavicular response to localised cooling (Malpique et al., 2018, Lee et al., 2016). When whole-body cooling (involving the supraclavicular region itself) has been used (e.g.: climatic chamber, full-body suit) changes in supraclavicular temperature are also indicative of thermogenesis, although an absolute rise in temperature is not always observed, supraclavicular skin temperature typically remains static or falls, but to a lesser degree than other regions (Yoneshiro et al., 2011, Jang et al., 2014, van der Lans et al., 2016). An increase in resting energy expenditure accompanied the rise in supraclavicular temperature observed in Study IV indicative of cold-induced thermogenesis.

Whether human BAT is metabolically relevant continues to be debated (Sanchez-Delgado et al., 2018, Marlatt et al., 2018). Reports between research groups are contradictory, with some proposing that human adult BAT could account for up to 20% of resting energy expenditure (Cypess et al., 2009) while others suggest that there may be no contribution at all (Sanchez-Delgado et al., 2018, Jensen, 2015). Most however, report a cold-induced increase in energy expenditure consistent with our findings

(Yoneshiro et al., 2011, Blondin et al., 2015b, Orava et al., 2011, Ouellet et al., 2012, van der Lans et al., 2013, UDin et al., 2016, Muzik et al., 2013). Though these tend to be of greater magnitude than that seen in Study IV, however, none of these other studies utilised such a mild stimulus. As observed in Study V, the greater the cold stimulation, the greater the $T_{SCR}$ response. The recent report of Blondin et al demonstrated a 1.8 fold increase in energy expenditure following 180 minutes of cold stimulation using a liquid perfused suit at 18˚C, a cooling protocol similar to those widely used for the study of adult BAT. This increase in energy expenditure occurred in association with an increase in BAT oxidative metabolism, and FDG uptake on PET-CT consistent with BAT thermogenesis. However, using EMG, it also identified significant muscular activity which was not clinically apparent to the investigator nor the participant during cooling, raising doubt that this rise in energy expenditure occurred exclusively through BAT activation (Blondin et al., 2015b). Findings also highlighted by U Din and co-workers (2016).

It may be argued that the response seen in Study IV is more representative of BAT thermogenesis than that seen in studies using similar degrees of cold stimulation as Blondin, particularly where an assumption of the absence of shivering is made using through self-reporting or visual/clinical examination. Whether the cold-induced rise in energy expenditure in Study IV was solely mediated by non-shivering thermogenesis in BAT is unclear. Even in the complete absence of shivering there is a possibility that some of this increase was mediated by alternative means, detailed discussion of these alternative mechanisms of non-shivering thermogenesis (such as sarcolipin calcium cycling, UCP3 proton leak, and creatine cycling) are beyond the scope of this thesis,

but are well summarised in the literature (Palmer and Clegg, 2017), although it must be noted that at the time of writing, the evidence for these in humans is limited.

Despite the possible confounding effect of subclinical shivering elicited by acute exposure to cold, measures of supraclavicular temperature using these types of cooling protocols have been shown to correlate with energy expenditure (Yoneshiro et al., 2011) FDG uptake on PET-CT (Lee et al., 2016, Law et al., 2018, Jang et al., 2014) and BAT volume (Jang et al., 2014), in groups of individuals previously defined as BAT positive on PET. This supports the use of supraclavicular skin temperature as a surrogate marker of BAT activity; in individuals with FDG detectable BAT at least.

Other aspects of the data obtained in both studies IV and V of individuals of unknown BAT status are also supportive of this. $T_{SCR}$ was consistently higher than any of the other body regions where the temperature was measured (Figure A5.2B in the Appendix to Study IV). This was observed in all individuals and at all time-points. Furthermore, this was the only site where skin temperature increased during cooling, at all other sites temperature fell or remained static (Figure A5.2 in the Appendix to Study IV) suggestive that this rise in temperature was confined to the SCR and not secondary to a generalised systemic thermogenesis.

Overall $T_{MSK}$ also fell in Study V during active forearm cooling in line with the peripheral vasoconstrictor response to cold (which occurs to reduce blood flow and subsequent heat loss from the core). Vasoconstriction typically occurs when skin temperature falls below 35˚C (Castellani and Young, 2016) and $T_{MSK}$ in this study was well below this in all subjects throughout. In this group of individuals, $T_{MSK}$ also fell rapidly during the

baseline period prior to active forearm cooling, indicating that these participants were not examined under thermoneutral conditions as had been intended (light clothing at a room temperature of c.22.9˚C). This may have resulted in a degree of BAT activation prior to forearm cooling and might obscure our interpretation of the time course of $T_{SCR}$ changes seen during active cooling.

Furthermore, the rate of $T_{MSK}$ decline was higher during the baseline period than during active cooling. $T_{MSK}$ was well above the threshold for maximal vasoconstriction (26 – 28˚C) (Charkoudian et al., 1999), which suggests that other heat-producing/preserving mechanisms may have been initiated. The maximal supraclavicular skin temperature increase during cooling was strongly correlated with rate of $T_{MSK}$ decline during the same period, whilst it is established that the rate of skin temperature change affects thermogenesis (Stocks et al., 2004) how this relates explicitly to BAT mediated thermogenesis has not been determined.

These findings give an insight into possible interplay between the different mechanisms that defend core temperature during exposure to mild cold, and repeating the Study V cooling protocol under confirmed thermoneutral conditions with simultaneous measurement of energy expenditure and muscle activity may help to tease out the kinetics of BAT activation and its contribution to the sequence of the thermoeffector response to mild cold exposure. Moreover, given the non-invasive methods used this could be explored in different age groups, including children.

At an ambient room temperature of 18˚C, in this small study, there was no change in $T_{SCR}$, nor did hand cooling elicit the increase in energy expenditure that was observed

at 23˚C. Many studies examine BAT under similar “cold-stimulated” conditions, but this study is one of the first to examine the capacity of BAT to respond to additional cold stimulation. Understanding the capacity for thermogenesis under normal physiological conditions is imperative to understanding how activity could be enhanced for metabolic benefit. It has been hypothesised that improving BAT function may improve both lipid clearance and glucose homeostasis (Bartelt et al., 2011, Blondin et al., 2017, Chondronikola et al., 2014), which in turn may be exploited for the treatment of insulin resistance, obesity or disorders of lipid metabolism, and importantly if targeted in early life could be utilised as a preventative measure. In the developed, western world, we are equipped to live almost entirely in thermal comfort. Certainly cold acclimation in adults can recruit FDG-detected BAT, and improve insulin sensitivity (Hanssen et al., 2016, van der Lans et al., 2013, Lee et al., 2014).

While acute cold exposure can induce thermogenesis, it can also elicit the cold pressor reflex response. If this exposure is sudden and painfully cold, a rapid, widespread discharge of the sympathetic nervous system occurs which results in stimulation of the cardiovascular system, leading to an increase in arterial pressure, heart rate and vascular resistance (Greene et al., 1965). This measurable immediate reflex response forms the basis of the ‘cold pressor test’, where typically subjects are asked to immerse their hand into ice water at 4 – 10˚C for 5 minutes, resulting in an increase in both heart rate and blood pressure.

Whilst the widespread sympathetic stimulation evoked by the cold pressor response may directly stimulate BAT thermogenesis, changes in supraclavicular skin

temperature may also be secondary to increased blood flow secondary to changes in blood pressure. An important consideration given the proximity of supraclavicular BAT to the large blood vessels within the neck and upper thorax (described in section 1.8). Therefore, Studies IV and V were designed to avoid this reflex response and aimed to determine if BAT thermogenesis could be evoked without major cardiovascular changes.

In Study IV I attempted to use the Finometer PRO® device (Finapres Medical Systems) to measure MABP from the ring finger. However, this failed to give adequate readings due to the peripheral vasoconstriction that occurred during immersion of the contralateral hand in cool water, especially at a room temperature of 18˚C. In Study V, using a standard automated blood pressure device with arm cuff, there were no significant changes in blood pressure or heart rate following active forearm cooling at 14˚C (Figure A5.1A in the Appendix to Study V). Whilst the sample size in this study was not sufficient to draw firm conclusions from this data, it is favourable that any changes in skin temperature observed within the supraclavicular region were not likely to be secondary to large systemic haemodynamic change. Furthermore, thermal nociceptors are typically activated at skin temperatures below 15˚C (although it is recognised that a small minority of people may find much milder cooling painful), and the temperature of the skin of the forearm in Study V was well above this threshold even after cooling (c. 18˚C).

Moreover, in published studies where cooling comprised intermittent immersion of feet into ice water (Virtanen et al., 2009), or placement on a block of ice (Yoneshiro et

al., 2011), the BAT response to cooling may have actually been the response to the reflex increase in sympathetic activity associated with the cold-pressor response rather than isolated BAT derived cold-induced thermogenesis.

In the early phases of Studies IV and V attempts were also made to try and measure skin perfusion within the supraclavicular region to determine the extent to which changes in skin perfusion during cooling were responsible for the observed changes of $T_{SCR}$. The laser doppler system available at the time of Study IV measured perfusion using a large adhesive probe that obscured the supraclavicular region and precluded concurrent measurement of $T_{SCR}$ and was also abandoned. Non-contact laser speckle contrast imaging systems may provide a solution to allow the simultaneous measurement of skin perfusion and temperature.

Children are often inappropriately considered “small adults” or “little people” and experience from clinical medicine tells us that this is not accurate. Children are physiologically very different in many ways, although research data on normal physiology throughout childhood is often lacking. Extrapolation of the findings from my studies of young adults to children should be undertaken with caution. Studies IV and V do however give some valuable insights into the feasibility of using mild cold stimulation to elicit a measurable increase in supraclavicular temperature in the context of the wider physiological response, simultaneously measuring both mean skin temperature and cardiovascular changes.

All experimental procedures undertaken in these studies were carefully chosen to be as non-invasive and child friendly as possible to allow for future replication of these

studies in subgroups of children. In doing so, this would enable us to determine how BAT contributes to the acute physiological response to mild cold during early life, and how this may change during development.

# CHAPTER 6

## Conclusions

### 6.1 General aims

This thesis aimed to assess the feasibility of using infrared thermography to measure supraclavicular temperature as a surrogate marker of BAT thermogenesis in children and to identify determinants of $T_{SCR}$ in early life.

This was undertaken through five studies. Two studies were undertaken in children and were designed to evaluate the supraclavicular thermogenic response to mild cold exposure and identify whether age, sex, BMI, ambient room temperature, diet and activity were determinants of $T_{SCR}$. As the response to cold exposure was much lower than expected, the remaining three studies were designed to investigate why this may have been, examining factors that may have affected the basal activity of BAT during baseline measurement; notably the impact of mild psychological stress, preceding ambient room temperature and severity and duration of cold exposure.

In all studies IRT was used to evaluate the temperature of the skin overlying supraclavicular BAT, this was utilised as a surrogate marker of BAT thermogenic output. Cooling was achieved using single hand immersion in cool (20.1˚C) tap water (Study I, II and IV) and using a water-perfused cooling servo-controlled blanket (set at 14˚C) wrapped circumferentially around the forearm (Study V). Although not intentional, cooling was also achieved passively in Study III and Study V, whilst participants sat immobile during imaging. The participants of Study III undertook a mental arithmetic test to invoke mild psychological stress, whilst the test itself did not produce a cortisol response suggestive of psychological stress, the anticipation of undertaking the test did.

### 6.2 Summary of study findings

Successful completion of the studies in this thesis has shown that IRT is both a feasible and practical method by which supraclavicular skin temperature can be measured in children and young adults. Subsequent to my studies, evidence has emerged that supports the use of $T_{SCR}$ as a surrogate marker of BAT activity in adults (Boon et al., 2014, Jang et al., 2014, Law et al., 2018, van der Lans et al., 2016, Thuzar et al., 2019). This has not yet been demonstrated in children, but given the practical, ethical and moral restrictions on the use of PET-CT imaging in healthy children, this is not unsurprising.

BMI percentile and sex were identified as determinants of $T_{SCR}$ and $\Delta T_{SCR}$ in children. While significant correlations between protein and vegetable intake and $T_{SCR}$ were identified in girls, these findings did not persist after adjustment for multiple comparisons. The studies in young adults identified anticipatory stress and ambient temperature as factors affecting $T_{SCR}$ and $\Delta T_{SCR}$. A small localised increase in $T_{SCR}$ with single hand immersion in cool water was identified in children and adults analogous to that reported by Symonds in 2012. The increase in $T_{SCR}$ in Study IV was accompanied by an increase in energy expenditure supportive of BAT activation. The magnitude of this response, was, however much smaller (c. 0.1 – 0.2˚C). Localised prolonged cooling of the whole forearm in a small group of adults yielded a larger more consistent response (c. 0.4˚C) which peaked at c. 30 minutes (beyond the period of IRT used in the children's study). This is the first report of prolonged isolated limb cooling used to activate BAT. Of note, in all studies where $T_{MSK}$ was recorded, despite undergoing an acclimatisation period of at least 30 minutes a decline in $T_{MSK}$ was observed during

baseline, suggesting that these studies were not undertaken at thermoneutrality as intended. Given that the thermoneutral zone for children is higher than adults (Kingma et al., 2012), and as the children's studies were undertaken at slightly lower ambient room temperatures, these children were also likely assessed outside of the thermoneutral zone.

The majority of BAT dedicated studies utilising cooling to elicit BAT activation have done so with intense cold exposure, often aiming to elicit maximal NST. In contrast, the studies in this thesis have demonstrated that one can also induce supraclavicular thermogenesis using relatively mild localised cold stimuli, particularly when the environmental conditions are carefully controlled. Moreover, they also identified that mild physiological stimuli can also influence $T_{SCR}$ and revealed the need to consider these when assessing BAT function with thermography carefully.

## 6.3 Limitations

### 6.3.1 Technical limitations

BMI and BMI percentile were used as indicators of body composition and adiposity. Although quick, easy and non-invasive BMI does not discriminate between excess fat, muscle or bone mass. This is particularly relevant in lean children where differences in BMI are often due to differences in fat-free mass (Freedman and Sherry, 2009). A more accurate assessment of adiposity in children and adults may have been achieved with Dual-Energy X-Ray Absorptiometry, air displacement plethysmography, skinfold thickness, isotope dilution and MRI, methods with their advantages and disadvantages (summarised by Wells and Fewtrell, 2009). BIA was used in Study IV, while useful for

population studies the accuracy of BIA is considered poor and is more suited to tracking the direction of change in body composition rather than accurate quantification (Wells and Fewtrell, 2006).

Dietary intake, activity and eating behaviour were assessed using parental reports via a validated questionnaire. Accuracy of this data is dependent on recall, may be subject to bias from socially desirable responding and provides very limited data on total energy intake. Furthermore, such questionnaires required a certain level of numeracy and literacy, which may have excluded some families from taking part in the study (e.g. non-English speaking families or low levels of literacy). More inclusive and accurate assessment may have been undertaken using 24 h recall via researcher interview, or written/audio recorded food diaries, although these methods are costly and labour intensive (Magarey et al., 2011).

Studies I and II did not make any formal assessment of pubertal status, given the proposed endocrine regulation of BAT differences in hormonal levels may have been significant. The validity of, non-pictorial self-reported assessment of pubertal status via interview (Petersen et al., 1988) and questionnaire (Carskadon and Acebo, 1993) has been demonstrated and is preferable to clinical examination or blood testing, particularly in healthy volunteer studies undertaken within the school setting.

Lastly, as previously discussed the MA test administered in Study III failed to elicit the expected stress response, and the acute response to stress could not be evaluated as planned. Further validation studies in subjects more representative of the general population should be undertaken to confirm the nature of this test, or further stress

testing should be undertaken with an established method such as the Trier Social Stress Test (Kirschbaum et al., 1993).

### 6.3.2 Limitations of study design

In addition to being a heterogeneous group of children in terms of age, sex, pubertal status and ethnicity, children were studied in a free-living environment. Ambient temperature was recorded but not controlled, there was no formal stabilisation/acclimatisation period between removal of school uniform and image acquisition in the study vest, and some children would have most certainly been in a post-prandial state when imaged after lunch or break time.

The experimental conditions of the children's studies may have been such that BAT was near maximally stimulated in a large proportion of participants even prior to hand immersion in cold water. This is highlighted in Study III where $T_{SCR}$ in adults was responsive not only to the anticipation of a mental arithmetic test, but also to the mild passive cooling associated with immobility, and in Study IV where $T_{SCR}$ only increased when participants were at an ambient room temperature of 23˚C, not 18˚C.

However, given the time course of the dynamic changes in $T_{SCR}$ observed in response to cold in young adults, it is also possible that the maximal or peak response was not captured within the 5 minute time frame of the children's studies and, that the attenuated response observed in children was due to an insufficient period of monitoring.

To adequately confirm this, further studies of children would be required, ideally conducted in a temperature-controlled laboratory, at confirmed thermoneutrality without the influence of dietary-induced thermogenesis. A shortened version of the cooling protocol developed in Study V has since been utilised in a study of children with diabetes at the University of Nottingham. Single forearm cooling for 5 minutes with a water-circulating blanket (15˚C), at an average ambient temperature of 23.3˚C resulted in an increase in $T_{SCR}$ of just c.0.1˚C (Law, Pending submission). A response which is still much less than that observed in the initial pilot study of Symonds et al in 2012. This supports the theory that in Study I and II supraclavicular BAT may have already been significantly active prior to cold exposure or that 5 minutes may not be sufficient to capture the complete supraclavicular BAT thermogenic response to cold stimulation.

Prolonging the exposure to a stimulus may be a simple means to ensure that the full response is captured. Where thermography is to be used to measure a dynamic response, the images taken at the specified time points should be comparable; ideally, there should be minimal movement between frames ensuring that the region of interest remains identical throughout. It was very clear from the initial pilot studies for Study I that very young children are not able to sit in one position for prolonged periods, and even with methods for repositioning, attaining adequate images for periods of longer than 10 minutes is technically challenging both for the research team and the child.

As technology has developed and higher specification thermal cameras have become available on the commercial market, the quality of thermograms has also improved. Figure 6.1 shows the contrast between an image obtained with the FLIR T440 and the FLIR B60 used in Symonds et al. 2012 (first camera purchased by the Department of Academic Child Health). The former producing images with anatomical detail that was not recognisable with earlier cameras. The course of superficial vessels such as the external jugular vein, or the thyroid veins are clear, and the course of deeper vascular structures are also evident.

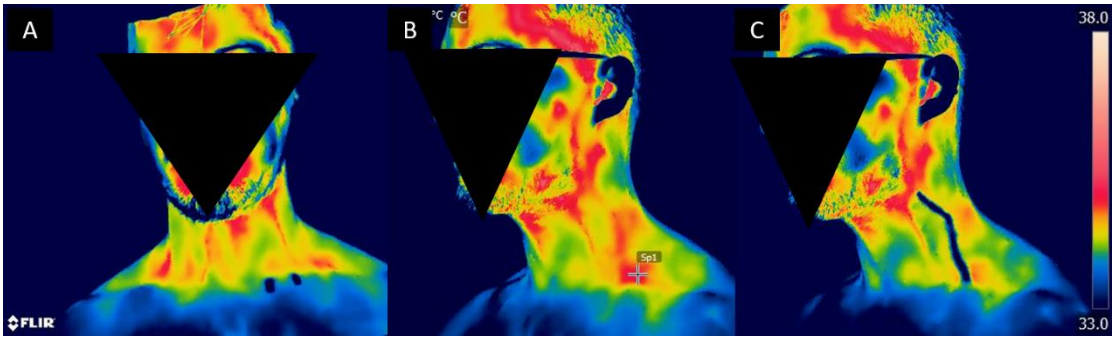



**Figure 6.1 Anterior and lateral thermograms of a male subject taken using a FLIR T540 thermal camera (resolution 464 x 348 pixels).** Details of vessels in the face and neck are apparent, image A and B were taken, then the course of a large vein was identified using ultrasound, and marked on the skin with a pen, a second thermal image taken immediately after (C), demonstrating the course of the vein in relation to the thermal patterns seen in thermogram B.

How the $T_{SCR}$ relates to these blood vessels is not clear and has not been formally explored to date. Furthermore, given Bonnot's anatomical descriptions of supraclavicular BAT in the adult and infant as surrounding the large vessels within the posterior triangle of the neck (Bonnot, 1908) this is perhaps not surprising. Study V did not find any substantial changes in blood pressure or heart rate in response to cold exposure, despite confirming a rise in supraclavicular temperature indicative of BAT

thermogenesis, although this study was small and underpowered with respect to the cardiovascular data, this suggests that changes in skin temperature were not secondary to large alterations in blood flow. Whether changes in $T_{SCR}$ represent smaller changes in blood flow or regional changes in microcirculation is unclear and warrant further investigation. Furthermore, even if these changes in temperature are as a result of changes in blood flow in superficial vessels, these themselves may be mediated by, or occur secondary to BAT thermogenesis. For example, heat is typically considered a vasodilator, during BAT thermogenesis heat transferred to the surrounding tissues may result in vasodilation of local blood vessels and increased blood flow.

Perhaps the most concerning limitation of $T_{SCR}$ as an assessment tool for BAT activity is the potential insulative effect of subcutaneous WAT overlying the BAT depot, especially when comparing groups with different body compositions (e.g. lean versus obese). This has been presented as an explanation by some for the relationship observed between BMI and $T_{SCR}$ in studies I, II and V. Such that those with a higher BMI have lower $T_{SCR's}$ not because their BAT is less active, but because their subcutaneous adipose tissue overlying their supraclavicular BAT is more plentiful and prevents heat loss to the skin surface.

It is well recognised that SCAT is inversely related to skin temperature (Salamunes et al., 2017). However, the degree to which this impacts heat transfer from supraclavicular BAT to the skin surface has not been quantified and whether this alters the detection of the thermogenic response is unclear. Attempts were made to

quantify the thickness of this subcutaneous layer using both ultrasound and MRI in studies IV and V. The layer of adipose tissue found immediately below the skin in the region of the posterior triangle of the neck was so small I was not able to measure it reproducibly with either method.

From this work, it is apparent that neither absolute $T_{SCR}$ nor $\Delta T_{SCR}$ offers a complete representation of BAT activity, or capacity for activation at this time, particularly in populations including individuals with dysfunctional and maximally active BAT as $\Delta T_{SCR}$ does not distinguish between the two. Acquisition of normative reference data may optimise the interpretation of these measures, or an alternative thermal index comprising both values plus additional variables (e.g. core temperature) may improve assessment of BAT.

Studies III to V were limited by the number of participants, and whilst identifying some interesting findings worthy of future study, these should be considered exploratory. These studies have however significantly refined the use of IRT for the study of BAT, and have optimised cooling protocols which in turn have been adopted and utilised by other researchers and PhD students in Academic Child Health and beyond.

### 6.3 Future perspectives

The assessment of BAT undertaken in studies IV and V could be extended to children to determine the supraclavicular BAT response to cold, including children of all ages. Establishing normative data for healthy individuals under controlled conditions will provide a reference for future clinical studies. With adaptation, and care to ensure they are conducted at thermoneutrality, these methods may also be suitable for

preschool infants and young children. These should be undertaken in a child-friendly temperature-controlled laboratory with consideration of the limitations described in section 6.3 and methods optimised where possible. Future work should also focus on optimising the assessment of $T_{SCR}$, and developing a robust thermal index with high sensitivity and specificity for BAT detection beyond that of the crude measure of absolute $T_{SCR}$ and $\Delta T_{SCR}$. Preferably, a thermal index that adjusts for relative adiposity and variations in ambient temperature. This will allow the detailed longitudinal study of BAT throughout the life cycle; from the neonatal period, through childhood and into adult life, providing data that is integral to the understanding of BAT developmental physiology and its role in metabolic health and disease. For clarity and transparency and future development, the methodology for image acquisition and thermographic analysis should be standardised and undertaken using contemporary guidance (Moreira et al., 2017).

Alternative methods for measuring $T_{SCR}$ may be preferred in very young children who are unable to remain still for the duration of imaging and should be explored. Contact thermometry with wireless data loggers, or with traditional surface wired thermocouples placed using IRT to locate the supraclavicular hotspot would allow greater flexibility during assessment.

### 6.4 Final remarks

This thesis has successfully used IRT to measure $T_{SCR}$ in children (and young adults). The supraclavicular thermogenic response to cold exposure (with a concurrent increase in energy expenditure) and anticipatory stress, suggest that these changes were consistent with BAT activation. Moreover, the thermogenic response was

isolated to the supraclavicular region and was not associated with gross systemic cardiovascular change indicative of the cold-pressor response, or a wider systemic thermogenic response. This work has identified BMI and sex as significant determinants of $T_{SCR}$ and the $T_{SCR}$ response to cooling in children for the first time and has provided data supportive to existing data that $T_{SCR}$ is also negatively associated with BMI in young adults.

In conclusion, these studies provide a snapshot of how supraclavicular BAT behaves in early childhood, and hints towards factors that may affect BAT development, and highlights some methodological issues that should be considered during assessment with thermography. Further work will be required to generate a complete picture of how BAT develops throughout childhood and adolescence, and whether adult BAT status can be optimised during early life.

## Appendix to Study I

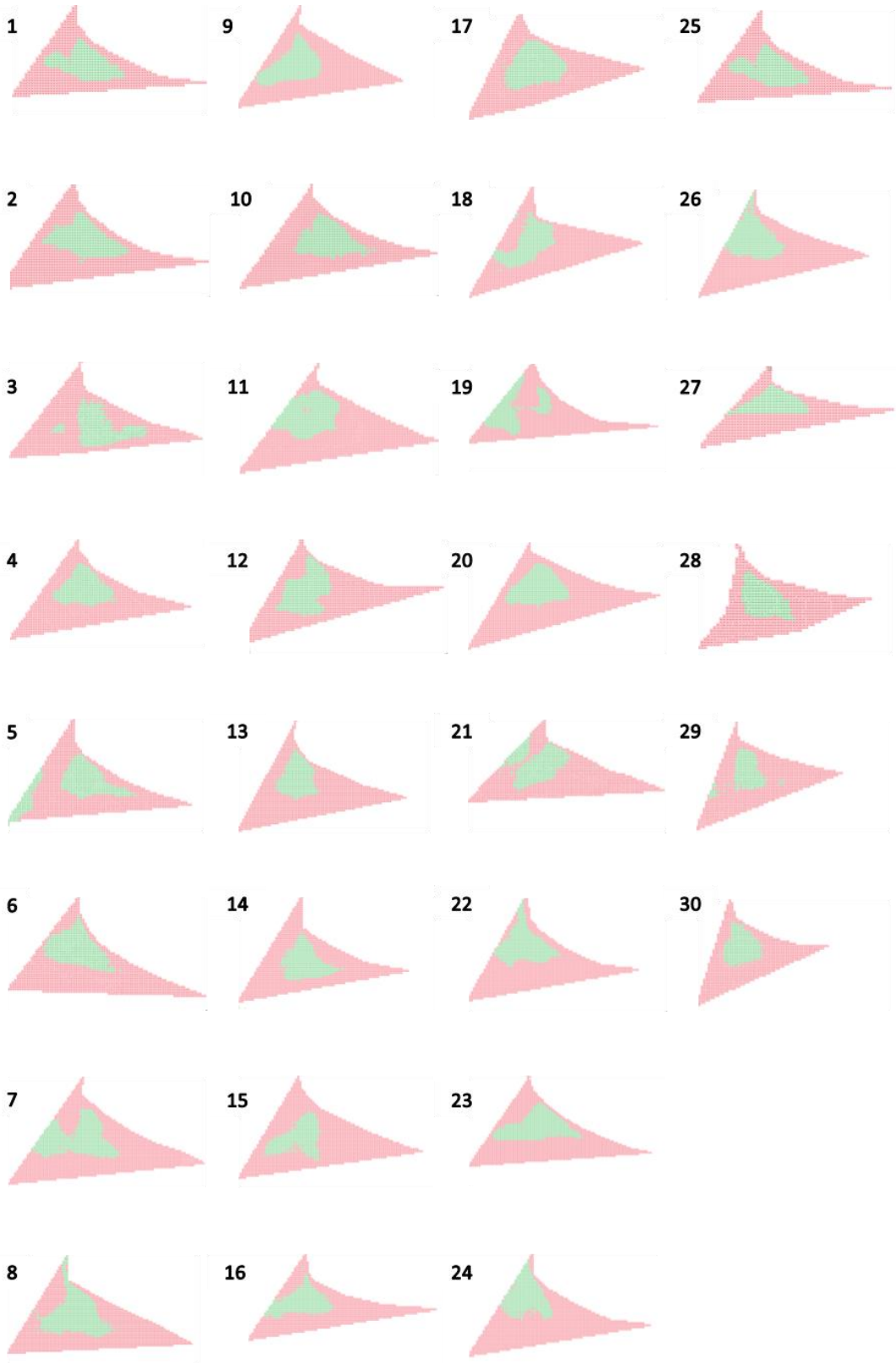



**Figure A3.1A Diagrammatic representation of the 25th upper percentile of temperature values.** The left polygonal supraclavicular region of interest from a randomly selected set of baseline images in 30 participants from Study I. Images constructed from the excel output obtained from ThermaCAM pro 2.1. Where green pixels represent the upper 25th percentile and red pixels the remaining ROI.

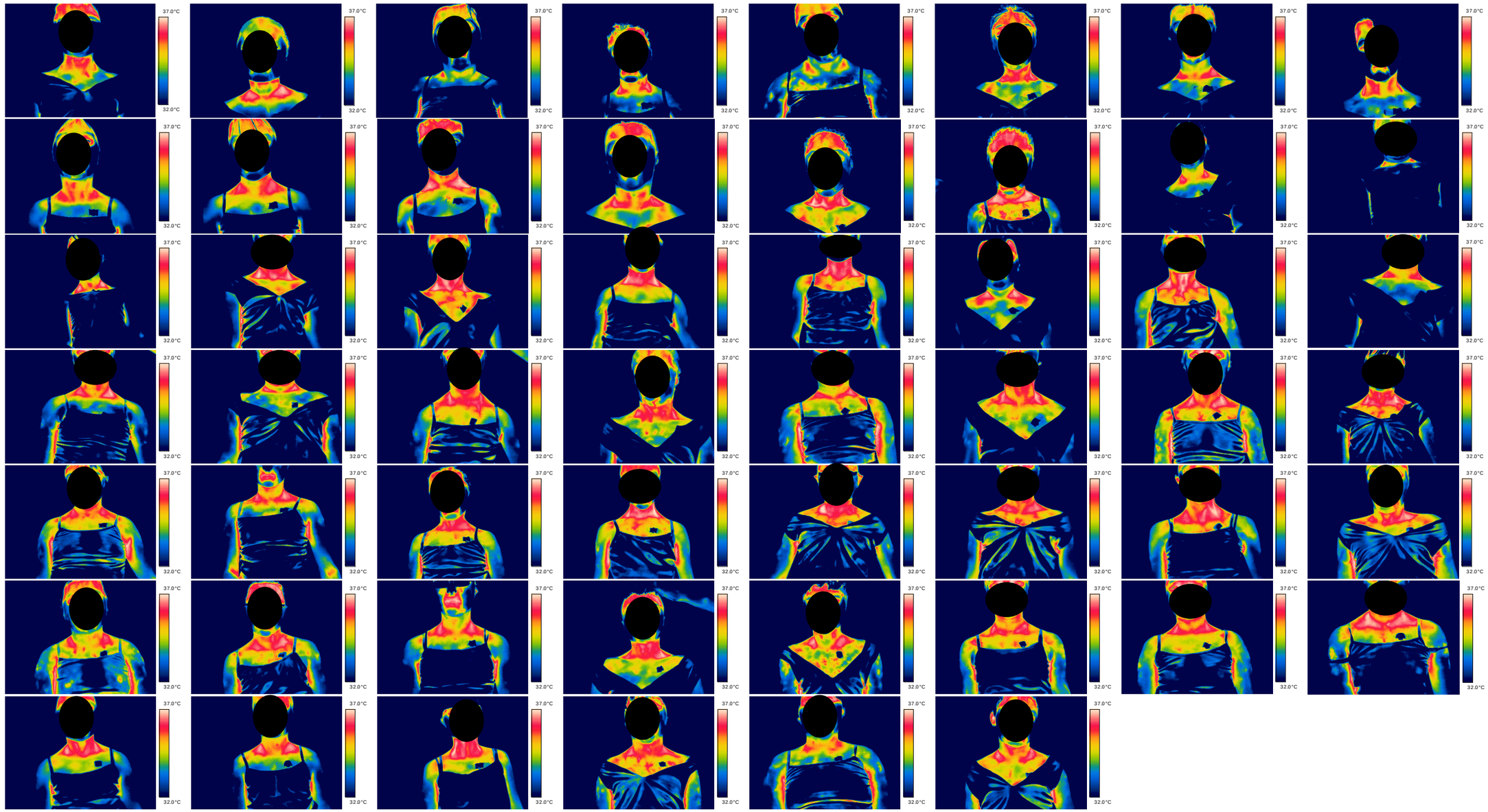
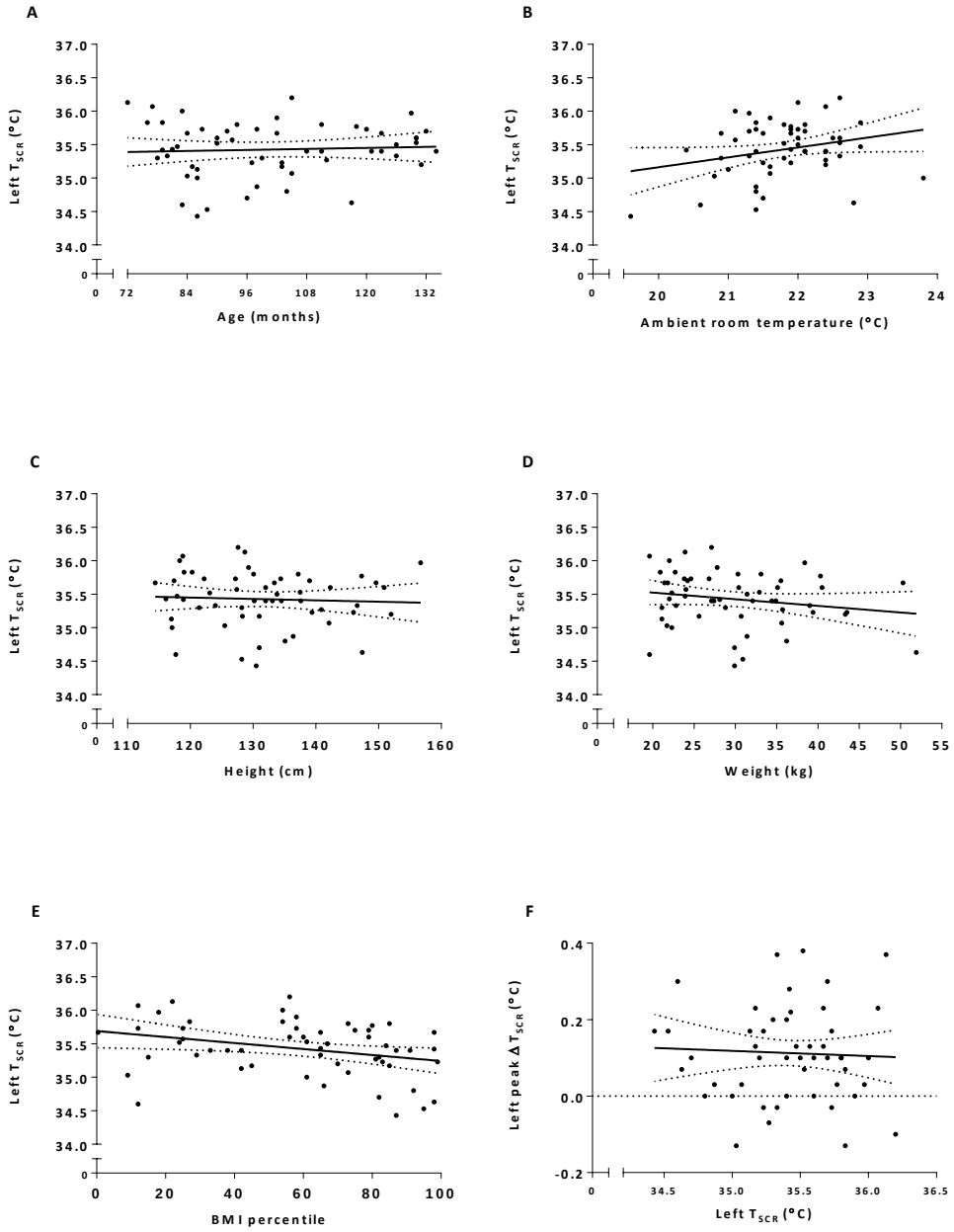
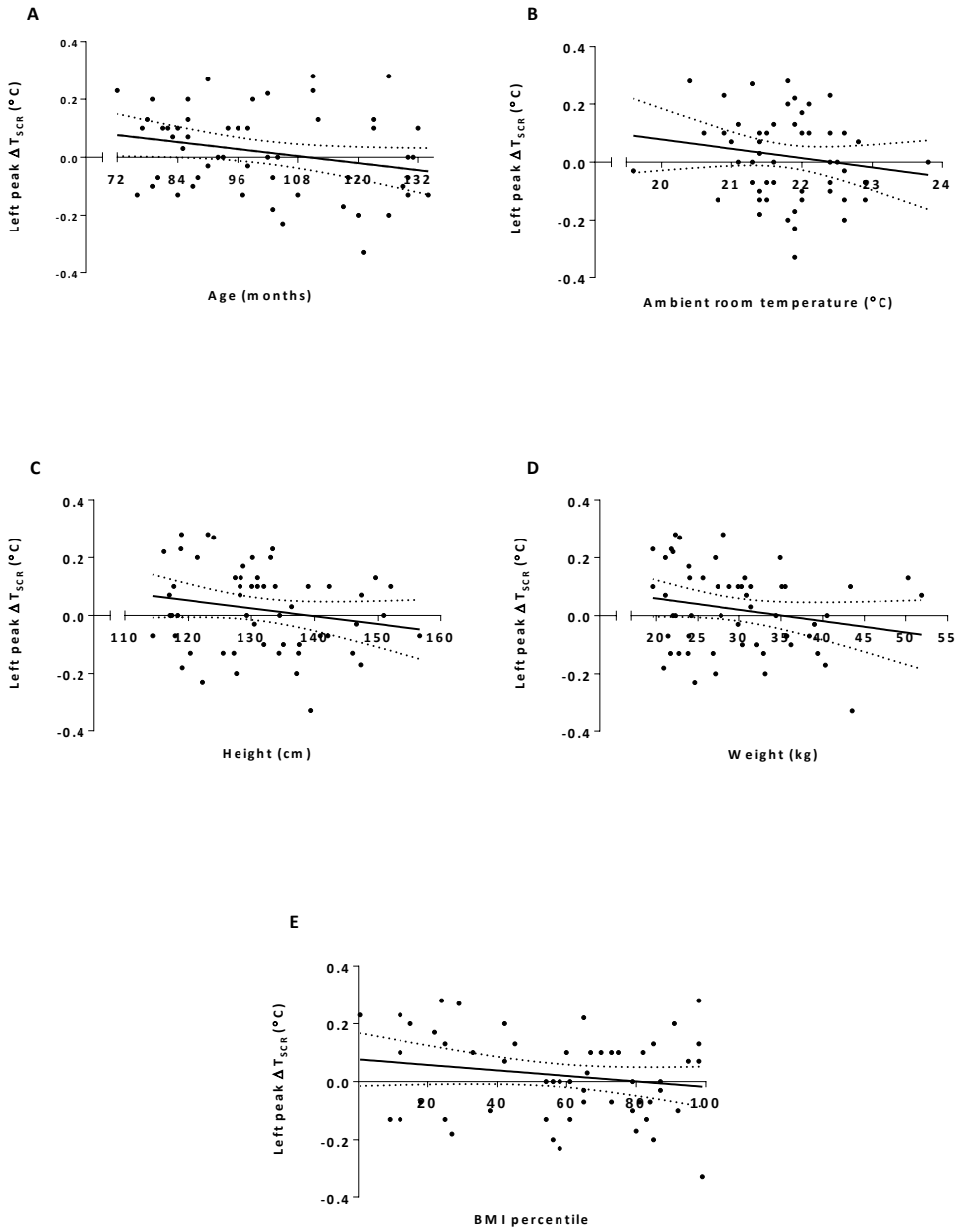



**Figure A3.1B Representative thermograms of the 55 children who underwent infrared thermography in Study I.** Images displayed in colour palette Rainbow 900 in FLIR ThermaCAM researcher Pro 2.1, minimum temperature displayed 32°C and maximum 37°C, a single image selected at random for each child (i.e. images do not represent the same time point for each child), anonymised but otherwise not manipulated.

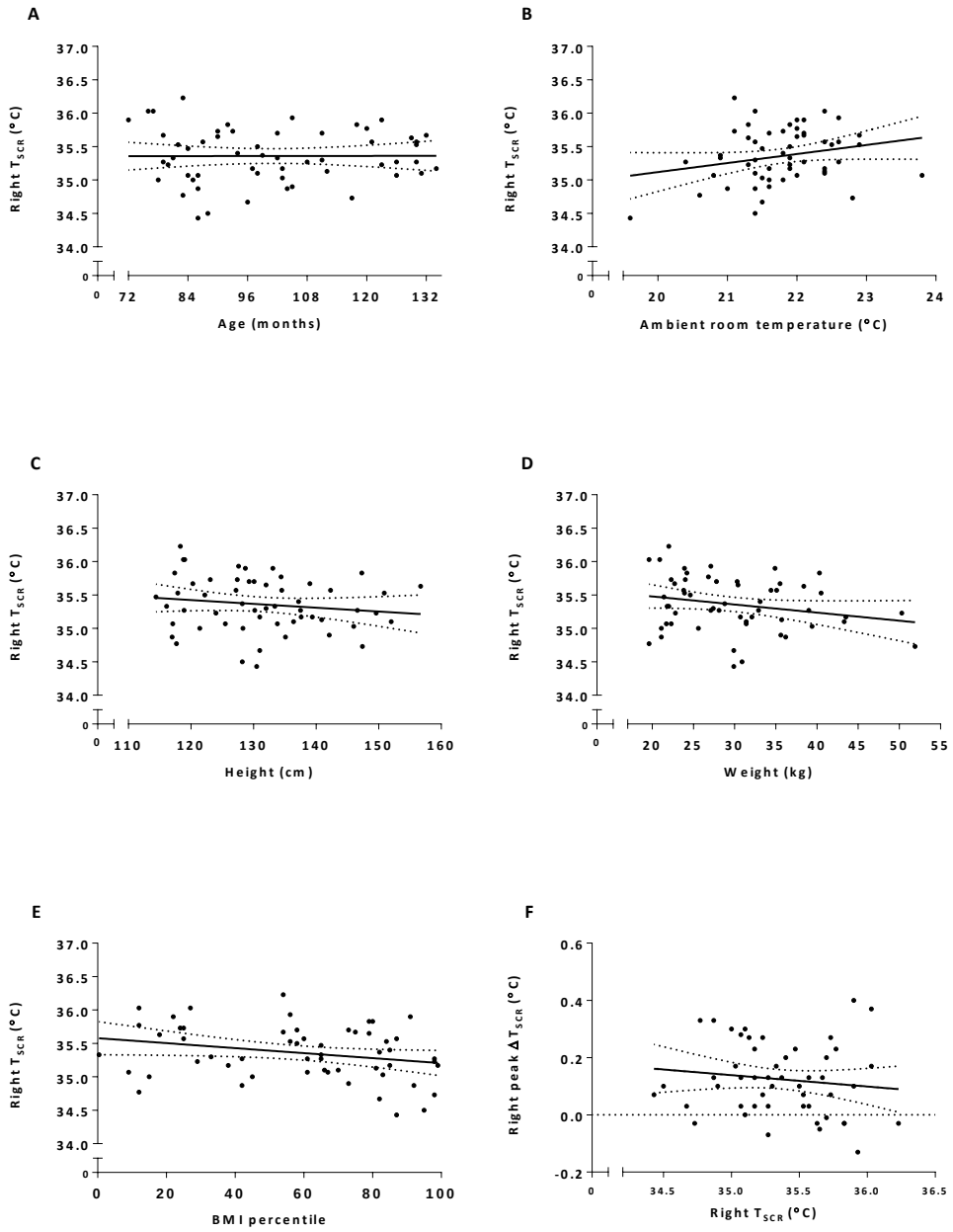



**Figures A3.2A – F Scatter plot and line of best fit ± 95% confidence intervals for A) age, B) ambient room temperature, C) height, D) weight and E) BMI percentile against left $T_{SCR}$ and, F) left baseline $T_{SCR}$ against response to hand cooling ($\Delta T_{SCR}$).**

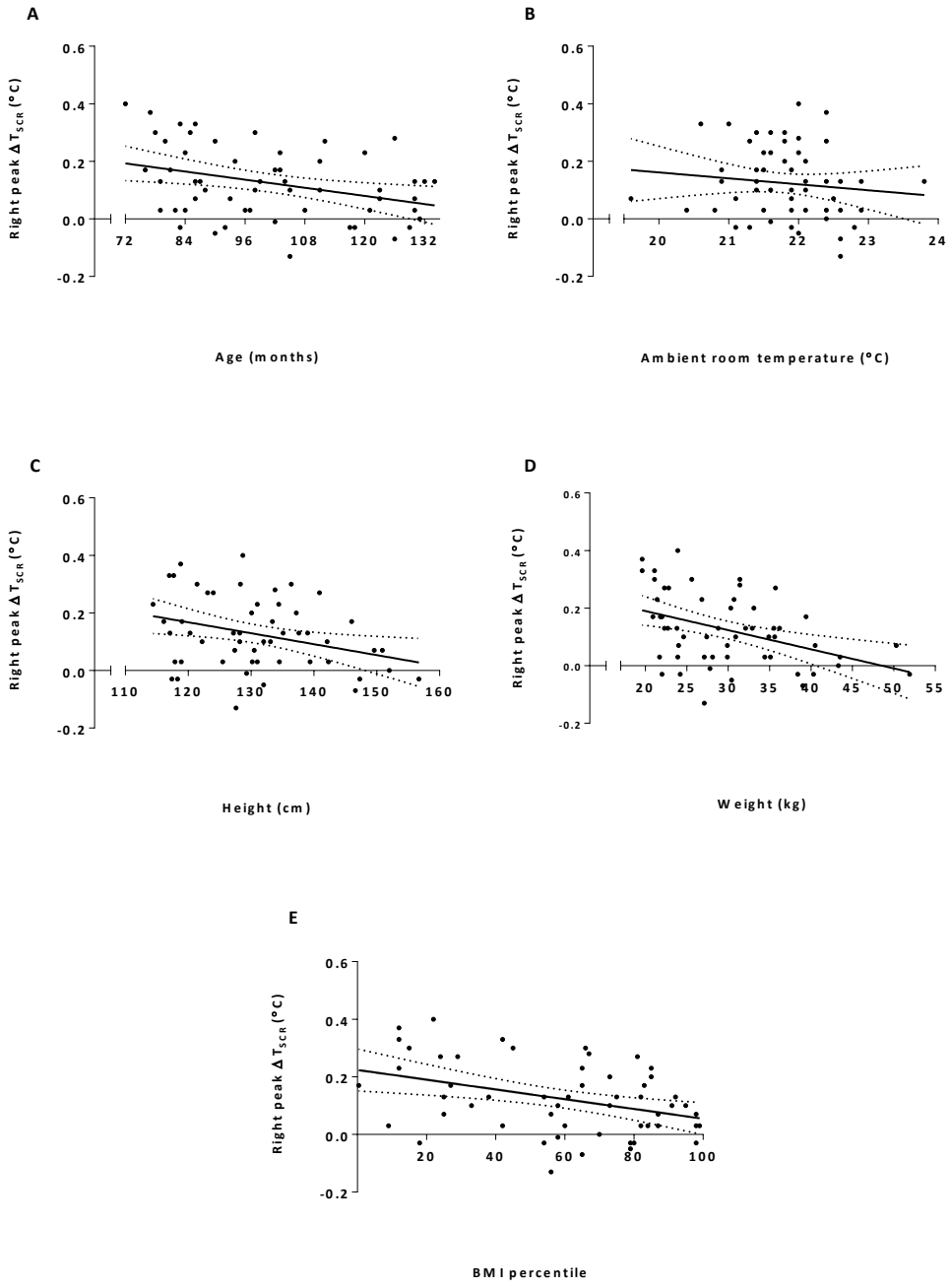
Linear regression identified BMI percentile as a significant predictor of left $T_{SCR}$ and a trend towards ambient temperature. Ambient temperature: $F(1, 53) = 3.75$, $P = 0.06$, $R^2 = 0.07$; BMI percentile: $F(1, 53) = 5.49$, $P = 0.02$ $R^2 = 0.09$. Age, height and weight were not predictors of left $T_{SCR}$. Age: $F(1, 53) = 0.17$, $P = 0.68$, $R^2 = 0.003$; weight: $F(1, 53) = 1.92$, $P = 0.17$, $R^2 = 0.04$; height: $F(1, 53) = 0.15$, $P = 0.70$, $R^2 = 0.003$ and there was no relationship between baseline left sided baseline $T_{SCR}$ and response to cold stimulation: $F(1,53) = 0.11$ , $P = 0.74$, $R^2 = 0.002$).




**Figures A3.3A – E. Scatter plot and line of best fit ± 95% confidence intervals for A) age, B) ambient room temperature, C) height, D) weight and E) BMI percentile against left-sided peak change in $T_{SCR}$ ($\Delta T_{SCR}$)**. Simple linear regression analysis identified no statistically significant predictors of left-sided peak $\Delta T_{SCR}$. Ambient temperature: $F(1,53) = 1.34$, $P = 0.25$, $R^2 = 0.03$; height: $F(1, 53) = 2.14$, $P = 0.15$, $R^2 = 0.04$; weight: $F(1, 53) = 2.38$, $P = 0.13$, $R^2 = 0.04$; BMI percentile: $F(1, 53) = 1.81$, $P = 0.18$, $R^2 = 0.03$. There was a trend towards age as a predictor of left $\Delta T_{SCR}$: $F(1, 53) = 3.62$, $P = 0.06$, $R^2 = 0.05$.




**Figures A3.4A – F Scatter plot and line of best fit ± 95% confidence intervals for A) age, B) ambient room temperature, C) height, D) weight and E) BMI percentile against right $T_{SCR}$ and, F) right baseline $T_{SCR}$ against response to hand cooling ($\Delta T_{SCR}$).** Linear regression analysis identified a trend towards ambient temperature, BMI percentile and weight as statistically significant predictors of right-sided $T_{SCR.}$ Ambient temperature: F (1, 53) = 3.22, P = 0.08, $R^2$ = 0.06; BMI percentile: F (1, 53) = 3.85, P = 0.06, $R^2$ = 0.07; weight: F (1, 53) = 3.03, P = 0.09, $R^2$ = 0.05. Age and height were not predictors of right $T_{SCR.}$ Age: F (1, 53) = 0.0006, P = 0.98, $R^2$ = 1.164e-005 and there was no relationship between baseline right sided $T_{SCR}$ and response to cold stimulation (F (1,53) = 0.90, P = 0.35, $R^2$ = 0.02).




**Figures A3.5A – E Scatter plot and line of best fit ± 95% confidence intervals for A) age, B) ambient room temperature, C) height, D) weight and E) BMI percentile against left-sided peak change in $T_{SCR}$ ($\Delta T_{SCR}$).** Linear regression identified BMI centile, height and weight and age as statistically significant predictors of right-sided peak $\Delta T_{SCR}$. Height: $F(1, 53) = 6.29$, $P = 0.02$, $R^2 = 0.11$; weight: $F(1,53) = 11.03$, $P = 0.002$, $R^2 = 0.17$; BMI percentile: $F(1, 53) = 9.15$, $P = 0.004$, $R^2 = 0.15$; age: $F(1, 53) = 7.26$, $P = 0.009$, $R^2 = 0.12$. Ambient temperature was not a predictor of right $\Delta T_{SCR}$: $F(1, 53) = 0.06$, $P = 0.81$, $R^2 = 0.001$.

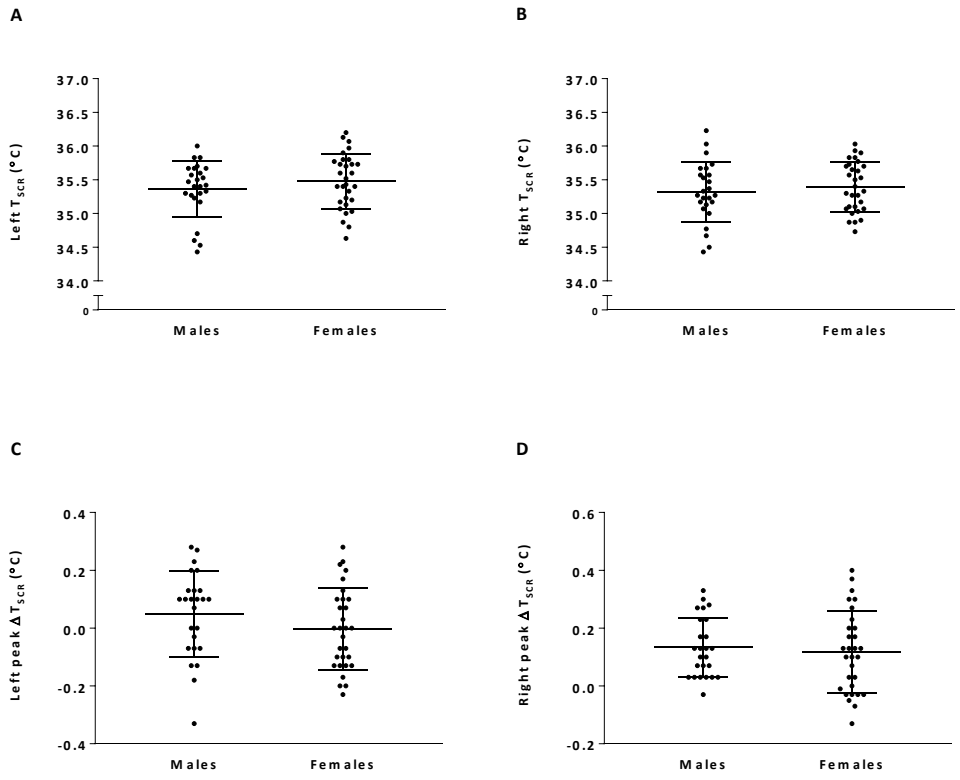



**Figure A3.6 Left and right sided baseline supraclavicular temperature (A and B) and response to hand cooling in males and females (C and D).** No significant differences in supraclavicular skin temperature ($T_{SCR}$) were identified between males (n = 25) and females (n = 30) at baseline, or in response to hand-cooling in healthy children aged 6 –11 years in Study I.

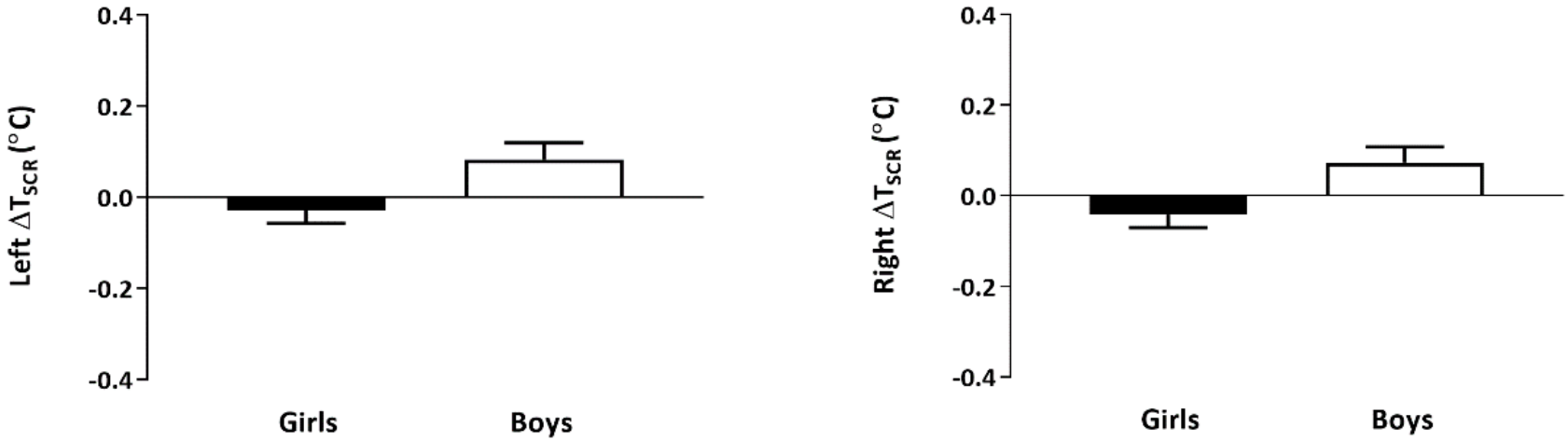



**Figure A3.7 Adjusted means for the left and right supraclavicular skin response to 5 minutes hand cooling (adjusted for BMI percentile) in the girls and boys from Study I aged 102 months and over**. ANCOVA analysis revealed a difference in change in supraclavicular temperature from baseline ($\Delta T_{SCR}$) between girls and boys following adjustment for BMI percentile. $\Delta T_{SCR}$ was greater in boys than girls on the left and right side with a mean difference of 0.11˚C (95%CI, 0.01 to 0.21˚C, p = 0.03) and 0.12 (95%CI, 0.02 to 0.29˚C, P = 0.02) respectively.

**Table A3.1 Correlation (Pearson's r) between supraclavicular skin temperature ($T_{SCR}$) values calculated in Study I using different methods of isolation of the supraclavicular region**

| | $T_{SCR87.5}$ [M] | $T_{SCR95}$ [M] |
|---|---|---|
| **Baseline left $T_{SCR87.5}$ [F]** | 0.99*** | 0.97*** |
| **Baseline right $T_{SCR87.5}$ [F]** | 0.99*** | 0.97*** |
| **Left $\Delta T_{SCR87.5}$ [F]** | 0.88*** | 0.93*** |
| **Right $\Delta T_{SCR87.5}$ [F]** | 0.77*** | 0.86*** |

*** $P < 0.0001$

[F] – Calculated using a manual method with FLIR's proprietary software

[M] – Calculated using a semi-automated method with a custom MATLAB script

$T_{SCR87.5}$ – $87.5^{th}$ centile value

$T_{SCR90}$ – $95^{th}$ centile value

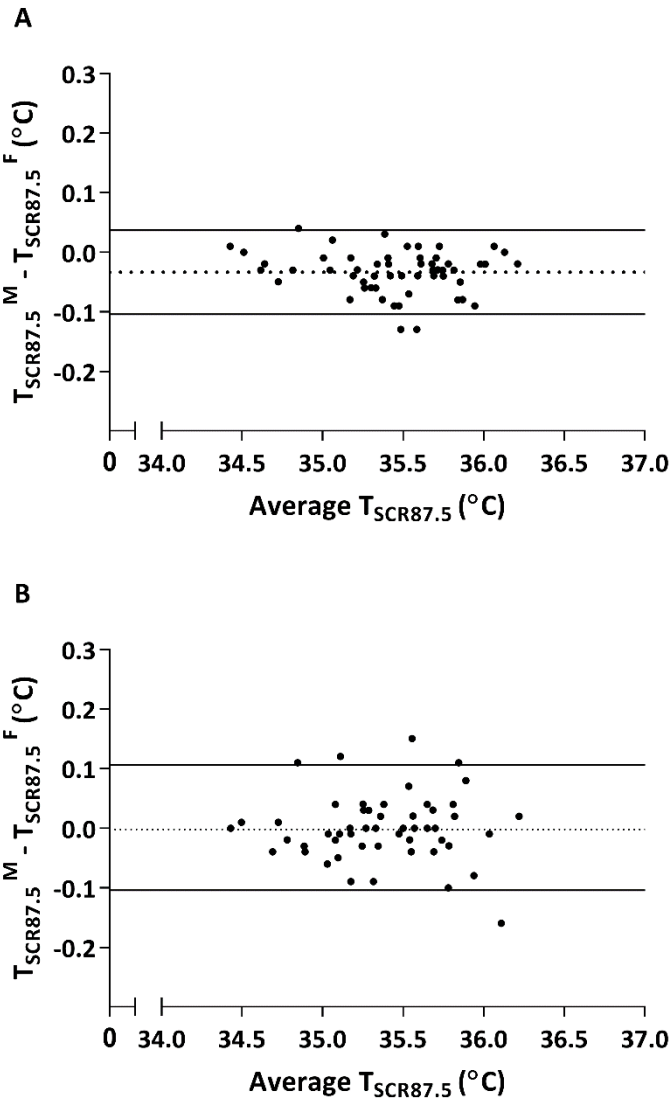



**Figure A3.8 Agreement between baseline $T_{SCR87.5}^{M}$ and $T_{SCR87.5}^{F}$ in Study I, displayed as Bland-Altman plots.** $T_{SCR}$ is supraclavicular temperature calculated as the 87.5$^{th}$ percentile value of the supraclavicular ROI, $^{F}$ – FLIR software, $^{M}$ – MATLAB. Mean Bias – dotted line and 95% limits of agreements – solid lines. A – left side, and B – right side.

**Table A3.2 Multiple regression analyses for left and right $T_{SCR95}$ as dependent variables and age, BMI percentile, ethnicity, sex and ambient temperature as independent variables for Study I (n = 55)**

| | Left $T_{SCR95}$ | | | | Right $T_{SCR95}$ | | | |
|---|---|---|---|---|---|---|---|---|
| **Variable** | **B** | **SE** | **β** | **P** | **B** | **SE** | **β** | **P** |
| **Constant** | 31.683 | 1.716 | - | < 0.01 | 30.963 | 1.778 | - | < 0.01 |
| **Age** | 0.000 | 0.003 | -0.017 | 0.902 | -0.001 | 0.003 | -0.033 | 0.814 |
| **BMI percentile** | -0.006 | 0.002 | -2.862 | 0.006 | -0.005 | 0.002 | -0.309 | 0.026 |
| **Ethnicity*** | 0.270 | 0.109 | 0.310 | 0.017 | 0.261 | 0.113 | 0.295 | 0.025 |
| **Sex Ψ** | -0.35 | 0.108 | -0.042 | 0.748 | 0.012 | 0.111 | 0.014 | 0.915 |
| **Ambient room temperature** | 0.160 | 0.079 | 0.274 | 0.048 | 0.187 | 0.082 | 0.082 | 0.027 |

Abbreviations: $T_{SCR95}$ – supraclavicular temperature (calculated as the 95$^{th}$ percentile value within the supraclavicular region); BMI – body mass index

Left $T_{SCR}$: $R^2$ = 0.257 (significant model P = 0.01); right $T_{SCR}$: $R^2$ = 0.221 (significant model P = 0.03)

* Caucasian compared with non-Caucasian

Ψ Females compared with males

**Table A3.3 Multiple regression analyses for left and right $\Delta T_{SCR95}$ as dependent variables age, BMI percentile, ethnicity, sex and ambient temperature as independent variables for Study I (n = 55)**

| | Left $\Delta T_{SCR95}$ | | | | Right $\Delta T_{SCR95}$ | | | |
|---|---|---|---|---|---|---|---|---|
| **Variable** | **B** | **SE** | **β** | **P** | **B** | **SE** | **β** | **P** |
| **Constant** | -0.018 | 0.637 | - | 0.977 | 0.074 | 0.635 | - | 0.907 |
| **Age** | -0.001 | 0.001 | -0.181 | 0.222 | -0.002 | 0.001 | -0.226 | 0.113 |
| **BMI percentile** | -0.001 | 0.001 | -0.196 | 0.174 | -0.001 | 0.001 | -0.248 | 0.075 |
| **Ethnicity*** | -0.023 | 0.040 | -0.077 | 0.568 | -0.076 | 0.040 | -0.244 | 0.065 |
| **Sex Ψ** | 0.072 | 0.040 | 0.254 | 0.075 | 0.052 | 0.040 | 0.176 | 0.194 |
| **Ambient room temperature** | 0.011 | 0.029 | 0.054 | 0.715 | 0.020 | 0.029 | 0.094 | 0.504 |

Abbreviations: $\Delta T_{SCR95}$ – change in supraclavicular temperature (calculated as the 95$^{th}$ percentile value within the supraclavicular region); BMI – body mass index

Left $\Delta T_{SCR}$: $R^2$ = 0.134 (Non-significant model P = 0.203); right $\Delta T_{SCR}$: $R^2$ = 0.205 (significant model P = 0.041)

* Caucasian compared with non-Caucasian

Ψ Females compared with male

## Appendix to Study II

**Table A3.1 Foods included for calculation of food consumption sum scores, reliability assessment of parental responses (Cronbach's alpha), and mean food consumption sum score in each food group**

| | Foods included in analysis categorised by group* | | | CA | MCSS |
|---|---|---|---|---|---|
| Carbohydrate | Cornflakes<br>Coco pops<br>Shreddies<br>Cheerios<br>Weetabix<br>Rice crispies<br>Sugar puffs<br>White bread<br>Brown bread | Potato (mashed)<br>Potato (Roast)<br>Potato (boiled)<br>Potato (baked)<br>Potato (chips)<br>Bread roll (white)<br>Bread roll (brown)<br>Yorkshire Pudding | Croissants<br>Pancake<br>Crumpet<br>Pitta bread<br>Pasta<br>Rice<br>Baguette<br>Potato Waffle | 0.81 | 120.7 |
| Dairy | Dairylea<br>Mozzarella<br>Milk | Cheese strings<br>Milkshake<br>Natural<br>Cheddar cheese | yoghurt<br>Flavoured yoghurt<br>Yoghurt drink | 0.54 | 41.4 |
| Fruit | Apple<br>Banana<br>Pear<br>Raspberry<br>Peach<br>Plum | Strawberry<br>Pineapple<br>Watermelon<br>Melon<br>Cherry<br>Kiwi | Blackberry<br>Mango<br>Grapes (red)<br>Grapes (green)<br>Orange | 0.7 | 84.6 |
| Protein | Eggs (scrambled)<br>Eggs (fried)<br>Eggs (boiled)<br>Chicken | Lamb<br>Fish fingers<br>Burgers<br>Sausages<br>Tuna&mayonnaise | Tuna<br>Baked beans<br>Kidney Beans | 0.72 | 62.8 |
| Savoury snack | Sausage Roll<br>Samosas<br>Spring rolls<br>Crisps | Hoolahoops<br>Cream Cracker<br>Ritz cracker | Wotsits<br>Doritos<br>Quavers | 0.73 | 53.6 |
| Sweet snack | Ice cream (strawberry)<br>Ice cream (chocolate)<br>Ice cream (vanilla)<br>Digestive Biscuit Chocolate Digestive | Fairy cake (plain)<br>Fairy cake (chocolate)<br>Angel delight (chocolate)<br>Angel delight (strawberry)<br>Jelly sweets<br>Boiled sweets<br>Jam doughnut | Cookie<br>Chocolate Éclair<br>Cheese Cake<br>Milk Chocolate<br>Dark Chocolate<br>White Chocolate<br>Bourbon<br>Custard Cream | 0.83 | 105.7 |
| Vegetable | Carrot<br>Cabbage (green)<br>Cucumber<br>Baby Sweetcorn<br>Sweetcorn | Corn on the cob<br>Tomato<br>Red Pepper<br>Green Pepper<br>Yellow<br>Sprouts<br>Peas | Pepper<br>Orange Pepper<br>Mushroom<br>Broccoli<br>Cauliflower<br>Onion | 0.80 | 85.8 |

* Food included in the grouped analysis only if < 25% of parental responses were "never tried"

CA – Cronbach's alpha, > 0.7 indicates good reliability; MCSS – mean consumption sum score

**Table A3.2 Relationship between Marlow-Crowne Social Desirability Score (MC-SDS) and responses to parental questionnaires regarding dietary intake, fussy eating behaviour, food consumption score and duration of TV watching**

| Variable | Correlation coefficient | P value |
|---|---|---|
| **Food consumption sum scores** | | |
| Carbohydrate | -0.09 | 0.62 |
| Dairy | -0.12 | 0.53 |
| Fruit | -0.22 | 0.24 |
| Protein | 0.01 | 0.60 |
| Savoury snack | 0.007 | 0.66 |
| Sweet snack | 0.004 | 0.72 |
| Vegetable | 0.07 | 0.15 |
| **TV watching** | 0.43* | 0.02 |
| **Picky eating** | -0.18 | 0.35 |

* Parental responses contaminated by socially desirable responding

**Table A3.3A and B Relationship between supraclavicular skin temperature ($T_{SCR}$) measured by infrared thermography and BMI percentile in healthy volunteer boys (A) and girls (B) aged 8 – 11 years (n = 36)**

**A**

| | Left supraclavicular temperature | | | Right supraclavicular temperature | | |
|---|---|---|---|---|---|---|
| | **Baseline** | **Cold exposed** | **$\Delta T_{SCR}$** | **Baseline** | **Cold exposed** | **$\Delta T_{SCR}$** |
| **r** | -0.53* | -0.67* | -0.46 | -0.49* | -0.64* | -0.44 |
| **95% CI** | -0.81 to -0.04 | -0.87 to -0.25 | -0.78 to 0.04 | -0.80 to 0.002 | -0.86 to -0.21 | -0.77 to 0.07 |
| **$R^2$** | 0.28 | 0.44 | 0.21 | 0.24 | 0.41 | 0.20 |
| **P value** | 0.04 | **0.005** | 0.07 | 0.05 | **0.008** | 0.09 |

**B**

| | Left supraclavicular temperature | | | Right supraclavicular temperature | | |
|---|---|---|---|---|---|---|
| | **Baseline** | **Cold exposed** | **$\Delta T_{SCR}$** | **Baseline** | **Cold exposed** | **$\Delta T_{SCR}$** |
| **r** | -0.71* | -0.68* | 0.08 | -0.76* | -0.73* | 0.13 |
| **95% CI** | -0.88 to -0.39 | -0.86 to -0.34 | -0.38 to 0.50 | -0.90 to -0.47 | -0.89 to -0.43 | -0.33 to 0.54 |
| **$R^2$** | 0.50 | 0.47 | 0.01 | 0.57 | 0.53 | 0.02 |
| **P value** | **0.0005** | **0.0009** | 0.74 | **0.0001** | **0.0003** | 0.59 |

*P < 0.05; bold type indicates statistical significance following adjustment for multiple comparisons.

## Appendix to Study IV

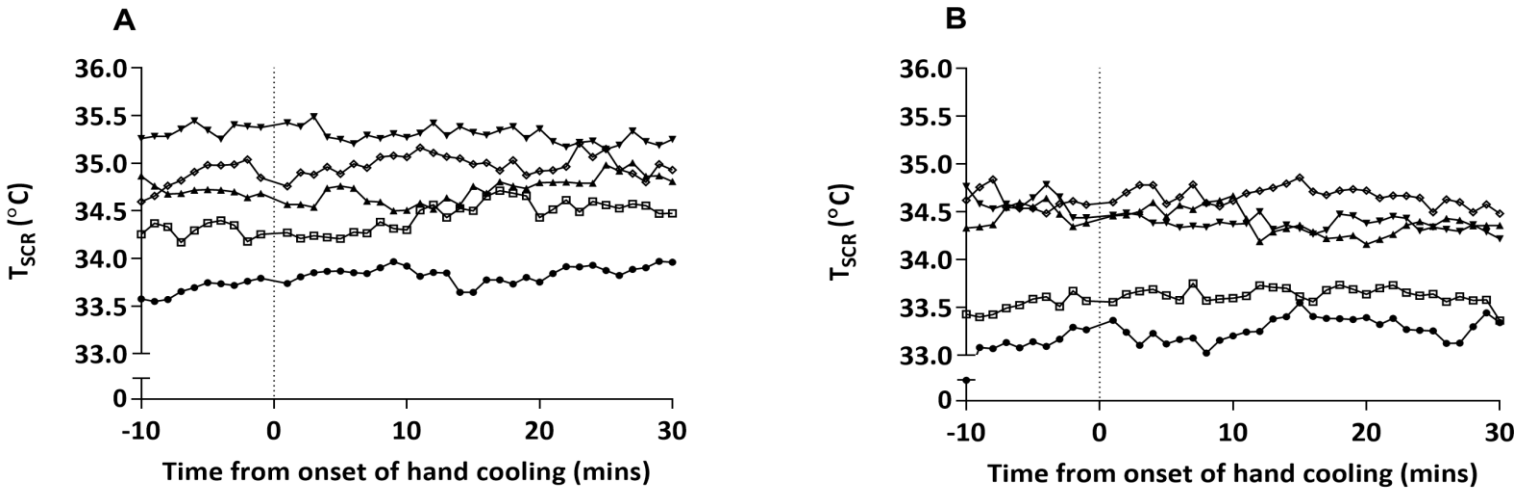



**Figure A5.1 A – B Supraclavicular skin temperature measured at 1 minute interval using infrared thermography prior to and during hand cooling at an ambient room temperature of A) 23˚C and B) 18˚C. Each symbol represents a single participant, n = 5.**

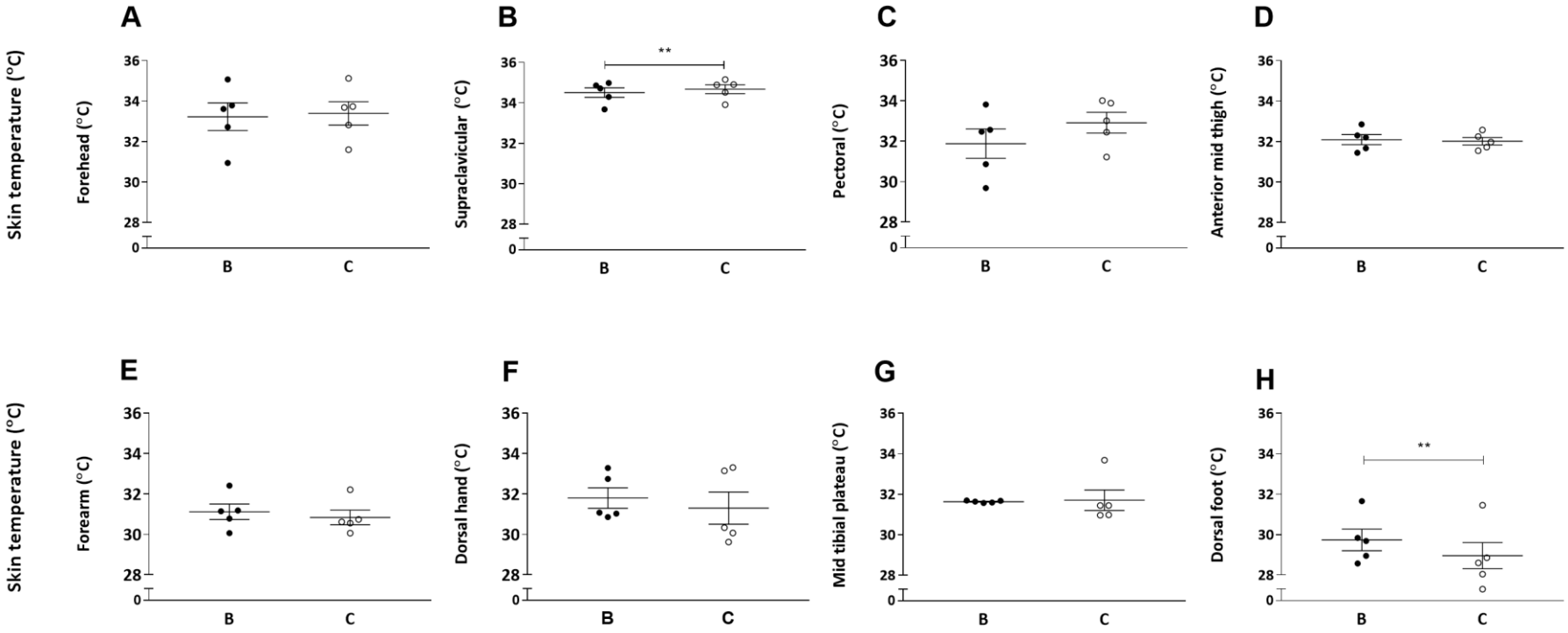



**Figure A5.2A – H Mean average skin temperature during the last 5 minutes of baseline (B) and hand cooling (C), measured using iButtons sited on the left side of the A) forehead, C) pectoral muscle, D) anterior mid-thigh E) mid forearm F) dorsum of the hand, G) mid-tibial plateau, H) dorsum of the foot and skin temperature from the right sided supraclavicular region measured using infrared thermography. ** P < 0.01. Individual data points shown with means ± SEM. Closed circle – baseline (B) and open circle (C) – hand cooling.**

## Appendix to Study V

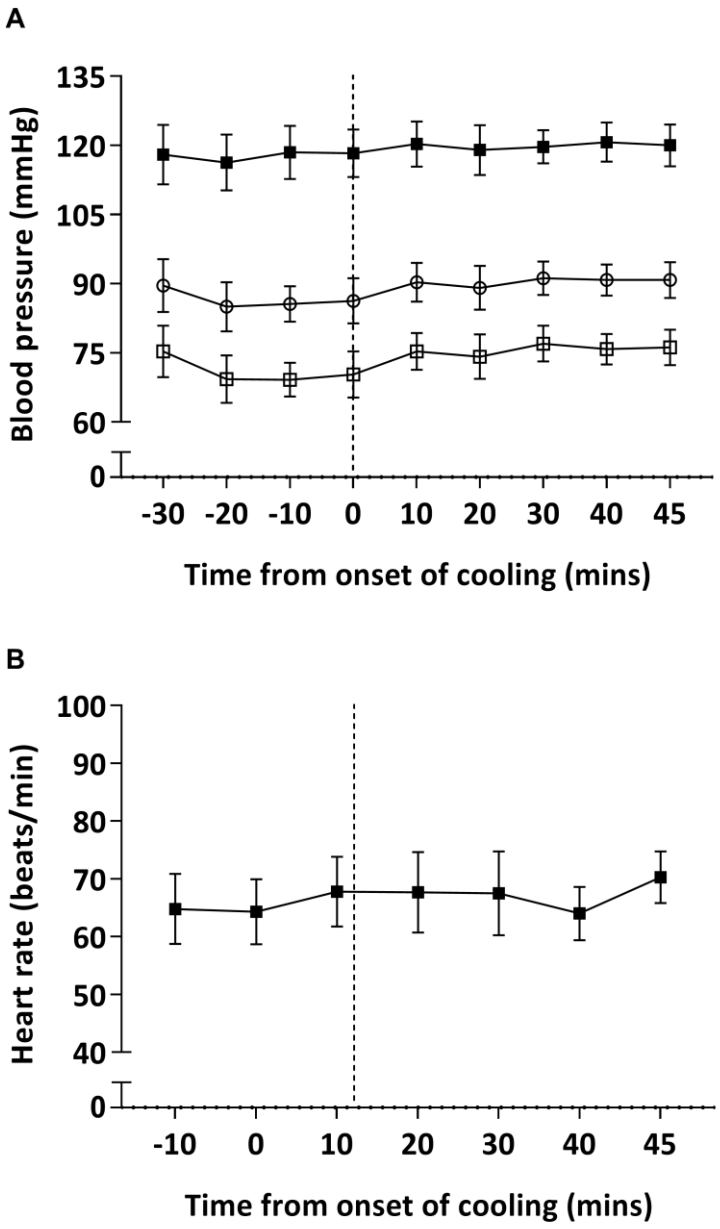



**Figure A5.1 A) Blood pressure and B) heart rate during baseline and active forearm cooling.** Data shown as mean ± SEM. Systolic blood pressure – closed square, mean arterial blood pressure – open circles, diastolic blood pressure – open squares, dotted line indicates onset of active forearm cooling with the Blanketrol II X device. n = 6.

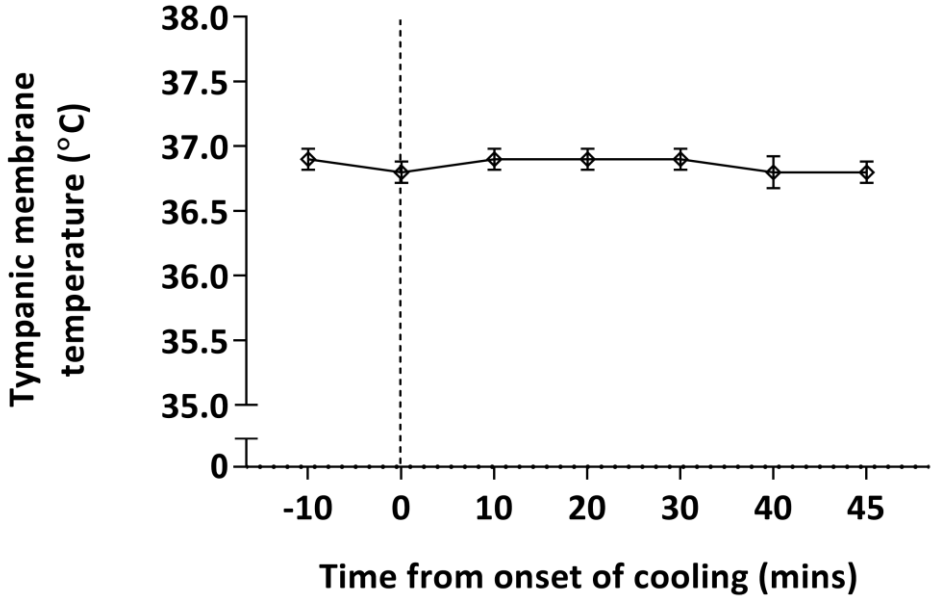



**Figure A5.2 Right sided tympanic membrane temperature during baseline and active forearm cooling with the Blanketrol II® device. n = 6.** Dotted line represents time zero at the onset of cooling.

## Other Authors' Declarations

For this thesis, we hereby declare that Lindsay Jane Robinson undertook the laboratory work (with the exception of paper no.3), data collection, statistical analysis, data interpretation and took the lead in writing the manuscripts for the following published papers and those currently under review:

1. ROBINSON, L., OJHA, S., SYMONDS, M. E. & BUDGE, H. 2014. Body mass index as a determinant of brown adipose tissue function in healthy children. *J Pediatr*, 164, 318-22 e1.
2. ROBINSON, L. J., LAW, J. M., SYMONDS, M. E. & BUDGE, H. 2016. Brown adipose tissue activation as measured by infrared thermography by mild anticipatory psychological stress in lean healthy females. *Exp Physiol*, 101, 549-57.
3. ROBINSON, L. J., LAW, J., ASTLE, V., GUTIERREZ-GARCIA, M., OJHA, S., SYMONDS, M. E., PITCHFORD, N. & BUDGE, H. 2019. Sexual Dimorphism of Brown Adipose Tissue Function. *J Pediatr*, 210, 166-172 e1.
4. ROBINSON, L. J., LAW, J., WAYNE, D., AUER, D., SYMONDS, M. E. & BUDGE, H. 2019. Effect of unilateral forearm cooling on supraclavicular brown adipose tissue thermogenesis, and its relationship to body composition in young adults (submitted to *Experimental Physiology*).
5. ROBINSON, L. J., SYMONDS, M. E., MACDONALD, I. A. & BUDGE, H. 2019. The supraclavicular skin temperature response to mild cold stimulation is dependent on ambient temperature (In Press).

James Law

shalini ojha
Shalini Ojha (signed electronically)

Valerie Astle

Helen Budge

Declan Wayne

Prof D P Auer

Director Precision Imaging Beacon

Nicola Pitchford

MICHAEL SYMONDS

## Copyright and permissions.

Where figures have been reproduced from a third party source they have been done so with permission from the author and/or publisher, or are licenced under the Commons Attribution 4.0 International License. This is indicated in the main body of the thesis as “reproduced with permission – see Appendix”. Full details of the original source and acknowledgement (where permission has been granted) in the format specified by the publisher is outlined below.

Figure 1.7 No longer under Copyright due to age, within the public domain.

Figure 1.9 Reproduced with permission from (Virtanen, K.A., Lidell, M.E., Orava, J., Heglind, M., Westergren, R., Niemi, T., Taittonen, M., Laine, J., Savisto, N.J., Enerback, S. & Nuutila, P. 2009. functional brown adipose tissue in healthy adults. N Engl J Med, 360, 1518-25.), Copyright Massachusetts Medical society.

Figure 1.10

A) Ang et al (2017) This article is distributed under the terms of the Creative Commons Attribution 4.0 International License (http://creativecommons.org/licenses/by/4.0/)

B) Kim, Mimi S.; Hu, Houchun H, Presence of Brown Adipose Tissue in an Adolescent With Severe Primary Hypothyroidism, The Journal of Clinical Endocrinology & Metabolism, 2014, 99, 9, E1686-990, by permission of Oxford University Press

C) Reprinted from Biochemical and Biophysical Research Communications, 504 /2, Jing Zhou, Nan-Nan Wu, Rui-Li Yin, Wei Ma, Cen Yan, Ying-Mei Feng, Chuan-Hai Zhang, Dong Zhao, Activation of brown adipocytes by placental growth factor, 470--477., Copyright (2018), with permission from Elsevier

D) Gatidis, S., Schmidt, H., Pfannenberg, C. A., Nikolaou, K., Schick, F. & Schwenzer, N. F. 2016. Is It Possible to Detect Activated Brown Adipose Tissue in Humans Using Single-Time-Point Infrared Thermography under Thermoneutral Conditions? Impact of BMI and Subcutaneous Adipose Tissue Thickness. PLoS One, 11, e0151152. Licenced under Commons Attribution 4.0 International License (http://creativecommons.org/licenses/by/4.0/)

E) Salem, V., Izzi-Engbeaya, C., Coello, C., Thomas, D. B., Chambers, E. S., Comninos, A. N., Buckley, A., Win, Z., Al-Nahhas, A., Rabiner, E. A., Gunn, R. N., Budge, H., Symonds, M. E., Bloom, S. R., Tan, T. M. & Dhillo, W. S. 2016. Glucagon increases energy expenditure independently of brown adipose tissue activation in humans.

Diabetes Obes Metab, 18, 72-81. Licenced under Commons Attribution 4.0 International License (http://creativecommons.org/licenses/by/4.0/)

F) Haq et al (2017) Licenced under Commons Attribution 4.0 International License (http://creativecommons.org/licenses/by/4.0/)

G) Reprinted by permission from [Springer]: Malpique, R., Gallego-Escuredo, J. M., Sebastiani, G., Villarroya, J., Lopez-bermejo, A., De Zegher, F., Villarroya, F. & Ibanez, L. 2018. Brown adipose tissue in prepubertal children: associations with sex, birthweight, and metabolic profile. Int J Obes (Lond). [COPYRIGHT] (2018)

Figure 1.11 Reprinted from The Journal of Pediatrics, 159, Laura A. Drubach, Edwin L. Palmer, Leonard P. Connolly, Amanda Baker, David Zurakowski, Aaron M. Cypess, Pediatric Brown Adipose Tissue: Detection, Epidemiology, and Differences from Adults, 949 - 944, Copyright (2011), with permission from Elsevier.

Figure 2.1 As the author of this Elsevier article, I retain the right to include it in a thesis or dissertation, provided it is not published commercially.

Chapter Three manuscripts are reproduced from Robinson et al (2014) and Robinson et al (2019) as the author of these Elsevier articles, I retain the right to include it in a thesis or dissertation, provided it is not published commercially, as specified by Elsevier.

ROBINSON, L., OJHA, S., SYMONDS, M. E. & BUDGE, H. 2014. Body mass index as a determinant of brown adipose tissue function in healthy children. *J Pediatr,* 164**,** 318-22 e1.

ROBINSON, L. J., LAW, J., ASTLE, V., GUTIERREZ-GARCIA, M., OJHA, S., SYMONDS, M. E., PITCHFORD, N. & BUDGE, H. 2019. Sexual Dimorphism of Brown Adipose Tissue Function. *J Pediatr,* 210**,** 166-172 e1.

Chapter Four manuscript reproduced from Robinson et al (2016) Brown adipose tissue activation as measured by infrared thermography by mild anticipatory psychological stress in lean healthy females/ Lindsay J. Robinson, James M. Law, Michael E. Symonds, et al/Experimental Physiology 101. Copyright (c) [2016] [John Wiley and Sons]

https://physoc.onlinelibrary.wiley.com/doi/full/10.1113/EP085642%4010.1111/%28ISSN%291469-445X.StressThermoregulation

Chapter Five manuscript reproduced from The Journal of Diabetes, Metabolism and its complications on the Science Repository. All the work at Science Repository is licensed under a Creative Commons Attribution 4.0 International License Authors at Science Repository retain copyright.

## References


ACOSTA, F. M., MARTINEZ-TELLEZ, B., SANCHEZ-DELGADO, G., ALCANTARA, J. M. A., ACOSTA-MANZANO, P., MORALES-ARTACHO, A. J. & RUIZ, J. R. 2018. Physiological responses to acute cold exposure in young lean men. *PLoS One,* 13**,** e0196543.

ADAMCZAK, M. & WIECEK, A. 2013. The adipose tissue as an endocrine organ. *Semin Nephrology,* 33**,** 2-13.

ADMIRAAL, W. M., HOLLEMAN, F., BAHLER, L., SOETERS, M. R., HOEKSTRA, J. B. & VERBERNE, H. J. 2013. Combining 123I-metaiodobenzylguanidine SPECT/CT and 18F-FDG PET/CT for the assessment of brown adipose tissue activity in humans during cold exposure. *J Nucl Med,* 54**,** 208-12.

AHERNE, W. & HULL, D. 1966. Brown adipose tissue and heat production in the newborn infant. *J Pathol Bacteriol,* 91**,** 223-34.

AMMER, K. 2005. Temperature readings from thermal images are less dependent on the number of pixels of the measurement area than on variation of room temperature. *Thermol Int,* 15**,** 131-133.

AMMER, K. 2008. The Glamorgan Protocol for recording and evaluation of thermal images of the human body. *Thermol Int,* 18**,** 125-9.

AMMER, K. 2017. The challenge of objective evaluation of infrared thermal images in health sciences. *Thermol Int,* 27**,** 93-97.

AMMER, K. & RING, F. J. 2013. Standard Procedures for Infrared Imaging in Medicine. *Medical Infrared Imaging: Principles and Practices.* 2nd ed. Boca Raton: CRC Press.

ANDERSSON, J., ROSWALL, J., KJELLBERG, E., AHLSTROM, H., DAHLGREN, J. & KULLBERG, J. 2019. MRI estimates of brown adipose tissue in children - Associations to adiposity, osteocalcin, and thigh muscle volume. *Magn Reson Imaging,* 58**,** 135-142.

ANG, Q. Y., GOH, H. J., CAO, Y., LI, Y., CHAN, S. P., SWAIN, J. L., HENRY, C. J. & LEOW, M. K. 2017. A new method of infrared thermography for quantification of brown adipose tissue activation in healthy adults (TACTICAL): a randomized trial. *J Physiol Sci,* 67**,** 395-406.

ASTRUP, A., BULOW, J., CHRISTENSEN, N. J. & MADSEN, J. 1984. Ephedrine-induced thermogenesis in man: no role for interscapular brown adipose tissue. *Clin Sci (Lond),* 66**,** 179-86.

AU-YONG, I. T., THORN, N., GANATRA, R., PERKINS, A. C. & SYMONDS, M. E. 2009. Brown adipose tissue and seasonal variation in humans. *Diabetes,* 58**,** 2583-7.

AZZOPARDI, D., STROHM, B., MARLOW, N., BROCKLEHURST, P., DEIERL, A., EDDAMA, O., GOODWIN, J., HALLIDAY, H. L., JUSZCZAK, E., KAPELLOU, O., LEVENE, M., LINSELL, L., OMAR, O., THORESEN, M., TUSOR, N., WHITELAW, A., EDWARDS, A. D. & GROUP, T. S. 2014. Effects of hypothermia for perinatal asphyxia on childhood outcomes. *N Engl J Med,* 371**,** 140-9.

BAL, N. C., SAHOO, S. K., MAURYA, S. K. & PERIASAMY, M. 2018. The role of sarcolipin in muscle non-shivering thermogenesis. *Front Physiol,* 9**,** 1217.

BARBATELLI, G., MURANO, I., MADSEN, L., HAO, Q., JIMENEZ, M., KRISTIANSEN, K., GIACOBINO, J. P., DE MATTEIS, R. & CINTI, S. 2010. The emergence of cold-induced brown adipocytes in mouse white fat depots is determined predominantly by white to brown adipocyte transdifferentiation. *Am J Physiol Endocrinol Metab,* 298**,** E1244-53.

BARCLAY, J. L., AGADA, H., JANG, C., WARD, M., WETZIG, N. & HO, K. K. 2015. Effects of glucocorticoids on human brown adipocytes. *J Endocrinol,* 224**,** 139-47.

BARKER, D. J. P. 2007. Obesity and early life. *Obes Rev,* 8 Suppl 1**,** 45-9.

BARKER, D. J. P., ERIKSSON, J. G., FORSÉN, T. & OSMOND, C. 2002. Fetal origins of adult disease: strength of effects and biological basis. *International journal of epidemiology,* 31**,** 1235.

BARLOW, S. E. & EXPERT, C. 2007. Expert committee recommendations regarding the prevention, assessment, and treatment of child and adolescent overweight and obesity: summary report. *Pediatrics,* 120 Suppl 4**,** S164-92.

BARRINGTON, S. F. & MAISEY, M. N. 1996. Skeletal muscle uptake of fluorine-18-FDG: effect of oral diazepam. *J Nucl Med,* 37**,** 1127-9.

BARTELT, A., BRUNS, O. T., REIMER, R., HOHENBERG, H., ITTRICH, H., PELDSCHUS, K., KAUL, M. G., TROMSDORF, U. I., WELLER, H., WAURISCH, C., EYCHMULLER, A., GORDTS, P. L., RINNINGER, F., BRUEGELMANN, K., FREUND, B., NIELSEN, P., MERKEL, M. & HEEREN, J. 2011. Brown adipose tissue activity controls triglyceride clearance. *Nat Med,* 17**,** 200-5.

BARTELT, A. & HEEREN, J. 2014. Adipose tissue browning and metabolic health. *Nat Rev Endocrinol,* 10**,** 24-36.

BARTESAGHI, S., HALLEN, S., HUANG, L., SVENSSON, P. A., MOMO, R. A., WALLIN, S., CARLSSON, E. K., FORSLOW, A., SEALE, P. & PENG, X. R. 2015. Thermogenic activity of UCP1 in human white fat-derived beige adipocytes. *Mol Endocrinol,* 29**,** 130-9.

BARTNESS, T. J., VAUGHAN, C. H. & SONG, C. K. 2010. Sympathetic and sensory innervation of brown adipose tissue. *Int J Obes (Lond),* 34 Suppl 1**,** S36-42.

BASKIN, A. S., LINDERMAN, J. D., BRYCHTA, R. J., MCGEHEE, S., ANFLICK-CHAMES, E., CERO, C., JOHNSON, J. W., O'MARA, A. E., FLETCHER, L. A., LEITNER, B. P., DUCKWORTH, C. J., HUANG, S., CAI, H., GARRAFFO, H. M., MILLO, C. M., DIECKMANN, W., TOLSTIKOV, V., CHEN, E. Y., GAO, F., NARAIN, N. R., KIEBISH, M. A., WALTER, P. J., HERSCOVITCH, P., CHEN, K. Y. & CYPESS, A. M. 2018. Regulation of human adipose tissue activation, gallbladder size, and bile acid metabolism by a beta3-adrenergic receptor agonist. *Diabetes,* 67**,** 2113-2125.

BEGAYE, B., PIAGGI, P., THEARLE, M. S., HASKIE, K., WALTER, M., SCHLOGL, M., BONFIGLIO, S., KRAKOFF, J. & VINALES, K. L. 2018. Norepinephrine and T4 are predictors of fat mass gain in humans with cold-induced brown adipose tissue activation. *J Clin Endocrinol Metab,* 103**,** 2689-2697.

BENJAMINI, Y. & YEKUTIELI, D. 2001. The control of the false discovery rate in multiple testing under dependency. *Annals of Statistics,* 29**,** 1165-1188.

BERTHOLET, A. M. & KIRICHOK, Y. 2017. UCP1: A transporter for H+ and fatty acid anions. *Biochimie,* 134**,** 28-34.

BERTHOLET, A. M. & KIRICHOK, Y. 2018. The mechanism FA-dependent H(+) transport by UCP1. *Handb Exp Pharmacol*.

BIANCHI, A., BRUCE, J., COOPER, A. L., CHILDS, C., KOHLI, M., MORRIS, I. D., MORRIS-JONES, P. & ROTHWELL, N. J. 1989. Increased brown adipose tissue activity in children with malignant disease. *Horm Metab Res,* 21**,** 640-1.

BIRO, F. M., PINNEY, S. M., HUANG, B., BAKER, E. R., WALT CHANDLER, D. & DORN, L. D. 2014. Hormone changes in peripubertal girls. *J Clin Endocrinol Metab,* 99**,** 3829-35.

BLONDIN, D. P., FRISCH, F., PHOENIX, S., GUERIN, B., TURCOTTE, E. E., HAMAN, F., RICHARD, D. & CARPENTIER, A. C. 2017a. Inhibition of intracellular triglyceride lipolysis suppresses cold-induced brown adipose tissue metabolism and increases shivering in humans. *Cell Metab,* 25**,** 438-447.

BLONDIN, D. P., LABBE, S. M., NOLL, C., KUNACH, M., PHOENIX, S., GUERIN, B., TURCOTTE, E. E., HAMAN, F., RICHARD, D. & CARPENTIER, A. C. 2015a. Selective

impairment of glucose but not fatty acid or oxidative metabolism in brown adipose tissue of subjects with type 2 diabetes. *Diabetes,* 64**,** 2388-97.

BLONDIN, D. P., LABBE, S. M., PHOENIX, S., GUERIN, B., TURCOTTE, E. E., RICHARD, D., CARPENTIER, A. C. & HAMAN, F. 2015b. Contributions of white and brown adipose tissues and skeletal muscles to acute cold-induced metabolic responses in healthy men. *J Physiol,* 593**,** 701-14.

BLONDIN, D. P., LABBE, S. M., TINGELSTAD, H. C., NOLL, C., KUNACH, M., PHOENIX, S., GUERIN, B., TURCOTTE, E. E., CARPENTIER, A. C., RICHARD, D. & HAMAN, F. 2014. Increased brown adipose tissue oxidative capacity in cold-acclimated humans. *J Clin Endocrinol Metab,* 99**,** E438-46.

BLONDIN, D. P., TINGELSTAD, H. C., NOLL, C., FRISCH, F., PHOENIX, S., GUERIN, B., TURCOTTE, E. E., RICHARD, D., HAMAN, F. & CARPENTIER, A. C. 2017b. Dietary fatty acid metabolism of brown adipose tissue in cold-acclimated men. *Nat Commun,* 8**,** 14146.

BLOOR, I. D. & SYMONDS, M. E. 2014. Sexual dimorphism in white and brown adipose tissue with obesity and inflammation. *Horm Behav,* 66**,** 95-103.

BONNOT, E. 1908. The Interscapular Gland. *J Anat Physiol,* 43**,** 43-58.

BOON, M. R., BAKKER, L. E., VAN DER LINDEN, R. A., PEREIRA ARIAS-BOUDA, L., SMIT, F., VERBERNE, H. J., VAN MARKEN LICHTENBELT, W. D., JAZET, I. M. & RENSEN, P. C. 2014. Supraclavicular skin temperature as a measure of 18F-FDG uptake by BAT in human subjects. *PLoS One,* 9**,** e98822.

BRAY, G. A. 2004. Medical consequences of obesity. *The Journal of Clinical Endocrinology & Metabolism,* 89**,** 2583-2589.

BRENDLE, C., WERNER, M. K., SCHMADL, M., LA FOUGERE, C., NIKOLAOU, K., STEFAN, N. & PFANNENBERG, C. 2018. Correlation of brown adipose tissue with other body fat compartments and patient characteristics: a retrospective analysis in a large patient cohort using PET/CT. *Acad Radiol,* 25**,** 102-110.

BRILLON, D. J., ZHENG, B., CAMPBELL, R. G. & MATTHEWS, D. E. 1995. Effect of cortisol on energy expenditure and amino acid metabolism in humans. *Am J Physiol,* 268**,** E501-13.

BROEDERS, E., BOUVY, N. D. & VAN MARKEN LICHTENBELT, W. D. 2015a. Endogenous ways to stimulate brown adipose tissue in humans. *Ann Med,* 47**,** 123-32.

BROEDERS, E. P., NASCIMENTO, E. B., HAVEKES, B., BRANS, B., ROUMANS, K. H., TAILLEUX, A., SCHAART, G., KOUACH, M., CHARTON, J., DEPREZ, B., BOUVY, N. D., MOTTAGHY, F., STAELS, B., VAN MARKEN LICHTENBELT, W. D. & SCHRAUWEN, P. 2015b. The Bile Acid Chenodeoxycholic Acid Increases Human Brown Adipose Tissue Activity. *Cell Metab,* 22**,** 418-26.

BROUGHAM, M. F. & WALLACE, W. H. 2005. Subfertility in children and young people treated for solid and haematological malignancies. *Br J Haematol,* 131**,** 143-55.

CANNON, B. & NEDERGAARD, J. 2004. Brown adipose tissue: function and physiological significance. *Physiol Rev,* 84**,** 277-359.

CANNON, B. & NEDERGAARD, J. 2012. Cell biology: Neither brown nor white. *Nature,* 488**,** 286-7.

CANNON, B. & NEDERGAARD, J. 2017. Brown Adipose Tissue: Development and Function. *Fetal and Neonatal Physiology*

5th ed.: Elsevier BV.

CANNON, W. B. 1916. *Bodily changes in pain, hunger, fear and rage - an account of recent researches into the function of emotional excitement*, D. Appleton.

CARDONE, D., PINTI, P. & MERLA, A. 2015. Thermal infrared imaging-based computational psychophysiology for psychometrics. *Computational and Mathematical Methods in Medicine*.

CAREY, A. L., FORMOSA, M. F., VAN EVERY, B., BERTOVIC, D., EIKELIS, N., LAMBERT, G. W., KALFF, V., DUFFY, S. J., CHERK, M. H. & KINGWELL, B. A. 2013. Ephedrine activates brown adipose tissue in lean but not obese humans. *Diabetologia,* 56**,** 147-55.

CAREY, A. L., PAJTAK, R., FORMOSA, M. F., VAN EVERY, B., BERTOVIC, D. A., ANDERSON, M. J., EIKELIS, N., LAMBERT, G. W., KALFF, V., DUFFY, S. J., CHERK, M. H. & KINGWELL, B. A. 2015. Chronic ephedrine administration decreases brown adipose tissue activity in a randomised controlled human trial: implications for obesity. *Diabetologia,* 58**,** 1045-54.

CAREY, A. L., VORLANDER, C., REDDY-LUTHMOODOO, M., NATOLI, A. K., FORMOSA, M. F., BERTOVIC, D. A., ANDERSON, M. J., DUFFY, S. J. & KINGWELL, B. A. 2014. Reduced UCP-1 content in in vitro differentiated beige/brite adipocytes derived from preadipocytes of human subcutaneous white adipose tissues in obesity. *PLoS One,* 9**,** e91997.

CARPENTIER, A. C., BLONDIN, D. P., VIRTANEN, K. A., RICHARD, D., HAMAN, F. & TURCOTTE, E. E. 2018. Brown adipose tissue energy metabolism in humans. *Front Endocrinol (Lausanne),* 9**,** 447.

CARSKADON, M. A. & ACEBO, C. 1993. A self-administered rating scale for pubertal development. *J Adolesc Health,* 14**,** 190-5.

CASTELLANI, J. W. & YOUNG, A. J. 2016. Human physiological responses to cold exposure: Acute responses and acclimatization to prolonged exposure. *Auton Neurosci,* 196**,** 63-74.

CELI, F. S., LE, T. N. & NI, B. 2015. Physiology and relevance of human adaptive thermogenesis response. *Trends Endocrinol Metab,* 26**,** 238-47.

CHALFANT, J. S., SMITH, M. L., HU, H. H., DOREY, F. J., GOODARZIAN, F., FU, C. H. & GILSANZ, V. 2012. Inverse association between brown adipose tissue activation and white adipose tissue accumulation in successfully treated pediatric malignancy. *Am J Clin Nutr,* 95**,** 1144-9.

CHAN, J. M., RIMM, E. B., COLDITZ, G. A., STAMPFER, M. J. & WILLETT, W. C. 1994. Obesity, fat distribution, and weight gain as risk factors for clinical diabetes in men. *Diabetes care,* 17**,** 961-969.

CHARKOUDIAN, N., STEPHENS, D. P., PIRKLE, K. C., KOSIBA, W. A. & JOHNSON, J. M. 1999. Influence of female reproductive hormones on local thermal control of skin blood flow. *J Appl Physiol (1985),* 87**,** 1719-23.

CHEN, K. Y., CYPESS, A. M., LAUGHLIN, M. R., HAFT, C. R., HU, H. H., BREDELLA, M. A., ENERBACK, S., KINAHAN, P. E., LICHTENBELT, W., LIN, F. I., SUNDERLAND, J. J., VIRTANEN, K. A. & WAHL, R. L. 2016. Brown Adipose Reporting Criteria in Imaging STudies (BARCIST 1.0): Recommendations for Standardized FDG-PET/CT Experiments in Humans. *Cell Metab,* 24**,** 210-22.

CHENG, W., ZHU, Z., JIN, X., CHEN, L., ZHUANG, H. & LI, F. 2012. Intense FDG activity in the brown adipose tissue in omental and mesenteric regions in a patient with malignant pheochromocytoma. *Clin Nucl Med,* 37**,** 514-5.

CHONDRONIKOLA, M., VOLPI, E., BORSHEIM, E., CHAO, T., PORTER, C., ANNAMALAI, P., YFANTI, C., LABBE, S. M., HURREN, N. M., MALAGARIS, I., CESANI, F. & SIDOSSIS, L. S. 2016. Brown adipose tissue is linked to a distinct thermoregulatory response to mild cold in people. *Front Physiol,* 7**,** 129.

CHONDRONIKOLA, M., VOLPI, E., BORSHEIM, E., PORTER, C., ANNAMALAI, P., ENERBACK, S., LIDELL, M. E., SARAF, M. K., LABBE, S. M., HURREN, N. M., YFANTI, C.,

CHAO, T., ANDERSEN, C. R., CESANI, F., HAWKINS, H. & SIDOSSIS, L. S. 2014. Brown adipose tissue improves whole-body glucose homeostasis and insulin sensitivity in humans. *Diabetes,* 63**,** 4089-99.

CHRISTENSEN, C. R., CLARK, P. B. & MORTON, K. A. 2006. Reversal of hypermetabolic brown adipose tissue in F-18 FDG PET imaging. *Clin Nucl Med,* 31**,** 193-6.

CICOGNANI, A., PASINI, A., PESSION, A., PIRAZZOLI, P., BURNELLI, R., BARBIERI, E., MAZZANTI, L. & CACCIARI, E. 2003. Gonadal function and pubertal development after treatment of a childhood malignancy. *J Pediatr Endocrinol Metab,* 16 Suppl 2**,** 321-6.

COHADE, C., MOURTZIKOS, K. A. & WAHL, R. L. 2003. "USA-Fat": prevalence is related to ambient outdoor temperature-evaluation with 18F-FDG PET/CT. *J Nucl Med,* 44**,** 1267-70.

COLE, T. J., FREEMAN, J. V. & PREECE, M. A. 1995. Body mass index reference curves for the UK, 1990. *Arch Dis Child,* 73**,** 25-9.

COLE, T. J. & LOBSTEIN, T. 2012. Extended international (IOTF) body mass index cut-offs for thinness, overweight and obesity. *Pediatr Obes,* 7**,** 284-94.

COLLABORATION, N. C. D. R. F. 2017a. Worldwide trends in body-mass index, underweight, overweight, and obesity from 1975 to 2016: a pooled analysis of 2416 population-based measurement studies in 128.9 million children, adolescents, and adults. *Lancet,* 390**,** 2627-2642.

COLLABORATION, N. R. F. 2017b. Worldwide trends in body-mass index, underweight, overweight, and obesity from 1975 to 2016: a pooled analysis of 2416 population-based measurement studies in 128.9 million children, adolescents, and adults. *The Lancet,* 390**,** 2627-2642.

COOLBAUGH, C. L., BUSH, E. C., GALENTI, E. S., WELCH, E. B. & TOWSE, T. F. 2018. An individualized, perception-based protocol to investigate human physiological responses to cooling. *Front Physiol,* 9**,** 195.

COUSINS, J., CZACHOWSKI, M., MUTHUKRISHNAN, A. & CURRIE, G. 2017. Pediatric Brown Adipose Tissue on (18)F-FDG PET: Diazepam Intervention. *J Nucl Med Technol,* 45**,** 82-86.

CRANDALL, J. P., GAJWANI, P., O, J. H., MAWHINNEY, D. D., STERZER, F. & WAHL, R. L. 2019. Repeatability of brown adipose tissue measurements on FDG PET/CT following a simple cooling procedure for BAT activation. *PLoS One,* 14**,** e0214765.

CRONIN, C. G., PRAKASH, P., DANIELS, G. H., BOLAND, G. W., KALRA, M. K., HALPERN, E. F., PALMER, E. L. & BLAKE, M. A. 2012. Brown fat at PET/CT: correlation with patient characteristics. *Radiology,* 263**,** 836-42.

CYPESS, A. M., CHEN, Y. C., SZE, C., WANG, K., ENGLISH, J., CHAN, O., HOLMAN, A. R., TAL, I., PALMER, M. R., KOLODNY, G. M. & KAHN, C. R. 2012. Cold but not sympathomimetics activates human brown adipose tissue in vivo. *Proc Natl Acad Sci U S A,* 109**,** 10001-5.

CYPESS, A. M., HAFT, C. R., LAUGHLIN, M. R. & HU, H. H. 2014. Brown fat in humans: consensus points and experimental guidelines. *Cell Metab,* 20**,** 408-15.

CYPESS, A. M., LEHMAN, S., WILLIAMS, G., TAL, I., RODMAN, D., GOLDFINE, A. B., KUO, F. C., PALMER, E. L., TSENG, Y. H., DORIA, A., KOLODNY, G. M. & KAHN, C. R. 2009. Identification and importance of brown adipose tissue in adult humans. *N Engl J Med,* 360**,** 1509-17.

CYPESS, A. M., WEINER, L. S., ROBERTS-TOLER, C., FRANQUET ELIA, E., KESSLER, S. H., KAHN, P. A., ENGLISH, J., CHATMAN, K., TRAUGER, S. A., DORIA, A. & KOLODNY, G. M. 2015. Activation of human brown adipose tissue by a beta3-adrenergic receptor agonist. *Cell Metab,* 21**,** 33-8.

CYPESS, A. M., WHITE, A. P., VERNOCHET, C., SCHULZ, T. J., XUE, R., SASS, C. A., HUANG, T. L., ROBERTS-TOLER, C., WEINER, L. S., SZE, C., CHACKO, A. T., DESCHAMPS, L. N., HERDER, L. M., TRUCHAN, N., GLASGOW, A. L., HOLMAN, A. R., GAVRILA, A., HASSELGREN, P. O., MORI, M. A., MOLLA, M. & TSENG, Y. H. 2013. Anatomical localization, gene expression profiling and functional characterization of adult human neck brown fat. *Nat Med,* 19**,** 635-9.

DAWKINS, M. J. & HULL, D. 1965. The Production of Heat by Fat. *Sci Am,* 213**,** 62-7.

DAWKINS, M. J. & SCOPES, J. W. 1965. Non-shivering thermogenesis and brown adipose tissue in the human new-born infant. *Nature,* 206**,** 201-2.

DEBOER, M. D. 2011. Ethnicity, obesity and the metabolic syndrome: implications on assessing risk and targeting intervention. *Expert Rev Endocrinol Metab,* 6**,** 279-289.

DENG, C., PAOLONI-GIACOBINO, A., KUEHNE, F., BOSS, O., REVELLI, J. P., MOINAT, M., CAWTHORNE, M. A., MUZZIN, P. & GIACOBINO, J. P. 1996. Respective degree of expression of beta 1-, beta 2- and beta 3-adrenoceptors in human brown and white adipose tissues. *Br J Pharmacol,* 118**,** 929-34.

DENG, J., NEFF, L. M., RUBERT, N. C., ZHANG, B., SHORE, R. M., SAMET, J. D., NELSON, P. C. & LANDSBERG, L. 2018. MRI characterization of brown adipose tissue under

thermal challenges in normal weight, overweight, and obese young men. *J Magn Reson Imaging,* 47**,** 936-947.

DENG, J., SCHOENEMAN, S. E., ZHANG, H., KWON, S., RIGSBY, C. K., SHORE, R. M. & JOSEFSON, J. L. 2015. MRI characterization of brown adipose tissue in obese and normal-weight children. *Pediatr Radiol,* 45**,** 1682-9.

DICKERSON, S. S. & KEMENY, M. E. 2004. Acute stressors and cortisol responses: a theoretical integration and synthesis of laboratory research. *Psychol Bull,* 130**,** 355-91.

DINSDALE, H., RIDLER, C. & ELLS, L. 2011. A simple guide to classifying body mass index in children. *National Obesity Observatory: Oxford*.

DODT, E. & ZOTTERMAN, Y. 1952. The discharge of specific cold fibres at high temperatures; the paradoxical cold. *Acta Physiol Scand,* 26**,** 358-65.

DRUBACH, L. A., PALMER, E. L., 3RD, CONNOLLY, L. P., BAKER, A., ZURAKOWSKI, D. & CYPESS, A. M. 2011. Pediatric brown adipose tissue: detection, epidemiology, and differences from adults. *J Pediatr,* 159**,** 939-44.

DUCHEN, M. R. & SZABADKAI, G. 2010. Roles of mitochondria in human disease. *Essays Biochem,* 47**,** 115-37.

EL HADI, H., FRASCATI, A., GRANZOTTO, M., SILVESTRIN, V., FERLINI, E., VETTOR, R. & ROSSATO, M. 2016. Infrared thermography for indirect assessment of activation of brown adipose tissue in lean and obese male subjects. *Physiol Meas,* 37**,** N118-N128.

ENERBACK, S. 2010. Human brown adipose tissue. *Cell Metab,* 11**,** 248-52.

ENGEL, H., STEINERT, H., BUCK, A., BERTHOLD, T., HUCH BONI, R. A. & VON SCHULTHESS, G. K. 1996. Whole-body PET: physiological and artifactual fluorodeoxyglucose accumulations. *J Nucl Med,* 37**,** 441-6.

ENTRINGER, S., RASMUSSEN, J., COOPER, D. M., IKENOUE, S., WAFFARN, F., WADHWA, P. D. & BUSS, C. 2017. Association between supraclavicular brown adipose tissue composition at birth and adiposity gain from birth to 6 months of age. *Pediatr Res,* 82**,** 1017-1021.

ERIKSSON, J. G., FORSEN, T., TUOMILEHTO, J., OSMOND, C. & BARKER, D. J. 2003. Early adiposity rebound in childhood and risk of Type 2 diabetes in adult life. *Diabetologia,* 46**,** 190-4.

FALKSTEDT, D., HEMMINGSSON, T., RASMUSSEN, F. & LUNDBERG, I. 2006. Body mass index in late adolescence and its association with coronary heart disease and stroke in middle age among Swedish men. *International Journal of Obesity,* 31**,** 777.

FAUL, F., ERDFELDER, E., LANG, A. G. & BUCHNER, A. 2007. G*Power 3: a flexible statistical power analysis program for the social, behavioral, and biomedical sciences. *Behav Res Methods,* 39**,** 175-91.

FAZELI, P. K., LUN, M., KIM, S. M., BREDELLA, M. A., WRIGHT, S., ZHANG, Y., LEE, H., CATANA, C., KLIBANSKI, A., PATWARI, P. & STEINHAUSER, M. L. 2015. FGF21 and the late adaptive response to starvation in humans. *J Clin Invest,* 125**,** 4601-11.

FDA. 2005. *NDA 21-870: FDG F 18 Injection* [Online]. Available: https://www.accessdata.fda.gov/drugsatfda_docs/label/2004/21768lbl.pdf [Accessed 21st October 2019 2019].

FEDORENKO, A., LISHKO, POLINA V. & KIRICHOK, Y. 2012. Mechanism of fatty-acid-dependent UCP1 uncoupling in brown fat mitochondria. *Cell,* 151**,** 400-413.

FELDMANN, H. M., GOLOZOUBOVA, V., CANNON, B. & NEDERGAARD, J. 2009. UCP1 ablation induces obesity and abolishes diet-induced thermogenesis in mice exempt from thermal stress by living at thermoneutrality. *Cell Metab,* 9**,** 203-9.

FIELD, A. E., COOK, N. R. & GILLMAN, M. W. 2005. Weight status in childhood as a predictor of becoming overweight or hypertensive in early adulthood **. *Obesity Research,* 13**,** 163-169.

FLETCHER, E., LEECH, R., MCNAUGHTON, S. A., DUNSTAN, D. W., LACY, K. E. & SALMON, J. 2015. Is the relationship between sedentary behaviour and cardiometabolic health in adolescents independent of dietary intake? A systematic review. *Obes Rev,* 16**,** 795-805.

FRANZ, D., KARAMPINOS, D. C., RUMMENY, E. J., SOUVATZOGLOU, M., BEER, A. J., NEKOLLA, S. G., SCHWAIGER, M. & EIBER, M. 2015. Discrimination between brown and white adipose tissue using a 2-point dixon water-fat separation method in simultaneous PET/MRI. *J Nucl Med,* 56**,** 1742-7.

FREEDMAN, D. S. & SHERRY, B. 2009. The validity of BMI as an indicator of body fatness and risk among children. *Pediatrics,* 124 Suppl 1**,** S23-34.

FUKUCHI, K., ONO, Y., NAKAHATA, Y., OKADA, Y., HAYASHIDA, K. & ISHIDA, Y. 2003. Visualization of interscapular brown adipose tissue using (99m)Tc-tetrofosmin in pediatric patients. *J Nucl Med,* 44**,** 1582-5.

FUKUCHI, K., TATSUMI, M., ISHIDA, Y., OKU, N., HATAZAWA, J. & WAHL, R. L. 2004. Radionuclide imaging metabolic activity of brown adipose tissue in a patient with pheochromocytoma. *Exp Clin Endocrinol Diabetes,* 112**,** 601-3.

GARCIA, C., BANDARU, V., VAN NOSTRAND, D., CHENNUPATI, S., ATKINS, F., ACIO, E., KULKARNI, K. & MAJD, M. 2010. Effective reduction of brown fat FDG uptake by controlling environmental temperature prior to PET scan: an expanded case series. *Mol Imaging Biol,* 12**,** 652-6.

GARCIA, C. A., VAN NOSTRAND, D., ATKINS, F., ACIO, E., BUTLER, C., ESPOSITO, G., KULKARNI, K. & MAJD, M. 2006. Reduction of brown fat 2-deoxy-2-[F-18]fluoro-D-glucose uptake by controlling environmental temperature prior to positron emission tomography scan. *Mol Imaging Biol,* 8**,** 24-9.

GARROW, J. S. 1987. Energy balance in man - an overview. *Am J Clin Nutr,* 45**,** 1114-9.

GASHI, G., MADOERIN, P., MAUSHART, C. I., MICHEL, R., SENN, J. R., BIERI, O. & BETZ, M. J. 2019. MRI characteristics of supraclavicular brown adipose tissue in relation to cold-induced thermogenesis in healthy human adults. *J Magn Reson Imaging*.

GATIDIS, S., SCHMIDT, H., PFANNENBERG, C. A., NIKOLAOU, K., SCHICK, F. & SCHWENZER, N. F. 2016. Is it possible to detect activated brown adipose tissue in humans using single-time-point infrared thermography under thermoneutral conditions? impact of BMI and subcutaneous adipose tissue thickness. *PLoS One,* 11**,** e0151152.

GELFAND, M. J., O'HARA S, M., CURTWRIGHT, L. A. & MACLEAN, J. R. 2005. Pre-medication to block [(18)F]FDG uptake in the brown adipose tissue of pediatric and adolescent patients. *Pediatr Radiol,* 35**,** 984-90.

GIFFORD, A., TOWSE, T. F., WALKER, R. C., AVISON, M. J. & WELCH, E. B. 2016. Characterizing active and inactive brown adipose tissue in adult humans using PET-CT and MR imaging. *Am J Physiol Endocrinol Metab,* 311**,** E95-E104.

GILLMAN, M. W. 2005. Developmental origins of health and disease. *N Engl J Med,* 353**,** 1848-50.

GILSANZ, V., CHUNG, S. A., JACKSON, H., DOREY, F. J. & HU, H. H. 2011. Functional brown adipose tissue is related to muscle volume in children and adolescents. *J Pediatr,* 158**,** 722-6.

GILSANZ, V., HU, H. H. & KAJIMURA, S. 2013. Relevance of brown adipose tissue in infancy and adolescence. *Pediatr Res,* 73**,** 3-9.

GILSANZ, V., HU, H. H., SMITH, M. L., GOODARZIAN, F., CARCICH, S. L., WARBURTON, N. M. & MALOGOLOWKIN, M. 2012a. The depiction of brown adipose tissue is related to disease status in pediatric patients with lymphoma. *Am J Roentgenol,* 198**,** 909-13.

GILSANZ, V., SMITH, M. L., GOODARZIAN, F., KIM, M., WREN, T. A. & HU, H. H. 2012b. Changes in brown adipose tissue in boys and girls during childhood and puberty. *J Pediatr,* 160**,** 604-609 e1.

GOLDEN, E. T., DICKSON, P. & SIMONEAUX, S. 2018. Brown fat necrosis with calcifications in the newborn: Risk factors, radiographic findings, and clinical course. *Indian J Radiol Imaging,* 28**,** 107-110.

GONZALEZ SOLVEYRA, C., ROMEO, H. E., ROSENSTEIN, R. E., ESTEVEZ, A. G. & CARDINALI, D. P. 1988. Benzodiazepine binding sites in rat interscapular brown adipose tissue: effect of cold environment, denervation and endocrine ablations. *Life Sci,* 42**,** 393-402.

GRAY, J. A. 1987. *The psychology of fear and stress*, CUP Archive.

GREANEY, J. L., STANHEWICZ, A. E., KENNEY, W. L. & ALEXANDER, L. M. 2015. Impaired increases in skin sympathetic nerve activity contribute to age-related decrements in reflex cutaneous vasoconstriction. *J Physiol,* 593**,** 2199-211.

GREEN, G. J., WEITZMAN, S. S. & PENCHARZ, P. B. 2008. Resting energy expenditure in children newly diagnosed with stage IV neuroblastoma. *Pediatr Res,* 63**,** 332-6.

GREENE, M. A., BOLTAX, A. J., LUSTIG, G. A. & ROGOW, E. 1965. Circulatory Dynamics during the Cold Pressor Test. *Am J Cardiol,* 16**,** 54-60.

GULLER, I., MCNAUGHTON, S., CROWLEY, T., GILSANZ, V., KAJIMURA, S., WATT, M. & RUSSELL, A. P. 2015. Comparative analysis of microRNA expression in mouse and human brown adipose tissue. *BMC Genomics,* 16**,** 820.

GUNNELL, D. J., FRANKEL, S. J., NANCHAHAL, K., PETERS, T. J. & DAVEY SMITH, G. 1998. Childhood obesity and adult cardiovascular mortality: a 57-y follow-up study based on the Boyd Orr cohort. *Am J Clin Nutr,* 67**,** 1111.

GUO, S. S., ROCHE, A. F., CHUMLEA, W. C., GARDNER, J. D. & SIERVOGEL, R. M. 1994. The predictive value of childhood body mass index values for overweight at age 35 y. *Am J Clin Nutr,* 59**,** 810-9.

GUPTA, P., BABYN, P. S., SHAMMAS, A. & MILLER, S. F. 2011. Brown fat distribution in the chest wall of infants-normal appearance, distribution and evolution on CT scans of the chest. *Pediatr Radiol,* 41**,** 1020-7.

HALL, J. A., RIBICH, S., CHRISTOFFOLETE, M. A., SIMOVIC, G., CORREA-MEDINA, M., PATTI, M. E. & BIANCO, A. C. 2010. Absence of thyroid hormone activation during development underlies a permanent defect in adaptive thermogenesis. *Endocrinology,* 151**,** 4573-82.

HANKIR, M. K., KRANZ, M., KEIPERT, S., WEINER, J., ANDREASEN, S. G., KERN, M., PATT, M., KLOTING, N., HEIKER, J. T., BRUST, P., HESSE, S., JASTROCH, M. & FENSKE, W. K. 2017. Dissociation Between Brown Adipose Tissue (18)F-FDG Uptake and Thermogenesis in Uncoupling Protein 1-Deficient Mice. *J Nucl Med,* 58**,** 1100-1103.

HANRAHAN, K., MCCARTHY, A. M., KLEIBER, C., LUTGENDORF, S. & TSALIKIAN, E. 2006. Strategies for salivary cortisol collection and analysis in research with children. *Appl Nurs Res,* 19**,** 95-101.

HANSSEN, M. J., BROEDERS, E., SAMMS, R. J., VOSSELMAN, M. J., VAN DER LANS, A. A., CHENG, C. C., ADAMS, A. C., VAN MARKEN LICHTENBELT, W. D. & SCHRAUWEN, P. 2015a. Serum FGF21 levels are associated with brown adipose tissue activity in humans. *Sci Rep,* 5**,** 10275.

HANSSEN, M. J., VAN DER LANS, A. A., BRANS, B., HOEKS, J., JARDON, K. M., SCHAART, G., MOTTAGHY, F. M., SCHRAUWEN, P. & VAN MARKEN LICHTENBELT, W. D. 2016. Short-term Cold Acclimation Recruits Brown Adipose Tissue in Obese Humans. *Diabetes,* 65**,** 1179-89.

HANSSEN, M. J., WIERTS, R., HOEKS, J., GEMMINK, A., BRANS, B., MOTTAGHY, F. M., SCHRAUWEN, P. & VAN MARKEN LICHTENBELT, W. D. 2015b. Glucose uptake in human brown adipose tissue is impaired upon fasting-induced insulin resistance. *Diabetologia,* 58**,** 586-95.

HANY, T. F., GHAREHPAPAGH, E., KAMEL, E. M., BUCK, A., HIMMS-HAGEN, J. & VON SCHULTHESS, G. K. 2002. Brown adipose tissue: a factor to consider in symmetrical tracer uptake in the neck and upper chest region. *Eur J Nucl Med Mol Imaging,* 29**,** 1393-8.

HAQ, T., CRANE, J. D., KANJI, S., GUNN, E., TARNOPOLSKY, M. A., GERSTEIN, H. C., STEINBERG, G. R. & MORRISON, K. M. 2017. Optimizing the methodology for measuring supraclavicular skin temperature using infrared thermography; implications for measuring brown adipose tissue activity in humans. *Sci Rep,* 7**,** 11934.

HARDY, J. D., DU BOIS, E. F. & SODERSTROM, G. 1938. The technic of measuring radiation and convection: one figure. *The Journal of Nutrition,* 15**,** 461-475.

HARDY, J. D. & OPPEL, T. W. 1938. Studies in Temperature Sensation. Iv. The Stimulation of Cold Sensation by Radiation. *J Clin Invest,* 17**,** 771-8.

HARMS, M. & SEALE, P. 2013. Brown and beige fat: development, function and therapeutic potential. *Nat Med,* 19**,** 1252-63.

HARTWIG, V., GUIDUCCI, L., MARINELLI, M., PISTOIA, L., TEGRIMI, T. M., IERVASI, G., QUINONES-GALVAN, A. & L'ABBATE, A. 2017. Multimodal imaging for the detection of brown adipose tissue activation in women: a pilot study using NIRS and infrared thermography. *J Healthc Eng,* 2017**,** 5986452.

HATAI, S. 1902. On the presence in human embryos of an interscapular gland corresponding to the so-called hibernating gland of lower mammals. *Anat Anz,* 21**,** 369-373.

HEATON, G. M., WAGENVOORD, R. J., KEMP JR, A. & NICHOLLS, D. G. 1978. brown-adipose-tissue mitochondria: photoaffinity labelling of the regulatory site of energy dissipation. *European Journal of Biochemistry,* 82**,** 515-521.

HEATON, J. M. 1972. The distribution of brown adipose tissue in the human. *J Anat,* 112**,** 35-9.

HEINEN, C. A., ZHANG, Z., KLIEVERIK, L. P., DE WIT, T. C., POEL, E., YAQUB, M., BOELEN, A., KALSBEEK, A., BISSCHOP, P. H., VAN TROTSENBURG, A. S. P., VERBERNE, H. J., BOOIJ, J. & FLIERS, E. 2018. Effects of intravenous thyrotropin-releasing hormone on (18)F-fluorodeoxyglucose uptake in human brown adipose tissue: a randomized controlled trial. *Eur J Endocrinol,* 179**,** 31-38.

HIGGINS, J. N., HADDOCK, J. A. & SHAW, D. G. 1993. Case report: soft tissue and perivisceral calcification occurring in an infant: a case of brown fat necrosis. *Br J Radiol,* 66**,** 366-8.

HIMMS-HAGEN, J., CUI, J. & LYNN SIGURDSON, S. 1990. Sympathetic and sensory nerves in control of growth of brown adipose tissue: Effects of denervation and of capsaicin. *Neurochem Int,* 17**,** 271-9.

HIMMS-HAGEN, J. & DESAUTELS, M. 1978. A mitochondrial defect in brown adipose tissue of the obese (obob) mouse: reduced binding of purine nucleotides and a failure to respond to cold by an increase in binding. *Biochemical and biophysical research communications,* 83**,** 628-634.

HIRSCH, J. D. 1984. Pharmacological and physiological properties of benzodiazepine binding sites in rodent brown adipose tissue. *Comp Biochem Physiol C,* 77**,** 339-43.

HOLSTILA, M., PESOLA, M., SAARI, T., KOSKENSALO, K., RAIKO, J., BORRA, R. J., NUUTILA, P., PARKKOLA, R. & VIRTANEN, K. A. 2017. MR signal-fat-fraction analysis and T2* weighted imaging measure BAT reliably on humans without cold exposure. *Metabolism,* 70**,** 23-30.

HOLSTILA, M., VIRTANEN, K. A., GRONROOS, T. J., LAINE, J., LEPOMAKI, V., SAUNAVAARA, J., LISINEN, I., KOMU, M., HANNUKAINEN, J. C., NUUTILA, P., PARKKOLA, R. & BORRA, R. J. 2013. Measurement of brown adipose tissue mass using a novel dual-echo magnetic resonance imaging approach: a validation study. *Metabolism,* 62**,** 1189-98.

HONG, T. S., SHAMMAS, A., CHARRON, M., ZUKOTYNSKI, K. A., DRUBACH, L. A. & LIM, R. 2011. Brown adipose tissue 18F-FDG uptake in pediatric PET/CT imaging. *Pediatr Radiol,* 41**,** 759-68.

HU, H. H., CHUNG, S. A., NAYAK, K. S., JACKSON, H. A. & GILSANZ, V. 2011. Differential computed tomographic attenuation of metabolically active and inactive adipose tissues: preliminary findings. *J Comput Assist Tomogr,* 35**,** 65-71.

HU, H. H. & GILSANZ, V. 2011. Developments in the imaging of brown adipose tissue and its associations with muscle, puberty, and health in children. *Front Endocrinol (Lausanne),* 2**,** 33.

HU, H. H., TOVAR, J. P., PAVLOVA, Z., SMITH, M. L. & GILSANZ, V. 2012. Unequivocal identification of brown adipose tissue in a human infant. *J Magn Reson Imaging,* 35**,** 938-42.

HU, H. H., WU, T. W., YIN, L., KIM, M. S., CHIA, J. M., PERKINS, T. G. & GILSANZ, V. 2014. MRI detection of brown adipose tissue with low fat content in newborns with hypothermia. *Magn Reson Imaging,* 32**,** 107-17.

HU, H. H., YIN, L., AGGABAO, P. C., PERKINS, T. G., CHIA, J. M. & GILSANZ, V. 2013. Comparison of brown and white adipose tissues in infants and children with chemical-shift-encoded water-fat MRI. *J Magn Reson Imaging,* 38**,** 885-96.

HUANG, Y. C., HSU, C. C., WANG, P. W., CHANG, Y. H., CHEN, T. B., LEE, B. F. & CHIU, N. T. 2012. Review analysis of the association between the prevalence of activated brown adipose tissue and outdoor temperature. *The Scientific World Journal,* 2012**,** 793039.

HUI, S. C. N., KO, J. K. L., ZHANG, T., SHI, L., YEUNG, D. K. W., WANG, D., CHAN, Q. & CHU, W. C. W. 2017. Quantification of brown and white adipose tissue based on Gaussian mixture model using water-fat and T2* MRI in adolescents. *J Magn Reson Imaging,* 46**,** 758-768.

HULL, D. 1976. The function of brown adipose tissue in the newborn. *Biochem Soc Trans,* 4**,** 226-8.

HWANG, J. J., YECKEL, C. W., GALLEZOT, J. D., AGUIAR, R. B., ERSAHIN, D., GAO, H., KAPINOS, M., NABULSI, N., HUANG, Y., CHENG, D., CARSON, R. E., SHERWIN, R. & DING, Y. S. 2015. Imaging human brown adipose tissue under room temperature conditions with (11)C-MRB, a selective norepinephrine transporter PET ligand. *Metabolism,* 64**,** 747-55.

ISRAELI, E., KORZETS, Z. E., TEKES-MANOVA, D., TIROSH, A., SCHOCHAT, T., BERNHEIM, J. & GOLAN, E. 2007. Blood-pressure categories in adolescence predict development of hypertension in accordance with the european guidelines. *American Journal of Hypertension,* 20**,** 705-709.

JACOBSSON, H., BRUZELIUS, M. & LARSSON, S. A. 2005. Reduction of FDG uptake in brown adipose tissue by propranolol. *Eur J Nucl Med Mol Imaging,* 32**,** 1130.

JANG, C., JALAPU, S., THUZAR, M., LAW, P. W., JEAVONS, S., BARCLAY, J. L. & HO, K. K. 2014. Infrared thermography in the detection of brown adipose tissue in humans. *Physiol Rep,* 2**,** e12167.

JEANGUILLAUME, C., METRARD, G., RICQUIER, D., LEGRAS, P., BOUCHET, F., LACOEUILLE, F., HINDRE, F., MOREL, O. & RAKOTONIRINA, H. 2013. Visualization of activated BAT in mice, with FDG-PET and its relation to UCP1. *Advances in Molecular Imaging,* 5**,** 19.

JENSEN, M. D. 2015. Brown adipose tissue- not as hot as we thought. *J Physiol,* 593**,** 489.

JESPERSEN, N. Z., LARSEN, T. J., PEIJS, L., DAUGAARD, S., HOMOE, P., LOFT, A., DE JONG, J., MATHUR, N., CANNON, B., NEDERGAARD, J., PEDERSEN, B. K., MOLLER, K. & SCHEELE, C. 2013. A classical brown adipose tissue mRNA signature partly overlaps with brite in the supraclavicular region of adult humans. *Cell Metab,* 17**,** 798-805.

JONES, B. F. & PLASSMANN, P. 2002. Digital infrared thermal imaging of human skin. *IEEE Eng Med Biol Mag,* 21**,** 41-8.

JOO HYUN, O., LODGE, M. A. & WAHL, R. L. 2016. Practical PERCIST: a simplified guide to PET response criteria in solid tumors 1.0. *Radiology,* 280**,** 576.

KAPLAN, A. S., ZEMEL, B. S. & STALLINGS, V. A. 1996. Differences in resting energy expenditure in prepubertal black children and white children. *J Pediatr,* 129**,** 643-7.

KATAOKA, N., HIOKI, H., KANEKO, T. & NAKAMURA, K. 2014. Psychological stress activates a dorsomedial hypothalamus-medullary raphe circuit driving brown adipose tissue thermogenesis and hyperthermia. *Cell Metab,* 20**,** 346-58.

KEIL, M. F. 2012. Salivary cortisol: a tool for biobehavioral research in children. *J Pediatr Nurs,* 27**,** 287-9.

KHANNA, A. & BRANCA, R. T. 2012. Detecting brown adipose tissue activity with BOLD MRI in mice. *Magn Reson Med,* 68**,** 1285-90.

KIEFER, F. W. 2016. Browning and thermogenic programing of adipose tissue. *Best Pract Res Clin Endocrinol Metab,* 30**,** 479-485.

KIEN, C. L. & CAMITTA, B. M. 1987. Close association of accelerated rates of whole body protein turnover (synthesis and breakdown) and energy expenditure in children with newly diagnosed acute lymphocytic leukemia. *JPEN J Parenter Enteral Nutr,* 11**,** 129-34.

KIM, M. S., HU, H. H., AGGABAO, P. C., GEFFNER, M. E. & GILSANZ, V. 2014. Presence of brown adipose tissue in an adolescent with severe primary hypothyroidism. *J Clin Endocrinol Metab,* 99**,** E1686-90.

KIM, S., KRYNYCKYI, B. R., MACHAC, J. & KIM, C. K. 2008. Temporal relation between temperature change and FDG uptake in brown adipose tissue. *Eur J Nucl Med Mol Imaging,* 35**,** 984-9.

KINGMA, B., FRIJNS, A. & VAN MARKEN LICHTENBELT, W. 2012. The thermoneutral zone: implications for metabolic studies. *Front Biosci (Elite Ed),* 4**,** 1975-85.

KIRSCHBAUM, C., GONZALEZ BONO, E., ROHLEDER, N., GESSNER, C., PIRKE, K. M., SALVADOR, A. & HELLHAMMER, D. H. 1997. Effects of fasting and glucose load on free cortisol responses to stress and nicotine. *J Clin Endocrinol Metab,* 82**,** 1101-5.

KIRSCHBAUM, C., PIRKE, K. M. & HELLHAMMER, D. H. 1993. The 'Trier Social Stress Test' - a tool for investigating psychobiological stress responses in a laboratory setting. *Neuropsychobiology,* 28**,** 76-81.

KNUDSEN, N., LAURBERG, P., RASMUSSEN, L. B., BULOW, I., PERRILD, H., OVESEN, L. & JORGENSEN, T. 2005. Small differences in thyroid function may be important for body mass index and the occurrence of obesity in the population. *J Clin Endocrinol Metab,* 90**,** 4019-24.

KOENIS, M. M., BROUWER, R. M., VAN BAAL, G. C., VAN SOELEN, I. L., PEPER, J. S., VAN LEEUWEN, M., DELEMARRE-VAN DE WAAL, H. A., BOOMSMA, D. I. & HULSHOFF POL, H. E. 2013. Longitudinal study of hormonal and physical development in young twins. *J Clin Endocrinol Metab,* 98**,** E518-27.

KOSKENSALO, K., RAIKO, J., SAARI, T., SAUNAVAARA, V., ESKOLA, O., NUUTILA, P., SAUNAVAARA, J., PARKKOLA, R. & VIRTANEN, K. A. 2017. Human brown adipose tissue temperature and fat fraction are related to its metabolic activity. *J Clin Endocrinol Metab,* 102**,** 1200-1207.

KRAUSS, S., ZHANG, C. Y. & LOWELL, B. B. 2005. The mitochondrial uncoupling-protein homologues. *Nat Rev Mol Cell Biol,* 6**,** 248-61.

KUJI, I., IMABAYASHI, E., MINAGAWA, A., MATSUDA, H. & MIYAUCHI, T. 2008. Brown adipose tissue demonstrating intense FDG uptake in a patient with mediastinal pheochromocytoma. *Ann Nucl Med,* 22**,** 231-5.

KUWABARA, H. & GJEDDE, A. 1991. Measurements of glucose phosphorylation with FDG and PET are not reduced by dephosphorylation of FDG-6-phosphate. *J Nucl Med,* 32**,** 692-8.

KWON, M. M., O'DWYER, S. M., BAKER, R. K., COVEY, S. D. & KIEFFER, T. J. 2015. FGF21-mediated improvements in glucose clearance require uncoupling protein 1. *Cell Rep,* 13**,** 1521-7.

LARSSON, B., BJORNTORP, P. & TIBBLIN, G. 1981. Health consequences of moderate obesity. *International Journal of Obesity,* 5**,** 97-116.

LAW, J. Pending submission. *Title to be confirmed.* PhD PhD, University of Nottingham.

LAW, J., CHALMERS, J., MORRIS, D. E., ROBINSON, L., BUDGE, H. & SYMONDS, M. E. 2017. The use of infrared thermography in the measurement and characterization of brown adipose tissue activation. *Temperature (Austin),* 5**,** 147-161.

LAW, J., MORRIS, D. E., IZZI-ENGBEAYA, C., SALEM, V., COELLO, C., ROBINSON, L., JAYASINGHE, M., SCOTT, R., GUNN, R., RABINER, E., TAN, T., DHILLO, W. S., BLOOM, S., BUDGE, H. & SYMONDS, M. E. 2018. Thermal imaging is a noninvasive alternative to PET/CT for measurement of brown adipose tissue activity in humans. *J Nucl Med,* 59**,** 516-522.

LAZARIDI, A. 2019. *Identification of factors that stimulate the brown adipose tissue in healthy adults and patients.* PhD, The University of Nottingham.

LEAN, M. E., JAMES, W. P., JENNINGS, G. & TRAYHURN, P. 1986. Brown adipose tissue uncoupling protein content in human infants, children and adults. *Clin Sci (Lond),* 71**,** 291-7.

LEBRON, L., CHOU, A. J. & CARRASQUILLO, J. A. 2010. Interesting image. Unilateral F-18 FDG uptake in the neck, in patients with sympathetic denervation. *Clin Nucl Med,* 35**,** 899-901.

LEE, J. H., KIM, J. M., CHOI, M. J., KANG, Y. E., JOUNG, K. H., YI, H. S., KIM, K. S., KU, B. J., KOO, B. S., SHONG, M. & KIM, H. J. 2018. Clinical Implications of UCP1 mRNA Expression in Human Cervical Adipose Tissue Under Physiological Conditions. *Obesity (Silver Spring),* 26**,** 1008-1016.

LEE, P., BOVA, R., SCHOFIELD, L., BRYANT, W., DIECKMANN, W., SLATTERY, A., GOVENDIR, M. A., EMMETT, L. & GREENFIELD, J. R. 2016. Brown adipose tissue exhibits a glucose-responsive thermogenic biorhythm in humans. *Cell Metab,* 23**,** 602-9.

LEE, P., GREENFIELD, J. R., HO, K. K. & FULHAM, M. J. 2010. A critical appraisal of the prevalence and metabolic significance of brown adipose tissue in adult humans. *Am J Physiol Endocrinol Metab,* 299**,** E601-6.

LEE, P., HO, K. K., LEE, P., GREENFIELD, J. R., HO, K. K. & GREENFIELD, J. R. 2011a. Hot fat in a cool man: infrared thermography and brown adipose tissue. *Diabetes Obes Metab,* 13**,** 92-3.

LEE, P., LINDERMAN, J. D., SMITH, S., BRYCHTA, R. J., WANG, J., IDELSON, C., PERRON, R. M., WERNER, C. D., PHAN, G. Q., KAMMULA, U. S., KEBEBEW, E., PACAK, K., CHEN, K. Y. & CELI, F. S. 2014a. Irisin and FGF21 are cold-induced endocrine activators of brown fat function in humans. *Cell Metab,* 19**,** 302-9.

LEE, P., SMITH, S., LINDERMAN, J., COURVILLE, A. B., BRYCHTA, R. J., DIECKMANN, W., WERNER, C. D., CHEN, K. Y. & CELI, F. S. 2014b. Temperature-acclimated brown adipose tissue modulates insulin sensitivity in humans. *Diabetes,* 63**,** 3686-98.

LEE, P., SWARBRICK, M. M., ZHAO, J. T. & HO, K. K. 2011b. Inducible brown adipogenesis of supraclavicular fat in adult humans. *Endocrinology,* 152**,** 3597-602.

LEE, P., WERNER, C. D., KEBEBEW, E. & CELI, F. S. 2014c. Functional thermogenic beige adipogenesis is inducible in human neck fat. *Int J Obes (Lond),* 38**,** 170-6.

LEE, W. L., SUNG, H. C., LIU, S. H. & CHANG, S. M. 2017. Meditative music listening to reduce state anxiety in patients during the uptake phase before positron emission tomography (PET) scans. *Br J Radiol,* 90**,** 20160466.

LEE, Y. H., PETKOVA, A. P., MOTTILLO, E. P. & GRANNEMAN, J. G. 2012. In vivo identification of bipotential adipocyte progenitors recruited by beta3-adrenoceptor activation and high-fat feeding. *Cell Metab,* 15**,** 480-91.

LEITNER, B. P., HUANG, S., BRYCHTA, R. J., DUCKWORTH, C. J., BASKIN, A. S., MCGEHEE, S., TAL, I., DIECKMANN, W., GUPTA, G., KOLODNY, G. M., PACAK, K., HERSCOVITCH, P., CYPESS, A. M. & CHEN, K. Y. 2017. Mapping of human brown adipose tissue in lean and obese young men. *Proc Natl Acad Sci U S A,* 114**,** 8649-8654.

LEITNER, B. P., WEINER, L. S., DESIR, M., KAHN, P. A., SELEN, D. J., TSANG, C., KOLODNY, G. M. & CYPESS, A. M. 2018. Kinetics of human brown adipose tissue activation and deactivation. *Int J Obes (Lond)*.

LEVY, S. B., KLIMOVA, T. M., ZAKHAROVA, R. N., FEDEROV, A. I., FEDOROVA, V. I., BALTAKHINOVA, M. E. & LEONARD, W. R. 2018. Brown adipose tissue, energy expenditure, and biomarkers of cardio-metabolic health among the Yakut (Sakha) of northeastern Siberia. *Am J Hum Biol,* 30**,** e23175.

LI, L., LAW, C. & POWER, C. 2007. Body mass index throughout the life-course and blood pressure in mid-adult life: a birth cohort study. *Journal of Hypertension,* 25**,** 1215-1223.

LIDELL, M. E., BETZ, M. J., DAHLQVIST LEINHARD, O., HEGLIND, M., ELANDER, L., SLAWIK, M., MUSSACK, T., NILSSON, D., ROMU, T., NUUTILA, P., VIRTANEN, K. A., BEUSCHLEIN, F., PERSSON, A., BORGA, M. & ENERBACK, S. 2013. Evidence for two types of brown adipose tissue in humans. *Nat Med,* 19**,** 631-4.

LIN, B., COUGHLIN, S. & PILCH, P. F. 1998. Bidirectional regulation of uncoupling protein-3 and GLUT-4 mRNA in skeletal muscle by cold. *Am J Physiol,* 275**,** E386-91.

LIN, C. S. & KLINGENBERG, M. 1980. Isolation of the uncoupling protein from brown adipose tissue mitochondria. *FEBS Lett,* 113**,** 299-303.

LIU, P., JI, Y., YUEN, T., RENDINA-RUEDY, E., DEMAMBRO, V. E., DHAWAN, S., ABU-AMER, W., IZADMEHR, S., ZHOU, B., SHIN, A. C., LATIF, R., THANGESWARAN, P., GUPTA, A., LI, J., SHNAYDER, V., ROBINSON, S. T., YU, Y. E., ZHANG, X., YANG, F., LU, P., ZHOU, Y., ZHU, L. L., OBERLIN, D. J., DAVIES, T. F., REAGAN, M. R., BROWN, A., KUMAR, T. R., EPSTEIN, S., IQBAL, J., AVADHANI, N. G., NEW, M. I., MOLINA, H., VAN KLINKEN, J. B., GUO, E. X., BUETTNER, C., HAIDER, S., BIAN, Z., SUN, L., ROSEN, C. J. & ZAIDI, M. 2017. Blocking FSH induces thermogenic adipose tissue and reduces body fat. *Nature,* 546**,** 107-112.

LKHAGVASUREN, B., NAKAMURA, Y., OKA, T., SUDO, N. & NAKAMURA, K. 2011. Social defeat stress induces hyperthermia through activation of thermoregulatory

sympathetic premotor neurons in the medullary raphe region. *Eur J Neurosci,* 34**,** 1442-52.

LOH, R. K. C., FORMOSA, M. F., LA GERCHE, A., REUTENS, A. T., KINGWELL, B. A. & CAREY, A. L. 2019. Acute metabolic and cardiovascular effects of mirabegron in healthy individuals. *Diabetes Obes Metab,* 21**,** 276-284.

LOWELL, B. B., V, S. S., HAMANN, A., LAWITTS, J. A., HIMMS-HAGEN, J., BOYER, B. B., KOZAK, L. P. & FLIER, J. S. 1993. Development of obesity in transgenic mice after genetic ablation of brown adipose tissue. *Nature,* 366**,** 740-2.

LUNDSTROM, E., STRAND, R., JOHANSSON, L., BERGSTEN, P., AHLSTROM, H. & KULLBERG, J. 2015. Magnetic resonance imaging cooling-reheating protocol indicates decreased fat fraction via lipid consumption in suspected brown adipose tissue. *PLoS One,* 10**,** e0126705.

MAGAREY, A., WATSON, J., GOLLEY, R. K., BURROWS, T., SUTHERLAND, R., MCNAUGHTON, S. A., DENNEY-WILSON, E., CAMPBELL, K. & COLLINS, C. 2011. Assessing dietary intake in children and adolescents: Considerations and recommendations for obesity research. *Int J Pediatr Obes,* 6**,** 2-11.

MALPIQUE, R., GALLEGO-ESCUREDO, J. M., SEBASTIANI, G., VILLARROYA, J., LOPEZ-BERMEJO, A., DE ZEGHER, F., VILLARROYA, F. & IBANEZ, L. 2018. Brown adipose tissue in prepubertal children: associations with sex, birthweight, and metabolic profile. *Int J Obes (Lond)*.

MANSON, J. E., WILLETT, W. C., STAMPFER, M. J., COLDITZ, G. A., HUNTER, D. J., HANKINSON, S. E., HENNEKENS, C. H. & SPEIZER, F. E. 1995. Body weight and mortality among women. *New England Journal of Medicine,* 333**,** 677-685.

MARINS, J. C. B., FORMENTI, D., COSTA, C. M. A., FERNANDES, A. D. & SILLERO-QUINTANA, M. 2015. Circadian and gender differences in skin temperature in militaries by thermography. *Infrared Physics & Technology,* 71**,** 322-328.

MARINS, J. C. B., MOREIRA, D. G., CANO, S. P., QUINTANA, M. S., SOARES, D. D., DE ANDRADE FERNANDES, A., DA SILVA, F. S., COSTA, C. M. A. & DOS SANTOS AMORIM, P. R. 2014. Time required to stabilize thermographic images at rest. *Infrared Physics & Technology,* 65**,** 30-35.

MARLATT, K. L., CHEN, K. Y. & RAVUSSIN, E. 2018. Is activation of human brown adipose tissue a viable target for weight management? *Am J Physiol Regul Integr Comp Physiol,* 315**,** R479-R483.

MARSHALL, J. M., STONE, A. & JOHNS, E. J. 1990. Analysis of vascular responses evoked in the cutaneous circulation of one hand by cooling the contralateral hand. *J Auton Nerv Syst,* 31**,** 57-66.

MARTINEZ-TELLEZ, B., GARCIA-RIVERO, Y., SANCHEZ-DELGADO, G., XU, H., AMARO-GAHETE, F. J., ACOSTA, F. M., RENSEN, P. C. N., BOON, M. R., LLAMAS-ELVIRA, J. M. & RUIZ, J. R. 2019a. Supraclavicular skin temperature measured by iButtons and (18)F-fluorodeoxyglucose uptake by brown adipose tissue in adults. *J Therm Biol,* 82**,** 178-185.

MARTINEZ-TELLEZ, B., PEREZ-BEY, A., SANCHEZ-DELGADO, G., ACOSTA, F. M., CORRAL-PEREZ, J., AMARO-GAHETE, F. J., ALCANTARA, J. M. A., CASTRO-PINERO, J., JIMENEZ-PAVON, D., LLAMAS-ELVIRA, J. M. & RUIZ, J. R. 2019b. Concurrent validity of supraclavicular skin temperature measured with iButtons and infrared thermography as a surrogate marker of brown adipose tissue. *J Therm Biol,* 82**,** 186-196.

MARTINEZ-TELLEZ, B., XU, H., SANCHEZ-DELGADO, G., ACOSTA, F. M., RENSEN, P. C. N., LLAMAS-ELVIRA, J. M. & RUIZ, J. R. 2018. Association of wrist and ambient temperature with cold-induced brown adipose tissue and skeletal muscle [(18)F]FDG uptake in young adults. *Am J Physiol Regul Integr Comp Physiol,* 315**,** R1281-R1288.

MARTINEZ DE MORENTIN, P. B., GONZALEZ-GARCIA, I., MARTINS, L., LAGE, R., FERNANDEZ-MALLO, D., MARTINEZ-SANCHEZ, N., RUIZ-PINO, F., LIU, J., MORGAN, D. A., PINILLA, L., GALLEGO, R., SAHA, A. K., KALSBEEK, A., FLIERS, E., BISSCHOP, P. H., DIEGUEZ, C., NOGUEIRAS, R., RAHMOUNI, K., TENA-SEMPERE, M. & LOPEZ, M. 2014. Estradiol regulates brown adipose tissue thermogenesis via hypothalamic AMPK. *Cell Metab,* 20**,** 41-53.

MATSUSHITA, M., YONESHIRO, T., AITA, S., KAMEYA, T., SUGIE, H. & SAITO, M. 2014. Impact of brown adipose tissue on body fatness and glucose metabolism in healthy humans. *Int J Obes (Lond),* 38**,** 812-7.

MEMON, M., MACDONALD, I. A. & BENNETT, T. 2013. Effect of mental stress on cardiovascular function at rest and after ingestion of fructose or sucralose in healthy, white European males. 43**,** 913-918.

MERKLIN, R. J. 1974. Growth and distribution of human fetal brown fat. *Anat Rec,* 178**,** 637-45.

MINN, H., ZASADNY, K. R., QUINT, L. E. & WAHL, R. L. 1995. Lung cancer: reproducibility of quantitative measurements for evaluating 2-[F-18]-fluoro-2-deoxy-D-glucose uptake at PET. *Radiology,* 196**,** 167-73.

MITCHELL, D. & WYNDHAM, C. H. 1969. Comparison of weighting formulas for calculating mean skin temperature. *J Appl Physiol,* 26**,** 616-22.

MOHAMMED, M., OOTSUKA, Y. & BLESSING, W. 2014. Brown adipose tissue thermogenesis contributes to emotional hyperthermia in a resident rat suddenly confronted with an intruder rat. *Am J Physiol Regul Integr Comp Physiol,* 306**,** R394-400.

MONTESI, L., EL GHOCH, M., BRODOSI, L., CALUGI, S., MARCHESINI, G. & DALLE GRAVE, R. 2016. Long-term weight loss maintenance for obesity: a multidisciplinary approach. *Diabetes Metab Syndr Obes,* 9**,** 37-46.

MOREIRA, D. G., COSTELLO, J. T., BRITO, C. J., ADAMCZYK, J. G., AMMER, K., BACH, A. J. E., COSTA, C. M. A., EGLIN, C., FERNANDES, A. A., FERNANDEZ-CUEVAS, I., FERREIRA, J. J. A., FORMENTI, D., FOURNET, D., HAVENITH, G., HOWELL, K., JUNG, A., KENNY, G. P., KOLOSOVAS-MACHUCA, E. S., MALEY, M. J., MERLA, A., PASCOE, D. D., PRIEGO QUESADA, J. I., SCHWARTZ, R. G., SEIXAS, A. R. D., SELFE, J., VAINER, B. G. & SILLERO-QUINTANA, M. 2017. Thermographic imaging in sports and exercise medicine: A Delphi study and consensus statement on the measurement of human skin temperature. *J Therm Biol,* 69**,** 155-162.

MORRISON, J. A., ALFARO, M. P., KHOURY, P., THORNTON, B. B. & DANIELS, S. R. 1996. Determinants of resting energy expenditure in young black girls and young white girls. *J Pediatr,* 129**,** 637-42.

MORRISON, J. A., GLUECK, C. J., HORN, P. S. & WANG, P. 2010. Childhood Predictors of Adult Type 2 Diabetes at 9- and 26-Year Follow-ups. *Archives of Pediatrics & Adolescent Medicine,* 164**,** 53-60.

MOSTYN, A., PEARCE, S., BUDGE, H., ELMES, M., FORHEAD, A. J., FOWDEN, A. L., STEPHENSON, T. & SYMONDS, M. E. 2003. Influence of cortisol on adipose tissue development in the fetal sheep during late gestation. *J Endocrinol,* 176**,** 23-30.

MOSTYN, A., PEARCE, S., STEPHENSON, T. & SYMONDS, M. E. 2004. Hormonal and nutritional regulation of adipose tissue mitochondrial development and function in the newborn. *Exp Clin Endocrinol Diabetes,* 112**,** 2-9.

MUROS-MOLINA, J., ROCHA, L. C., BOSCHERIO, D., MORRIS, D. E., LAW, J., BUDGE, H. & SYMONDS, M. E. 2019. Differences in brown adipose tissue activity with sex and anthopometry as determined by thermal imaging. *EMS Obesity Research Journal,* 1**,** 002.

MUST, A., JACQUES, P. F., DALLAL, G. E., BAJEMA, C. J. & DIETZ, W. H. 1992. Long-term morbidity and mortality of overweight adolescents. A follow-up of the Harvard Growth Study of 1922 to 1935. *The New England journal of medicine,* 327**,** 1350.

MUST, A., SPADANO, J., COAKLEY, E. H., FIELD, A. E., COLDITZ, G. & DIETZ, W. H. 1999. The disease burden associated with overweight and obesity. *JAMA,* 282**,** 1523-9.

MUZIK, O., MANGNER, T. J., LEONARD, W. R., KUMAR, A. & GRANNEMAN, J. G. 2017. Sympathetic innervation of cold-activated brown and white fat in lean young adults. *J Nucl Med,* 58**,** 799-806.

MUZIK, O., MANGNER, T. J., LEONARD, W. R., KUMAR, A., JANISSE, J. & GRANNEMAN, J. G. 2013. 15O PET measurement of blood flow and oxygen consumption in cold-activated human brown fat. *J Nucl Med,* 54**,** 523-31.

NAGANO, G., OHNO, H., OKI, K., KOBUKE, K., SHIWA, T., YONEDA, M. & KOHNO, N. 2015. Activation of classical brown adipocytes in the adult human perirenal depot is highly correlated with PRDM16-EHMT1 complex expression. *PLoS One,* 10**,** e0122584.

NANDAGOPAL, R., LAVERDIERE, C., MULROONEY, D., HUDSON, M. M. & MEACHAM, L. 2008. Endocrine late effects of childhood cancer therapy: a report from the Children's Oncology Group. *Horm Res,* 69**,** 65-74.

NEDERGAARD, J., BENGTSSON, T. & CANNON, B. 2007. Unexpected evidence for active brown adipose tissue in adult humans. *Am J Physiol Endocrinol Metab,* 293**,** E444-52.

NEDERGAARD, J. & CANNON, B. 2010. The changed metabolic world with human brown adipose tissue: therapeutic visions. *Cell Metab,* 11**,** 268-72.

NEDERGAARD, J. & CANNON, B. 2013. How brown is brown fat? It depends where you look. *Nature medicine,* 19**,** 540.

NGUYEN, Q. M., SRINIVASAN, S. R., XU, J.-H., CHEN, W. & BERENSON, G. S. 2008. Changes in risk variables of metabolic syndrome since childhood in pre-diabetic and type 2 diabetic subjects: the Bogalusa Heart Study. *Diabetes care,* 31**,** 2044.

NHS CHOICES. *NHS Choices. What is your BMI?* [Online]. Available: https://www.nhs.uk/live-well/healthy-weight/ [Accessed November 7th 2013].

NICHOLLS, D. G. & LOCKE, R. M. 1984. Thermogenic mechanisms in brown fat. *Physiol Rev,* 64**,** 1-64.

NICHOLLS, D. G. & RIAL, E. 1999. A history of the first uncoupling protein, UCP1. *J Bioenerg Biomembr,* 31**,** 399-406.

NIRENGI, S., HOMMA, T., INOUE, N., SATO, H., YONESHIRO, T., MATSUSHITA, M., KAMEYA, T., SUGIE, H., TSUZAKI, K., SAITO, M., SAKANE, N., KUROSAWA, Y. & HAMAOKA, T. 2016. Assessment of human brown adipose tissue density during daily ingestion of thermogenic capsinoids using near-infrared time-resolved spectroscopy. *J Biomed Opt,* 21**,** 091305.

NIRENGI, S., YONESHIRO, T., SUGIE, H., SAITO, M. & HAMAOKA, T. 2015. Human brown adipose tissue assessed by simple, noninvasive near-infrared time-resolved spectroscopy. *Obesity (Silver Spring),* 23**,** 973-80.

NIU, H. H., LUI, P. W., HU, J. S., TING, C. K., YIN, Y. C., LO, Y. L., LIU, L. & LEE, T. Y. 2001. Thermal symmetry of skin temperature: normative data of normal subjects in Taiwan. *Zhonghua Yi Xue Za Zhi (Taipei),* 64**,** 459-68.

NUNALLY, J. 1978. *Psychometric Theory*, McGraw-Hill.

OJHA, S., FAINBERG, H. P., WILSON, V., PELELLA, G., CASTELLANOS, M., MAY, S. T., LOTTO, A. A., SACKS, H., SYMONDS, M. E. & BUDGE, H. 2016. Gene pathway development in human epicardial adipose tissue during early life. *JCI Insight,* 1**,** e87460.

OKUYAMA, C., SAKANE, N., YOSHIDA, T., SHIMA, K., KUROSAWA, H., KUMAMOTO, K., USHIJIMA, Y. & NISHIMURA, T. 2002. (123)I- or (125)I-metaiodobenzylguanidine visualization of brown adipose tissue. *J Nucl Med,* 43**,** 1234-40.

OKUYAMA, C., USHIJIMA, Y., KUBOTA, T., YOSHIDA, T., NAKAI, T., KOBAYASHI, K. & NISHIMURA, T. 2003. 123I-Metaiodobenzylguanidine uptake in the nape of the neck of children: likely visualization of brown adipose tissue. *J Nucl Med,* 44**,** 1421-5.

OLSEN, J. M., CSIKASZ, R. I., DEHVARI, N., LU, L., SANDSTROM, A., OBERG, A. I., NEDERGAARD, J., STONE-ELANDER, S. & BENGTSSON, T. 2017. beta3-Adrenergically induced glucose uptake in brown adipose tissue is independent of UCP1 presence or activity: Mediation through the mTOR pathway. *Mol Metab,* 6**,** 611-619.

OLSEN, J. M., SATO, M., DALLNER, O. S., SANDSTRÖM, A. L., PISANI, D. F., CHAMBARD, J.-C., AMRI, E.-Z., HUTCHINSON, D. S. & BENGTSSON, T. 2014. Glucose uptake in brown fat cells is dependent on mTOR complex 2–promoted GLUT1 translocation. *J Cell Biol,* 207**,** 365-374.

ONG, F. J., AHMED, B. A., ORESKOVICH, S. M., BLONDIN, D. P., HAQ, T., KONYER, N. B., NOSEWORTHY, M. D., HAMAN, F., CARPENTIER, A. C., MORRISON, K. M. & STEINBERG, G. R. 2018. Recent advances in the detection of brown adipose tissue in adult humans: a review. *Clin Sci (Lond),* 132**,** 1039-1054.

ORAVA, J., NUUTILA, P., LIDELL, M. E., OIKONEN, V., NOPONEN, T., VILJANEN, T., SCHEININ, M., TAITTONEN, M., NIEMI, T., ENERBACK, S. & VIRTANEN, K. A. 2011. Different metabolic responses of human brown adipose tissue to activation by cold and insulin. *Cell Metab,* 14**,** 272-9.

ORESKOVICH, S. M., ONG, F. J., AHMED, B. A., KONYER, N. B., BLONDIN, D. P., GUNN, E., SINGH, N. P., NOSEWORTHY, M. D., HAMAN, F. & CARPENTIER, A. C. 2019. Magnetic resonance imaging reveals human brown adipose tissue is rapidly activated in response to cold. *Journal of the Endocrine Society*.

OUELLET, V., LABBE, S. M., BLONDIN, D. P., PHOENIX, S., GUERIN, B., HAMAN, F., TURCOTTE, E. E., RICHARD, D. & CARPENTIER, A. C. 2012. Brown adipose tissue oxidative metabolism contributes to energy expenditure during acute cold exposure in humans. *J Clin Invest,* 122**,** 545-52.

OUELLET, V., ROUTHIER-LABADIE, A., BELLEMARE, W., LAKHAL-CHAIEB, L., TURCOTTE, E., CARPENTIER, A. C. & RICHARD, D. 2011. Outdoor temperature, age, sex, body mass index, and diabetic status determine the prevalence, mass, and glucose-uptake activity of 18F-FDG-detected BAT in humans. *J Clin Endocrinol Metab,* 96**,** 192-9.

PALMER, B. F. & CLEGG, D. J. 2017. Non-shivering thermogenesis as a mechanism to facilitate sustainable weight loss. *Obes Rev,* 18**,** 819-831.

PANDITA, A., SHARMA, D., PANDITA, D., PAWAR, S., TARIQ, M. & KAUL, A. 2016. Childhood obesity: prevention is better than cure. *Diabetes Metab Syndr Obes,* 9**,** 83-9.

PARYSOW, O., MOLLERACH, A. M., JAGER, V., RACIOPPI, S., SAN ROMAN, J. & GERBAUDO, V. H. 2007. Low-dose oral propranolol could reduce brown adipose tissue F-18 FDG uptake in patients undergoing PET scans. *Clin Nucl Med,* 32**,** 351-7.

PEARSON, N. & BIDDLE, S. J. 2011. Sedentary behavior and dietary intake in children, adolescents, and adults. A systematic review. *Am J Prev Med,* 41**,** 178-88.

PERKINS, A. C., MSHELIA, D. S., SYMONDS, M. E. & SATHEKGE, M. 2013. Prevalence and pattern of brown adipose tissue distribution of 18F-FDG in patients undergoing PET-CT in a subtropical climatic zone. *Nucl Med Commun,* 34**,** 168-74.

PETERSEN, A. C., CROCKETT, L., RICHARDS, M. & BOXER, A. 1988. A self-report measure of pubertal status: Reliability, validity, and initial norms. *J Youth Adolesc,* 17**,** 117-33.

PETERSON, C. M., OROOJI, M., JOHNSON, D. N., NARAGHI-POUR, M. & RAVUSSIN, E. 2017. Brown adipose tissue does not seem to mediate metabolic adaptation to overfeeding in men. *Obesity (Silver Spring),* 25**,** 502-505.

PETROVIC, N., WALDEN, T. B., SHABALINA, I. G., TIMMONS, J. A., CANNON, B. & NEDERGAARD, J. 2010. Chronic peroxisome proliferator-activated receptor gamma (PPARgamma) activation of epididymally derived white adipocyte cultures reveals a population of thermogenically competent, UCP1-containing adipocytes molecularly distinct from classic brown adipocytes. *J Biol Chem,* 285**,** 7153-64.

PFANNENBERG, C., WERNER, M. K., RIPKENS, S., STEF, I., DECKERT, A., SCHMADL, M., REIMOLD, M., HARING, H. U., CLAUSSEN, C. D. & STEFAN, N. 2010. Impact of age on the relationships of brown adipose tissue with sex and adiposity in humans. *Diabetes,* 59**,** 1789-93.

PI-SUNYER, F. X. 2002. The obesity epidemic: pathophysiology and consequences of obesity. *Obesity research,* 10**,** 97S-104S.

PICTON, S. V. 1998. Aspects of altered metabolism in children with cancer. *Int J Cancer Suppl,* 11**,** 62-4.

PLATTNER, O., SEMSROTH, M., SESSLER, D. I., PAPOUSEK, A., KLASEN, C. & WAGNER, O. 1997. Lack of nonshivering thermogenesis in infants anesthetized with fentanyl and propofol. *Anesthesiology,* 86**,** 772-7.

PONRARTANA, S., AGGABAO, P. C., CHAVEZ, T. A., DHARMAVARAM, N. L. & GILSANZ, V. 2016. Changes in Brown Adipose Tissue and Muscle Development during Infancy. *J Pediatr,* 173**,** 116-21.

PONRARTANA, S., AGGABAO, P. C., HU, H. H., ALDROVANDI, G. M., WREN, T. A. & GILSANZ, V. 2012. Brown adipose tissue and its relationship to bone structure in pediatric patients. *J Clin Endocrinol Metab,* 97**,** 2693-8.

PONRARTANA, S., HU, H. H. & GILSANZ, V. 2013. On the relevance of brown adipose tissue in children. *Ann N Y Acad Sci,* 1302**,** 24-29.

PORTER, C., CHONDRONIKOLA, M. & SIDOSSIS, L. S. 2015. The Therapeutic Potential of Brown Adipocytes in Humans. *Front Endocrinol (Lausanne),* 6**,** 156.

QUESADA, J. I. P., KUNZLER, M. R. & CARPES, F. P. 2017. Methodological Aspects of Infrared Thermography in Human Assessment. *Application of Infrared Thermography in Sports Science***,** 49-79.

RABOI, C. A. & SMITH, W. 1999. Brown fat necrosis in the setting of congenital heart disease and prostaglandin E1 use: a case report. *Pediatr Radiol,* 29**,** 61-3.

RAMAGE, L. E., AKYOL, M., FLETCHER, A. M., FORSYTHE, J., NIXON, M., CARTER, R. N., VAN BEEK, E. J., MORTON, N. M., WALKER, B. R. & STIMSON, R. H. 2016. Glucocorticoids Acutely Increase Brown Adipose Tissue Activity in Humans, Revealing Species-Specific Differences in UCP-1 Regulation. *Cell Metab,* 24**,** 130-41.

RASMUSSEN, J. M., ENTRINGER, S., NGUYEN, A., VAN ERP, T. G., BURNS, J., GUIJARRO, A., OVEISI, F., SWANSON, J. M., PIOMELLI, D., WADHWA, P. D., BUSS, C. & POTKIN, S. G. 2013. Brown adipose tissue quantification in human neonates using water-fat separated MRI. *PLoS One,* 8**,** e77907.

RATZIU, V., GIRAL, P., CHARLOTTE, F., BRUCKERT, E., THIBAULT, V., THEODOROU, I., KHALIL, L., TURPIN, G., OPOLON, P. & POYNARD, T. 2000. Liver fibrosis in overweight patients. *Gastroenterology,* 118**,** 1117-1123.

RCPCH. 2013. *Boys and girls body mass index (BMI) chart 2-20 years* [Online]. Available: https://www.rcpch.ac.uk/sites/default/files/2018-03/boys_and_girls_bmi_chart.pdf [Accessed 23rd August 2019].

RICE, S. P., ZHANG, L., GRENNAN-JONES, F., AGARWAL, N., LEWIS, M. D., REES, D. A. & LUDGATE, M. 2010. Dehydroepiandrosterone (DHEA) treatment in vitro inhibits adipogenesis in human omental but not subcutaneous adipose tissue. *Mol Cell Endocrinol,* 320**,** 51-7.

RICQUIER, D., GERVAIS, C., KADER, J. C. & HEMON, P. 1979. Partial purification by guanosine-5'-diphosphate--agarose affinity chromatography of the 32,000 molecular weight polypeptide from mitochondria of brown adipose tissue. *FEBS Lett,* 101**,** 35-8.

RICQUIER, D. & KADER, J. C. 1976. Mitochondrial protein alteration in active brown fat: a soidum dodecyl sulfate-polyacrylamide gel electrophoretic study. *Biochem Biophys Res Commun,* 73**,** 577-83.

ROBINSON, L., OJHA, S., SYMONDS, M. E. & BUDGE, H. 2014. Body mass index as a determinant of brown adipose tissue function in healthy children. *J Pediatr,* 164**,** 318-22 e1.

ROBINSON, L. J., LAW, J., ASTLE, V., GUTIERREZ-GARCIA, M., OJHA, S., SYMONDS, M. E., PITCHFORD, N. & BUDGE, H. 2019. Sexual Dimorphism of Brown Adipose Tissue Function. *J Pediatr,* 210**,** 166-172 e1.

ROBINSON, L. J., LAW, J. M., SYMONDS, M. E. & BUDGE, H. 2016. Brown adipose tissue activation as measured by infrared thermography by mild anticipatory psychological stress in lean healthy females. *Exp Physiol,* 101**,** 549-57.

ROCKALL, A. G., AVRIL, N., LAM, R., IANNONE, R., MOZLEY, P. D., PARKINSON, C., BERGSTROM, D., SALA, E., SARKER, S. J., MCNEISH, I. A. & BRENTON, J. D. 2014. Repeatability of quantitative FDG-PET/CT and contrast-enhanced CT in recurrent ovarian carcinoma: test-retest measurements for tumor FDG uptake, diameter, and volume. *Clin Cancer Res,* 20**,** 2751-60.

ROCKSTROH, D., LANDGRAF, K., WAGNER, I. V., GESING, J., TAUSCHER, R., LAKOWA, N., KIESS, W., BUHLIGEN, U., WOJAN, M., TILL, H., BLUHER, M. & KORNER, A. 2015. Direct evidence of brown adipocytes in different fat depots in children. *PLoS One,* 10**,** e0117841.

RONTI, T., LUPATTELLI, G. & MANNARINO, E. 2006. The endocrine function of adipose tissue: an update. *Clin Endocrinol (Oxf),* 64**,** 355-65.

ROSENWALD, M., PERDIKARI, A., RULICKE, T. & WOLFRUM, C. 2013. Bi-directional interconversion of brite and white adipocytes. *Nat Cell Biol,* 15**,** 659-67.

RUTHERFORD, M., RAMENGHI, L. A., EDWARDS, A. D., BROCKLEHURST, P., HALLIDAY, H., LEVENE, M., STROHM, B., THORESEN, M., WHITELAW, A. & AZZOPARDI, D. 2010. Assessment of brain tissue injury after moderate hypothermia in neonates with hypoxic-ischaemic encephalopathy: a nested substudy of a randomised controlled trial. *Lancet Neurol,* 9**,** 39-45.

SACKS, H. S., FAIN, J. N., HOLMAN, B., CHEEMA, P., CHARY, A., PARKS, F., KARAS, J., OPTICAN, R., BAHOUTH, S. W., GARRETT, E., WOLF, R. Y., CARTER, R. A., ROBBINS, T., WOLFORD, D. & SAMAHA, J. 2009. Uncoupling protein-1 and related messenger ribonucleic acids in human epicardial and other adipose tissues: epicardial fat functioning as brown fat. *J Clin Endocrinol Metab,* 94**,** 3611-5.

SAITO, M. 2013. Brown adipose tissue as a regulator of energy expenditure and body fat in humans. *Diabetes Metab J,* 37**,** 22-9.

SAITO, M., OKAMATSU-OGURA, Y., MATSUSHITA, M., WATANABE, K., YONESHIRO, T., NIO-KOBAYASHI, J., IWANAGA, T., MIYAGAWA, M., KAMEYA, T., NAKADA, K., KAWAI, Y. & TSUJISAKI, M. 2009. High incidence of metabolically active brown adipose tissue in healthy adult humans: effects of cold exposure and adiposity. *Diabetes,* 58**,** 1526-31.

SAITO, M., YONESHIRO, T. & MATSUSHITA, M. 2016. Activation and recruitment of brown adipose tissue by cold exposure and food ingredients in humans. *Best Pract Res Clin Endocrinol Metab,* 30**,** 537-547.

SALAMUNES, A. C. C., STADNIK, A. M. W. & NEVES, E. B. 2017. The effect of body fat percentage and body fat distribution on skin surface temperature with infrared thermography. *Journal of Thermal Biology,* 66**,** 1-9.

SALEM, V., IZZI-ENGBEAYA, C., COELLO, C., THOMAS, D. B., CHAMBERS, E. S., COMNINOS, A. N., BUCKLEY, A., WIN, Z., AL-NAHHAS, A., RABINER, E. A., GUNN, R. N., BUDGE, H., SYMONDS, M. E., BLOOM, S. R., TAN, T. M. & DHILLO, W. S. 2016. Glucagon increases energy expenditure independently of brown adipose tissue activation in humans. *Diabetes Obes Metab,* 18**,** 72-81.

SAMPATH, S. C., SAMPATH, S. C., BREDELLA, M. A., CYPESS, A. M. & TORRIANI, M. 2016. Imaging of brown adipose tissue: state of the art. *Radiology,* 280**,** 4-19.

SANCHEZ-DELGADO, G., MARTINEZ-TELLEZ, B., GARCIA-RIVERO, Y., ALCANTARA, J. M. A., ACOSTA, F. M., AMARO-GAHETE, F. J., LLAMAS-ELVIRA, J. M. & RUIZ, J. R. 2018. Brown adipose tissue and skeletal muscle (18)F-FDG activity after a personalized cold exposure is not associated with cold-induced thermogenesis and nutrient oxidation rates in young healthy adults. *Front Physiol,* 9**,** 1577.

SANCHEZ-GURMACHES, J. & GUERTIN, D. A. 2014. Adipocytes arise from multiple lineages that are heterogeneously and dynamically distributed. *Nat Commun,* 5**,** 4099.

SARASNIEMI, J. T., KOSKENSALO, K., RAIKO, J., NUUTILA, P., SAUNAVAARA, J., PARKKOLA, R. & VIRTANEN, K. A. 2018. Skin temperature may not yield human brown adipose tissue activity in diverse populations. *Acta Physiol (Oxf),* 224**,** e13095.

SCHAPIRA, D. V., CLARK, R. A., WOLFF, P. A., JARRETT, A. R., KUMAR, N. B. & AZIZ, N. M. 1994. Visceral obesity and breast cancer risk. *Cancer,* 74**,** 632-639.

SCHILPEROORT, M., HOEKE, G., KOOIJMAN, S. & RENSEN, P. C. 2016. Relevance of lipid metabolism for brown fat visualization and quantification. *Curr Opin Lipidol,* 27**,** 242-8.

SCHLEIN, C., TALUKDAR, S., HEINE, M., FISCHER, A. W., KROTT, L. M., NILSSON, S. K., BRENNER, M. B., HEEREN, J. & SCHEJA, L. 2016. FGF21 lowers plasma triglycerides by accelerating lipoprotein catabolism in white and brown adipose tissues. *Cell Metab,* 23**,** 441-53.

SCHNEIDER, C. A., RASBAND, W. S. & ELICEIRI, K. W. 2012. NIH Image to ImageJ: 25 years of image analysis. *Nat Methods,* 9**,** 671-5.

SCHUBRING, C. 1986. Temperature regulation in healthy and resuscitated newborns immediately after birth. *J Perinat Med,* 14**,** 27-33.

SCOTNEY, H., SYMONDS, M. E., LAW, J., BUDGE, H., SHARKEY, D. & MANOLOPOULOS, K. N. 2017. Glucocorticoids modulate human brown adipose tissue thermogenesis in vivo. *Metabolism,* 70**,** 125-132.

SEALE, P., BJORK, B., YANG, W., KAJIMURA, S., CHIN, S., KUANG, S., SCIME, A., DEVARAKONDA, S., CONROE, H. M., ERDJUMENT-BROMAGE, H., TEMPST, P., RUDNICKI, M. A., BEIER, D. R. & SPIEGELMAN, B. M. 2008. PRDM16 controls a brown fat/skeletal muscle switch. *Nature,* 454**,** 961-7.

SEIXAS, A., AZEVEDO, J., PIMENTA, I., AMMER, K., CARVALHO, R., VILAS-BOAS, J. P., MENDES, J. & VARDASCA, R. 2018. Skin temperature of the foot: Reliability of infrared image analysis based in the angiosome concept. *Infrared Physics & Technology,* 92**,** 402-408.

SENN, J. R., MAUSHART, C. I., GASHI, G., MICHEL, R., LALIVE D'EPINAY, M., VOGT, R., BECKER, A. S., MULLER, J., BALAZ, M., WOLFRUM, C., BURGER, I. A. & BETZ, M. J. 2018. Outdoor temperature influences cold induced thermogenesis in humans. *Front Physiol,* 9**,** 1184.

SHAI, I., JIANG, R., MANSON, J. E., STAMPFER, M. J., WILLETT, W. C., COLDITZ, G. A. & HU, F. B. 2006. Ethnicity, obesity, and risk of type 2 diabetes in women: a 20-year follow-up study. *Diabetes Care,* 29**,** 1585-90.

SHARP, L. Z., SHINODA, K., OHNO, H., SCHEEL, D. W., TOMODA, E., RUIZ, L., HU, H., WANG, L., PAVLOVA, Z., GILSANZ, V. & KAJIMURA, S. 2012. Human BAT possesses molecular signatures that resemble beige/brite cells. *PLoS One,* 7**,** e49452.

SHATTOCK, S. G. 1909. On Normal Tumour-like Formations of Fat in Man and the Lower Animals. *Proc R Soc Med,* 2**,** 207-70.

SHORAKAE, S., JONA, E., DE COURTEN, B., LAMBERT, G. W., LAMBERT, E. A., PHILLIPS, S. E., CLARKE, I. J., TEEDE, H. J. & HENRY, B. A. 2019. Brown adipose tissue thermogenesis in polycystic ovary syndrome. *Clin Endocrinol (Oxf),* 90**,** 425-432.

SIDOSSIS, L. & KAJIMURA, S. 2015. Brown and beige fat in humans: thermogenic adipocytes that control energy and glucose homeostasis. *J Clin Invest,* 125**,** 478-86.

SIDOSSIS, L. S., PORTER, C., SARAF, M. K., BORSHEIM, E., RADHAKRISHNAN, R. S., CHAO, T., ALI, A., CHONDRONIKOLA, M., MLCAK, R., FINNERTY, C. C., HAWKINS, H. K., TOLIVER-KINSKY, T. & HERNDON, D. N. 2015. Browning of subcutaneous white adipose tissue in humans after severe adrenergic stress. *Cell Metab,* 22**,** 219-27.

SILVENTOINEN, K., MAGNUSSON, P. K. E., TYNELIUS, P., BATTY, G. D. & RASMUSSEN, F. 2009. Association of body size and muscle strength with incidence of coronary

heart disease and cerebrovascular diseases: a population-based cohort study of one million Swedish men. *International Journal of Epidemiology,* 38**,** 110-118.

SIMMONDS, M., LLEWELLYN, A., OWEN, C. G. & WOOLACOTT, N. 2016. Predicting adult obesity from childhood obesity: a systematic review and meta-analysis. *Obesity Reviews,* 17**,** 95-107.

SKILLEN, A., CURRIE, G. M. & WHEAT, J. M. 2012. Thermal control of brown adipose tissue in 18F-FDG PET. *J Nucl Med Technol,* 40**,** 99-103.

SMITH, R. E. 1964. Thermoregulatory and adaptive behavior of brown adipose tissue. *Science,* 146**,** 1686-9.

SMITH, R. E. & HOCK, R. J. 1963. Brown fat: thermogenic effector of arousal in hibernators. *Science,* 140**,** 199-200.

SODERLUND, V., LARSSON, S. A. & JACOBSSON, H. 2007. Reduction of FDG uptake in brown adipose tissue in clinical patients by a single dose of propranolol. *Eur J Nucl Med Mol Imaging,* 34**,** 1018-22.

SOUMANO, K., DESBIENS, S., RABELO, R., BAKOPANOS, E., CAMIRAND, A. & SILVA, J. E. 2000. Glucocorticoids inhibit the transcriptional response of the uncoupling protein-1 gene to adrenergic stimulation in a brown adipose cell line. *Mol Cell Endocrinol,* 165**,** 7-15.

SPIELBERGER, C. 1983. Manual for the state-trait anxiety inventory. Spieberger CD (Ed). STAI Manual. Palo Alto Calif Consulting. *Psychologist Press*.

STALLINGS, V. A., VAISMAN, N., CHAN, H. S., WEITZMAN, S. S., HAHN, E. & PENCHARZ, P. B. 1989. Energy metabolism in children with newly diagnosed acute lymphoblastic leukemia. *Pediatr Res,* 26**,** 154-7.

STAMPFER, M. J., MACLURE, K. M., COLDITZ, G. A., MANSON, J. & WILLETT, W. C. 1992. Risk of symptomatic gallstones in women with severe obesity. *Am J Clin Nutr,* 55**,** 652-658.

STAUSS, J., FRANZIUS, C., PFLUGER, T., JUERGENS, K. U., BIASSONI, L., BEGENT, J., KLUGE, R., AMTHAUER, H., VOELKER, T., HOJGAARD, L., BARRINGTON, S., HAIN, S., LYNCH, T., HAHN, K. & EUROPEAN ASSOCIATION OF NUCLEAR, M. 2008. Guidelines for 18F-FDG PET and PET-CT imaging in paediatric oncology. *Eur J Nucl Med Mol Imaging,* 35**,** 1581-8.

STEINBERG, J. D., VOGEL, W. & VEGT, E. 2017. Factors influencing brown fat activation in FDG PET/CT: a retrospective analysis of 15,000+ cases. *Br J Radiol,* 90**,** 20170093.

STEINHERZ, L. J., STEINHERZ, P. G., TAN, C. T., HELLER, G. & MURPHY, M. L. 1991. Cardiac toxicity 4 to 20 years after completing anthracycline therapy. *JAMA,* 266**,** 1672-7.

STEVENS, J. C. & CHOO, K. K. 1998. Temperature sensitivity of the body surface over the life span. *Somatosens Mot Res,* 15**,** 13-28.

STOCKS, J. M., TAYLOR, N. A., TIPTON, M. J. & GREENLEAF, J. E. 2004. Human physiological responses to cold exposure. *Aviat Space Environ Med,* 75**,** 444-57.

STRACK, A. M., BRADBURY, M. J. & DALLMAN, M. F. 1995. Corticosterone decreases nonshivering thermogenesis and increases lipid storage in brown adipose tissue. *Am J Physiol,* 268**,** R183-91.

STRAHAN, R. & GERBASI, K. C. 1972. Short, homogeneous versions of the Marlow-Crowne social desirability scale. *J Clin Psychol,* 28**,** 191-193.

SURASI, D. S., BHAMBHVANI, P., BALDWIN, J. A., ALMODOVAR, S. E. & O'MALLEY, J. P. 2014. (1)(8)F-FDG PET and PET/CT patient preparation: a review of the literature. *J Nucl Med Technol,* 42**,** 5-13.

SUZUKI, M., MURAKAMI, M., SHIRAI, M., HASHIMOTO, O., KAWADA, T., MATSUI, T. & FUNABA, M. 2018. Role of estradiol and testosterone in Ucp1 expression in brown/beige adipocytes. *Cell Biochem Funct,* 36**,** 450-456.

SVENSSON, P. A., LINDBERG, K., HOFFMANN, J. M., TAUBE, M., PEREIRA, M. J., MOHSEN-KANSON, T., HAFNER, A. L., RIZELL, M., PALMING, J., DANI, C. & SVENSSON, M. K. 2014. Characterization of brown adipose tissue in the human perirenal depot. *Obesity (Silver Spring),* 22**,** 1830-7.

SYMONDS, M. E., ANDREWS, D. C. & JOHNSON, P. 1989. The control of thermoregulation in the developing lamb during slow wave sleep. *J Dev Physiol,* 11**,** 289-98.

SYMONDS, M. E., BUDGE, H., PERKINS, A. C. & LOMAX, M. A. 2011. Adipose tissue development--impact of the early life environment. *Prog Biophys Mol Biol,* 106**,** 300-6.

SYMONDS, M. E., HENDERSON, K., ELVIDGE, L., BOSMAN, C., SHARKEY, D., PERKINS, A. C. & BUDGE, H. 2012a. Thermal imaging to assess age-related changes of skin

temperature within the supraclavicular region co-locating with brown adipose tissue in healthy children. *J Pediatr,* 161**,** 892-8.

SYMONDS, M. E., POPE, M. & BUDGE, H. 2012b. Adipose tissue development during early life: novel insights into energy balance from small and large mammals. *Proc Nutr Soc,* 71**,** 363-70.

SYMONDS, M. E., POPE, M., SHARKEY, D. & BUDGE, H. 2012c. Adipose tissue and fetal programming. *Diabetologia,* 55**,** 1597-606.

TAM, C. S. & RAVUSSIN, E. 2012. Energy balance: an overview with emphasis on children. *Pediatr Blood Cancer,* 58**,** 154-8.

TATTERSALL, G. J. 2015. Thermimage: Functions for Handling Thermal Images. .

TATTERSALL, G. J. 2016. Infrared thermography: A non-invasive window into thermal physiology. *Comparative Biochemistry and Physiology Part A: Molecular & Integrative Physiology,* 202**,** 78-98.

THUZAR, M., LAW, W. P., DIMESKI, G., STOWASSER, M. & HO, K. K. Y. 2019. Mineralocorticoid antagonism enhances brown adipose tissue function in humans: A randomized placebo-controlled cross-over study. *Diabetes Obes Metab,* 21**,** 509-516.

THUZAR, M., LAW, W. P., RATNASINGAM, J., JANG, C., DIMESKI, G. & HO, K. K. Y. 2018. Glucocorticoids suppress brown adipose tissue function in humans: A double-blind placebo-controlled study. *Diabetes Obes Metab,* 20**,** 840-848.

TIMMONS, J. A., WENNMALM, K., LARSSON, O., WALDEN, T. B., LASSMANN, T., PETROVIC, N., HAMILTON, D. L., GIMENO, R. E., WAHLESTEDT, C., BAAR, K., NEDERGAARD, J. & CANNON, B. 2007. Myogenic gene expression signature establishes that brown and white adipocytes originate from distinct cell lineages. *Proc Natl Acad Sci U S A,* 104**,** 4401-6.

TIROSH, A., SHAI, I., AFEK, A., DUBNOV-RAZ, G., AYALON, N., GORDON, B., DERAZNE, E., TZUR, D., SHAMIS, A., VINKER, S. & RUDICH, A. 2011. Adolescent BMI trajectory and risk of diabetes versus coronary disease. *N Engl J Med,* 364**,** 1315-25.

TISDALE, M. J. 1997. Cancer cachexia: metabolic alterations and clinical manifestations. *Nutrition,* 13**,** 1-7.

TOWNSEND, E. & PITCHFORD, N. J. 2012. Baby knows best? The impact of weaning style on food preferences and body mass index in early childhood in a case-controlled sample. *BMJ Open,* 2**,** e000298.

TRAYHURN, P., THURLBY, P. & JAMES, W. 1977. Thermogenic defect in pre-obese ob/ob mice. *Nature,* 266**,** 60.

TRUONG, M. T., ERASMUS, J. J., MUNDEN, R. F., MAROM, E. M., SABLOFF, B. S., GLADISH, G. W., PODOLOFF, D. A. & MACAPINLAC, H. A. 2004. Focal FDG uptake in mediastinal brown fat mimicking malignancy: a potential pitfall resolved on PET/CT. *Am J Roentgenol,* 183**,** 1127-32.

UDIN, M., RAIKO, J., SAARI, T., KUDOMI, N., TOLVANEN, T., OIKONEN, V., TEUHO, J., SIPILA, H. T., SAVISTO, N., PARKKOLA, R., NUUTILA, P. & VIRTANEN, K. A. 2016. Human brown adipose tissue [(15)O]O2 PET imaging in the presence and absence of cold stimulus. *Eur J Nucl Med Mol Imaging,* 43**,** 1878-86.

UEMATSU, S. 1985. Symmetry of skin temperature comparing one side of the body to the other. *Thermology,* 1**,** 4-7.

UEMATSU, S., EDWIN, D. H., JANKEL, W. R., KOZIKOWSKI, J. & TRATTNER, M. 1988. Quantification of thermal asymmetry. Part 1: Normal values and reproducibility. *J Neurosurg,* 69**,** 552-5.

UNICEF 2018. WHO, The World Bank Group. Joint Child Malnutrition Estimates-Levels and Trends 2018.

VALENCAK, T. G., OSTERRIEDER, A. & SCHULZ, T. J. 2017. Sex matters: The effects of biological sex on adipose tissue biology and energy metabolism. *Redox Biol,* 12**,** 806-813.

VAN DER LANS, A. A., HOEKS, J., BRANS, B., VIJGEN, G. H., VISSER, M. G., VOSSELMAN, M. J., HANSEN, J., JORGENSEN, J. A., WU, J., MOTTAGHY, F. M., SCHRAUWEN, P. & VAN MARKEN LICHTENBELT, W. D. 2013. Cold acclimation recruits human brown fat and increases nonshivering thermogenesis. *J Clin Invest,* 123**,** 3395-403.

VAN DER LANS, A. A., VOSSELMAN, M. J., HANSSEN, M. J., BRANS, B. & VAN MARKEN LICHTENBELT, W. D. 2016. Supraclavicular skin temperature and BAT activity in lean healthy adults. *J Physiol Sci,* 66**,** 77-83.

VAN MARKEN LICHTENBELT, W. D. & SCHRAUWEN, P. 2011. Implications of nonshivering thermogenesis for energy balance regulation in humans. *Am J Physiol Regul Integr Comp Physiol,* 301**,** R285-96.

VAN MARKEN LICHTENBELT, W. D., VANHOMMERIG, J. W., SMULDERS, N. M., DROSSAERTS, J. M., KEMERINK, G. J., BOUVY, N. D., SCHRAUWEN, P. & TEULE, G. J.

2009. Cold-activated brown adipose tissue in healthy men. *N Engl J Med,* 360**,** 1500-8.

VARDASCA, R., RING, E., PLASSMANN, P. & JONES, C. 2012. Thermal symmetry of the upper and lower extremities in healthy subjects. *Thermology international,* 22**,** 53-60.

VARKEVISSER, R., VAN STRALEN, M., KROEZE, W., KET, J. & STEENHUIS, I. 2019. Determinants of weight loss maintenance: a systematic review. *Obesity Reviews,* 20**,** 171-211.

VIENGCHAREUN, S., PENFORNIS, P., ZENNARO, M. C. & LOMBES, M. 2001. Mineralocorticoid and glucocorticoid receptors inhibit UCP expression and function in brown adipocytes. *Am J Physiol Endocrinol Metab,* 280**,** E640-9.

VIJGEN, G. H., BOUVY, N. D., TEULE, G. J., BRANS, B., HOEKS, J., SCHRAUWEN, P. & VAN MARKEN LICHTENBELT, W. D. 2012. Increase in brown adipose tissue activity after weight loss in morbidly obese subjects. *J Clin Endocrinol Metab,* 97**,** E1229-33.

VIJGEN, G. H., BOUVY, N. D., TEULE, G. J., BRANS, B., SCHRAUWEN, P. & VAN MARKEN LICHTENBELT, W. D. 2011. Brown adipose tissue in morbidly obese subjects. *PLoS One,* 6**,** e17247.

VILLARROYA, F. & GIRALT, M. 2015. The beneficial ffects of brown fat transplantation: further evidence of an endocrine role of brown adipose tissue. *Endocrinology,* 156**,** 2368-70.

VILLARROYA, J., CEREIJO, R. & VILLARROYA, F. 2013. An endocrine role for brown adipose tissue? *Am J Physiol Endocrinol Metab,* 305**,** E567-72.

VINER, R., HARGREAVES, D. & CHEUNG, C. 2017. State of child health: report 2017. *London: Royal College of Paediatrics & Child Health*.

VINER, R., WARD, J., CHEUNG, R., WOLF, I. & HARGREAVES, D. 2018. State of Child Heath short report: Child Health in England: comparison with other wealthy countries. London: Royal College of Paediatrics and Child Health.

VIRTANEN, K. A., LIDELL, M. E., ORAVA, J., HEGLIND, M., WESTERGREN, R., NIEMI, T., TAITTONEN, M., LAINE, J., SAVISTO, N. J., ENERBACK, S. & NUUTILA, P. 2009. Functional brown adipose tissue in healthy adults. *N Engl J Med,* 360**,** 1518-25.

VOGEL, W. V., VALDES OLMOS, R. A., TIJS, T. J., GILLIES, M. F., VAN ELSWIJK, G. & VOGT, J. 2012. Intervention to lower anxiety of 18F-FDG PET/CT patients by use of audiovisual imagery during the uptake phase before imaging. *J Nucl Med Technol,* 40**,** 92-8.

VOSSELMAN, M. J., VAN DER LANS, A. A., BRANS, B., WIERTS, R., VAN BAAK, M. A., SCHRAUWEN, P. & VAN MARKEN LICHTENBELT, W. D. 2012. Systemic beta-adrenergic stimulation of thermogenesis is not accompanied by brown adipose tissue activity in humans. *Diabetes,* 61**,** 3106-13.

WAHL, R. L., JACENE, H., KASAMON, Y. & LODGE, M. A. 2009. From RECIST to PERCIST: Evolving Considerations for PET response criteria in solid tumors. *J Nucl Med,* 50 Suppl 1**,** 122S-50S.

WALDEN, T. B., HANSEN, I. R., TIMMONS, J. A., CANNON, B. & NEDERGAARD, J. 2012. Recruited vs. nonrecruited molecular signatures of brown, "brite," and white adipose tissues. *Am J Physiol Endocrinol Metab,* 302**,** E19-31.

WANG, Q., ZHANG, M., XU, M., GU, W., XI, Y., QI, L., LI, B. & WANG, W. 2015. Brown adipose tissue activation is inversely related to central obesity and metabolic parameters in adult human. *PLoS One,* 10**,** e0123795.

WANG, Q. A., TAO, C., GUPTA, R. K. & SCHERER, P. E. 2013. Tracking adipogenesis during white adipose tissue development, expansion and regeneration. *Nat Med,* 19**,** 1338-44.

WARDLE, J., SANDERSON, S., LEIGH GIBSON, E. & RAPOPORT, L. 2001. Factor-analytic structure of food preferences in four-year-old children in the UK. *Appetite,* 37**,** 217-23.

WEIR, G., RAMAGE, L. E., AKYOL, M., RHODES, J. K., KYLE, C. J., FLETCHER, A. M., CRAVEN, T. H., WAKELIN, S. J., DRAKE, A. J., GREGORIADES, M. L., ASHTON, C., WEIR, N., VAN BEEK, E. J. R., KARPE, F., WALKER, B. R. & STIMSON, R. H. 2018. Substantial Metabolic Activity of Human Brown Adipose Tissue during Warm Conditions and Cold-Induced Lipolysis of Local Triglycerides. *Cell Metab,* 27**,** 1348-1355 e4.

WEIR, J. B. 1949. New methods for calculating metabolic rate with special reference to protein metabolism. *J Physiol,* 109**,** 1-9.

WELLS, J. C. & FEWTRELL, M. S. 2006. Measuring body composition. *Arch Dis Child,* 91**,** 612-7.

WESCHE, M. F., WIERSINGA, W. M. & SMITS, N. J. 1998. Lean body mass as a determinant of thyroid size. *Clin Endocrinol (Oxf),* 48**,** 701-6.

WHO 2018. Taking action on childhood obesity report. www.WHO.int.

WHO. 2019. *Health topics: obesity* [Online]. World Health Organisation. Available: https://www.who.int/topics/obesity/en/ [Accessed 23/9/2019].

WIJERS, S. L., SARIS, W. H. & VAN MARKEN LICHTENBELT, W. D. 2010. Cold-induced adaptive thermogenesis in lean and obese. *Obesity (Silver Spring),* 18**,** 1092-9.

WINTHER, S., ISIDOR, M. S., BASSE, A. L., SKJOLDBORG, N., CHEUNG, A., QUISTORFF, B. & HANSEN, J. B. 2018. Restricting glycolysis impairs brown adipocyte glucose and oxygen consumption. *Am J Physiol Endocrinol Metab,* 314**,** E214-E223.

WISKIN, A. E., DAVIES, J. H., WOOTTON, S. A. & BEATTIE, R. M. 2011. Energy expenditure, nutrition and growth. *Arch Dis Child,* 96**,** 567-72.

WU, J., BOSTROM, P., SPARKS, L. M., YE, L., CHOI, J. H., GIANG, A. H., KHANDEKAR, M., VIRTANEN, K. A., NUUTILA, P., SCHAART, G., HUANG, K., TU, H., VAN MARKEN LICHTENBELT, W. D., HOEKS, J., ENERBACK, S., SCHRAUWEN, P. & SPIEGELMAN, B. M. 2012. Beige adipocytes are a distinct type of thermogenic fat cell in mouse and human. *Cell,* 150**,** 366-76.

XUE, B., RIM, J. S., HOGAN, J. C., COULTER, A. A., KOZA, R. A. & KOZAK, L. P. 2007. Genetic variability affects the development of brown adipocytes in white fat but not in interscapular brown fat. *J Lipid Res,* 48**,** 41-51.

YAMAGA, L. Y., THOM, A. F., WAGNER, J., BARONI, R. H., HIDAL, J. T. & FUNARI, M. G. 2008. The effect of catecholamines on the glucose uptake in brown adipose tissue demonstrated by (18)F-FDG PET/CT in a patient with adrenal pheochromocytoma. *Eur J Nucl Med Mol Imaging,* 35**,** 446-7.

YEUNG, H. W., GREWAL, R. K., GONEN, M., SCHODER, H. & LARSON, S. M. 2003. Patterns of (18)F-FDG uptake in adipose tissue and muscle: a potential source of false-positives for PET. *J Nucl Med,* 44**,** 1789-96.

YONESHIRO, T., AITA, S., KAWAI, Y., IWANAGA, T. & SAITO, M. 2012. Nonpungent capsaicin analogs (capsinoids) increase energy expenditure through the activation of brown adipose tissue in humans. *Am J Clin Nutr,* 95**,** 845-50.

YONESHIRO, T., AITA, S., MATSUSHITA, M., KAMEYA, T., NAKADA, K., KAWAI, Y. & SAITO, M. 2011a. Brown adipose tissue, whole-body energy expenditure, and thermogenesis in healthy adult men. *Obesity (Silver Spring),* 19**,** 13-6.

YONESHIRO, T., AITA, S., MATSUSHITA, M., KAYAHARA, T., KAMEYA, T., KAWAI, Y., IWANAGA, T. & SAITO, M. 2013. Recruited brown adipose tissue as an antiobesity agent in humans. *J Clin Invest,* 123**,** 3404-8.

YONESHIRO, T., AITA, S., MATSUSHITA, M., OKAMATSU-OGURA, Y., KAMEYA, T., KAWAI, Y., MIYAGAWA, M., TSUJISAKI, M. & SAITO, M. 2011b. Age-related decrease

in cold-activated brown adipose tissue and accumulation of body fat in healthy humans. *Obesity (Silver Spring),* 19**,** 1755-60.

YONESHIRO, T., MATSUSHITA, M., NAKAE, S., KAMEYA, T., SUGIE, H., TANAKA, S. & SAITO, M. 2016. Brown adipose tissue is involved in the seasonal variation of cold-induced thermogenesis in humans. *Am J Physiol Regul Integr Comp Physiol,* 310**,** R999-R1009.

ZHOU, J., WU, N. N., YIN, R. L., MA, W., YAN, C., FENG, Y. M., ZHANG, C. H. & ZHAO, D. 2018. Activation of brown adipocytes by placental growth factor. *Biochem Biophys Res Commun,* 504**,** 470-477.

ZINGARETTI, M. C., CROSTA, F., VITALI, A., GUERRIERI, M., FRONTINI, A., CANNON, B., NEDERGAARD, J. & CINTI, S. 2009. The presence of UCP1 demonstrates that metabolically active adipose tissue in the neck of adult humans truly represents brown adipose tissue. *FASEB J,* 23**,** 3113-20.

ZOTTERMAN, Y. 1959. Thermal sensations. *Handbook of physiology,* 1**,** 431-458.

ZUKOTYNSKI, K. A., FAHEY, F. H., LAFFIN, S., DAVIS, R., TREVES, S. T., GRANT, F. D. & DRUBACH, L. A. 2009. Constant ambient temperature of 24 degrees C significantly reduces FDG uptake by brown adipose tissue in children scanned during the winter. *Eur J Nucl Med Mol Imaging,* 36**,** 602-6.

ZUKOTYNSKI, K. A., FAHEY, F. H., LAFFIN, S., DAVIS, R., TREVES, S. T., GRANT, F. D. & DRUBACH, L. A. 2010. Seasonal variation in the effect of constant ambient temperature of 24 degrees C in reducing FDG uptake by brown adipose tissue in children. *Eur J Nucl Med Mol Imaging,* 37**,** 1854-60.